THÈSE POUR OBTENIR LE GRADE DE DOCTEUR DE L'UNIVERSITÉ DE MONTPELLIER

En Sciences de la Terre et de l'Eau

École doctorale GAIA

Unité de recherche HydroSciences Montpellier

Multidisciplinary study for the characterization of volcanic aquifers hydrogeological functioning. Case of Bromo-Tengger volcano (East Java, Indonesia)

Présentée par Alix TOULIER

Le 6 décembre 2019

Sous la direction de Hervé JOURDE

Devant le jury composé de

Jean-Lambert JOIN, Professeur, Université de la Réunion	Rapporteur
François BEAUDUCEL, Directeur de recherche, IPGP-IRD, Yogyakarta	Rapporteur
Benoît DEWANDEL, Chargé de recherche HDR, BRGM Montpellier	Examinateur
Alexandre PRYET, Maître de conférences, ENSEGID Bordeaux	Examinateur
Patrick LACHASSAGNE, Chercheur HDR, Danone waters, Evian-les-Bains	Invité
Olivier BEON, Ingénieur, Danone waters, Evian-les-Bains	Invité
Adrien SELLES, Chargé de recherche, BRGM Inde	Invité
Heru HENDRAYANA, Associated Professor, UGM Yogyakarta	Invité
Hervé JOURDE, Professeur, HSM-UM, Montpellier	Directeur de thèse
Véronique DE MONTETY, Maître de conférences, HSM-UM, Montpellier	Co-encadrante de thèse

UNIVERSITÉ DE MONTPELLIER

« Indonesia, Negeri yang gemah ripah loh jinawi »

**Indonesia has so much amazing nature which is so peaceful.*

À mes parents…

Abstract

Résumé

Les volcans sont des espaces qui combinent aléas et ressources naturelles, ces dernières justifiant la forte densité de population vivant sur de nombreux volcans actifs en milieu tropical. Certains volcans sont ainsi considérés comme de véritables châteaux d'eau au travers desquels les eaux souterraines circulent vers des systèmes aquifères complexes et parfois artésiens. Ces derniers offrent de nombreuses possibilités en matière d'alimentation en eau, que ce soit pour l'agriculture ou l'eau potable, parfois à des fins commerciales (eau embouteillée).

Le système aquifère du volcan Bromo-Tengger, localisé à l'Est de l'Ile de Java (Indonésie), représente une ressource stratégique. En effet, sa principale source artésienne à fort débit (Umbulan), alimente en partie la deuxième plus grande ville d'Indonésie (Surabaya). Depuis plus d'une décennie, cette ressource en eau est soumise à une pression croissante liée à une constante augmentation des prélèvements d'eau à des fins agricoles ou industrielles et à l'accroissement de la population, favorisée par l'accessibilité des populations à des techniques de forage de plus en plus performantes. Connu comme l'un des stratovolcans les plus visités au monde, le potentiel aquifère du Bromo-Tengger n'était jusqu'ici que très peu connu.

Dans le cadre de ce travail, une approche multidisciplinaire a été mise en œuvre pour préciser l'hydrogéologie du flanc Nord du Bromo-Tengger et ses relations avec l'aquifère volcano-sédimentaire localisé en aval, dans la plaine de Pasuruan. Diverses campagnes géologiques et géophysiques ont permis de préciser la lithologie et la géométrie des formations aquifères du volcan, mais également d'identifier le contexte d'émergence de leurs exutoires naturels, essentiellement des sources artésiennes de piedmonts volcaniques à fort débit.

L'installation de stations météorologiques le long du flanc Nord du volcan, complétée par l'instrumentation d'un bassin versant représentatif, ont permis de préciser le contexte hydro-météorologique. L'analyse de ces données et de l'information hydrochimique et isotopique recueillie sur les eaux souterraines et les précipitations, ont permis de préciser la distribution de la recharge et d'élaborer un modèle conceptuel de fonctionnement hydrogéologique. La recharge s'effectue de façon identique sur tout le flanc du volcan (≈66% de la pluie) avec une zone préférentielle de recharge identifiée vers 1000 m d'altitude due principalement aux effets orographiques. Conceptuellement, les eaux infiltrées alimentent un réseau d'aquifères perchés alimentant à leur tour un aquifère libre dont la partie terminale devient captive vers la plaine volcano-sédimentaire avale. Les conditions artésiennes de cet aquifère associées à une géométrie multicouche expliquent les fortes productivités de la plaine de Pasuruan.

Afin d'estimer les propriétés hydrodynamiques et le niveau piézométrique en différents points de cet aquifère, un dispositif de mesure sur forages artésiens permettant la mesure transitoire de la charge hydraulique jusqu'à l'équilibre a été développé. Les résultats obtenus ont permis de proposer une carte piézométrique de l'aquifère artésien afin de définir les principales directions et systèmes d'écoulement, et d'estimer des temps de transit. La pertinence du modèle conceptuel proposé a ensuite été appréciée au moyen de deux modèles numériques d'écoulement en régime permanent. Ces modèles permettent de représenter le fonctionnement hydrogéologique actuel et celui antérieur à la mise en place des forages dans la plaine de Pasuruan. Le croisement de l'information hydrodynamique simulée avec les informations relatives à l'âge de l'eau souterraine dans la plaine, a permis d'identifier le modèle d'écoulement le plus représentatif à considérer à l'échelle du système.

Les résultats obtenus dans le cadre de cette étude multidisciplinaire contribuent ainsi à améliorer la connaissance du fonctionnement hydrogéologique des stratovolcans en position d'arc volcanique, incluant une caldera, des aquifères perchés de haute altitude ainsi qu'une plaine volcano-sédimentaire multicouche et artésienne.

Mots-clés : Hydrogéologie, aquifères volcaniques, système artésien, recharge, volcano-sédimentaire, étude multidisciplinaire, volcan Bromo-Tengger, Indonésie

Abstract

Volcanoes are environments which combine hazards and natural resources, the latter accounting for the high population density living on many active volcanoes in tropical contexts. Beyond being a source of construction materials, some volcanoes are considered as "water towers", providing considerable possibilities for the drinking water supply through complex aquifer systems sometimes showing an artesian condition. The Bromo-Tengger volcano aquifer system in East Java, Indonesia, is a strategic resource with its main artesian spring Umbulan, which partly supplies the second largest city of Indonesia (Surabaya). For more than a decade, this resource has been under mounting pressure with an increase of water abstraction for agricultural practices, industrial development and population growth. The anthropogenic impact was heightened as drilling techniques became more accessible. The Bromo-Tengger volcano is one of the most visited stratovolcanoes worldwide. However, to date, the aquifer potential of the Bromo-Tengger has so far been poorly studied.

As part of this thesis project, a multidisciplinary approach was used to characterize the hydrogeology of the northern flank of the volcano and its downstream artesian plain. The geological and geophysical results have clarified the lithology and the geometry of the aquifer formations around the volcano, but also have helped identify the outflow context of the natural major artesian springs of volcanic piedmont areas like Umbulan.

The climatic conditions were characterized by the installation of new meteorological stations along the northern flank and completed by the monitoring of a representative watershed. Comparing the climatic conditions with hydrochemical and isotopic data has enabled a quantitative analysis of the distribution of the recharge and the development of a first hydrogeological conceptual model. The recharge covers the whole northern flank of the volcano (≈66% of rainfall) with a preferential recharge zone identified at about 1000 m elevation mainly due by orographic effects. Conceptually, infiltrated waters supply a binary system that is composed of a network of high-elevation perched aquifers feeding all or part of a main basal aquifer. The latter becomes confined towards the plain through a multi-layered artesian aquifer which explains the high aquifer productivity of the area.

A new measurement device for free-flowing artesian wells has been developed, combining hydraulic tests and piezometric head measurements. Interpreting the results enables to estimate the hydrodynamic parameters and draw up a piezometric map of the artesian aquifer of Pasuruan. These results allowed to define the main directions and flow systems and estimate groundwater transit time.

A first numerical steady-flow model shows good consistency with the conceptual model previously developed. It allows for a better understanding of the hydrogeological functioning in the present and under pre-exploitation conditions. Comparing the model results with the water age analyses allowed us to put forward the most realistic flow model that can be considered at the scale of the aquifer system.

This research helps provide insights to improve hydrogeology knowledge of stratovolcanoes in volcanic arc setting, in environments which comprise a caldera, high-level perched aquifers and a multi-layered artesian volcano-sedimentary plain.

Keywords: Hydrogeology, volcanic aquifers, artesian system, recharge, volcano-sedimentary, multidisciplinary study, Bromo-Tengger volcano, Indonesia

Forewords

This PhD thesis was carried out from October 2016 to October 2019 within the Hydrosciences laboratory of the University of Montpellier (France), under the supervision of the Prof. Hervé Jourde.

This research is part of the framework of Rejoso Kita project, started in 2015 with the international collaboration of UM (Université de Montpellier), UGM (Universitas Gadjah Mada), ICRAF (The World Agroforestry Centre), SII (Social Investment of Indonesia), and CKNet (Collaborative Knowledge Network Indonesia) institutions with the financial support of an industrial partner (Danone Aqua Indonesia). This research was authorized by the Ministry of Research, Technology and Higher Education of Indonesia (RISTEKDIKTI) and the Bromo Tengger Semeru National Park (TNBTS) who have facilitated the access to the Bromo-Tengger zones.

Laboratory analyses have been performed in France by Hydrosciences – LAMA (Montpellier), Géosciences Montpellier, CONDATEau (Rennes), EMMAH (Avignon), SARM (Nancy), BRGM (Orléans), but also abroad at UW-EIL (Canada), Geotop (Canada) and in Gadjah Mada Lab (Indonesia).

To facilitate the sharing of the phD results, this thesis was written in English with a research paper structure corresponding to each chapter. This language was chosen in order to make this study accessible to any person interested in the topics, and especially to share the results to our Indonesian colleagues and partners.

Acknowledgements

Pour certains, la géologie commence tôt dans l'enfance, et d'une manière douce avec une première collection de jolis minéraux achetés quotidiennement au bureau de tabac du coin. Pour mes frères et moi, les premières notions de géologie s'apparentaient plus à d'innombrables brouettes de pierres que nous ramassions dans le jardin familial à chaque fois que nous étions punis… et dieu sait qu'on en a rempli des brouettes ! « Allez, encore une brouette car il reste des pierres apparentes », nous disait mon père. Heureusement à l'époque, je ne savais pas que notre maison était construite sur une terrasse alluviale de l'Isère communément appelée gravière… Et paradoxalement, c'est sûrement ces satanées brouettes de pierres blanches, jaunes, marrons et parfois étincelantes qui ont aiguisé ma curiosité pour les roches et la géologie en général. 20 ans plus tard et quelques années d'études au compteur, je commence donc par remercier ces brouettes d'histoires géologiques et par la même occasion le goût du labeur que nous aura inculqué mon père.

Revenons-en à la Thèse, et à cette partie des remerciements qui aura, je l'espère, le plus gros impact factor de ce manuscrit : Seule et unique partie du manuscrit qui ne soit soumise à aucun cadre rédactionnel et qui permette au thésard de sortir durant quelques lignes de la monotonie du discours scientifique. Alors autant en profiter…

En France :

Je voudrais commencer par remercier mon directeur de thèse Hervé Jourde pour m'avoir proposé ce sujet de recherche lorsque je vivais en Nouvelle Zélande loin de la science…. Merci de m'avoir fait confiance tout au long de ce projet et de m'avoir donné les moyens de conduire à bien ces recherches, je lui en suis très reconnaissant. Je remercie également ma co-encadrante Véronique de Montety pour son soutien et ses conseils avisés.

Je remercie vivement les membres du jury d'avoir accepté de juger mes travaux de recherche qui, je l'espère, seront à la hauteur de leur exigence scientifique.

Toujours dans l'atmosphère Montpelliéraine, je remercie Séverin Pistre et Véronique Léonardi d'être venus m'aider sur le terrain en Indonésie, lorsque les ascensions de volcans sous la chaleur, l'humidité et les serpents en aurait terrassé plus d'un… Désormais le Mont Semeru, le Rinjani, le Merapi et le Kawah Ijen n'ont plus de secret pour nous ce qui aura largement comblé mes entrainements de triathlon en France. Sur l'aspect monitoring, je voudrais remercier l'expertise de Jean-Pierre Briquet sur l'installation des stations météo et celle de Pierre Marchand sur l'installation de stations hydrologiques. Merci également à tout le personnel d'Hydrosciences qui a contribué à l'avancée de la démarche scientifique de cette thèse. Les discussions sur l'approche isotopique avec Nicolas Patris et Jean Denis Taupin m'ont permis d'approfondir mes connaissances et pousser davantage les interprétations dans ce domaine pour lequel les hydrogéologues ont souvent moins d'affinité, c'était mon cas.

Côté Géosciences Montpellier, c'est bien évidemment à ce super volcanologue, Jean-Marie Dautria que j'adresse mes sincères remerciements pour sa disponibilité, sa bonne humeur sur le terrain et nos longues discussions autour de ces quelques « cailloux » ramenés du pays des volcans… à ce plongeon inattendu mais effectué avec tant de grâce qui t'a permis de revêtir le traditionnel Saroug Indonésien ! J'espère avoir la même capacité à manier le marteau de géologue passé la retraite. Merci également à Erik Doerflinger pour son aide sur l'utilisation du GPS différentiel en Indonésie. J'ai mis un pied dans ce vaste domaine qu'est la Géodésie et je connais désormais l'importance de considérer le gradient du géoïde local dans la construction d'une carte piézométrique.

Participer à votre encadrement de stage de master aura été clairement une expérience des plus enrichissantes durant cette thèse. Merci donc à Théophile Chomet, Léopold Fontant et Benjamin Baud d'avoir accepté d'être le coéquipier d'un forcené de terrain, qui ne vous laissait que peu de répit pour dormir… j'espère vous avoir donné l'envie de vous lancer vous aussi dans cette formidable aventure qu'est la Thèse. Benjamin, j'espère que notre premier papier scientifique te sera utile dans ce début prometteur de jeune chercheur !

Venons-en maintenant aux fameux thésards d'Hydrosciences. Je crois pouvoir dire que la vraie force d'un doctorant réside dans sa capacité à échanger avec les autres thésards qui l'entourent, que ce soit pour décompresser devant une bonne bière ou pour débattre de théories scientifiques farfelues devant la cafetière du labo… Un grand merci à vous tous de m'avoir fait me sentir bien lors de mes périodes en France ! A Marlène pour tes conseils sur R et ta faculté à transmettre ton optimisme et le sentiment qu'il y a plus important dans la vie que le travail (#Baby). A Victor mon co-bureau qui n'aura pas perdu une occasion de nous faire part de ces fameuses blagues niçoises, ses répliques de Kaamelott et qui aura participé activement à la propagation de grands « Et merdeuhh !!! » dans le couloir. Jeu inventé par nos soins dans le but de simuler de violents excès de colère qui pourraient réveiller les quelques chercheurs encore vivants au sous-sol du laboratoire. Tu auras été un sacré « Challenger » ! A Camille, mon fidèle coéquipier de footing et toujours partant pour m'expliquer ses dernières trouvailles d'hydrologue. A ce fameux joker (Ponce et Shetty, 1995), qui nous aura permis de résoudre habilement bon nombre de questions scientifiques de hauts rangs ! Merci à toi Laïna pour ta gentillesse, ton rire tonitruant (à moins que ce soit le mien qui résonnait ?) et ton aide sur les données de Gaz, une discipline exigeante et encore très prometteuse. J'espère voir ton nom dans de futurs articles gazeux. Merci Marie-Amélie pour ton aide sur la modélisation, qui complétée par la solide expérience de Yvan Rossier, m'auront permis de créer ce premier modèle 3D.

Enfin merci à tous les autres thésards et post-doc, Yohann, Lise, Alexandre, Marie, Mohammed, Antoine et bien d'autres pour leurs échanges ainsi que les repas hilarants au RA, qui ont sûrement marqué, voir choqué certaines tables voisines (non je ne te dénonce pas Alexandre !). Vous avez contribué à me remplir la tête de beaux souvenirs de labo.

Faire une Thèse à l'autre bout du monde n'aurait jamais été possible sans le soutien administratif des gestionnaires d'HSM. Je tiens particulièrement à remercier Bérengère Baldit pour son efficacité et sa sympathie en toute circonstance face à un thésard qui lui a donné du fil à retordre avec ses nombreuses missions en Indonésie…

Je voudrais remercier toutes les équipes de Danone waters en France et en Indonésie qui, en plus d'avoir financé cette Thèse, ont su insuffler une bonne synergie à ce projet. Merci tout d'abord à Olivier Beon, d'avoir initié ce projet et continué à le suivre depuis la France. A Jean Luc Bonjour, qui a rejoint l'équipe en cours de route et a toujours été de bons conseils avec une touche d'humour plus qu'appréciée. Mes remerciements très chaleureux à Patrick Lachassagne qui m'a « coaché » de la genèse à l'aboutissement de cette Thèse, sur le terrain comme en rédaction d'article. Merci pour son implication « sans faille » et ses idées débordantes qui m'ont permis de constamment remettre en question mes interprétations pour mieux les défendre.

In Indonesia and elsewhere:

My Indonesian experiences have gone far beyond the scientific framework of this thesis. I think back on the small town of Pasuruan where I spent more than a year living the real Indonesian lifestyle. It was a huge "culture-bump" when I first arrived in front of this impressive Bromo-Tengger volcano, and a member of the project exclaimed "Well, here, you are project manager Alix, good luck!" It was not a foregone conclusion for the only "bule" of the town,

but Indonesian smiles are more than legend. They really know how to motivate you to keep pushing through difficult times. I am living proof of that.

I want to thank everyone who has allowed me to be part of and grow in this wonderful country. In the field, between rice fields and canyons to the most remote roads, I was lucky to work with Mas Sangka, Yudah, then Ahmad. The collection of field data would have been very different without your help. Great job and Matursuwun masbro! Thanks to our official driver-pilot Mas Heri who always took care of us anywhere we went, and kept us alive during many complicated field trips, "Are you sure this is a negotiable road? Yes, of course... Al hamdoulillah!" This dear "basecamp" was well where the days of processing data cohabiting with mosquitoes were interrupted by the traditional dinners "liwetan," and were very appreciated during the Ramadan periods. Thank you to all the members of SII team, Mas Kevin, Ratib, Dayat, Bu lili, Pak Fajar and Musmin for making this basecamp so welcoming! The installation of our scientific equipment would not have been possible without the exceptional skills of Pak Bambang, our "superhero" as we called him. He has done nothing short of the impossible for us!

I do not forget Danone Aqua Indonesia from Jakarta with Azwar, Endah, Fainta, Reza, Arif, Harie, Arya, Sangka to Pasuruan with Sunarno, Hari, Huda and the others who helped me during the long geophysical surveys and welcomed me for the many PhD progress meetings. It was a really pleasure to work with you guys. Terima kasih banyak teman teman dan sampai jumpa lagi di Indonesia! In Yogyakarta, Thanks to François Beauducel for the scientific advice about volcanoes.

From the University of Gadjah Mada, I would like to thank Pak Heru for his logistical support and Pak Lucas for his broad knowledge of the Indonesian volcanic environment. The long research visa procedures and KITAS would not have been possible without the valued help of Bu Wita. I am grateful to her. Many thanks to mas Haris, the other PhD student of this ambitious thesis project. Your help in the field was more than welcome. I wish you a very good end of dissertation and many research papers. Selamat sukses mas.

A special thought for this farmer on the banks of this Pasuruan river, who warned me in extremis that crocodiles were possibly in the river while I was going inside to perform gauging sections..." Buaya, Buaya! ", the word in Bahasa Indonesia that I will never forget.

Je remercie également les autres personnes de plusieurs continents qui ont eu un rôle de près ou de loin dans cette thèse. A Tim mon frangin de Bora Bora qui m'a permis de reprendre un bon départ. A Teva Victor de Tahiti qui m'a fait découvrir une autre belle façon d'aborder la géologie : la sculpture sur basalte. A Sophie ma colloque en Nouvelle Zélande avec qui j'ai remis un pied en milieu volcanique à Rotorua…quel beau pays !

A Adrien Selles en Inde qui tout au long de ma thèse m'a fait l'honneur de partager son expérience sur le volcan Merapi. Et enfin en France, à mes amis d'enfance les « Artistes » comme j'aime à les appeler, qui se reconnaitront. Désolé d'avoir été si loin durant ces 3 dernières années, mais trouver de l'eau sur un volcan avec une baguette de sourcier ça prend du temps... !

Je terminerai cette longue envolée lyrique par ces quelques lignes pour remercier avec beaucoup de tendresse mes parents et mes frères et sœurs pour leur soutien indéfectible. L'aboutissement de ces trois années de thèse n'auraient pu se réaliser sans vous.

En passant de la Nouvelle Zélande, au Canada puis en Indonésie, un immense merci à celle qui a partagé ma vie et m'a soutenu dans cette aventure depuis son commencement.

Table of Content

Abstract iii
Acknowledgements vii
Table of Content xi
List of Figures xv
List of Tables xxi
General Introduction 2
Scientific and study context 2
Scientific Approach 4
Time line 5
Thesis content 6
Chapter 1. General context 11
1.1 Geographical context 12
1.1.1 The Indonesian archipelago 12
1.1.2 Java island and the Bromo-Tengger volcano 13
1.2 Geological and tectonic context 14
1.2.1 Geodynamic origin of Java 14
1.2.2 Regional tectonic settings 17
1.2.3 Bromo-Tengger complex 21
1.2.4 Architecture of Bromo-Tengger deposits 25
1.3 Hydrogeological context 30
1.3.1 Volcanic islands 30
1.3.2 Hydrogeological features of volcanic rocks 31
1.3.3 Recharge processes 34
1.3.4 Groundwater occurrence 35
1.3.5 Hydrogeological conceptual model 38
1.3.6 Hydrochemical features of volcanic rocks 42
1.4 Climatic context 43
1.4.1 Tropical climate 43
1.4.2 Atmospheric circulation in Java 43
1.4.3 Local climate 45
1.5 Land and water uses 46
1.5.1 Land use 46
1.5.2 Water use 48
1.6 Synthesis 50
Instrumentation 51
Overview 51
Weather stations 52
Probe monitoring 54

Chapter 2. Geological and hydrogeological characterization of piedmont artesian springs related to the coastal volcano-sedimentary deposits of Pasuruan, Indonesia 59

2.1 Introduction 61

2.2 Study area 62

2.3 Methodology 63

2.3.1 Groundwater points inventory and database 63

2.3.2 Geological and drilling surveys 64

2.3.3 Geophysical survey 66

2.4 Results 69

2.4.1 Groundwater inventory 69

2.4.2 Geological survey 71

2.4.3 Drilling survey 75

2.4.4 Geophysical survey 78

2.5 Discussion 85

2.5.1 Geological and hydrogeological characterization 85

2.5.2 Outflow context of artesian springs of volcanic piedmont area 87

2.6 Conclusion 92

Chapter 3. Multidisciplinary study with quantitative analysis of isotopic data for the assessment of recharge and functioning of volcanic aquifers. Case of Bromo-Tengger volcano, Indonesia. 96

3.1 Introduction 98

3.2 Study area 100

3.2.1 Geology 100

3.2.2 Climate 103

3.2.3 Hydrogeology 105

3.3 Methodology 106

3.3.1 Geological study 106

3.3.2 Monitoring network for recharge assessment 107

3.3.3 Quantitative estimation of stable isotopes signature for recharge area delineation 111

3.4 Results and interpretations 115

3.4.1 Geological synthesis and hydrogeological implications 115

3.4.2 Hydro-climatological monitoring of the northern flank of the Bromo-Tengger 119

3.4.3 Hydrochemistry 124

3.4.4 Isotopic composition of groundwater and rainfall 129

3.4.5 Quantitative modeling of groundwater isotopic signature 132

3.5 Discussion and implications for the conceptual hydrogeological model 137

3.5.1 Hydrogeological structure and functioning 137

3.5.2 Recharge distribution and hydrogeological balance 138

3.5.3 Towards a conceptual hydrogeological model 139

3.5.4 Perspectives 139

3.6 Conclusion 141

3.6.1 Acknowledgements 142

Chapter 4. A cost-effective methodology to estimate aquifer transmissivity and hydraulic head from free-flowing artesian wells. Case study of Bromo-Tengger volcano-sedimentary aquifer 145

4.1 Introduction 147

4.2 Methodology 148

4.2.1 Basic concepts concerning artesian aquifers 148

4.2.2 Design of the free-flowing artesian well device (FFAWD) 149

4.2.3 Measurement procedures 151

4.2.4 Hydrodynamic response analysis 152

4.2.5 Computation of the piezometric head at free-flowing well 154

4.2.6 Piezometric mapping 156

4.3 Description of the study site 157

4.4 Results 159

4.4.1 Computation of hydrodynamic parameters 159

4.4.2 Piezometric head computation 162

4.4.3 Piezometric mapping 164

4.4.4 Evaluation of groundwater transit time 166

4.5 Discussion 168

4.5.1 Device 168

4.5.2 Method of measurement 168

4.5.3 Data interpretation 169

4.5.4 Case study 170

4.6 Conclusion 171

4.6.1 Acknowledgements 172

Chapter 5. Validation of the hydrogeological conceptual model through numerical modeling coupled with age dating analyses. 175

5.1 Introduction 177

5.2 Methodology 178

5.2.1 Theoretical background 178

5.2.2 Model design 178

5.2.3 Modeling strategy 185

5.2.4 Age dating sampling 187

5.3 Results 193

5.3.1 Groundwater flow modeling 193

5.3.2 Groundwater age dating results 197

5.4 Discussion 202

5.4.1 Groundwater flow modeling 202

5.4.2 Identification of conceptual models for groundwater flow 205

5.5 Conclusion 209

Conclusion and Perspectives 211

References 221

Appendices 236

List of Figures

Figure 1. 1. a. Location map of the Indonesian archipelago (modified from Gertisser and Keller, 2003). **b**. Location of the Bromo-Tengger volcano in the Eastern part of Java Island (modified from the free access library of ArcGIS online).....12

Figure 1. 2. View of the Bromo-Tengger volcanic massif showing the caldera summit "sea of sand".....13

Figure 1. 3. a. Geology and tectonic settings of Java island (modified after Caudron et al., 2015; Clements et al., 2009; Smyth, 2005). **b.** Regional cross-section of the eastern Java margin (modified after Marliyani, (2016)).. .16

Figure 1. 4. Simplified geological cross-section (N-S) showing the structural evolution of Java Island from the Middle Eocene to the present day. 18

Figure 1. 5. Synthesis schema of the geological, paleoenvironmental and geodynamic features of the East Kendeng basin of the Pasuruan region. 19

Figure 1. 6. a. Hillshade map of the Bromo-Tengger-Semeru volcanic complex. **b.** Main notable structures and eruptive centres of Bromo-Tengger (modified after Solikhin, (2017)). **c.** The Tengger caldera, seen from Mt Penanjakan at 2 700 m.a.s.l.; Mt Bromo seen on the left, currently active. **d.** 3D map of the Tengger caldera zone created with the digital elevation model STRM30m developed by the USGS.....21

Figure 1. 7. Simplified geochronology of the major eruptive and collapse events. 22

Figure 1. 8. a. View of Mount Bromo during a period of quiescence (April 2018), from drone aerial photography. **b.** Mount Bromo during a period of eruptive activity (April 2019).....23

Figure 1. 9. Geological map of Bromo-Tengger complex published by CVGHM, (2010) (from Zaennudin et al., 1994). 25

Figure 1. 10. Main lithologies described in the literature concerning Bromo Tengger, **a.** Lava flows (lamellar and fractured andesite) of the Kronto unit, **b.** Ash fall deposits of the Tengger wall unit, **c.** Ignimbrite of the Sakapura unit, **d.** Dark sand of the sand sea caldera, **e.** Lahar deposits of the Madakaripura valley, **f.** Recent alluvial deposits in the Sapikerep valley. The location name refers to the maps in **Figure 1. 6**. 27

Figure 1. 11. Conceptual model of the distribution of volcanoclastic facies associated with andesitic stratovolcanoes, as adapted for the eastern flank of Merapi volcano. The proximal to distal variation and the lateral distribution of facies depend on the dynamics of valleys and interfluves (Selles et al., 2015).....28

Figure 1. 12. Review of hydraulic conductivities reported in basaltic and andesitic contexts (modified after Pryet, (2011)). (1) from a review of undifferentiated basaltic contexts by Custodio, (2007), other examples from pumping tests performed in insular volcanic contexts: (2) Gingerich, (1999), (3) Rotzoll et al. (2007), (4) Hunt, (1996), (5) Join, (1991) supplemented by (6) Selles, (2014) and (7) Charlier et al. (2011) in andesitic contexts.....34

Figure 1. 13. Types of springs identified in andesitic volcanic-subduction contexts (modified from Selles, (2014)) with **A**. Lithological contact springs occur where aquifer layers overlying a less permeable formation are incised by erosion (e.g. Sumber Pitu in Malang, East Java). **B.** Depression springs occur where the groundwater table intersects the surface topography (e.g. Tirtoageng spring in Probolinggo, East Java). **C.** Contact fault springs (artesian springs) triggered by faults or intrusive bodies which can favour vertical groundwater circulation (e.g. Ranggojalu spring in Probolinggo, East Java). 37

Figure 1. 14. Hydrogeological conceptual models of young oceanic volcanoes (modified from Join et al. (2016)). 38

Figure 1. 15. Conceptual hydrogeological model of the eastern flank of Merapi volcano (from Selles, (2014)). 41

Figure 1. 16. Mean sea-surface temperature (STT in the tropical Pacific Ocean for the period January 1982-December2012, modified after Clarke, (2014)). 44

Figure 1. 17. Mean interannual rainfall at 10 rainfall stations, as a function of their elevation (m.a.s.l.) (data from BMKG, (2018) of Malang city). 45

Figure 1. 18. Land use and land cover map of the Pasuruan district in 2015. 46

Figure 1. 19. Drone aerial view of Pasuruan plain with **a.** Paddy field plantations and **b.** The city of Pasuruan with the Arjuno-Arjuna volcanic complex in the background. 47

Figure 1. 20. Types of water point for agriculture, drinking water supply, domestic and industrial uses divided into three main types: springs, wells and river intake. Spring-type water points are divided into (1) gravity springs and (2) artesian springs. The wells are divided into shallow (3) dug wells, (4) pump wells and deep (5) artesian wells (mostly free-flowing). The rest of the water used comes from (6) river intake. 49

Figure 1. 21. 3D Conceptual schema of the northern flank of Bromo-Tengger 51

Figure 1. 22. Location of rain gauges and weather stations installed on the northern volcano flank, **b, c.** Aqua Kebon Candi plant, **d, e.** Kronto village, **f, g.** Wonorejo village, **h.** Seruni caldera summit, **i.** Temple in the sand sea caldera....53

Figure 1. 23. Installation of new probes on the northern volcano flank (**a**) with TD Diver for gauging stations (**b, e, g**) and piezometric artesian well monitoring (**h**), CTD Diver for physico-chemical....55

Figure 2. 1. a. Relief map of the North-Eastern part of Java Island (USGS SRTM30 dataset) with location of the studied area. **b.** Drone view of the Umbulan artesian springs. **c.** Drone view of the Banyu Biru artesian spring..62

Figure 2. 2. Bromo-Tengger database developed with the Access Microsoft platform. 64

Figure 2. 3. Location map of the geological and geophysical investigations. 65

Figure 2. 4. Core drill method applied in the Pasuruan plain. 66

Figure 2. 5. Principle of resistivity measurements with four electrodes (modified after Knödel et al., (2007)) and two arrays configurations presented (WS & GM). 67

Figure 2. 6. Location map of the geophysical profiles performed in three main investigation zones. 68

Figure 2. 7. Location map of the inventoried groundwater points....69

Figure 2. 8. Artesian wells inventoried in paddy fields (left, middle) and in a village (right). 71

Figure 2. 9. Steps of lava flow weathering with **a.** Massive slightly fractured fresh lava flow (key outcrop n° 3), **b.** Old lava flow with "onion skin" weathering (key outcrop n° 4), **c.** Weathering of lava flow leading to saprolite formation, **d.** Final weathering stage of the top lava flow unit represented by lava boulders (blocks field) in surface. 72

Figure 2. 10. Geological description of the alluvial quarry near Banyu Biru spring. 73

Figure 2. 11. Cores and cutting samples provided from the drilling survey with **a.** andesitic lava core collected at well FD1 at 15 m depth, **b.** Coarse-grained volcanic sand collected at Aqua wash well at 80 m depth, **c.** Cemented pyroclastic deposits, **d.** Clayey and cemented lahar deposits collected at well FD4 at 70 m depth. Well logging video performed in artesian well B33, with **e.** A vertical downhole view, and a horizontal view with different types of cemented pyroclastic deposits (**f, g, h**). 76

Figure 2. 12. Compilation of geological and hydrogeolgoical data along a S-N-NE cross section of the Pasuruan plain....77

Figure 2. 13. 2D and 3D representation of the geophysical profiles of zone 1 surrounding the Banyu Biru spring. 80

Figure 2. 14. 2D and 3D representation of the geophysical profiles of zone 2 surrounding the FD1 well log. 82

Figure 2. 15. 2D and 3D representation of the geophysical profiles of zone 3 surrounding the Umbulan artesian spring....84

Figure 2. 16. Reservoir conceptual model for the plain of Pasuruan. 86

Figure 2. 17. Map showing location of cross-sections on the plain of Pasuruan. 87

Figure 2. 18. Correlation of five topographic cross-sections along the supposed strike-slip fault on the volcano-sedimentary plain of Pasuruan. 88

Figure 2. 19. Drilling and geophysical surveys synthesis projected into 3 N-S cross-sections related to the main geophysics zones....89

Figure 2. 20. Hydrogeological interpretations of the outflow context of a. Umbulan and b. Banyu Biru artesian springs. 90

Figure 3. 1. a Relief map of the North-Eastern part of the Java Island (USGS SRTM30 dataset) with the location of the studied artesian springs, among which Umbulan, and the main volcanoes active vents. The major active faults systems (Watukosek and Pasuruan) and the meteorological stations from BMKG are indicated, and completed by the satellite data provided by the Tropical Rainfall Measuring Mission (TRMM) (3b42v7; Zone: 25x25 km). **b** The Tengger caldera, seen from Mt Penanjakan at 2700masl. Mt Bromo still active on the left. **c** South-North view of the Umbulan artesian spring with the new adduction pipe that supplies the Surabaya city with drinking water (drone view). The main spring outflow is located in the southern part of the basin in the catchwork visible on the photo. 102

Figure 3. 2. a Mean interannual rainfall at 10 rainfall stations, as a function of their elevation (m.a.s.l.) (data from BMKG of Malang city); the location of each rainfall station is reported on Fig. 1 a. **b** Mean monthly precipitation for the 10 rain gauges. **c** Normalised rainfall index (i) and annual cumulative rainfall from 2000 to 2017 hydrological years, estimated from the TRMM data (3b42v7, 2011). The index is given by the equation: $i = (P_i - P_{mean})/\sigma$ where P_i = annual cumulative rainfall, P_{mean} = mean interannual rainfall and σ = standard deviation of the total annual cumulate rainfall. 104

Figure 3. 3. Location of the sampling sites on the Bromo-Tengger-Semeru area plotted on a DEM (STRM30m). The sampling points are divided in 5 types: 1) Gravity springs, 2) Artesian springs, 3) Artesian wells, 4) Ranu Grati lake (Maar) and (5) Rainwater from raingauges. 109

Figure 3. 4. Quantitative modeling method for recharge area delineation of the Bromo-Tengger hydrogeological system. 114

Figure 3. 5 a Geological map of the Northern flank of the Bromo Tengger, modified after Mulyadi, (1992); Santosa et al., (1992); Zaennudin et al., (1994). **b** Schematic geological cross section of the Northern flank of the Bromo Tengger from the Caldera summit (A) to the north coast of Pasuruan (B). Detailed drilling logs are provided in chapter 2, **Figure 2. 12**. 117

Figure 3. 6. a Monthly rainfall monitored at the 5 meteorological stations installed during this research along the Northern flank of Bromo-Tenger. **b** Annual rainfall, mean annual temperature and relative humidity for each meteorological station. The Aqua temperature and humidity have been inferred from the temperature altitudinal 120

Figure 3. 7. a Location map of the Kronto river representative watershed and the monitoring network. **b** water budget parameter. **c** Tables of results: 1) periods for each type of computation, 2) water budget computations at each meteorological station 3) Kronto watershed water budget. 123

Figure 3. 8. a Piper diagram of major ions analysed in springs, wells and lake. **b** Binary plot $[Ca^{2+}]$ vs $[Mg^{2+}]$ for same groundwater samples. 125

Figure 3. 9. a Location map of the water sampled on the Northern flank of the Bromo-Tengger, **b.** $\delta D/\delta^{18}O$ graph, **c.** $\delta^{18}O$/elevation graph. 131

Figure 3. 10. Discretization of the aquifer potential recharge surface area. 132

Figure 3. 11. Computed annual water budget components (R, RET and ER), potential recharge (Re) and $\delta^{18}O$ gradient (BSWL) as a function of the elevation. The isotopic signature of the recharge in the caldera is provided by the Temple meteorological station at 2150 m mean elevation. 133

Figure 3. 12. Recharge distribution vs elevation. 134

Figure 3. 13. Hydrogeological conceptual model of the northern part of Bromo-Tengger volcano with **a.** The location map showing the main hydrogeological units, the main recharge area (whole flank), the groundwater samples plotted according four elevation groups and types. Arrow with full and dashed black line show respectively the groundwater flow circulation identified or assumed. **b.** Schematic N-S cross section of northern volcano flank showing the groundwater flow paths according to the identified recharge locations and the atmospheric circulation features from the sea to the Tengger caldera summit. 140

Figure 4. 1. Conceptual model and technical terms for confined and unconfined aquifers (modified from Chen et al., (2017)). 149

Figure 4. 2. **a.** Description of the free-flowing artesian well device (FFAWD) and measurement protocol, **b.** Typical pressure data set recorded by the probe over time during the test of well n°8. The characteristics of free-flowing well n°8 shown here are described in **Table 4. 1**.....150

Figure 4. 3. Schematic evolution of well discharge, piezometric head in the confined aquifer, and pressure measured with a probe installed at the top of the well head (or in our device). Modified after Sun and Xu (2014). 153

Figure 4. 4. Methodology applied to correct the piezometric head measurements from the recovery tests considering an example of three free-flowing artesian wells with different hydrodynamic parameters. 156

Figure 4. 5. Location map of the Pasuruan artesian basin in East Java (Indonesia) with description of water types, showing water points selected for recovery tests with or without continuous pressure monitoring or not. The map and location data are provided in UTM zone 49S coordinates, using the WGS84 datum.....158

Figure 4. 6. Representative piezometric head data recorded during the tests, sorted into three categories: **a.** Recovery curve without any visible influence, except for post-production effects, **b.** Recovery curve influenced by surge effect during the first ten seconds of the test (=sinusoidal curve) and **c.** Recovery curve influenced by leaky well or internal leakage from the aquifer itself. All the recovery test periods are interpreted with the Cooper-Jacob solution. 159

Figure 4. 7. Comparison of the duration of the post-production effect between computed values (formula from Forkasiewicz, (1972)) and values graphically determined from the derivative curve. 160

Figure 4. 8. Compilation of the 33 piezometric head values classified into 2 types: H1: reliable value (extrapolated or interpolated); H2: inaccurate value without any continuous pressure measurements.....163

Figure 4. 9. **a.** Piezometric map of the Pasuruan artesian basin in East Java (Indonesia). The map and the location data are provided in UTM zone 49S coordinates, using the WGS84 datum. **b.** Transmissivity map of the artesian aquifer basin (=confined aquifer) using ordinary kriging from the recovery test results. **c.** Map of hydraulic conductivity derived from the piezometric map and different selected groundwater flow paths. 165

Figure 5. 1. Design of model for the northern flank of the Bromo-Tengger volcano with **a.** the outer limit of the domain that consider geomorphological and hydrogeological limits, **b.** 2D areal finite element mesh with the distinctive volcanic edifice and the volcano-sedimentary plain of Pasuruan from which the nodes of the artesian wells are refined. **c.** Vertical discretization of the 2D mesh considering 5 layers (6 slices) ranging from the surface to -300 m.a.s.l. over the model domain. **d.** Discretization of the volcano-sedimentary unit with a confining unit located in layer 2 (10 m thick). 180

Figure 5. 2. **a.** hydraulic conductivity of slice 3 over the model domain, **b.** cross-section (A-B) between the volcano-sedimentary plain and the volcanic edifice, illustrating the K values of the five model layers. **c.** description of the boundary conditions applied over the model domain. **d.** recharge distribution applied to slice 1 (ground surface).....184

Figure 5. 3. Compilation of discharge data (literature and PhD monitoring) for Umbulan and Banyu Biru artesian springs. 186

Figure 5. 4. Location map with the water point features of the age dating sampling in 2018. 187

Figure 5. 5. **a.** Sampling process for noble gas collection using glass bottle and immerged pump at the Banyu Biru spring outflow (- 4m depth underwater). **b.** Sampling kits used for groundwater age dating analyses.....188

Figure 5. 6. Variation of atmospheric concentrations of the different tracers used to estimate groundwater age, interpolated to 2020. **a.** ^{3}H atmospheric concentrations provided by the GNIP stations at Quezon (Philippines) and Jakarta (Indonesia), (IAEA, 2017). **b.** ^{14}C atmospheric concentrations (IAEA, 2017) and **c.** atmospheric concentrations of dissolved gases (USGS, 2018).....192

Figure 5. 7. Calibration performance of the groundwater flow model in the Pasuruan plain zone with **a.** the hydraulic head calibration results and **b.** the spring's discharge calibration results 193

Figure 5. 8. **a.** 2D map view (slice 3) of the model in steady state in 2018, **b.** water budget results and **c.** 2D vertical cross-section of the model along the conceptual schema of the water budget. 195

Figure 5. 9. Natural flow conditions model in 1980 with **a.** the hydraulic head distribution in slice 3, **b.** the associated water budget. 196

Figure 5. 10. a Values of $\delta^{13}C$ versus latitude, **b.** Values of ^{14}C versus latitude and c. Values of $\delta^{13}C$ versus ^{14}C. The intercept at $^{14}C = 0$ provides an estimate of the $\delta^{13}C$ of magmatic CO_2 (-2.5%). 198

Figure 5. 11. Tritium and ^{14}C dating results for the plain of Pasuruan 199

Figure 5. 12. a. Variation in atmospheric concentrations of CFCs and SF_6. **b. c. d.** and **e.** The results of CFCs and SF_6 concentration in groundwater samples according the main flow models. 201

Figure 5. 13. Conceptual models for groundwater flow paths in the Bromo-Tengger aquifer system..... 207

List of Tables

Table 1. 1. Deployment of instrumentation. 52

Table 1. 2. Monitoring set-up with new instrumentation probes. 54

Table 2. 1 Inventory of groundwater points up to April 2019. 69

Table 2. 2. Selection of key outcrops from the 2016-2017 geological survey. 71

Table 2. 3. Results of the resistivity calibration from **a.** key outcrops and well logs and **b.** from electrical conductivity (converted to resistivity value) of the groundwater from artesian springs/wells and dug wells (i.e. confined and unconfined aquifers). 78

Table 3. 1. Hydrochemical and isotopic results. Samplings and water analyses were repeated for some locations (b and c letters). *NA:* not available; *BDL:* below detection limit. 126

Table 3. 2. Hydrochemical and isotopic results. Samplings and water analyses were repeated for some locations (b and c letters). (-): not available; 127

Table 3. 3. Results of the sensitivity analysis. The reference scenario is based on recharge in half of the caldera and satisfying (1) the $\delta^{18}O$ measured at Umbulan spring and (2) the outflow measured in the plain. In comparison with the reference scenario, various adjustments are tested (1). no contribution of the caldera or full caldera and (2). +/- 15% of rainfall). 136

Table 4. 1. Characteristics of Artesian water points and results obtained. The piezometric data refer to 4 types: artesian springs (AS), non-flowing artesian well (NFAW), free-flowing artesian well (FFAW) and surface water (LAKE). 161

Table 4. 2. Kinematic velocity and groundwater transit time results for each selected flow path (1, 2 and 3), located in **Figure 4. 9. c**. 167

Table 5. 1. Initial hydraulic conductivity values of the model domain 181

Table 5. 2. Boundary conditions in the model domain. 183

Table 5. 3. Mean age estimation from anthropogenic gases 200

Introduction

General Introduction

Scientific and study context

A suitable understanding of the hydrogeology of volcanic regions is fundamental for the management of their water resources, especially in tropical volcanic islands where rainfall distribution is highly heterogeneous both in time and space. In tropical contexts, the wet season provides a high amount of rainfall through the monsoon events. Conversely, the dry season is characterized by a period with practically no precipitation leading to limited surface water resource during extent drought, which may be notably accentuated by recurrent atmospheric convection such as El Niño events. In volcanic regions where a significant part of the population lives on volcanic slopes, surface water is mostly ephemeral. The freshwater supply is compensated by exploiting groundwater from volcanic aquifers which sometimes becomes the only water resource. Groundwater from volcanic aquifers usually constitutes a perennial water resource, generally of higher quality than surface water. However, the groundwater occurrence depends on the geological features and recharge processes related to climate patterns. In many places, the groundwater resource thus becomes a socio-economic issue due to excessive water abstraction without any anticipated sustainable management.

Two main volcanic hydrogeological conceptual models, the "Hawaian" and the "Canarian" models (Custodio, 2004; Join et al., 2005; Peterson and Morre, 1987), are classically considered to explain groundwater flow in a volcanic context. They are based on the consideration of different hydrodynamics, controlled by the mode of genesis of the volcano, its geological structure, age, and state of erosion, as well as distinct climate and precipitation context. Understanding the complexity of the internal structure of volcanoes, which results from several stages of upbuilding and dismantlement, is currently an essential research topic for the hydrogeologist community interested in volcanic regions.

Even if special attention has been paid to volcanic islands (Nichols et al., 1996; Singhal and Gupta, 2010), the hydrogeological functioning of volcanic aquifers remains, to some extent, poorly known. Consequently, the identification of groundwater occurrence, the quantification of the available resources and understanding of groundwater flow circulation remains a major challenge to improve and promote a sustainable management.

Indonesia is located at the boundaries of several tectonic plates known as the "Pacific ring of fire" (Pambudi, 2017), known worldwide for its impressive number of volcanoes. More than 130 are still active, accounting for approximately 14% of the world's active volcanoes. Mount Samalas located on Lombok Island is known as the source of one of the powerful Plinian eruptions (VEI 7 magnitude) that upset the global climate in 1257 (Guillet et al., 2017). Volcanoes in the Indonesian archipelago, represent a concentration of deadly hazards (landslides, earthquakes, eruptions, floods and tsunamis) with around 10% of the Indonesian population living in places at risk of volcanic eruptions. By contrast, volcanoes also often offer

beautiful landscapes with abundant natural resources including construction materials (volcanic sand and rock), geothermal energy (Bertani, 2016; Murakami et al., 2000), and fertile soil favourable for agricultural practices, and more importantly provide an important groundwater resource supporting the livelihood of the population. Over the last four decades, groundwater needs have gradually increased, due to the development of the country associated with the growth of both the population and economy.

On the Eastern part of the Java island (Indonesia), the Bromo-Tengger volcano is one of the most visited active volcanoes in the world (Bromo-Tengger Semeru national park (TNBTS), FAO 1982; Cochrane, 2006). Since the 1980s, the spectacular view of the "sea of sand caldera" became the most accessible outstanding natural attraction in Java. Mt. Bromo's last eruption in 2010 was unusual as it continued for 9 months, the longest period in its recorded history, and caused severe effects on agriculture, tourism activity and damage to infrastructures (Bachri et al., 2015). More than a profitable touristic spot, the massif also provides an important drinking water resource to the local population through groundwater. The main artesian spring of the area (Umbulan), with a continuous discharge of about 3500 L s^{-1}, is mainly used for population needs such as rice irrigation and drinking water. It also partly supplies the second biggest city of Indonesia (Surabaya) located 80 km North of the volcano. Thus, the Bromo-Tengger aquifer is a regional and strategic groundwater resource. However, there is a growing pressure on the water supply due to population growth, highly productive rice cropping and the development of industrial sectors. In the Pasuruan Plain, located at the northern foot of Bromo-Tengger, the easy-access to drilling technology can be blamed for the hundreds of private artesian wells continuously flowing in the area (mainly for paddy fields). As there is no sustainable management or protection policy to regulate these wells, a significant part of freshwater is therefore lost towards canals, rivers and then into the ocean.

Awareness of the groundwater issue started in the 2000s, with the discharge decrease of the Umbulan Spring, for which the last oral testimonies report a discharge of about 5000 L s^{-1} in the 1980s. Gauging measurements performed in 2007 by a local organization (Cknet foundation) seem to confirm the decreasing trend of the Umbulan discharge, and therefore of the artesian conditions of the Pasuruan plain volcano sedimentary aquifer. In 2019, the Indonesian government completed the construction of a pipeline, directly connecting Umbulan spring to the city of Surabaya. In the long term, the pipeline should provide several thousand litres per second of drinking water to Surabaya. This regional project has already triggered water use conflicts with Pasuruan local farmers. As a result, it might expect an increase of new private artesian wells in the Pasuruan plain which would result in both intensifying the pressure on the groundwater resource and, hence increasing the tensions between water consumers.

This context highlights the need for a better knowledge regarding the hydrogeology of the Bromo-Tengger volcano. Indeed, previous studies have mostly focused on the volcanology and seismic aspects of Mt. Bromo and its caldera, while others have addressed the geological architecture of the volcanic edifice but without any hydrogeological description. Therefore, there is an urgent need to characterize the hydrogeological functioning of the Bromo-Tengger aquifer system to adequately manage the groundwater resource.

Scientific Approach

This PhD dissertation, as part of the "Rejoso Kita Project," aims to undertake the first hydrogeological study of the northern flank of the Bromo-Tengger volcano with the objective to propose a first hydrogeological conceptual model. The improvement in hydrogeological knowledge was guided by a scientific approach aiming at gathering and assembling data and evidences to i) to acquire a better understanding of the extent, geometry and hydrodynamic properties of the aquifer's formations, and ii) to quantify the input and output components of the water budget to provide a first estimation of both the main recharge processes and a delineation of the preferential recharge area.

Another objective of this PhD thesis is to understand the hydrodynamic functioning of the main aquifer bodies, notably to assess the artesian conditions of the volcano-sedimentary Pasuruan plain. The results provide scientific data to implement numerical modeling to assess the aquifer's response to anthropogenic and climate changes.

As a tool for understanding complex volcanic aquifers systems, a multidisciplinary approach has thus been applied by combining "lines of evidence" from different types of analysis conducted through scientific investigations.

In view of this, scientific investigations were conducted following three research thematic approaches related to the hydrogeology of the Bromo-Tengger volcano:

I) **Volcanic architecture**: geological surveys and geophysical investigations to determine the architecture and aquiferous properties of the main geological bodies.

II) **Hydrogeological conceptual model**: by means of an experimental site implemented by climatic monitoring, the input and output components obtained enabled to estimate a first water budget. Based on complementary hydrochemical and isotopic data, the most likely recharge distribution is proposed at the scale of the northern flank of the volcano, along with a first conceptual model.

III) **The groundwater flow:** The groundwater flow and hydrodynamic properties of the aquifer systems are estimated by hydrodynamic investigations (aquifer tests and piezometric surveys). Complementary sampling for age dating, allows determine groundwater residence time and identify the most suitable groundwater flow model required for the study of past and present-day scenarios.

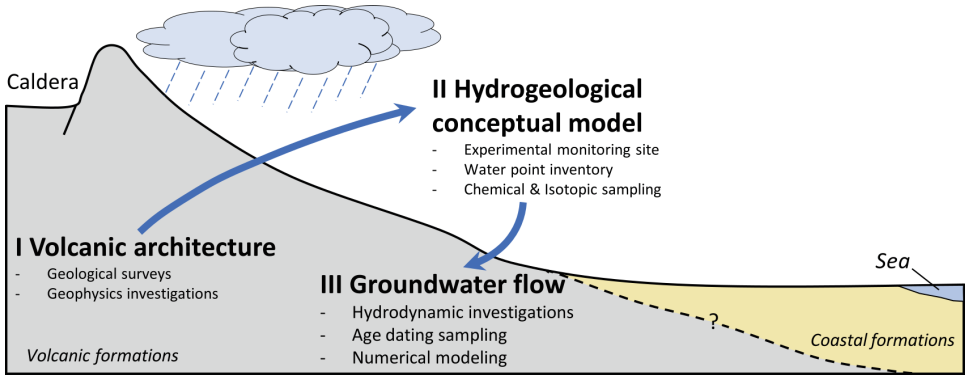

Figure. 1. Guideline research topics of the thesis project with the main investigations conducted on the northern flank of the Bromo-Tengger volcano.

Time line

This thesis work was carried out from October 2016 to October 2019, including more than 12 months of field work in Indonesia divided into 5 missions over the three years:

- The first year (2016-2017), essentially focused on the collection of a first hydrogeological dataset (groundwater points inventory) and the updating of the geological map of Bromo-Tengger through exploratory field work. Geophysical ERT investigations were carried out around the main springs of the Pasuruan Plain. A monitoring network was set up on the northern flank of the volcano during the summer of 2017, with the installation of weather stations and water level recorders at springs, rivers and piezometers. The visa procedures and authorizations requests to lead the research in Indonesia were noticeably time consuming during the first missions in Indonesia.

- The second year (2017-2018), focused on sampling for hydrochemical and isotopic analyses, including age dating. In parallel, a new free-flowing well device was designed and applied at the scale of the Pasuruan Plain to define the hydrodynamic features of the artesian basin.

- The last year (2018-2019) was dedicated to the complementary hydrogeological data collection required to implement a 3D numerical model of the Bromo-Tengger aquifer system. Hydrogeological data processing was performed leading to a numerical groundwater flow model. The ultimate 4 months were focused on the writing the dissertation and research papers.

Thesis content

This thesis is divided into five chapters, each intended to be self-standing but also complementary to follow a common research guideline according to the three previous research topics applied to the Bromo-Tengger volcano. Except for the *Chapter 1*, which describes the overall context of the study area, each chapter follows the classical structure of scientific communications:

- Chapter 1: introduces the global context of the study area related to the geography, geology and climate supplemented by land and water uses occurring in the area. Since no hydrogeological data existed in the literature about the Bromo-Tengger volcano, we present a review of the volcanic hydrogeology to outline the scientific context of such multidisciplinary study.

- Chapter 2: *Why do high artesian springs occur within the piedmont area of the Bromo-Tengger volcano?* This second chapter introduces the geological and the hydrogeological features of an artesian volcano-sedimentary basin such as the Pasuruan Plain. The complementary geological field investigations allow to explain the outflow context of piedmont volcanic springs. Finally, we provide a schematic geological conceptual model.

- Chapter 3: *What is the recharge process and hydrogeological conceptual model for this stratovolcano in a tropical context?* (article published in *Journal of Hydrology: regional studies*). This Chapter is based on a multidisciplinary approach combining hydrogeological field studies, hydro-climatological monitoring, as well as hydrochemical and isotopic sampling. A quantitative analysis method is proposed to better assess the recharge distribution at the scale of the volcano's northern flank. The results from each discipline allow to propose an adequate hydrogeological conceptual model of the Bromo-Tengger volcano.

- Chapter 4: *How to assess the hydraulics and flow of an artesian aquifer such as occurring within the Pasuruan Basin?* (article to be submitted to *Hydrogeology Journal*). An artesian free-flowing well device is designed to estimate, both the hydraulic head and the hydrodynamic parameters in various measurement locations on the volcano-sedimentary of the Pasuruan Plain. A piezometric map is drawn up to assess groundwater flow circulation and estimate transit time at the scale of the volcano-sedimentary plain.

- Chapter 5: *Does the hydrogeological conceptual model allow numerical modeling of groundwater flow and transit time distribution in agreement with groundwater age data?* Proposes a 3D numerical flow model based on the new insights acquired during this thesis project (conceptual model, water budget, hydrodynamic parameters). The present-day hydrogeological conditions allow the testing of conceptual assumptions and the assessment of current groundwater flow in the main basal aquifer. Based on

age dating data, the most reliable flow model and the water residence times are discussed and compared to the groundwater transit times estimated in *Chapter 4*.

From a research point of view, the results of this thesis should help improve the general knowledge of the hydrogeological conceptual models of stratovolcano volcano, in volcanic arc setting, in environment with a caldera, high-level perched aquifers with multilayered and artesian volcano-sedimentary plain.

In other respects, this research should also provide a scientific basis for effective water resource management at the scale of the Bromo-Tengger aquifer system. This sustainable management might improve the living conditions of local inhabitants and provide guidelines for the conservation of freshwater ecosystems.

Chapter I



View of the North Pasuruan plain with the Bromo-Tengger volcano in the background

Chapter 1. General context

This first chapter describes the global context of the study area to better understand the research issues related to the groundwater resource. Indeed, some factors impact the occurrence of groundwater and its development. These controlling factors are presented here according to the following structure.

This chapter is divided into five main sections, the first one defining the geographical framework and boundaries of the study area.

The second section introduces the main geological features of the Bromo-Tengger volcano, including the regional and local tectonics, as well as the genesis of the volcano with his eruptive history that allows to distinguish the main volcanic formations.

The third section proposes a review of the hydrogeological settings in a volcanic context. This part presents some fundamental features of volcanic hydrogeology and introduces the geodynamic contexts at the origin of basaltic and andesitic volcanic island arcs and describes the hydrogeological potential of the main volcanic formations. The recharge processes and groundwater occurrences on such volcanic islands are presented and illustrated by hydrogeological conceptual models developed for basaltic (Hawaii vs. Canary Islands) and andesitic contexts (Merapi volcano). The distinctions between the major conceptual models are discussed and compared with some specific features observed in andesitic contexts. This section is concluded by a short overview of the specific hydrochemical issues in volcanic environments.

A fourth section presents the climatic context of Java Island with the main atmospheric circulation patterns that control the regional climate. The local climate of the study area is presented based on meteorological data provided by the Indonesian climatic center (BMKG) for the 2008-2017 period. This allows a first overview of the precipitation pattern and seasonal effects.

The fifth section focuses on the land and water uses in the study area and presents the main anthropogenic pressures affecting the Bromo-Tengger hydrogeological system.

A final section summarizes this chapter.

1.1 Geographical context

1.1.1 The Indonesian archipelago

Indonesia is located in Southeast Asia between the Indian and Pacific oceans. The territory comprises more than 13 000 Islands, and represents the largest archipelago in the world with a surface area of about 2 million km² and more than 270 million inhabitants in 2019, making it the fourth most populated country in the world. The islands of this archipelago are essentially located according to the main tectonic features of Southeast Asian, which are themselves related to major subduction zones associated with the convergence of the Indo-Australian, Eurasian and Pacific plates (**Figure 1. 1. a**). Indonesia extends on both sides of the equator and is bounded to the North by Malaysia and the Philippines, to the East by New Guinea and to the South by Timor and Australia. The Indonesian territory is covered by more than 130 active volcanoes characterized by explosive eruptive dynamics, and numerous earthquakes, which is a common feature in subduction regimes.

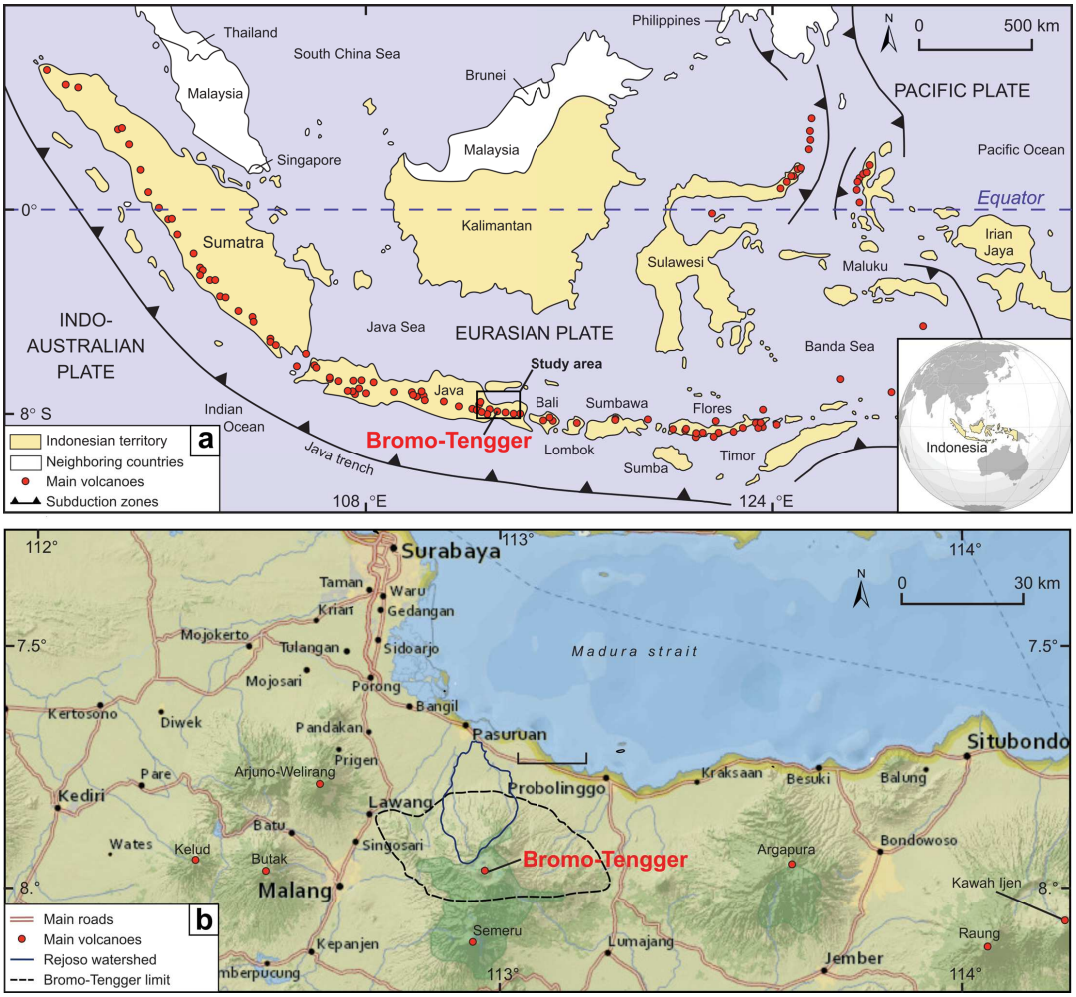

Figure 1. 1. a. Location map of the Indonesian archipelago (modified from Gertisser and Keller, 2003). **b**. Location of the Bromo-Tengger volcano in the Eastern part of Java Island (modified from the free access library of ArcGIS online).

1.1.2 Java island and the Bromo-Tengger volcano

The island of Java (*Jawa*) is bordered to the south by the Indian Ocean and to the North by the Java Sea, with Sumatra lying to the northwest, Bali to the east and Borneo to the north. It is the main island of Indonesia, where about 60% of the total population lives. The Bromo-Tengger volcano is among the 45 active volcanoes on the Island of Java, being located in East Java (**Figure 1. 1**. **b.**) between the cities of Surabaya, Malang, Probolinggo and Lumajang, which lie, respectively, to the North, West, East and South. The Bromo-Tengger volcano has a surface area of about 1 300 km², culminating at 2 770 m.a.s.l. (Mount Penandjakan), comprising a wide caldera summit with a diameter of about 9 km, and the last active vent represented by Mount Bromo. The volcanic massif extends northwards towards the Strait of Madura, across a plain whose main city is Pasuruan with about 200 000 inhabitants. Its southern part is bordered by the Semeru volcano, which represents the highest point on the island of Java at an elevation of 3 676 m (Mahameru).

The Arjuno-Welirang volcanic complex and Lamongan volcano border the Bromo-Tengger to the west and east, respectively.

The Bomo-Tengger and Semeru volcanoes are both included in the Bromo-Tengger-Semeru National Park (Cochrane, 2003). The park is a famous touristic site, especially the caldera (called the Tengger Caldera or Sea of Sand caldera) and several freshwater mountain lakes on the southern slopes of Mt. Semeru (Hakim and Miyakawa, 2013).

The study area is constrained by the complex and fragmented territorial organization of Bromo-Tengger between several administrative entities. The volcano is located within the district of Pasuruan and also shares part of its territory with the districts of Malang (West), Probolinggo (North-East) and Lumjang (South-East).

The Rejoso Watershed (blue line, **Figure 1. 1**. **b**) covers 630 km² and forms part of the Welang-Rejoso Watershed located in Pasuruan district. This latter watershed refers to the hydrological boundary based on data from the Watershed Management Center (BPDAS) of KLHK Indonesia. Part of the northern flank of Bromo-Tengger is included in the Rejoso watershed, which is currently the subject of a socio-environmental study of the water resource carried out by the Rejoso project.



Figure 1. 2. View of the Bromo-Tengger volcanic massif showing the caldera summit “sea of sand”.

1.2 Geological and tectonic context

1.2.1 Geodynamic origin of Java

A volcanic arc is a chain of volcanoes formed along a convergent tectonic plate boundary (e.g. Pacific Ring of Fire). Volcanic arcs result from the subduction of an oceanic tectonic plate under another, and are often parallel to the oceanic trench. These arcs should not be confused with hotspot volcanic chains, where volcanoes often form one after another in the middle of a tectonic plate, as the plate moves over the hotspot, and so the volcanoes progress in age from one end of the chain to the other (e.g. Hawaiian archipelago and La Réunion).

Java is part of a volcanic island arc situated in the Indonesian archipelago at the southern margin of the Eurasian Plate. Sundaland belongs to the continental core of SE Asia, and has been accreting onto Eurasia since Early Mesozoic times, corresponding to a landmass which now underlies the shallow seas to the north of Java (Clements et al., 2009). To the south of Java, subduction of the Indo-Australia Plate beneath the Eurasian Plate has taken place along the Java Trench (**Figure 1. 3**. **a.**) from the middle Eocene (ca. 45 Ma) to the present day (Hall, 2002). As a consequence of subduction since the Early Cenozoic, Java is essentially made up of the products of active and ancient volcanism. The volcanoes of the modern Sunda Arc are distributed along the length of the island and a second older volcanic arc of Eocene to Miocene age forms the Southern Mountains of East Java (Smyth, 2005).

Based on field observations carried out in different parts of Java, Clements et al. (2009) distinguish several distinct structural sectors that broadly correspond to the regions of West, Central and East Java.

- In West and East Java, the overthrust volcanic arc is still preserved, whereas Central Java exposes a deeper structural level below the volcanic arc, which has been largely removed by erosion.
- According to a similar differentiation as suggested by Van Bemmelen, (1949), East Java can be subdivided into four parts, broadly parallel to the E-W elongation of the island, represented by: (1) the early Cenozoic Southern Mountains Arc, (2) the Kendeng basin, and (3) a marine shelf north of the basin (Sunda shelf), (Smyth, 2005).

1- The Southern Mountains Arc consists of a volcanic arc and ophiolitic rocks of Cretaceous age. A volcanic arc was built upon basement rocks from the middle Eocene to the Miocene in southern Java, with a probable thickness > 2 500 m and a width of about 50 km (Smyth, 2005).

2- The Kendeng Basin lies directly behind and to the north of the Southern Mountains Arc, representing the main Cenozoic depocentre in onshore East Java. This deep flexural basin dated as Eocene to Miocene contains a sedimentary sequence about 10 km thick, as suggested by the strong negative Bouguer anomaly (Untung and Sato, 1978). It is now partially exposed at the surface in the Kendeng Fold-Thrust Belt (**Figure 1. 2. b.**).

3- The early Cenozoic Sunda Shelf is made up of pre-Cenozoic basement rocks (ophiolitic and arc rocks), which include chert, basic volcanic rocks and metasedimentary rocks (Hamilton, 1988). Basin development began in the Eocene. There are between 2 000 and 6 000 m of Eocene to Pliocene shallow marine clastic and extensive carbonate sedimentary rocks located within fault-controlled basins (Ardhana et al., 1993). The sedimentary deposits have been deformed by (1) open E-W-oriented folds, (2) northward-verging, E-W-oriented thrusts and (3) ENE-WSW normal faults (Chotin et al., 1984).

The modern volcanic arc is mainly built on the Kendeng Basin (**Figure 1. 3. b.**) and is represented by many andesitic-basaltic stratovolcanoes exceeding 2 500 m in elevation. The volcanic activity here started in the late Miocene (ca. 10 Ma), mostly dominated by explosive type eruptions. This explosive activity results from the incorporation of sediments from the continental crust into the magma, thus increasing the water and CO_2 content and giving rise to more viscous lavas at lower temperature near the land surface (Custodio, 2007). The eruptive and epiclastic products contribute to fertilizing the surrounding soils. Some of these stratovolcanoes have cinder cones and/or lava domes (Kelud and Merapi), calderas with a crater lake (Ijen) or with an inner cone (Bromo-Tengger), or with an open vent system (Semeru), as in the case of central and parasitic cones.

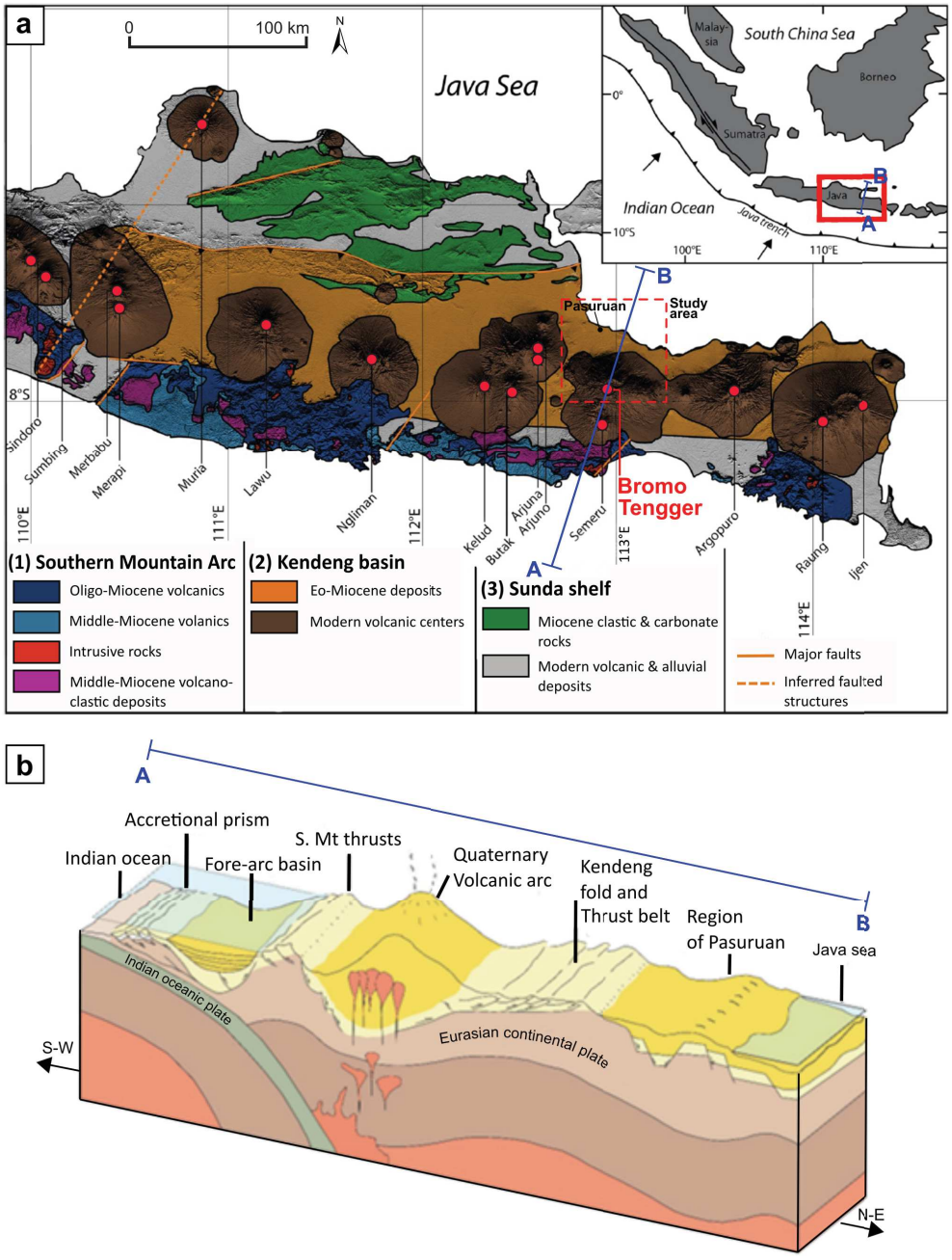

Figure 1. 3. a. Geology and tectonic settings of Java island (modified after Caudron et al., 2015; Clements et al., 2009; Smyth, 2005). **b.** Regional cross-section of the eastern Java margin (modified after Marliyani, (2016)).

1.2.2 Regional tectonic settings

The Pasuruan region is composed of a Tertiary-Quaternary back-arc sedimentary basin, where the main regional stress is related to the northward convergence and subduction of the Indo-Australian plate beneath the Eurasian plate which began in the Late Cretaceous – Early Eocene (Hadi Nugroho et al., 2018; Romario et al., 2015; Satyana et al., 2004; Simandjuntak, 1993; Susilohadi, 1995). The main regional features are summarized on **Figure 1. 5**.
The stratigraphy and the geodynamic evolution can be divided into three periods:

1.2.2.1 Middle Eocene to Middle Miocene

The extensional regional stress caused by the subduction led to the formation of a 400-km-long back-arc basin, called the Kendeng basin (Romario et al., 2015; Smyth, 2005): the local subsidence caused the reactivation of basement structures and the formation of several E-W-trending half-grabens as illustrated in **Figure 1. 3** (Susilohadi, 1995). The syn-tectonic sedimentation was derived from the erosion of volcanogenic deposits in the South volcanic arc (Southern Mountains) as well as from the shallow marine environment, with an asymmetrical geometry thickening southward. The sediments are mainly composed of volcanic conglomerates, volcanic sandstones, fluviatile deposits, tuffaceous mudstones, mudstones with foraminifera, shallow marine marls and limestones, etc. (Husein, 2015; Smyth et al., 2008; Surya Nugraha and Hall, 2013).

The low abundance of volcanoclastic materials in the formations located in the northern part of East Java, far from the South volcanic arc, can be explained by the marine transgression caused by local subsidence, which started in the Middle Oligocene, along with the cessation of volcanic activity in the Middle Miocene. On the contrary, the shallow marine environment led to the extensive deposition of carbonate rocks in this region (Pelang and Kujung Fms.), which are actually the main target formations for petroleum exploration in the Kendeng basin (Moscariello et al., 2018; Satyana et al., 2004; Surya Nugraha and Hall, 2013).

1.2.2.2 Middle-Late Miocene to Holocene

The regional stress was inverted and became compressive: the uplift of Java led to a minor local regressive trend and the deposition of calcareous sandstones (Kerek Fm.). The Pliocene eustatic marine transgression led to the deposition of marly limestones (Kalibeng Fm.). Finally, a renewed regression from the Late Pliocene to Holocene resulted in the more terrigenous and volcanogenic/volcanoclastic deposits of the Pucangan, Kabuh and Jombang formations (Susilohadi, 1995): this period is indeed heavily influenced by the Quaternary volcanic activity, concentrated in the present-day arc which is located several kilometres north of the Southern Mountains Arc (Surya Nugraha and Hall, 2013; Waltham et al., 2008).

During the Plio-Pleistocene, northward compression induced several tectonic structures: in this way, the major normal and dextral strike-slip faults – which were inherited from the basement - became reverse and sinistral while conserving the same strike (respectively E-W and NE-SW) across the entire Kendeng basin. Moreover, the Quaternary volcanism built a new

volcanic arc which was affected by a syn-sedimentary fold-and-thrust belt: the reverse E-W thrust faults are shallower than the pre-existing faults and appear to root on the ductile mudstones at the base of the Pucangan formations (De Genevraye and Samuel, 1972; Smyth, 2005; Susilohadi, 1995). Since the Pliocene, 10 to 30 km of shortening has been produced by this structure (Smyth et al., 2008).

During the Late Pliocene, the regional compressive stress also led to the formation of an alternating system of E-W-trending anticlines and synclines in the Kendeng basin: the two onshore expressions of these anticlines - which extend from Central to East Java - are the northern Rembang Zone, represented by Madura island, and the highly eroded southern Kendeng Zone, whose southern flank may correspond to the plain of Pasuruan (**Figure 1. 4**). The offshore Madura strait thus represents the syncline separating the two previous structures (De Genevraye and Samuel, 1972; Hadi Nugroho et al., 2018; Moscariello et al., 2018; Susilohadi, 1995). Because of this local uplift, the Oligo-Miocene limestones crop out on Madura island, while the Pleistocene volcanogenic formations of Kabuh and Pucangan are found in the Kendeng hills, in the western part of Pasuruan (Tsuji et al., 1986).

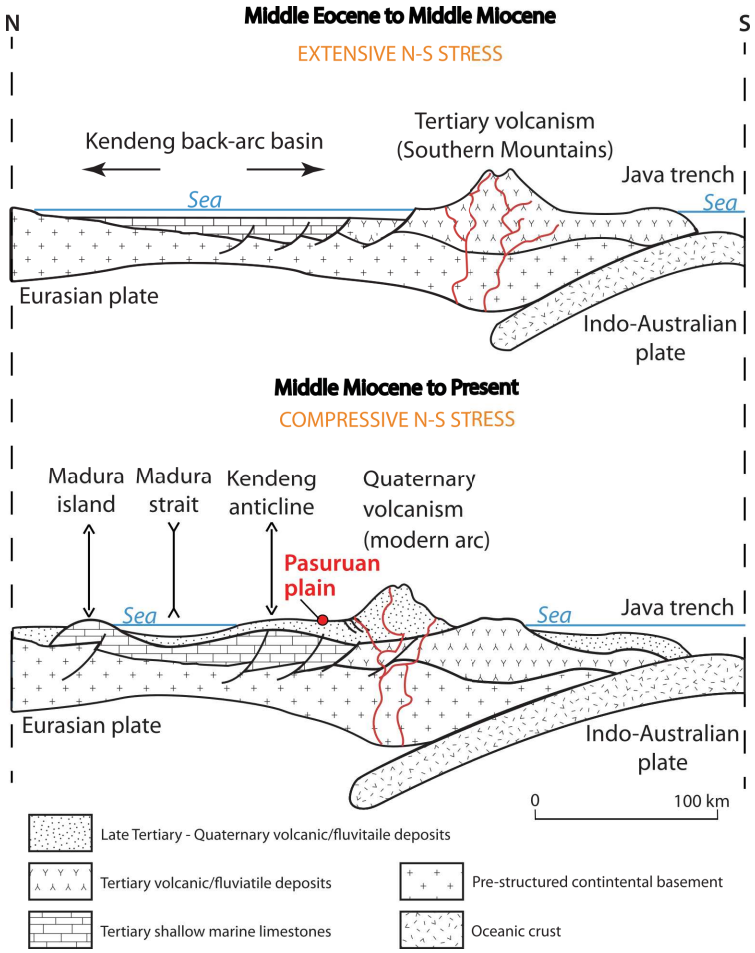

Figure 1. 4. Simplified geological cross-section (N-S) showing the structural evolution of Java Island from the Middle Eocene to the present day.

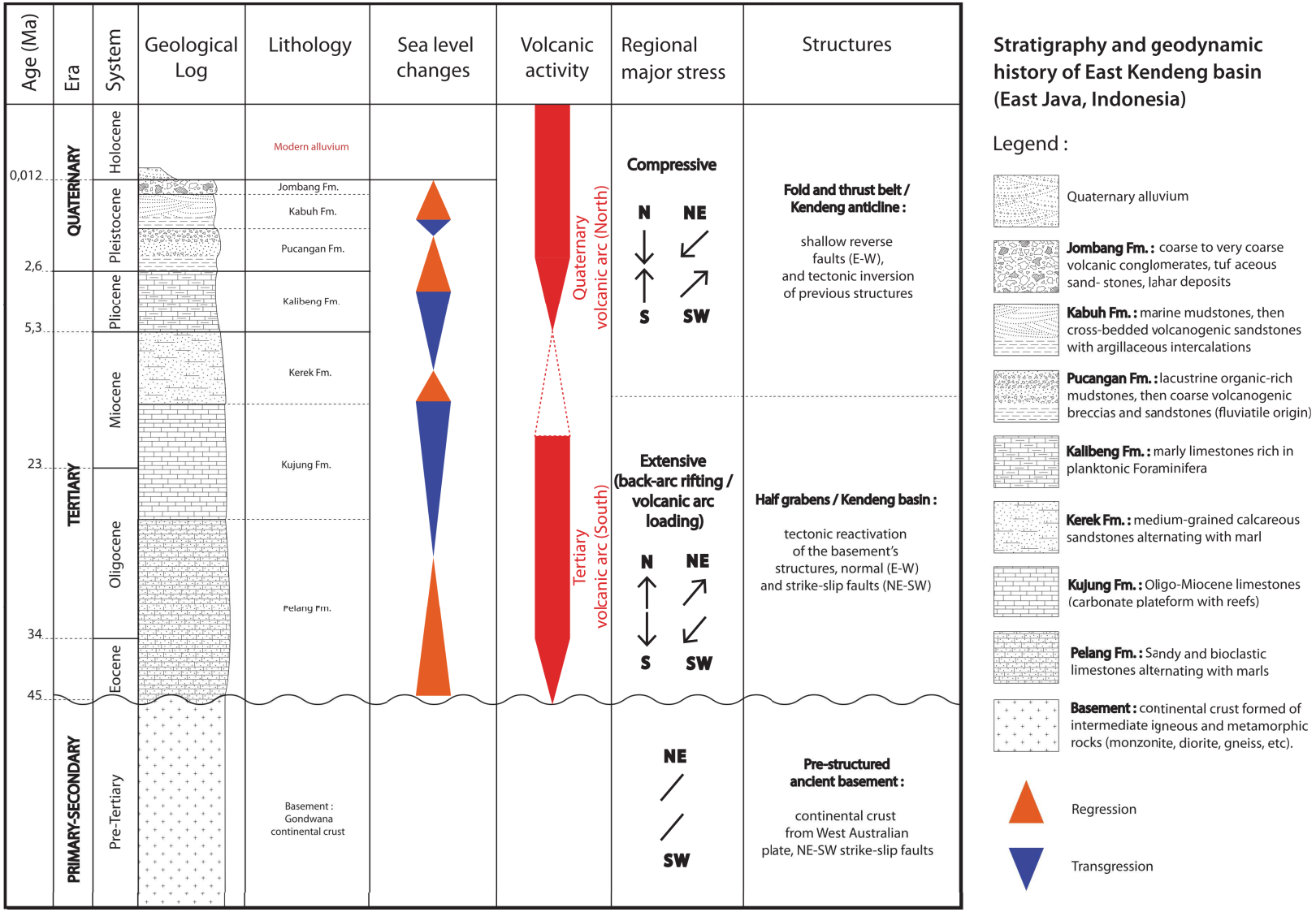

Figure 1. 5. Synthesis schema of the geological, paleoenvironmental and geodynamic features of the East Kendeng basin of the Pasuruan region.

1.2.2.3 Present day

In Java, there is limited evidence of active faults, mostly because the humid climatic system triggers intense erosion and the presence of eruptive products which cover the surface expressions of active faulting. However, several field tectonics studies provide some structural insights.

The present-day major structures of East Java are represented by normal faults (E-W) and strike-slip faults (NE-SW) inherited from pre-existing geodynamic contexts (Marliyani, 2016; Simandjuntak, 1993; Susilohadi, 1995). The deepest faults are those that have been reactivated from the basement (De Genevraye and Samuel, 1972). Java is one of the most active subduction zones worldwide: archives show that seismic events may occur not only along the dipping slab but also onshore, which demonstrate the continuing tectonic activity on Java. Indeed, the displacement caused by the subduction is compensated by the slab as well as the overriding plate (Koulali et al., 2016).

In the Kendeng zone, the East-West trending fold-and-thrust belt formed during the Plio-Pleistocene compression is still active in some segments, as well as numerous strike-slip faults (Koulali et al., 2016; Marliyani et al., 2019): for example, the Watukosek fault system, which was at the origin of the Lusi mud volcano eruption in May 2006, is a NE-SW sinistral strike-slip fault following the alignment of several volcanic edifices (Moscariello et al., 2018).

In the Eastern part of Pasuruan, Marliyani et al., (2019) have identified an active fault. This fault is a high-angle normal fault with prominent youthful scarps cutting Pleistocene deltaic sediments (mostly gravelly tuffaceous sandstone). It can be traced over a distance of 13 km, along which the southern block is downfaulted in relation to the northern block, with an offset of approximately 50 m. Geological field investigations have demonstrated the recent activity of this fault, associated with at least 6 seismic events during the last 4000 years: the more recent event was in November 1852, with an estimated magnitude of 6.6 on Richter's scale.

Mazzini et al., (2017) present the following stratigraphic log in the region of the Lusi mud volcano located about 20 km northwest of Pasuruan:

- Holocene composed of shallow alluvial sediments (300 m thick).
- Pleistocene alternating sandstones and shales of the Pucangan formation, (600 m).
- Pleistocene bluish grey clay of the Upper Kalibeng formation (1300 m).
- Plio-Pleistocene volcaniclastics (1 000 m); Oligocene-Miocene carbonates belonging to the Kujung sequence (probably more than 900 m).
- Eocene organic-rich shale rock (more than 800 m).

To summarize, Pasuruan is located on the southern flank of the Kendeng anticline basin. This region corresponds to back-arc region of the Java subduction system in the immediate vicinity of the present-day volcanic arc represented by the Bromo-Tengger-Semeru volcanic complex. This region is impacted by local subsidence and fault systems. The Pasuruan basin may correspond to a N-S graben structure infilled by about 300 m of recent alluvial deposits and probably bounded to the North by the only active normal E-W fault system identified in the basin.

1.2.3 Bromo-Tengger complex

1.2.3.1 Geological and morphological history

The Bromo-Tengger volcano is included in the Semeru-Tengger volcanic complex which comprises a cluster of calderas and strato-cones mainly aligned from North to South (**Figure 1. 6. a**) over an area of more than 2 000 km². The Bromo-Tengger massif is a "young" composite/stratovolcano (~1.4 Ma) whose summit was situated at 4 500 m.a.s.l during the paroxysmal building stage (Van Gerven and Pichler, 1995). Nowadays, the northern flank spreads towards the Madura strait and leads to a horseshoe-shaped rift zone. According to this latter author, the volcanic edifice was built up from 4 main eruptive centres over the last 1.4 Ma (**Figure 1. 6. b**); these centres are named (I.) Nongkojajar, (II.) Ngadisari, (III.) Cemorrolawang, and (IV) Tengger.

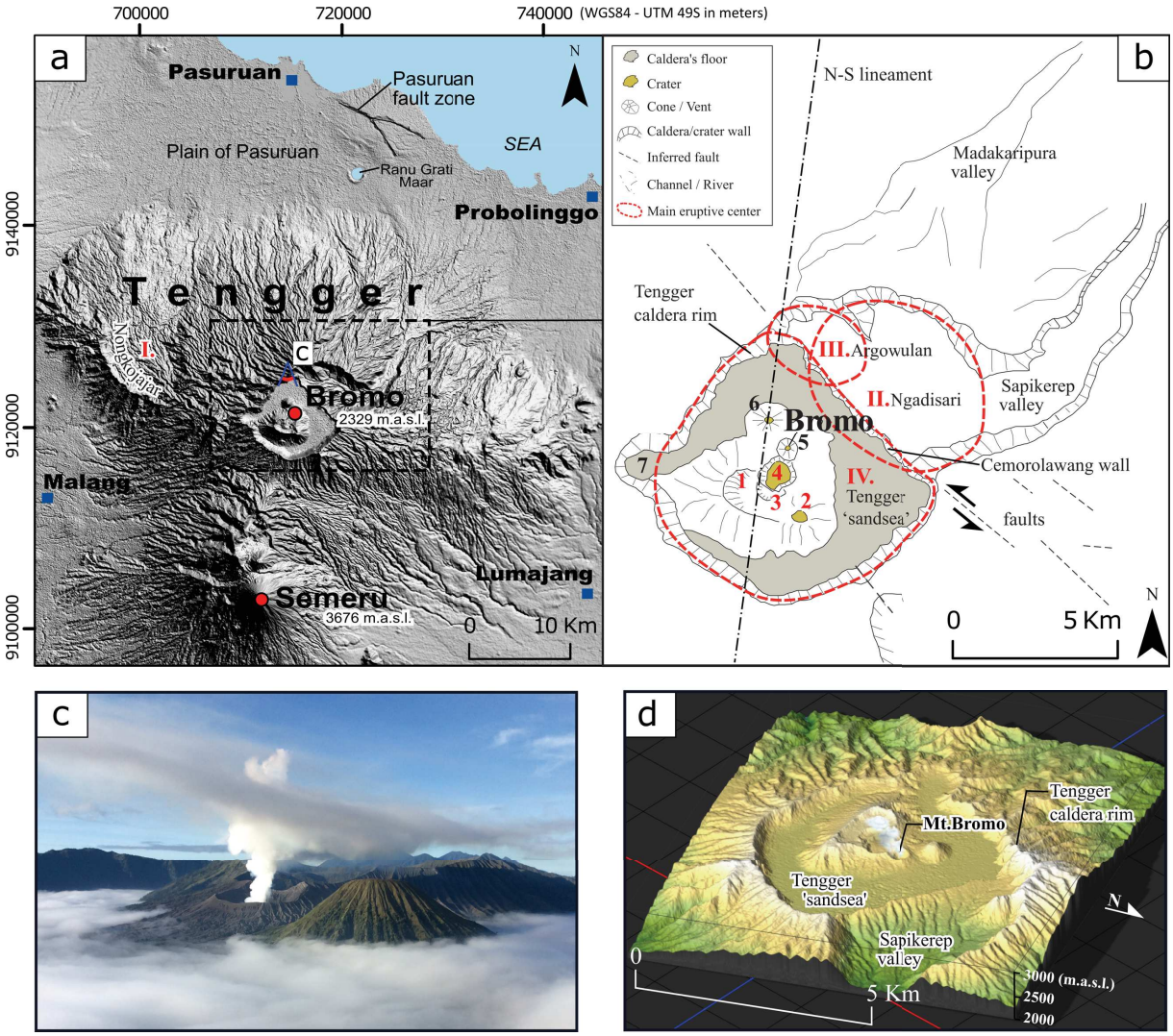

Figure 1. 6. a. Hillshade map of the Bromo-Tengger-Semeru volcanic complex. **b.** Main notable structures and eruptive centres of Bromo-Tengger (modified after Solikhin, (2017)). **c.** The Tengger caldera, seen from Mt Penanjakan at 2 700 m.a.s.l.; Mt Bromo seen on the left, currently active. **d.** 3D map of the Tengger caldera zone created with the digital elevation model STRM30m developed by the USGS.

The northern flank was initially considered by Van Bemmelen, (1949), as:

- a slippage zone inducing a "growing rift", with a vast structure of 25 km lateral amplitude corresponding to the area of the slide;
- a northwest slipped block, an anticlinorium affecting Pliocene-Pleistocene marine lands corresponding to the frontal area of the slide.

However, (Mulyadi, 1992), showed that this "growing rift" was as polygenetic structure corresponding to a curved alignment of eruptive centres that have been active over time.

Based on the radiometric dating of rocks (K/Ar), the chronology of the major eruptive events and collapse can be described as follows (**Figure 1. 7**):

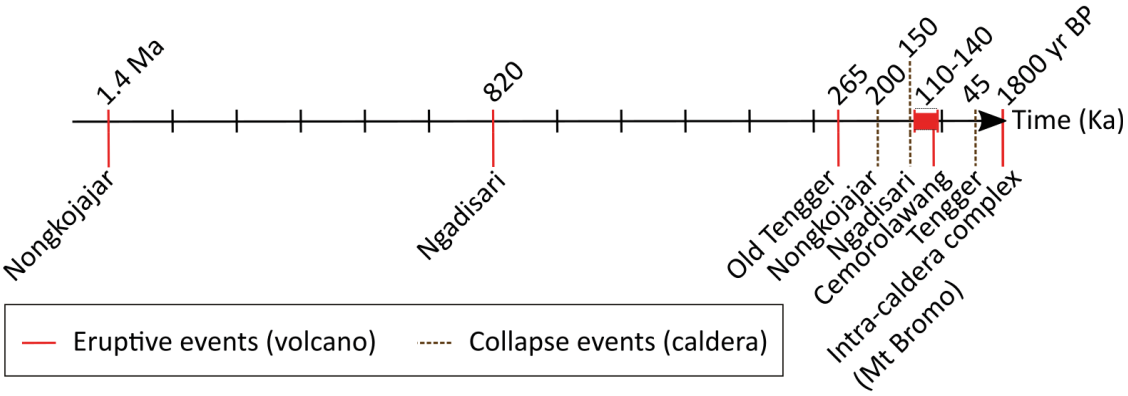

Figure 1. 7. Simplified geochronology of the major eruptive and collapse events.

The building phase is mainly related to the volcanoes (in chronological order) of Nongkojajar, Ngadisari, old Tengger, the Cemorolawang strato-cone and the intra-caldera complex of Tengger, while the dismantlement phase is represented by weathering/erosion processes and the caldera-collapse of the previous eruptive centres.

The most recent stage of volcanic activity is characterized by the intra-caldera activity of Tengger at six eruptive vents, which started prior to about 1 800 yrs BP. These vents, which become younger from North to South, are illustrated in **Figure 1. 6. b**, and show phreatomagmatic-andesitic tuff cones/rings: (1) Widodaren, (2) Kursi, (3) Segarawedi Kidul, (4) Segarawedi Lor, (5) Bromo and (6) the Strombolian-basaltic cone of Batok. Parasitic cones are located to the Southwest inside the Tengger caldera, (7) Mount Ijo and another cone outside the Caldera named "Mount Keciri". The last active crater is now displaying magmatic degassing through Mount Bromo, which is in a solfatoric and fumarolic stage (**Figure 1. 6**. **d**; **Figure 1. 8**).

According to Van Gerven and Pichler, (1995) and Zaennundin, (1990), it is possible to summarize the genesis of the Bromo-Tengger volcanic massif in terms of two main units which comprise three main calderas (Ngadisari, Tengger and Argowulan/Cemorolawang):

(1) the pre-caldera formation: exposed in the steep Tengger caldera wall, which is up to 650 m high (Mt Penanjdakan), while the straight wall of Cemorolawang in the Northeast caldera is the lowest part, with an elevation of only 100 m above the caldera floor;
(2) the post-caldera formations: represented by the Tengger intra-caldera complex.

The current Tengger caldera (**Figure 1. 6**. **a, b**) culminates at more than 2 750 m above sea level (Mt Penanjakan), and the inner caldera floor (Sand sea) is at around 2 100 m.a.s.l. The caldera has a roughly circular shape with a width of 10 km from east to west and 9 km from north to south; it is truncated in the northeast part by the Cemorolawang wall. The latter feature continues towards the North-East through the valley of Sapikerep, which is related to the collapse of an ancient volcanic edifice (Kundi-Baruklinting-Sapikerep).

1.2.3.2 Recent eruptive history and hazards

Mount Bromo is the last relic of the intense volcanic activity of the Bromo-Tengger edifice in the past, involving eruptions that were alternatively explosive and effusive. With a crater of about 800 m in diameter and more than 100 m depth, Mount Bromo has erupted at least 50 times since 1775 (mainly VEI = 2), with an estimated frequency of about one eruption every 6 - 7 years (Kumalasari et al., 2017; Zaennudin, 2010). The last major eruptions occurred in 2004, 2010-2011, 2016 and 2019, dominated by ash explosions (brown smoke) that produced 300 to 3000 m high columns and deposits of fine-grained volcanic materials as well as volcanic bombs (**Figure 1. 8**. **b**).



Figure 1. 8. a. View of Mount Bromo during a period of quiescence (April 2018), from drone aerial photography. **b.** Mount Bromo during a period of eruptive activity (April 2019).

Since 1989, the deformation of the volcano has been monitored by a Global Positioning System (GPS) and Electronic Distance Measurement (EDM). Complementary monitoring with camera and seismometer has been installed since the years 2000, allowing a continuous surveillance of volcanic activity (CVGHM, 2010). The potential hazards from eruptions of Bromo are due to ejected (glowing) rock fragments, heavy ashfalls and toxic gases (e.g. H_2S). So far, hazards due to lahars have never occurred during eruptions of Mt Bromo, and only one fact of casualty was reported in 2004 when two tourists were killed after getting too close to the active vent (Bani et al., 2013). The latest geophysical studies show that the deformation of Mt Bromo before and after eruption is relatively small, with a displacement of only about a few cm, with the pressure source being about 1 km beneath the active vent (Abidin et al., 2004). The SO_2 emission rate of Mt Bromo is estimated at 22 - 32 t d^{-1} during the declining eruptive phase, which represents a major source of volcanic degassing into the atmosphere (Bani et al., 2013). Nowadays, there is no clear evidence of hydrothermal activity within the Bromo-Tengger massif, only a few springs with yellow Sulphur deposits are observed in the vicinity of the Widodaren volcanic vent in the sea of sand caldera.

1.2.3.3 Local tectonic settings

In terms of local tectonics, there is very sparse knowledge concerning the fault system of the Bromo-Tengger volcanic massif. The major tectonic structures of East Java are normal (E-W) and strike-slip (NE-SW) faults, inherited from the subduction context (Marliyani, 2016; Susilohadi, 1995). However, Bromo-Tengger does not seem to follow the same tectonic pattern. The intra-caldera complex appears to follow a roughly North-South lineament (**Figure 1. 6. b**), aligned with Semeru in the South and the Ranu Grati maar on the North Pasuruan plain (Neumann van Padang, 1951). Some authors describe the structure as a circular-open caldera associated with normal caldera-bounding faults probably existing within the Tengger caldera (Cabusson, 2012; Cole et al., 2005). In particular, as regards the Tengger caldera, the wall of Cemorolawang on the northeast margin (**Figure 1. 6. b**) is linear, suggesting a control by NW-SE strike-slip faults (Newhall and Dzurisin, 1988). No other fault system on Bromo-Tengger is described in the literature.

1.2.4 Architecture of Bromo-Tengger deposits

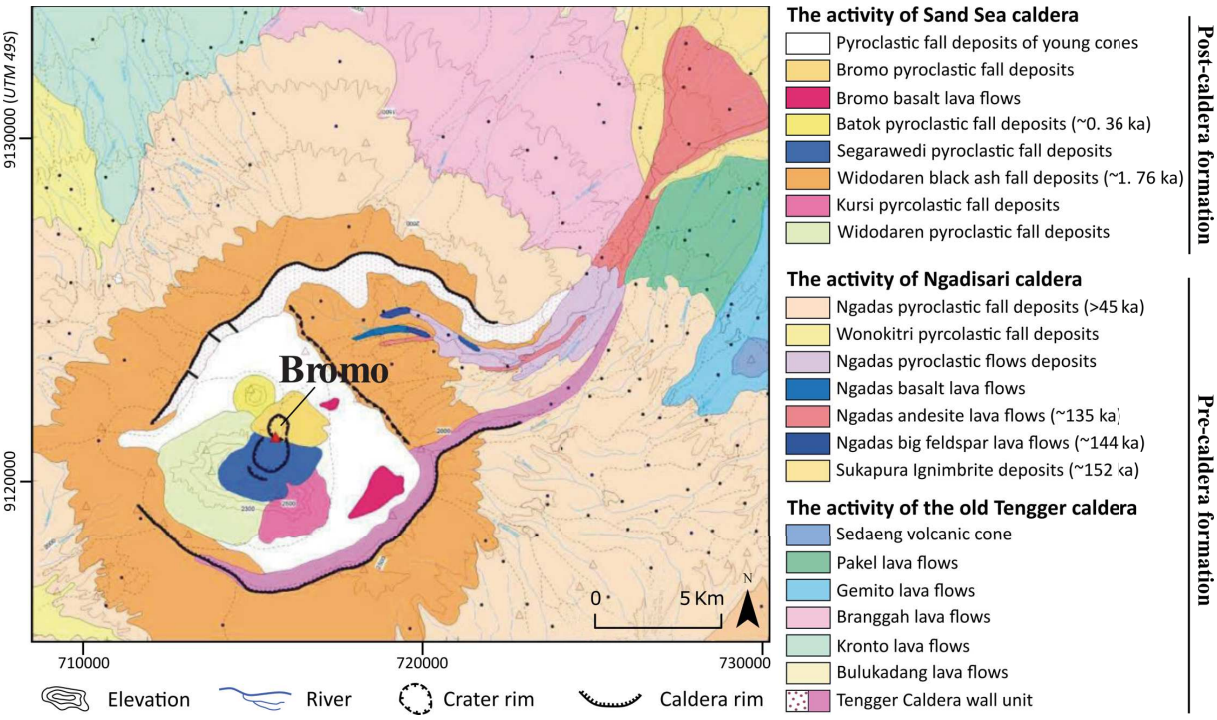

Figure 1. 9. Geological map of Bromo-Tengger complex published by CVGHM, (2010) (from Zaennudin et al., 1994).

The geological map provided by (Zaennudin et al., 1994) describes the lithological units according to three main groups related to (1) the post-caldera formations and (2) the pre-caldera formations (**Figure 1. 9**). The main lithologies described below are illustrated in **Figure 1. 10**.

1.2.4.1 Pre-caldera formations

- The old Tengger volcano produced a huge accumulation of lava flows and subordinate pyroclastic deposits (ashfalls, lapilli, pyroclastic flow) visible on the old Tengger caldera wall and probably cut by some dykes representing the framework of the central zone (Thouret, 1999). An intrusive core zone is a common feature in the central part of many volcanoes, even if not actually visible due to coverage by recent volcanic formations (Custodio, 2007). The main lava types of the pre-caldera formations are basaltic, basaltic andesite and scarce scoriaceous basalts (Van Gerven and Pichler, 1995). The lava flows are usually massive and thick (> 5-10m), fractured in some locations. Large volumes of lava flows can fill the valleys, with intense erosion sometimes leading to an inverted topography. The lava flows are classically found with interlocking autoclastic breccias, which are themselves covered by baked paleo-soils (red layers) (del Potro and Hürlimann, 2008).

- The Sakapura ignimbrite (152 ka) is partly welded in some localities and associated with the formation of the Ngadisari caldera. This formation covers a delta-shaped area extending towards the Madura strait about 31 km from the caldera and could represent

a volume of about 3.8 km^3 (Hadisantono, 1990). The distal part, near the Pasuruan coast, is often reworked into lahars or fluviatile deposits. A thickness of more than 70 m can be observed at outcrop in some valleys (between Sakapura and Patalan). According to Mulyadi, (1992), the Ranu Grati maar located on the plain of Pasuruan could cut across this ignimbrite (**Figure 1. 6. a**). Two additional formations (the Tosari and Ngadas ignimbrites) are suggested by this author as being associated with the formation of the Tengger caldera. In fact, these two latter formations are a simplification of several lithologies (tephra falls, phreatomagmatic surges, pyroclastic flows).

1.2.4.2 Post-caldera formations

- The six intra-caldera tuff cones (Widodaren, Segarawedi Kidul, Segarawedi Lor and Bromo) are landforms of essentially phreatomagmatic origin with a small proportion of magmatic products (from basaltic andesite to andesite composition). Only the Mt. Batok is composed of a Strombolian basaltic cinder cone. The main post-caldera formations outside the caldera are characterized by the Widodaren black ash-fall deposits (1.76 ka), which spread out radially from the old Tengger caldera wall. The current sand sea caldera floor is composed of a thin layer of dark brown sand (ash and lapilli-fall deposits). Ephemeral streams have largely eroded the sands, leading to runoff incision whose distal part follows a delta-like pattern. The lava flows of the post-caldera formations are vesicle-rich, dark colored rocks containing large (up to 0.5 cm) plagioclase phenocrysts (Susilohadi, 1995).

At the scale of the Bomo-Tengger massif, the volcanic activity gave rise to a large range of lavas including 6 main rock types (basalt, basalt-andesite, andesite, basaltic trachyandesite, trachyandesite and dacite), (Miftakhul Fajar and Nogroho, 2018; Mulyadi, 1992; Van Gerven and Pichler, 1995). Basaltic lava is erupted at a temperature of ca. 1200 °C and is relatively fluid, which leads to continuous degassing and effusive eruptions. The lava chemistry evolves from basalt to more acidic andesite due to magmatic fractionation and contamination by crustal materials. The decrease in temperature reduces the mobility of lava, such as observed with andesite (1100°C) or dacite (1000°C).

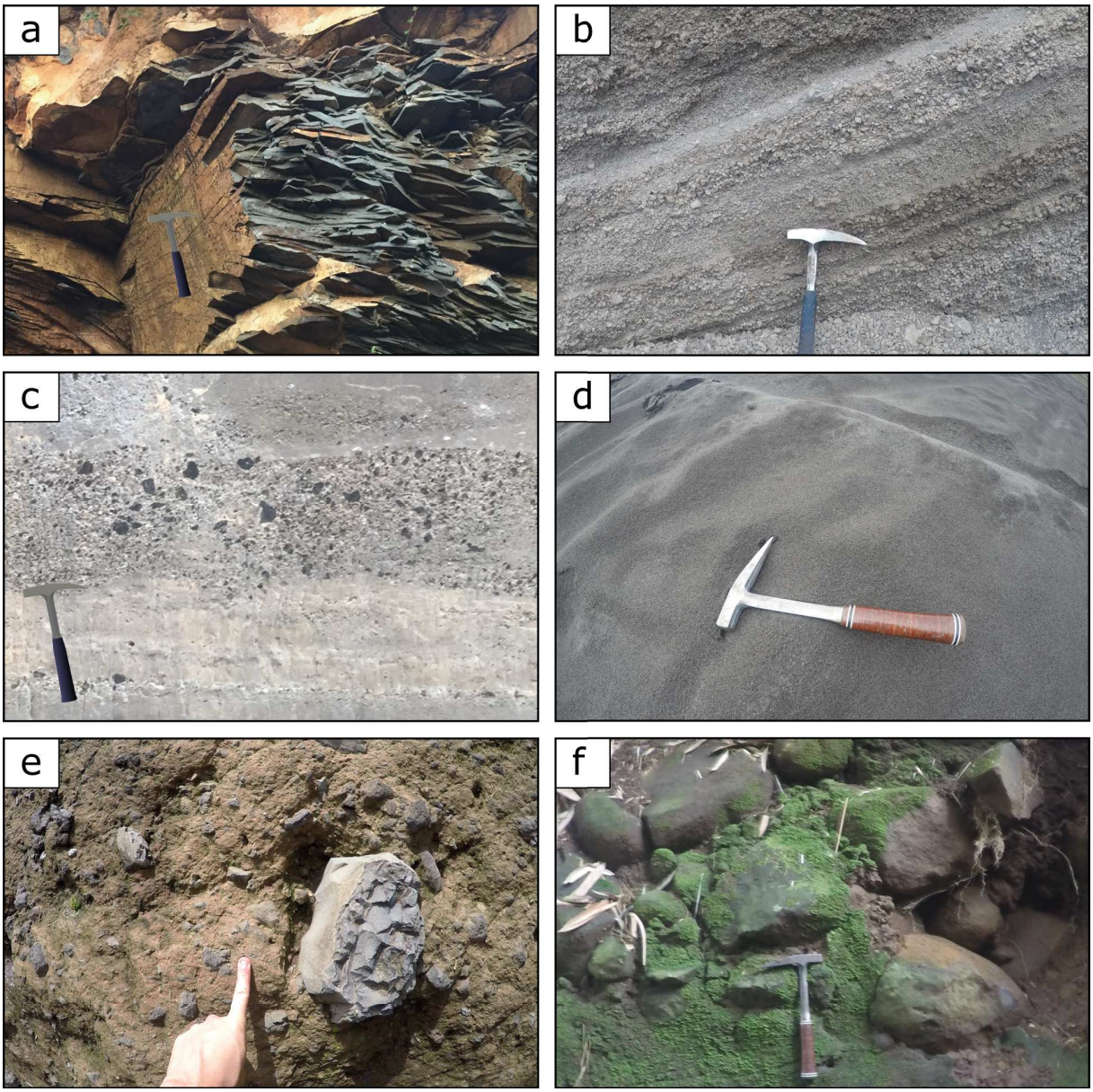

Figure 1. 10. Main lithologies described in the literature concerning Bromo Tengger, **a.** Lava flows (lamellar and fractured andesite) of the Kronto unit, **b.** Ash fall deposits of the Tengger wall unit, **c.** Ignimbrite of the Sakapura unit, **d.** Dark sand of the sand sea caldera, **e.** Lahar deposits of the Madakaripura valley, **f.** Recent alluvial deposits in the Sapikerep valley. The location name refers to the maps in **Figure 1. 6**.

1.2.4.3 Geological conceptual model of andesitic stratovolcano

Based on the eastern flank of Merapi, a conceptual model for the architecture of an andesitic stratovolcano has been recently proposed by Selles et al., (2015) (see **Figure 1. 11**).

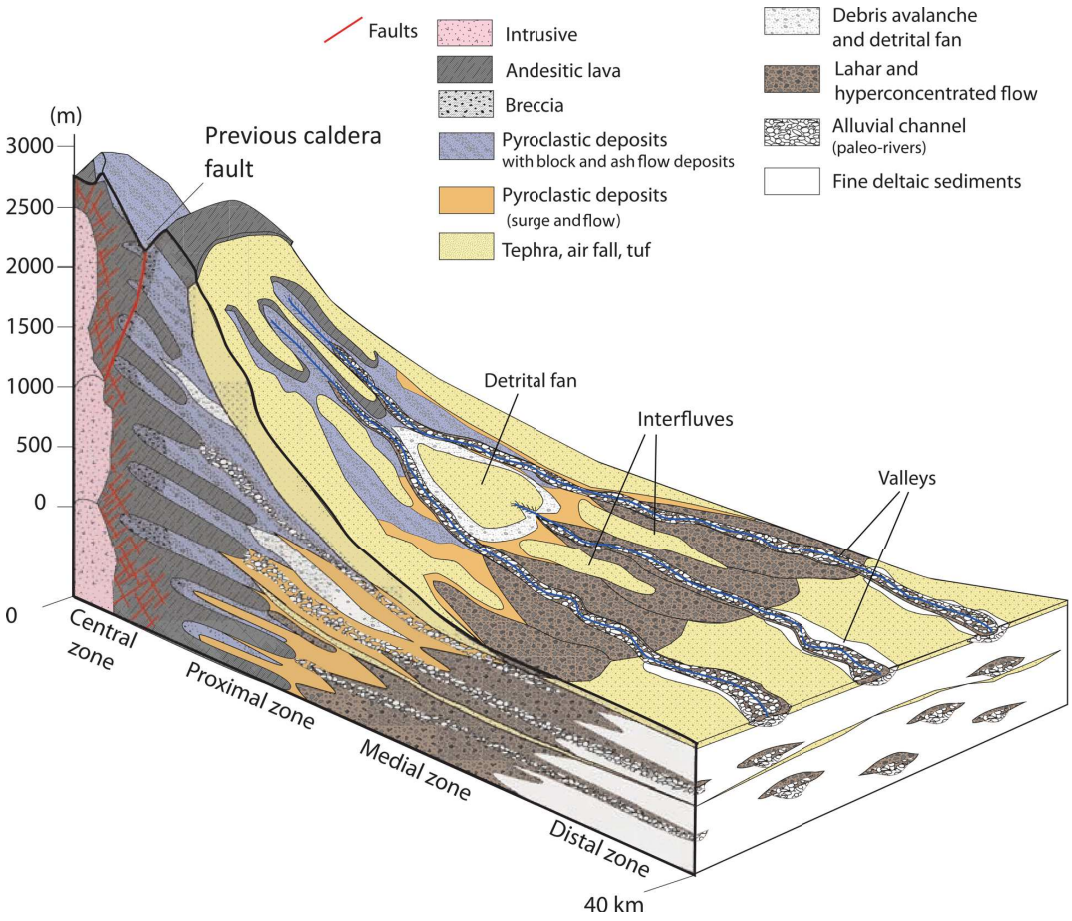

Figure 1. 11. Conceptual model of the distribution of volcanoclastic facies associated with andesitic stratovolcanoes, as adapted for the eastern flank of Merapi volcano. The proximal to distal variation and the lateral distribution of facies depend on the dynamics of valleys and interfluves (Selles et al., 2015).

The facies distribution around the volcano is divided into four main parts according to elevation, corresponding to (1) central zone, (2) proximal zone, (3) medial zone and (4) distal zone:

1) The central zone is mainly composed of lava flows intercalated with auto-breccias, surrounding a core zone characterized by a dyke network or other intrusive body. The block and ash formations spread away close to the vent. Subsequent lava flows may spread over pre-existing formations and lead to "baking" of the underlying material which then usually acquires a reddish color (rubefaction). This red layer is known as a baked paleo-soil or bole formation (Naud, 1971; Singhal and Gupta, 2010).

2) The lava flow units progressively disappear as the pyroclastic deposits (surge and flow, tephra, airfall, tuff) become thicker. Due to intense erosion, relief inversion of the massive lava flows is a common geomorphological feature. The drainage network starts to incise the upper slopes, which favors the accumulation of lahars and alluvial deposits (paleo-channels) as well as pyroclastic flows. Instability of the slope combined with

meteoric/fluvial infiltration can trigger large-scale slumping and landslides, such as debris avalanches associated with detrital fans. These landforms may be at the origin of a drainage anomaly inducing modifications of the surface and groundwater flow systems (Join et al., 2005);

3) The decrease of the slope in the medial zone favors the accumulation of low-energy deposits, with lahars in the more distal part corresponding to detrital fans farther upstream. Because of the gentle slope, the most distal voluminous blocks are usually accumulated in this zone. However, because of the torrential flow of streams in a tropical climate, sand, boulders, gravel and andesitic lava blocks of metric to decametric size may be transported as far as 20 km from the summit;

4) The downstream part of the volcano is represented by a plain in the coastal area with an accumulation of inter-eruption deposits characterized by coarse-fine and partly stratified sediments provided by the dismantling of volcanic formations. Locally, some lava blocks can be observed in river beds and are controlled by the migration of river channels (paleo-channels). The plain is built up by fluvial clastic supply as well as by syn-eruption aerial deposits (e.g. ashfalls) if the volcano is still active.

Both constructive (eruptions) and destructive (erosion) processes operate simultaneously during the active life of the volcano, after which destructive agents alone control the geomorphological evolution (Pryet, 2011). For instance, chemical weathering and hydrolysis of the lava flows result in the formation of erodible soils and thick clay-rich saprolites. At the outcrop, "onion skin" weathering of lava boulders is usually visible, in common with saprolites found in granitic contexts (Dewandel et al., 2017). In warm tropical climates, late-stage weathering eventually produces a lateric or bauxitic cover with iron oxy-hydroxides and kaolinite-illite rich soils (Weijden and Pacheco, 2003). Erosion and weathering processes may occur even during the upbuilding of the volcano, creating paleo-channels extending from the proximal to the distal zone.

Despite the very detailed geological conceptual model proposed by Selles et al., (2015), the architecture of Bromo-Tengger appears rather different since lava flows extend as far as the Pasuruan plain in the distal zone, corresponding to the first relief on the volcano flanks. It is unclear how to define the transition zone between these lava flows and the volcano-sedimentary formations of the distal zone. This question concerning the scope of the field investigations is addressed in chapter 2 of this thesis.

1.3 Hydrogeological context

1.3.1 Volcanic islands

Volcanic activity at the origin of islands can be divided into three broad classes: (1) hot-spot volcanism (e.g. Hawaiian and Canary islands or La Réunion island), (2) divergent plate boundary volcanism (e.g. Iceland, Azores and submarine mid-ocean ridge) and (3) island-arc volcanism (e.g. Java or Japan islands) (Custodio, 2007). Most volcanic islands consist of a large pile of submarine volcanics, capped by subaerial effusive formations; they can be summarized into two types (Singhal and Gupta, 2010):

- oceanic islands, with rocks mainly of basaltic composition (e.g. Hawaii and French Polynesia);
- island-arc, with rocks mainly of andesitic composition (e.g. Indonesia and Guadeloupe).

Erupted from one or several shield volcanoes, basaltic volcanic islands are the visible part of larger massifs built up several kilometres above the deep ocean floor (Pryet, 2011). Depending on their viscosity, lava flows are classified into two types (1) pahoehoe (ropy) and (2) aa (blocky/clinker), terms derived from the Hawaiian language. Basaltic lavas with low viscosity give rise to flows covering an extensive area (Walker, 1971). In contrast to basaltic volcanism, the more viscous andesitic lavas related to island-arc settings do not usually extend over wide areas. Andesitic volcanism results in large and thick formations along long strips, often making up steep-sided bulbous domes and stratovolcanoes (e.g. Japan and Indonesia). Andesitic-type formations, predominantly generated by explosive activity, generally show a wider range of lithological variety, giving rise to a very high spatial and vertical variability of the structure and hydrodynamic properties of the aquifers (Charlier et al., 2011). Andesitic islands in subduction zones are much less well known, but useful knowledge can be derived from other volcanoes in continental or oceanic settings, considering that many volcanic hydrogeological concepts remain valid in such contexts. Among these concepts, a common feature of volcanic islands is the multi-phase volcanic activity involving a succession of constructive events (effusive and/or explosive) and destructive events (caldera collapse, landslides, weathering), which accounts for their complex internal structure. On all volcanic islands, groundwaters may occur in aquifers under either perched, unconfined or confined conditions.

In spite of common processes at their origin, each volcanic island has its own geological history and climatic regime, which strongly influence its specific hydrogeological setting.

1.3.2 Hydrogeological features of volcanic rocks

From a hydrogeological point of view, volcanic rocks mostly represent a heterogeneous and anisotropic environment (Custodio, 2007). This environment can be considered as a simultaneously porous and fractured medium reflecting the massive lithology (e.g. lava flows), separated by a network of conductive features such as fractures or interflow sediments. In some configurations, volcanics are considered as a continuous, anisotropic medium with relatively high porosity.

The primary porosity and permeability depend on the rate of cooling, viscosity of the magma and degassing during cooling. Because of the higher viscosity compared to basaltic lavas, acidic volcanic rocks usually do not extend over wide areas but are instead mostly represented by large and thick formations occurring in long strips, which induces a lower porosity and permeability.

According to Singhal and Gupta, (2010), porosity and permeability in volcanic rocks are imparted by voids that may be associated with (a) scoriae, (b) autoclastic breccia zones between lava flows, (c) cavities between fluid lava flows, (d) shrinkage cracks, parallel to the flow surfaces or columnar joints, (e) gas vesicles, (f) lava tubes, and (g) fractures and lineaments. The hydrogeological settings of the main volcanic units are summarized below.

1.3.2.1 Lava flows

The lava flow type, (1) pahoehoe and (2) aa, and the arrangement of pore spaces govern the hydrogeological characteristics.

(1) The vertical and horizontal joints (lamellar in **Figure 1. 10. a** or columnar) associated with voids within the autoclastic breccia impart initial high porosity and permeability to recent pahoehoe lavas (Mathers and Zalasiewicz, 1994). The existence of lava tube and gas vesicles may enhance the hydrogeological properties.

(2) In aa lava flows, the high initial permeability is mainly related to clinker zones located at the top and bottom of the flow. This clinker zone (or autoclastic breccia) is analogous to the intergranular porosity of coarse gravel, while the central massive core of aa flows is characterized by a low permeability and porosity under unfractured conditions.

The nature of the lava flow interlayers (e.g. sediment or scoria), is an important factor in controlling the hydraulic properties. “Widespread beds of weakly weathered clinker contribute to increase horizontal permeability while the occurrence of unconformities such as impervious baked-soils, weakly fractured massive lava flows, lahar or welded tuff present a barrier to the vertical permeability” (Pryet, 2011). With these configurations, relatively high anisotropy ratios may occur in lava flow sequences. For instance, in the Gran Canaria, Spain, the anisotropy K_h/K_v is reported to be between 20 and 100 (Custodio, 1985).

1.3.2.2 Cooked paleo-soil (red bole)

This formation results from the heating a pre-existing soil layer by an overlying lava flow. This type of alteration is due to thermal or chemical processes, and gives rise to a reddish coloration (sometimes green) and a very low permeability similar to baked clay (Inamdar and Kumar, 1994). Being rich in clay, this unit may lead to the development of perched aquifers in the unsaturated zone, with many "under lava springs" located at the foot of cliffs, in the interface between the porous autoclastic breccia and the red baked paleo-soil. It also serves as a confining or semi-confining layer in another context (Hunt, 1996; Nichols et al., 1996). A widespread extent of this impermeable layer may contribute to constraining the groundwater flow direction, particularly where lava flows are associated with ancient paleo-valleys. If the red layers are fractured, the infiltration may occur deeper or form a local aquifer of low transmissivity (Versey and Singh, 1983).

1.3.2.3 Dykes and sills

Intrusive igneous bodies within the volcanic massif are classically defined as "dykes" in the case of vertical or steeply dipping bodies or as "sills" if they are nearly horizontal tabular bodies. A high-density dyke network is commonly located near the eruptive centre (volcanic core), while sills usually follow the bedding of enclosing sedimentary rocks or lava flows. Massive and unweathered dykes may act as vertical barriers for lateral groundwater flow, forming compartments of water bodies (dyke-impounded aquifers) such as in the Hawaiian Islands (Nichols et al., 1996). On the other hand, if fractures are well developed within the adjacent country rocks and the dyke (or sill) itself, this may result in a good permeability forming a potential source of groundwater (Izquierdo, 2011; Matter et al., 2006).

1.3.2.4 Pyroclastic deposits

Eruptive explosions commonly generate a large diversity of juvenile lithic elements (pyroclasts) thrown into the air and transported to the surface. For simplification, this term refers to all pyroclasts varying in size from coarse blocks to fine dust (ash), including ash, cinder, scoria, clinker, lapilli, larger blocks as well as reworked pyroclasts. The permeability of pyroclastic deposits depends on the degree of consolidation and welding. These formations may be deposited as loosely consolidated cooled fragments (usually permeable) or formed at high temperature by the fusion of rock fragments (e.g. welded tuffs) characterized mostly by a very low permeability (Dominguez, 2017). Despite a relatively good porosity, the fined-grained nature of ash layers induces mostly a low permeability. The unconsolidated reworked pyroclastic deposits (volcano-sedimentary deposits) show a higher conductivity such as in coastal areas of Indonesia (Singhal and Gupta, 2010). However, the hydrogeological settings of these volcano-sedimentary formations are very poorly defined in the literature.

1.3.2.5 Ignimbrite

Particularly in the context of andesitic-type volcanism, explosive events may trigger gravity-driven mass flows commonly named pyroclastic flows (Takahashi and Tsujimoto, 2000). An ignimbrite can be defined as a combination of successive pyroclastic deposits (fall, surge and flow) composed of several flow units. Ignimbrites may be intensively or partly welded due to the high temperatures during deposition, or remain more or less loose, with abundant vitreous particulate material (Custodio, 2007). The low primary permeability of dense welded ignimbrites may act as an impervious barrier for groundwater flow. However, in the same way as with massive lava flows or dykes, a dense fracture network in ignimbrite deposits may produce an aquifer formation such as observed in the Merapi volcano (Selles, 2014) or near Sibolangit in Sumatra where several dozens of springs (~500 L s^{-1}) emerge from fissures (de Roever, 1966).

1.3.2.6 Lahars (landslide deposits)

Erosion, earthquakes and uplift associated with heavy rainfall are at the origin of large landslides that deeply affect volcanic formations. Landslides may be accompanied by lahar deposits (mudflows) mainly composed of clay-rich and polygenic blocks constituting an impervious layer.

The volcanic units discussed above show a high variability of hydrogeological settings. In addition, fault systems may affect the volcanic layers at the regional scale. Normal faults are related to the extensional regime of the back-arc basin or result from the collapse of the volcano's flank. These faults may act as preferential drainage for groundwater and play a hydrogeological key role through their isotropic effect on the regional permeability (Caine et al., 1996).

In contrast, hydrothermal activity progressively fills the pre-existing fissures and pores with secondary minerals (zeolite, calcite, secondary silica) and imparts a very low permeability in the vicinity of the eruptive center (R et al., 2012). For instance, on La Réunion island, the formation of zeolite in the pores of basalt greatly decreases the rock's porosity (Join, 1991). Weathering processes may also dramatically reduce permeability. Clay minerals are the result of intense weathering, such as in the case of saprolites (described in section 1.2.4), or the chemical alteration of ashes. Based on field surveys in volcanic contexts (gas-permeameter and pumping tests), it has been demonstrated than both hydrothermal activity and weathering processes induce a reduction of the porosity and permeability with time and depth (Cruz, 2003; Folio, 2001; A. Pryet et al., 2012). This is due to the clogging of fractures and voids at depth where hydrothermalism and lithostatic pressure increase. Rock weathering may become conspicuous in a few years in humid tropical climates, especially for calc-alkaline rocks (Custodio, 2007).

The conventional methods for pumping tests in isotropic and homogeneous media are generally applied to volcanic rocks (Jacob, Theis and Hantush methods) and provide reasonable results. Hydrodynamic properties are particularly scale dependent in volcanic contexts. Depending on the scale considered, the permeability may vary over 9 orders of magnitude.

Several examples of the hydraulic conductivity in andesitic and basaltic type volcanic contexts are summarized in **Figure 1. 12**.

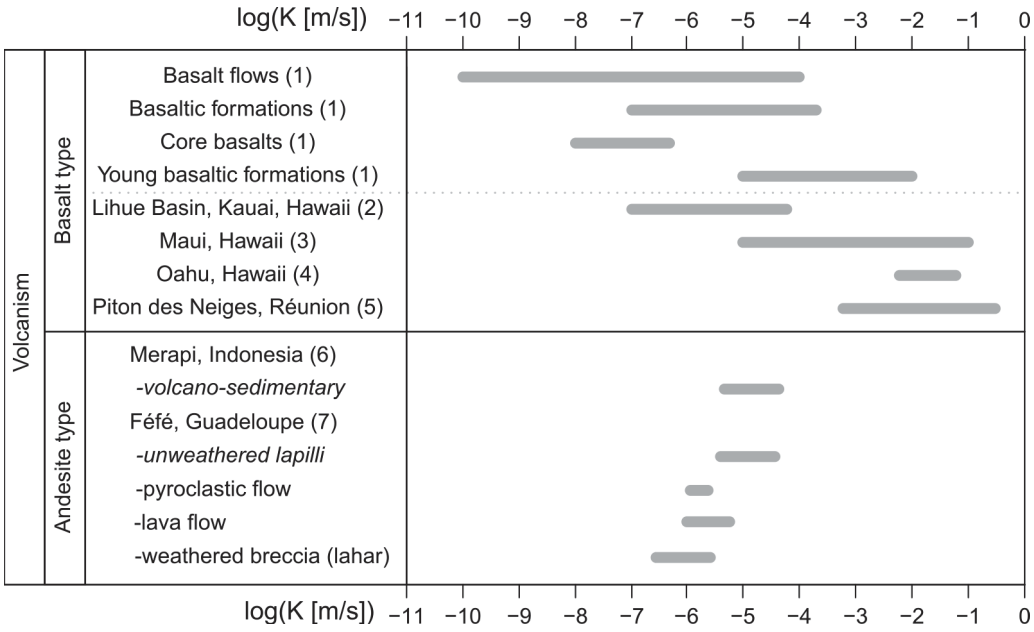

Figure 1. 12. Review of hydraulic conductivities reported in basaltic and andesitic contexts (modified after Pryet, (2011)). (1) from a review of undifferentiated basaltic contexts by Custodio, (2007), other examples from pumping tests performed in insular volcanic contexts: (2) Gingerich, (1999), (3) Rotzoll et al. (2007), (4) Hunt, (1996), (5) Join, (1991) supplemented by (6) Selles, (2014) and (7) Charlier et al. (2011) in andesitic contexts.

1.3.3 Recharge processes

Recharge is the hydrological process whereby water moves downward from the surface to an aquifer. In volcanic environments, the recharge is mainly influenced by:

1) The climatic conditions: the amount of precipitation can be extremely heterogeneous both in space and time, especially in a tropical context. In such a context, the distribution of precipitation is affected by large discrepancies between the wet and windward side and the more arid leeward side (Pryet, 2011). Tropical islands with relative high temperatures and exposed to persistent trade winds show seasonal effects as well as orographic effects. The latter are commonly observed on the wet windward side through an increase in precipitation according to the elevation.
   In addition, the occurrence of fog may increase the effective precipitation due to cloud-water interception. The “fog drip” from the vegetation may be consider as an additional source of recharge such as in Hawaii (Scholl et al., 2002), the Canary Islands (Ritter et al., 2008) and Indonesia (Toulier et al., 2019).

2) Soil properties: recharge in older volcanic rocks (> 2 Ma) is generally low because of the high run-off related to low-permeability layers that are mostly weathered. The

unconsolidated and porous pyroclastic materials usually covering the volcano summit may favour infiltration, while run-off may dominate on massive unfractured lava flows.

3) Land cover: the existence of dense vegetation may favor water interception, storing water in the canopy (soil moisture storage) or releasing it via evapotranspiration. The root network may also lead to deeper infiltration and a decreased erosion rate.

4) Geomorphology: in young permeable volcanic rocks associated with steep and elongated watersheds, the infiltration can be very intense such as observed in Hawaii where the streams are mostly of seasonal flash-flood type (Peterson, 1972).

The amount of groundwater recharge is the total volume of rainfall and fog drip minus the actual evapotranspiration and runoff. Indeed, this assumes that hydraulic properties, slope and the thickness of soils control the groundwater recharge, which mainly occurs through the rock matrix in a volcanic context (Custodio, 2007). There are numerous methods to assess the groundwater recharge such as an empirical approach using the water budget (Thornthwaite, 1948), remote sensing (e.g. TRMM or GLEAM satellite data), hydrological monitoring (lysimeter) or physically-based models (Herrera and Custodio, 2014).
In volcanic contexts, the water budget results indicate a groundwater recharge that ranges from 0 to 64% of incident precipitation in Hawaii (Izuka et al., 2010), about 59% at Féfé in Guadeloupe (Charlier et al., 2011) and from about 33% to 45% at Merapi, in Indonesia (Selles, 2014). These results seems to suggest that, in a volcanic and tropical context, the recharge rate is generally high, typically ranging between 10 and 50% of incipient precipitation on a regional scale according to Gingerich and Oki (2000).

1.3.4 Groundwater occurrence

Groundwater in volcanic rocks occurs under perched, unconfined and confined conditions. On volcanic islands, a basal aquifer is typically observed which corresponds to “the main water table below which all permeable rocks are saturated” (Stearns et al., 1930) or can be defined as a lens-shaped water body floating on saltwater with a flat water table related to the Ghyben-Hertzberg principle (Join et al., 2016). High-level aquifers are also observed in relation to dyke-impounded groundwater or perched aquifers that may be detected from the outflow of high-elevation springs. The term “perched aquifer” is defined as a saturated perched layer formed when the vertical percolation flux is impounded by an impervious formation such as sills, ash beds, baked paleo-soils or massive lava flows (Hinds et al., 1999; Singhal and Gupta, 2010). Groundwater may be stored and flow sub-horizontally within relatively permeable units (e.g. within an autoclastic breccia covering a baked paleo-soil). Perched aquifers may remain buried (generally in young islands) or outcrop in deeply incised valleys.

1.3.4.1 Spring types

In a volcanic context, three main types of springs have been identified (Fetter, 1994; Selles, 2014) and are illustrated in **Figure 1. 13**:

- Type A: *Lithological contact springs* occur when erosion reveals the boundary between aquiferous layers overlying less permeable rock or aquitards (e.g. red bole layer). It is the most abundant spring type in volcanic contexts, usually represented by under-lava springs (or inter-flow springs) observed in the cliff walls of erosion canyons and cirques. This type of spring is abundant in the Coiron massif in Ardèche (France) (Naud, 1971). Join et al., (2016) distinguish these springs from emergences related to the outflow of the deep saturated zone (the basal aquifer) such as the Cascade Grand Galet on la Reunion Island (Lachassagne and Marechal, 2011). The discharge may be low (< 1 L s^{-1}) and ephemeral from perched horizons or important and perennial from basal aquifers (> 100 L s^{-1}) depending on the aquifer extent, the thickness of the saturated zone and the density of spring outflows (**Figure 1. 13. A**).

- Type B: *Depression springs* are formed when the superficial groundwater table intersects the surface topography. They are generally associated with a drainage anomaly along the volcano's flank (e.g. detrital fans from landslide events). Depending on the recharge surface and the material properties, their discharge is usually small or ephemeral (**Figure 1. 13. B**).

- Type C: *Contact fault springs (artesian springs):* Contact fault springs lie along fault lines making up a transmissive zone of preferential groundwater circulation leading to the surface. The lithological formations may be offset against each other along the fault plane, forming a barrier or a drain to groundwater movement. It may not be excluded than other intrusive bodies such as dykes could be at the origin of the artesian springs. This type of spring is perennial with an important discharge from 100 L s^{-1} to more than 1000 L s^{-1}, depending on the hydraulic head of the confined aquifer. In Indonesia, these springs may form large "pools" with artesian outflows that are visible underwater due to numerous diffuse sand boils (**Figure 1. 13. C**).

Other spring outflow configurations can be found in volcanic contexts, such as submarine springs (e.g. Pearl Harbor springs in Hawaii) or lava tube springs (e.g. Laufbalavatn lava tube in Iceland) as well as hot springs associated with geothermal activity giving rise to mud pools or geysers (e.g. Lady Knox geyser in Rotorua, New Zealand), (Detay et al., 2012; Kiernan et al., 2003; Nichols et al., 1996).

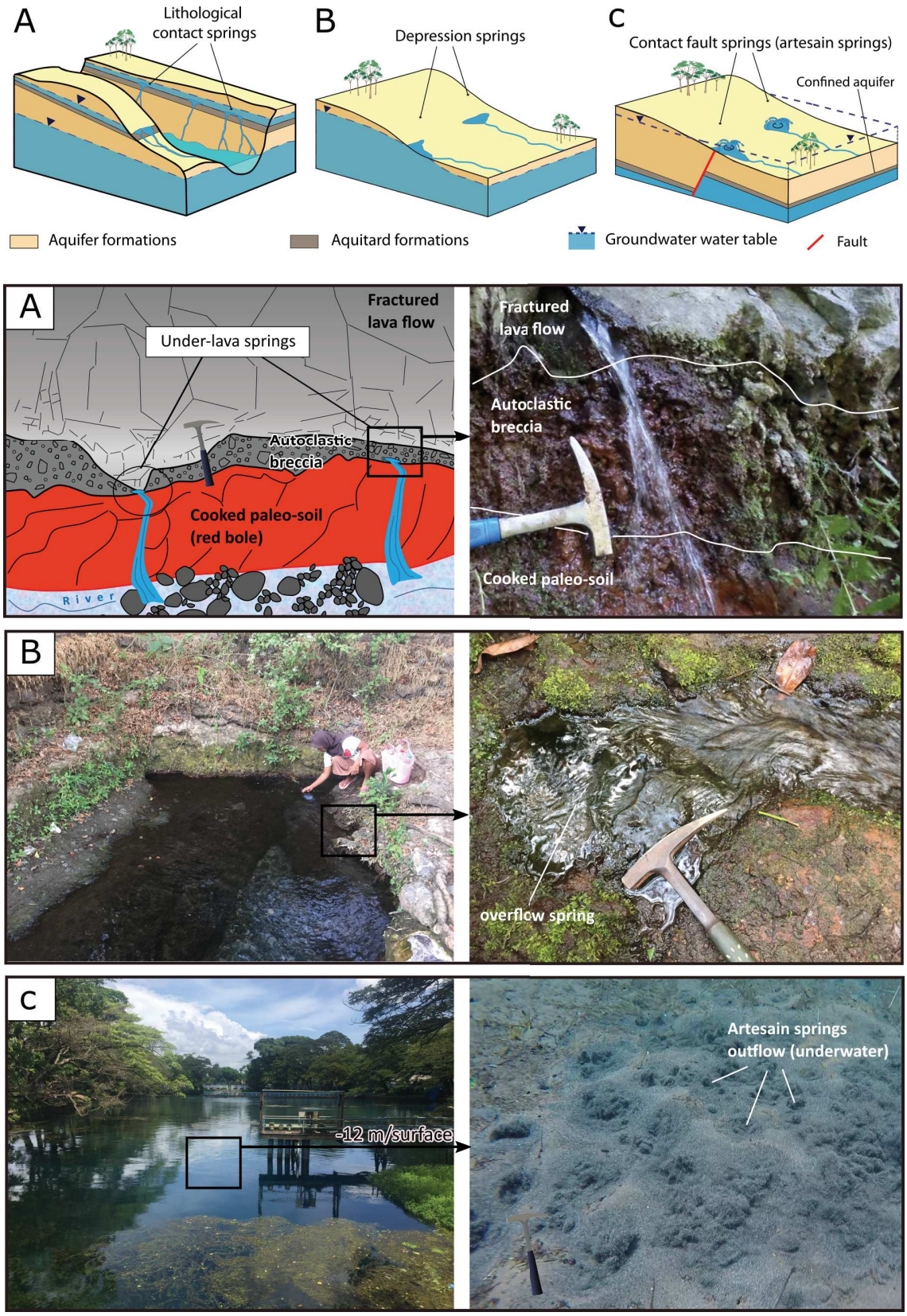

Figure 1. 13. Types of springs identified in andesitic volcanic-subduction contexts (modified from Selles, (2014)) with **A**. Lithological contact springs occur where aquifer layers overlying a less permeable formation are incised by erosion (e.g. Sumber Pitu in Malang, East Java). **B.** Depression springs occur where the groundwater table intersects the surface topography (e.g. Tirtoageng spring in Probolinggo, East Java). **C.** Contact fault springs (artesian springs) triggered by faults or intrusive bodies which can favour vertical groundwater circulation (e.g. Ranggojalu spring in Probolinggo, East Java).

1.3.5 Hydrogeological conceptual model

1.3.5.1 Basaltic type

In the literature, groundwater occurrence in volcanic basaltic islands is explained by two main hydrogeological conceptual models: the (1) Hawaiian and the (2) Canarian models (**Figure 1. 14**):

(1) A low-lying basal aquifer linked to inland dyke-impounded and perched aquifers such as on the island of Oahu in Hawaii (Nichols et al., 1996; Peterson, 1972) or the young Piton de la Fournaise (La Réunion) (Violette et al., 1997), Madeira (Prada et al., 2005) and Cape Vert (Heilweil et al., 2009). The water table shows a low hydraulic gradient as a consequence of the high permeability of the volcanic formations within which a very thick vadose zone may be developed (> 100 m thick);

(2) A continuous basal aquifer extending far inland and at rather high elevation, which is well described in the Canary Islands such as on Tenerife (Custodio, 2007), and also on Kauai (Hawaii) (Izuka and Gingerich, 2003), the old Piton des Neiges (La Réunion) (Join et al., 1997) and Easter Island (Chile) (Herrera and Custodio, 2008). The water table reaches several hundreds of metres above sea level and is marked by steep hydraulic gradients. Older volcanic formations are more likely to show this type of configuration.

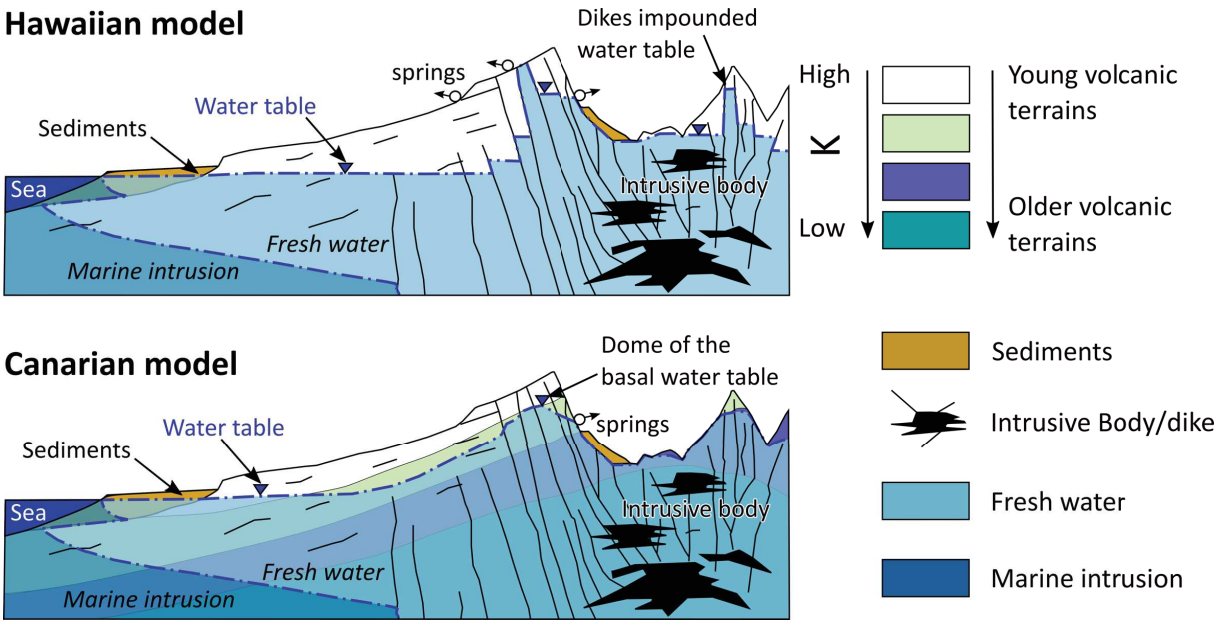

Figure 1. 14. Hydrogeological conceptual models of young oceanic volcanoes (modified from Join et al. (2016)).

In fact, the "Hawaiian" and the "Canarian" hydrogeological models do not represent two different conceptual models, since they are both based on hydrodynamics and the mode of formation of the volcano (Custodio, 2007). There is a wide range of possibilities according to the particular structure, age and state of erosion of the materials, as well as climate and

precipitation. The simple hydrogeological conceptual model of a single hot-spot intraplate volcano, whether it is an oceanic island or in a continental setting, is based on distinguishing (1) a low-permeability core, (2) a more permeable cover and (3) a transmissive apron surrounding the massif. The changes are not always sharp and transitions may be gradual and complex.

The core includes the dyke zone (even cone sheets), the older compacted volcanic formations and even the upper part of the magma chamber and the ocean floor if erosion is deep enough, and parts of the volcanic massif that have been intensely thermally and hydrothermally altered. This appears to be a common pattern, even if not visible due to recent volcanic cover. On La Palma Island, the sequence is clearly exposed in the almost 1 000-m-high wall of a large landslide affecting the centre of the northern volcano (Camacho et al., 2009). The core area may show a large collapse caldera later filled by intra-caldera recent volcanics and eroded materials as well as the corresponding extra-caldera cover. This fill may form a high-elevation aquifer if enclosed or be reduced to a recharge area if opened up by major landslides causing deep erosion, as in the case of Tenerife and Gran Canaria (Custodio et al., 2016; Marrero-Diaz et al., 2015). Core conditions can be recognized also on La Gomera, Madeira and La Réunion (Izquierdo, 2011; Join et al., 2005; Prada et al., 2005). The cover formations receives the high-altitude recharge and groundwater then flows outward to the periphery. Depending on permeability, recharge and thickness, springs and streams may or may not appear. While large springs appear on Oahu and La Reunion, and to some extent on Madeira and La Palma, they do not form in the well-recharged Tenerife aquifer due to the continuous cover of thick young volcanics. The water table may be shallow in the case of old islands (Fuerteventura) (Herrera and Custodio, 2014) or up to several hundreds of metres thick (Tenerife) (Custodio et al., 2016).

Whether or not continuous, and depending on the state of erosion and the effect of large landslides, aprons may be narrow or extensive as in the case of Honolulu in Hawaii (Nichols et al., 1996). Water-table (unconfined) aquifers are commonly developed on the apron, but may become semi-confined in lower-lying areas due to the deposition of finer sediments on the slope or supplied from the coast, even under flowing conditions. Free-flowing artesian conditions are reported in some cases such as in the Honnolulu artesian basin (Nichols et al., 1996), the Eastern basin of Merapi in Indonesia (Selles, 2014) or in the Deccan traps (Singhal, 1997). Coastal aquifers in volcano-sedimentary deposits may be an important source of water supply tapped by artesian wells, but their hydrogeological settings are very poorly studied in the literature.

This configuration (core, cover and apron) is a valid model for a single main volcano under ideal conditions. But reality is more complex since there may be more than one main volcano, either separated from each other or partially overlapping, with a wide spectrum of different cumulative structures and states of erosion, and under very different climatic conditions. According to local conditions, very different hydrogeological models can be proposed, often with numerous uncertainties due to lack of data. Some models simply judiciously apply the concept of core, cover and apron, focusing on hydrodynamics, and adapting the concept to local circumstances. This latter approach is usually favored, which makes it easier to formulate local hydrogeological models. In some cases, when the inner structure cannot be inferred, this approach allows to formulate alternative hypotheses, as for

Easter Island (Herrera and Custodio, 2008). In the case of rift-related islands, as is partially the case of the Azores, there is less knowledge of recent cover formations under a humid climate, without deep gullying. Although the number of boreholes is limited, it seems that the approach presented above is applicable, at least in part to western Sao Miguel (Cruz, 2003).

However, andesitic islands in subduction zones are much less well known, but useful knowledge can be derived from large volcanoes in continental settings, such as in the Andean Altiplano (highland) of northern Chile (Montgomery et al., 2003). Similar conditions are found along the Andes and as far as Sierra Madre in Guanajuato, Mexico (Morales et al., 2015). The core, cover and apron concept seems to account for the observations, especially in mountain-front settings between volcanoes and infilled lateral depressions. In this latter situation, aquifers are hosted in volcanic calderas with large graben-like collapses, such as La Pacana (Chile), but recharge under arid conditions is mostly transferred from the cover of the volcano, which seems to surround a core. However, there is a possible main difference with respect to basaltic volcanism: the greater importance of thick and extensive ignimbrite deposits, both in intra- and extra-caldera positions. The hydrogeological role of these deposits is still poorly understood and may have a stronger conditioning effect than a single groundwater system (Custodio, 2007).

1.3.5.2 Andesitic type

In the recent literature, Selles, (2014) proposed a hydrogeological conceptual model for the flank of a young andesitic stratovolcano (Merapi in Indonesia, >~400 ka), with an extensive cover of volcano-sedimentary deposits (**Figure 1. 15**). At the regional scale, the eastern flank of the Merapi volcano is described as heterogeneous multi-layered system composed of an alternation of aquitard and aquifer formations that can be divided into three hydrogeological units:

1) The upper part (> 800 m.a.s.l.): where perched aquifers of limited extent are developed in coarse pyroclastic flows and ignimbrite deposits with a relatively low hydraulic conductivity (~1.0 x10-8 m s-1). These aquifers overlie aquitard formations mainly composed of unfractured lavas, dykes and welded tuff formations. In this unit, several lithological contact springs can be observed emerging from a perched aquifer.

2) The spring belt 1, zone SB1 (400-800 m.a.s.l.): extreme flank collapses have led to a drainage anomaly associated with a shallow aquifer (mainly pyroclastic and detritic materials, K~1.0 x 10^{-5} m s^{-1}) providing groundwater to perennial *depression springs* mostly of small discharge.

3) The spring belt 2, zone SB2 (200-300 m.a.s.l.): corresponds to the main discharge zone, showing important and perennial *artesian springs* with a discharge higher than 1 m^3 s^{-1}. (e.g. Umbul Ponggok spring at Klaten, Central Java). According to the

present author, the occurrence of springs is probably caused by regional faults which create a preferential vertical groundwater circulation to the surface. These springs drain a deep confined multi-layered aquifer through a paleo-channel network (K~2.0 x10^{-4} m s-1) buried beneath the air-fall deposits, tuffs and lahar formations. The hydraulic gradient inferred from field surveys is low (~7.0 x 10^{-3} m s^{-1}), suggesting a relatively high permeability of the volcanic formations;

Compared to the conceptual models for young oceanic volcanoes (**Figure 1. 14**), it seems that Merapi shows many similarities with the Hawaiian type, such as the existence of high-level water bodies (perched aquifers) probably also caused by impounding due to dykes. The low hydraulic gradient observed at Merapi remains a common feature of young basaltic islands, along with the existence of an artesian basal aquifer which is also observed in the coastal part of Oahu Island in Hawaii (Honolulu artesian basin). The presence of extensive ignimbrite deposits and well-developed paleo-channel networks within the volcano-sedimentary deposits seems to be a specific hydrogeological feature of andesitic islands in subduction zones.

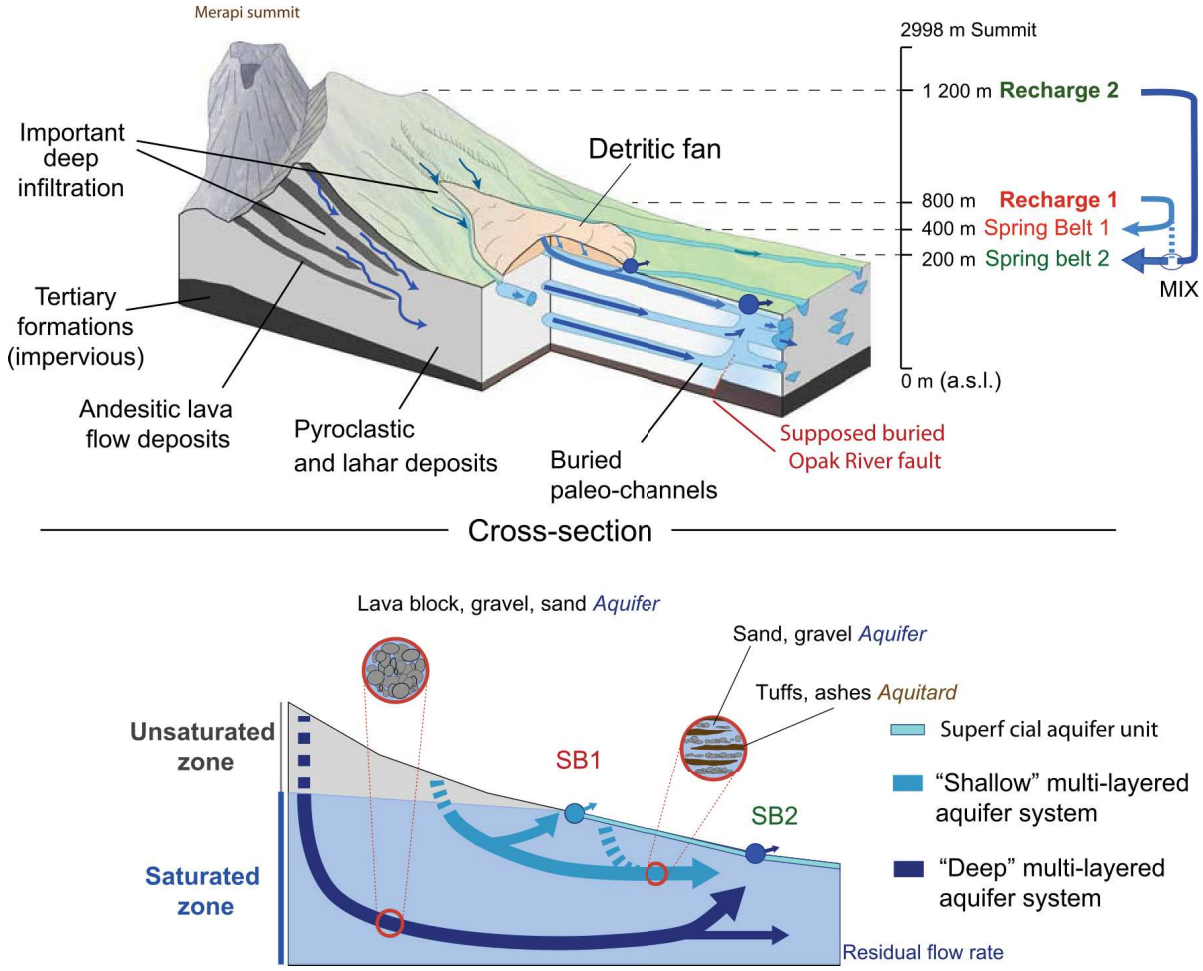

Figure 1. 15. Conceptual hydrogeological model of the eastern flank of Merapi volcano (from Selles, (2014)).

1.3.6 Hydrochemical features of volcanic rocks

The general principles of hydrochemistry and the isotopic tools developed in crystalline, carbonate or other sedimentary contexts are also applicable to volcanic rocks (Appelo and Postma, 2004). The stable isotopes of water (^{18}O and D) are particularly efficient tools in volcanic environments for assessing recharge areas where the high relief of volcanoes may favour the altitude-dependent isotope variations (i.e. isotopic altitudinal gradient) (Parisi et al., 2011). However, on volcanic island with occurrence of persistent fog, the isotopic composition may be influenced by a fog drip (Scholl et al., 2002). Since volcanic rocks are carbon-free, the recharge of ^{13}C and ^{14}C contents is usually not affected by geochemical water/rock interactions. However, an addition of deep-originated CO_2 or calcite in fracture infillings may influence the C isotopic composition, that makes difficult the ^{14}C interpretation, possibly causing an age overestimation (Custodio, 2007).

Volcanic rocks are rich in alkaline earth elements (Ca^{2+} and Mg^{2+}) contained in plagioclase and ferromagnesian minerals which are partly dissolved during rapid weathering. The low amount of alkalis in the dissolved phase is explained by the much slower release of Na^+ and K^+. Depending on the pH and temperature condition, Ca^{2+} may remain in the dissolved phase or be precipitated as carbonate; HCO_3^- often constitutes the dominant anion in groundwaters. In basalts, the groundwater type is usually Ca-Mg-HCO3 while higher concentrations of SiO_2 and Na^+ are observed in groundwaters from acidic volcanic rocks (rhyolite), leading to a Na-HCO3 type. Active vents may also produce volcanic emissions rich in Cl^-, SO_4^{2-}, H_2S or SO_2, which later may later enter the dissolved phase. Except near active volcanic vents, groundwaters mostly show an electrical conductivity lower than 150-200 µS cm^{-1} related to the low solubility of volcanic rocks, with pH ranging from 6.7 to 8.5 (Singhal and Gupta, 2010).

Groundwater in volcanic rocks is generally of good quality because of the natural high filtration capacity of the volcanic formations (e.g. lapilli). Under confined conditions, the absence of oxygen limits the occurrence of pathogenic bacteria indicative of fecal contamination and therefore the eventual downward migration of contaminants is minimized. Therefore, volcanic artesian systems can easily provide a source of drinking water from artesian wells. Water quality issues in volcanic contexts are essentially related to pesticide contamination from agriculture practices or due to lack of sewage systems on the volcano flanks; this contamination may reach the basal aquifer after a more or less prolonged transit. Agriculture and industrial activities in the downstream part of volcanoes also remain a serious challenge for the sustainability of the groundwater resource. Groundwater abstraction in coastal areas has also has an impact on seawater intrusion, especially in areas where recharge rates are low and permeability is high.

1.4 Climatic context

1.4.1 Tropical climate

Humid tropical zones are generally defined as being located on both sides of the equator (between latitudes 23°N and 23°S). From the classification of Köpen (Peel et al., 2007), the temperature is relatively high and stable over the year with a mean monthly temperature higher than 18°C. The annual precipitation is about 2 000 mm, enhanced by strong periods of monsoon, and exceeds the annual evapotranspiration (Kottek et al., 2006).
These particular climatic conditions generally result in a dense vegetation and highly permeable soils (Charlier, 2008). In tropical climates, characterization of the main hydrological processes may be complicated by large seasonal variations in all aspects of the water budget (Cook et al., 1998).

1.4.2 Atmospheric circulation in Java

Java island is included in the Indo-Pacific Warm Pool (IPWP), which is a large body of open-ocean water characterized by a permanent sea-surface temperature (SST) higher than 28 °C (**Figure 1. 16)**, and is therefore called the 'heat engine' of the globe (De Deckker, 2016; Pierrehumbert, 2000). The IPWP is thought to play a key role in the propagation and amplification of climate changes through its influence on the global distribution of heat and water vapour (Abram et al., 2009).
Climate variability in the IPWP region is influenced by three major climate systems:

1) The El Nino-Southern Oscillation (ENSO) which refers to a coupled ocean-atmosphere instability associated with El Nino (EN) and the Southern Oscillation (SO) climatic phenomenon (Clarke, 2014). El Nino refers to a warming period (and La Nina to a cooling period) induced by a SST anomaly, while the Southern Oscillation refers to a sea-level pressure variation, which appears every two to five years and lasts for several months or even a few years. The Walker circulation (atmospheric circulation cell) is an integral component of the El Niño–Southern Oscillation and its fluctuation can lead to extreme weather conditions in Java. Drought conditions typically occur during El Nino, when SSTs surrounding Indonesia are cool and the Walker circulation is weakened, resulting in anomalous surface easterlies across Indonesia (Hendon, 2003). Conversely, rainfall during the dry season may occur through the development of La Nina, associated with a warm SST anomaly;

2) The Indian Ocean Dipole (IOD) is an irregular oscillation of SST in which the western Indian Ocean becomes alternately warmer and then cooler than the eastern part of the ocean. In Indonesia, inter-annual variations in rainfall are strongly related to the inter-annual variation of the tropical SST in the Indian Ocean (Aldrian and Dwi Susanto, 2003);

3) The Asian–Australian monsoon is defined by subtropical seasonal reversals in the atmospheric circulation and associated precipitation, leading to two distinct phases, the "rainy" and "dry" seasons (Webster et al., 1998). In Java, the rainy season occurs from October to May when the cross-equatorial flow turns westerly, bringing heavy precipitation from the northwest (Hamada et al., 2002). The dry season occurs from June to September, influenced by dry south-easterly trade winds and characterized by a low-level inversion which caps the deep convection (Rodysill et al., 2013).

The conjunction of the above three climate systems governs the temperature, wind trends and rainfall variability over Java Island. In East Java, the annual rainfall easily exceeds 2 000 mm per year, especially in areas with high relief such as volcanoes (BMKG, 2018). The mean annual temperature in East Java ranges from 22°C to 29°C with a relative humidity higher than 75% (BMKG, 2018).

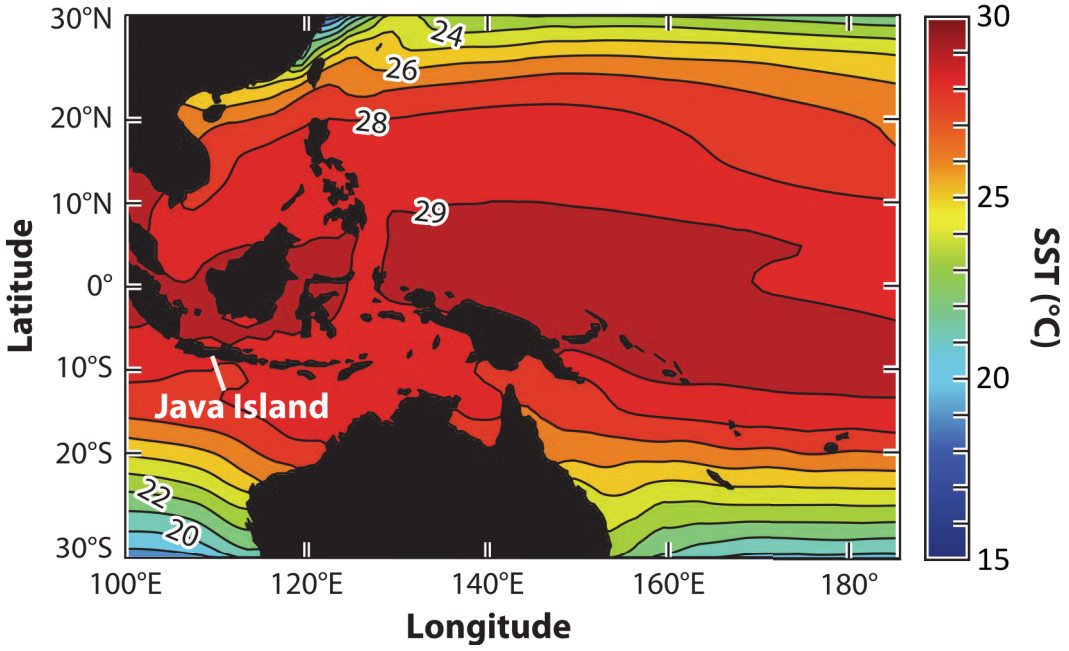

Figure 1. 16. Mean sea-surface temperature (STT in the tropical Pacific Ocean for the period January 1982-December2012, modified after Clarke, (2014)).

1.4.3 Local climate

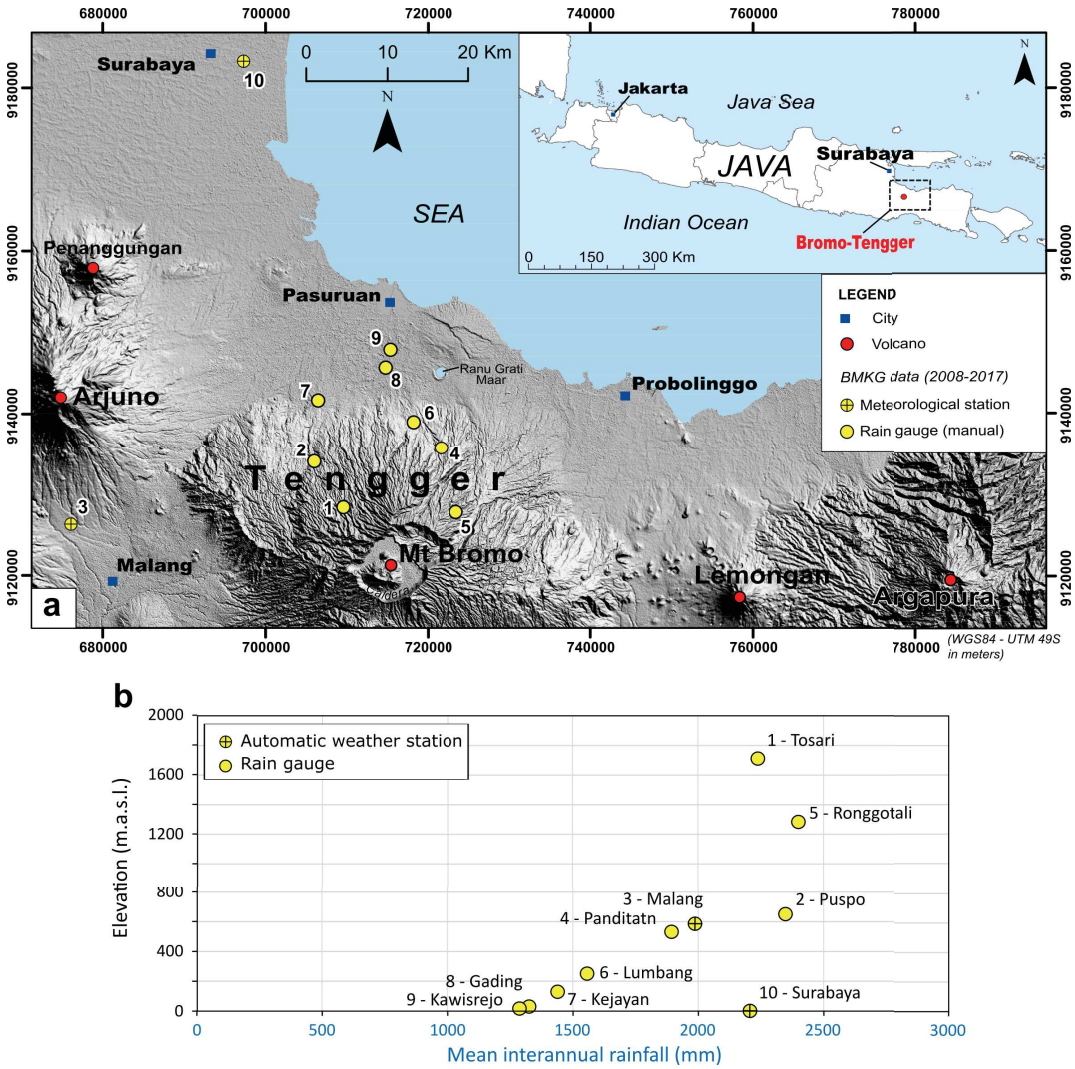

Figure 1. 17. Mean interannual rainfall at 10 rainfall stations, as a function of their elevation (m.a.s.l.) (data from BMKG, (2018) of Malang city).

According to Badan Meteorologi, Klimatologi dan Geofisika of Malang (BMKG, 2018) the precipitation recorded around the Bromo-Tengger volcano for the 2008-2017 period ranges from 1 290 to 2 400 mm year^{-1} for station 9 and 5, respectively (**Figure 1. 17. a**). The mean interannual precipitation is estimated at about 2000 mm, based on 6 rain gauges (n° 1, 2, 4, 5, 6, 7; **Figure 1. 17. b**) regularly located on the northern flank of Bromo-Tengger, with a maximum amount of rainfall from December to February. Unfortunately, BMKG data are not precise enough to map rainfall on Tengger volcano because of numerous and long gaps observed in the data from all rain gauges. In such a steep topographic environment, the rainfall usually increases from the coastal low-lying areas to the highest areas inland, but also depends on the wind direction. From the data from Surabaya and Malang, the annual average wind direction is about N150° (NW-SE), with a mean velocity of about 5 km h^{-1} and an annual average humidity of 76 %. The 2008-2018 annual average temperature shows a minimum and maximum temperature of 18.3°C for Malang (580 m.a.s.l.) and 32.1 °C for Surabaya (10 m.a.s.l.).

1.5 Land and water uses

1.5.1 Land use

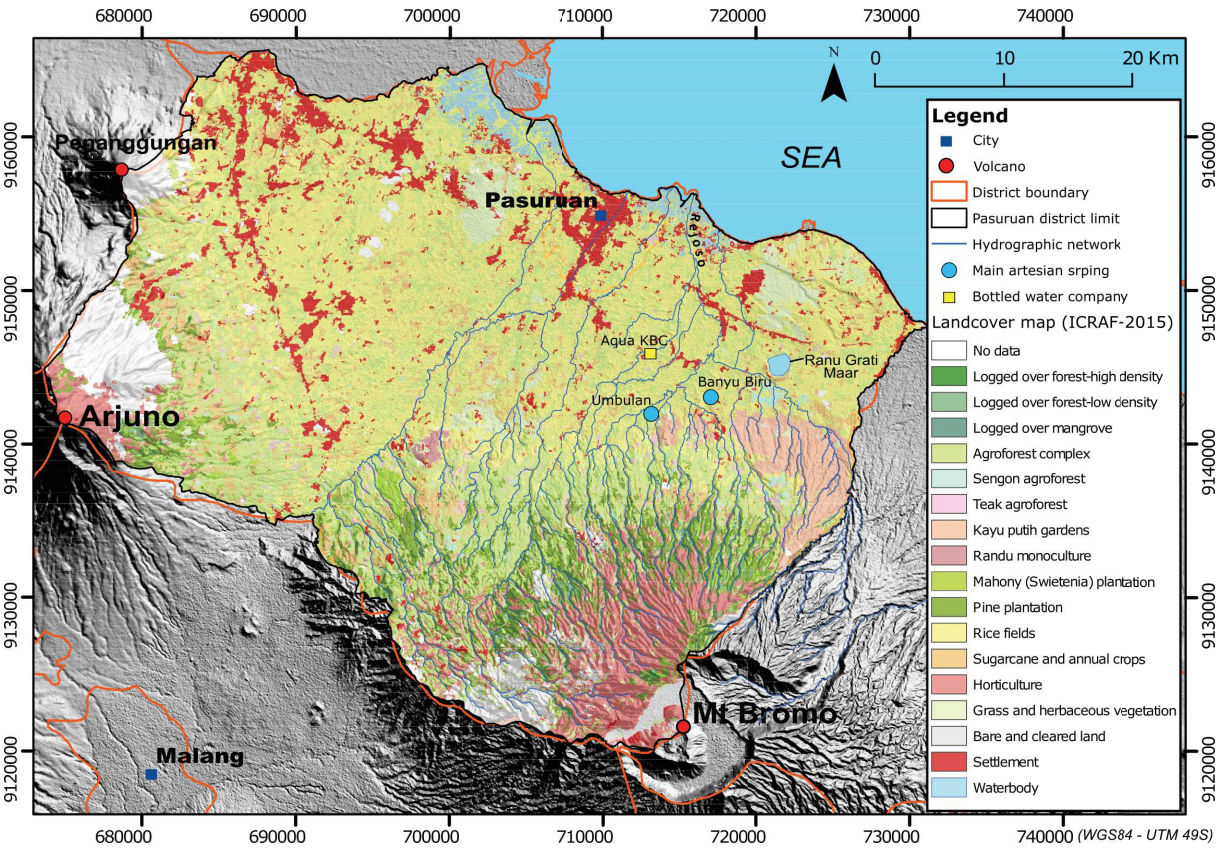

Figure 1. 18. Land use and land cover map of the Pasuruan district in 2015 (modified from ICRAF, 2015).

The successive eruptions of the Bromo-Tengger volcano over time have largely contributed to fertilizing the surrounding soils, which has given rise to a thriving agriculture in the district of Pasuruan, acting as an income source for the local population (**Figure 1. 18**).

The land use and land cover map provided by Amaruzaman et al. (2018) is dominated by paddy fields (rice plantations) and complex agroforest (mixed garden). Horticulture, sugarcane and pine plantations are also relatively common practices. Paddy fields and sugarcane plantations are abundant in the downstream area. Complex agroforest dominates the middle stream area of the watershed, and horticulture and pine plantation are mostly found in the upstream area. The settlements are located in the centre of the paddy field and complex agroforest areas.

From 1990 to 2015, complex agroforest was converted to paddy fields (**Figure 1. 19**) almost every year, stimulated by water abundance, especially in the downstream part through permanent rivers, farmers' wells and natural groundwater springs (e.g. Umbulan spring). As consequence, farmers grow rice 2 to 3 times per year, which represents a perennial income for the local population.

The drainage network extends radially away from the volcano summit with large steep canyons. This network is mostly supplied by ephemeral streams on the Bromo-Tengger flank. The stream density seems to decrease westwards probably due to the gentle slope related to the old caldera of Nongkojajar. On the plain of Pasuruan, numerous canals collect waters from streams on the northern flank, which are then delivered to the main rivers of the plain such as the Rejoso River.

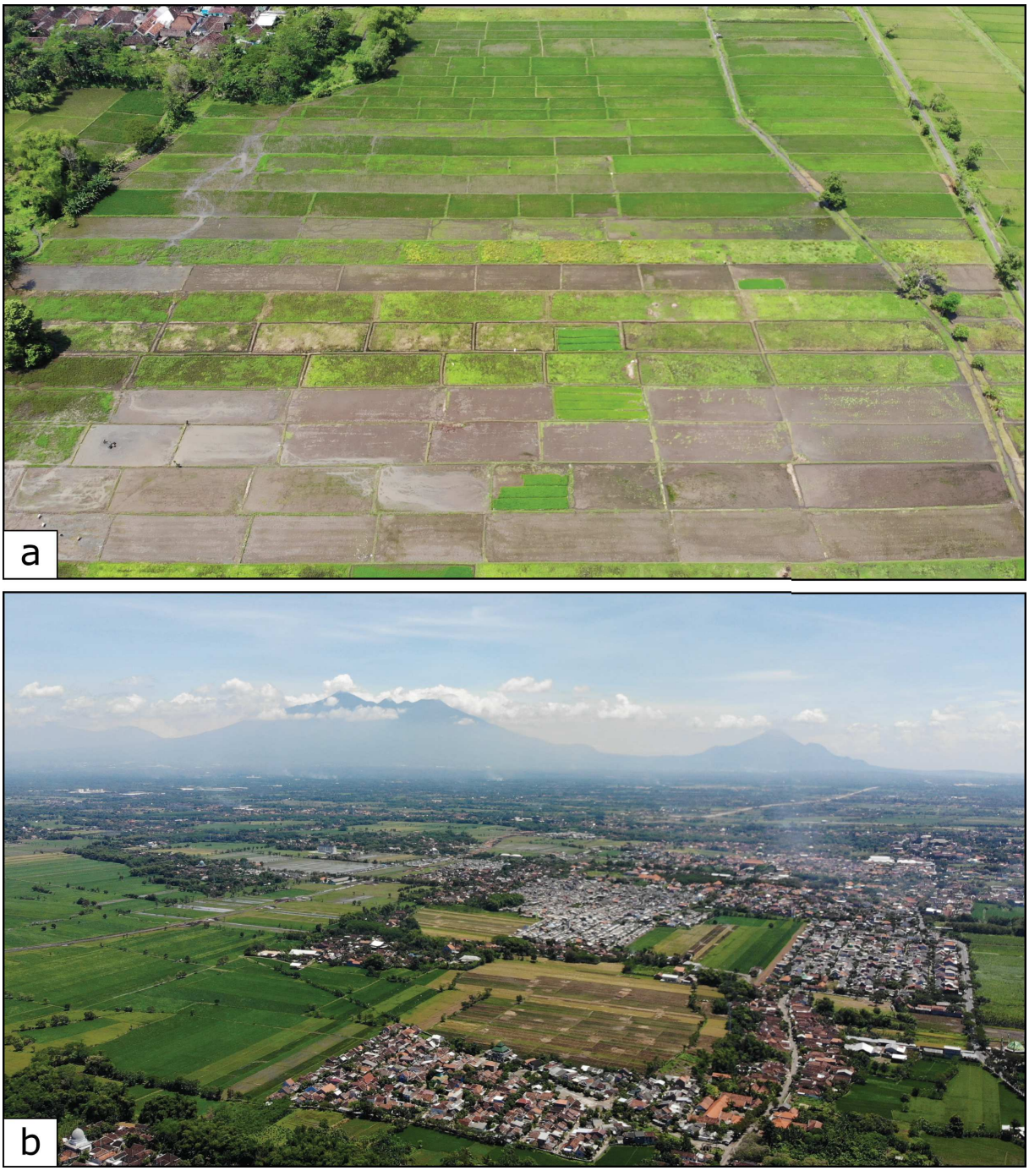

Figure 1. 19. Drone aerial view of Pasuruan plain with **a.** Paddy field plantations and **b.** The city of Pasuruan with the Arjuno-Arjuna volcanic complex in the background.

1.5.2 Water use

From the northern flank of the Bromo-Tengger volcano down onto the plain of Pasuruan, the water used can be divided into three main origins: groundwater from springs, wells (shallow or deep) and surface water mainly from river intake. In fact, it is possible to distinguish six types of water points related to their specific outflow context, as illustrated in **Figure 1. 20**.

1.5.2.1 Springs

Groundwater may flow from (1) natural or permanent gravity springs, where the water table intersects the surface topography or (2) artesian springs, where a conductive weakness zone (fault, intrusive body, etc.) in the confining layer triggers a preferential vertical groundwater flowpath to the surface. For more hydrogeological details, see the previous section 1. 3. 4. Gravity springs are mainly used for domestic purposes in the upstream part of the volcano flank (e.g. Wonorejo village) as they constitute the only source of water in a zone where streams are ephemeral. Artesian springs show a higher discharge and can provide both drinking water (no water treatment required) and irrigation for paddy fields through the dense canal network on the plain. The most important artesian springs around Pasuruan are Umbulan (~ 3500 L s^{-1}) and Banyu Biru (~ 300 L s^{-1}) (**Figure 1. 18**.). Umbulan is mostly used for drinking water supply (e.g. PDAM Pasuruan, PDAM Surabaya) and other irrigation needs such as paddy fields, while Banyu Biru is mostly used as a recreational area. However, in 2019, the Indonesian government completed the construction of a pipeline (> 60 km from Umbulan to Surabaya), which directly connects the Umbulan spring to Surabaya city. In the long term, this pipeline should provide several thousands of litres per second of drinking water to Surabaya and may increase the pressure on the groundwater resource of Pasuruan.

1.5.2.2 Wells

On the lowlands, some of the water used comes from shallow wells and artesian deep wells. The shallow wells rarely reach more than 20-30 m depth and are divided into two types according to the abstraction process: (3) using an electric pump or with a manual bucket, mostly for domestic uses that require less amounts of water, (4) using a motor pump several hours each day, mostly for irrigation. The pumping rate ranges from 5 to 10 L s^{-1}, depending on the pump power.

Deep artesian wells, usually called “free-flowing artesian wells”, can reach more than 100 m depth, (several are 200 m deep according to oral testimonies) and provide a discharge of several litres per second of drinking water. Due to water abundance in this cluster, several local and national drinking water treatment plants operate in the area (e.g. Aqua Indonesia company) and some of the water is used for car washing. Despite a relatively high water abundance, the waste of groundwater is significant since the waters from farmers’ artesian wells are flowing continuously into the environment without any control.

1.5.2.3 Rivers

A proportion of the water used comes from (6) river intake independently in the upstream and downstream parts of the volcano. This river intake is generally controlled by manual weirs or dam infrastructures most of which were probably built during the Dutch colonization before 1942.

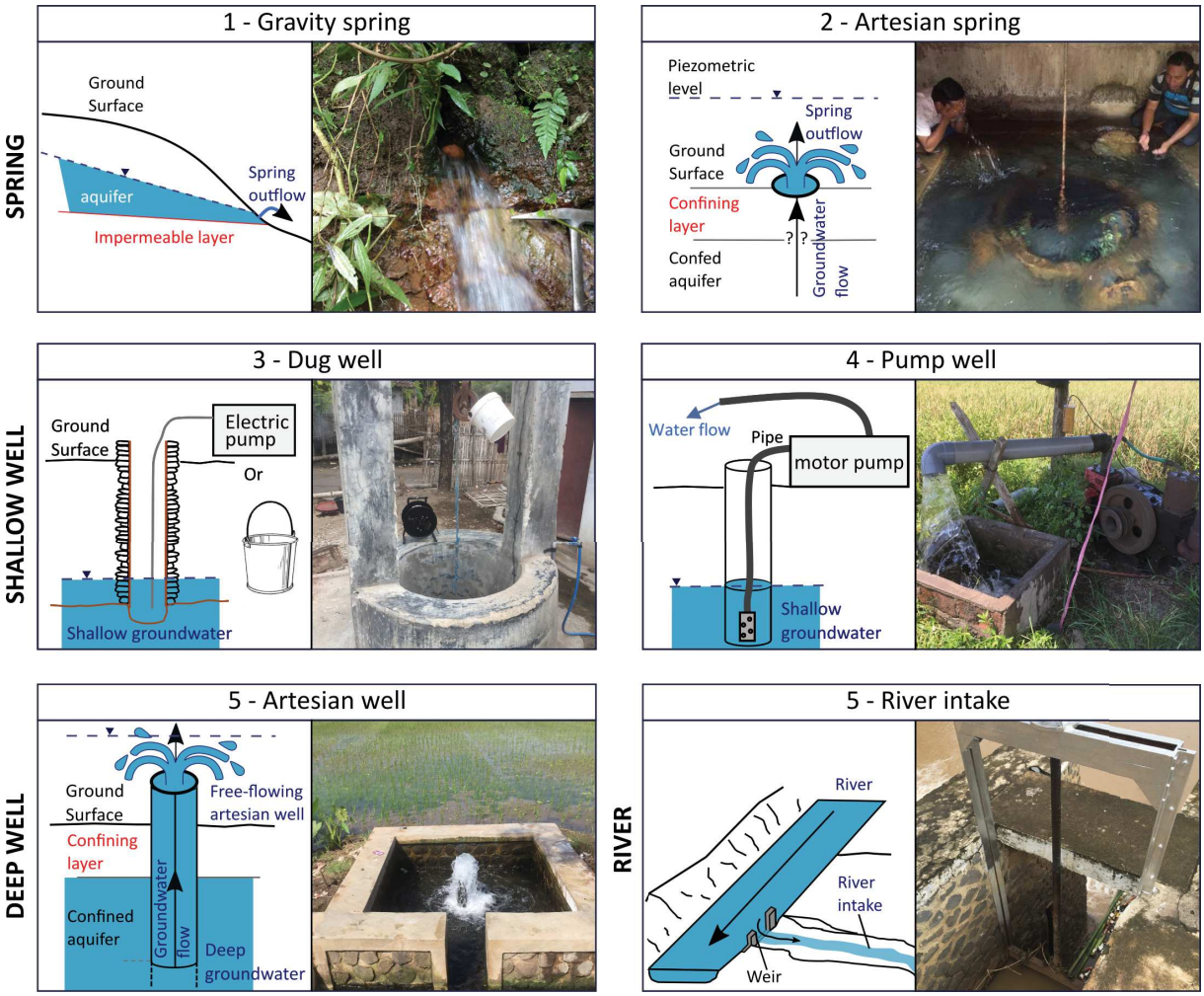

Figure 1. 20. Types of water point for agriculture, drinking water supply, domestic and industrial uses divided into three main types: springs, wells and river intake. Spring-type water points are divided into (1) gravity springs and (2) artesian springs. The wells are divided into shallow (3) dug wells, (4) pump wells and deep (5) artesian wells (mostly free-flowing). The rest of the water used comes from (6) river intake.

1.6 Synthesis

The Bromo-Tengger volcano is an andesitic stratovolcano in a volcanic arc setting, where the volcanic activity is conditioned by subduction along the Java trench. The geological history of the volcano is relatively recent (< 1.4 Ma) but complex. Volcanic formations are heterogeneous and form complex structures related to multiphase building/dismantlement stages linked to several main eruptive centres and caldera collapses over time. Nowadays, the last active vent is Mount Bromo located in the wide "sand sea" caldera of Tengger well known as a famous touristic site. Despite a period of relative quiescence, Mount Bromo remains a source of hazards due to recurrent explosive eruptions, with the most recent important event occurring in 2010.

Many studies have focused on the geological and volcanic features of this massif (especially the summit caldera), but no hydrogeological study has been published until now. The hydrogeological characteristics of volcanic formations are highly variable and depend on many factors such as the distance from the source point, the fracture network and the degree of consolidation (welded or loose), as well as the weathering and remobilization processes (e.g. interbedded layers or paleo-channels). Even if volcanic rocks are often considered as porous media, reality is more complex because of the wide range of hydrodynamic properties of such materials (e.g. permeability varies over 9 orders of magnitude). The aquifer formations are mainly associated with loosely consolidated pyroclastic deposits and fractured lava flows with porous autoclastic breccias. In the same way as massive lava flows or dykes, a dense fracture network in ignimbrite deposits may produce an aquifer formation. Conversely, welded pyroclastics (tuffs), ashfall deposits, unfractured massive lava flows, dykes (sills) or ignimbrites as well as landslide formations (lahars or debris avalanche) are mostly aquitard formations. The understanding of the geometry and hydraulic connectivity between all these formations is a serious challenge to define a valid hydrogeological conceptual model. The latter is poorly developed in andesitic compared to basaltic contexts. Special attention needs to be paid to the geometry and artesian conditions of some coastal volcano-sedimentary formations, since many scientific issues remain to be addressed.

The Bromo-Tengger volcano is located in a region with tropical climate conditions characterized by a monsoon regime with rainy and dry seasons occurring, respectively, from October to May and from June to September. The precipitation easily exceeds 2000 mm y^{-1}. According to the literature, recharge processes on a volcano in this type of humid tropical climate may be influenced by orographic effects, fog occurrence, land cover (vegetation), hydraulic properties and the weathering state of the volcanic formations directly related to their age. From the northern flank Bromo-Tengger to the downstream plain of Pasuruan, water comes from groundwater through springs (gravity or artesian), shallow wells (dug and pump wells) or deep wells (free-flowing artesian wells). A remaining proportion of the water comes from river intake. Although the relatively high abundance of water in the region supports a thriving agriculture (e.g. paddy fields), pressure on the groundwater resource is increasing with a growing demography, uncontrolled illegal farmer's wells and major water supply projects managed by the Indonesian government (e.g. Umbulan-Surabaya project). In this context, there is an urgent need to characterize the hydrogeological functioning of the Bromo-Tengger aquifer system for an adequate management of the groundwater resource.

Instrumentation

Overview

The first field work was aimed at deploying a network of measuring instruments to assess a hydrogeological water budget and characterize the hydrodynamic behavior of the northern flank of the Bromo-Tengger volcano aquifer system (**Figure 1. 21**). To define the "inflow - outflow" conditions of the hydrosystem, the following equipment was installed:

- Four new weather stations on the northern flank of the volcano, from 550 m.a.s.l. to 2 700 m.a.s.l., including one station located within the sand sea caldera at 2 100 m.a.s.l. The daily time step dataset allow an altitudinal characterization of rainfall, temperature and humidity. In the event of failure of the weather stations, manual rain gauges have been installed in the vicinity of some of them.

- A gauging station in a representative watershed (Kronto), to assess the hydrological behavior of a typical river of the northern flank.

- Gauging stations installed at the two main artesian springs of the Pasuruan plain (Umbulan and Banyu Biru), supplemented by two other physico-chemical probes (T°C and electrical conductivity) to record the hydrodynamic behavior of these springs.

- A piezometer to monitor the piezometric level within the Pasuruan artesian aquifer. It is used to define the trend of the hydraulic head of the artesian aquifer over time.

This instrumentation is supplemented by two barometers, one in the plain at Umbulan and the other at the Kronto gauging station to correct the measured water levels. Data collection from the new instrumentation was performed at monthly intervals. Additional gauging section measurements were carried out to allow data processing and analysis of hydrological stations.

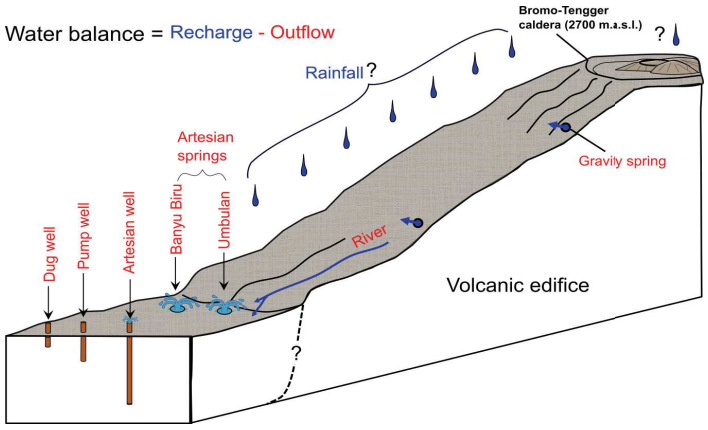

Figure 1. 21. 3D Conceptual schema of the northern flank of Bromo-Tengger

Weather stations

In order to define the recharge conditions along the northern flank, four new weather stations (Cimpod RTU - CIMEL) were judiciously installed on sites allowing a good distribution of measurements according to an altitudinal profile, an easy road access, and guaranteeing the safety of the equipment (**Figure 1. 22**). These stations include the sites of Kronto, Wonorejo, Seruni and Temple. Three additional rain gauges were installed near the weather stations, in case of failures. The four new weather stations record rainfall, T°C and relative humidity with a daily time step, while the station already existing at the Aqua bottling plant only allows a daily rainfall measurement (**Table 1. 1**). To protect the stations, a concrete support was built, equipped with an iron fence as well as a locked door (**Figure 1. 22. g, h, i**).

In addition, each new weather station was connected to a water tank to collect the rain measured by a tipping bucket. This water collector is filled with one litre of oil to avoid evaporation. The final volume of water in this tank is measured at the end of the monitoring period to check the good calibration of the CIMEL rain station. The blue water tank is visible at Wonorejo and Temple (**Figure 1. 22. g, h**). The instrumentation of the weather stations was completed at the end of March 2017.

Due to technical and logistical problems, only the first year of measurements (April 2017 - April 2018) is considered as reliable and the data are used here to calculate the hydrogeological water budget discussed in *Chapter 3*.

Table 1. 1. Deployment of instrumentation.

Location	**UTM - 49S**			**Rain gauge**	**Weather station**	**Daily monitoring (UTC)**		
	X (m)	Y (m)	Z (m.a.s.l.)	(*installed*)	(*installed*)	Rainfall (mm)	T°C (°C)	Humidity (%)
Aqua KBC	713215	9145908	17	*31/03/2017*	*From Aqua*	yes	-	-
Kronto	713990	9136958	545	*16/11/2016*	*January 2013 17/03/2017*	yes	yes	yes
Wonorejo	714071	9133211	1158	*29/11/2016*	*27/03/2017*	yes	yes	yes
Seruni	715323	9126121	2681	-	*30/03/2017*	yes	yes	yes
Temple	715445	9122585	2154	-	*30/03/2017*	yes	yes	yes

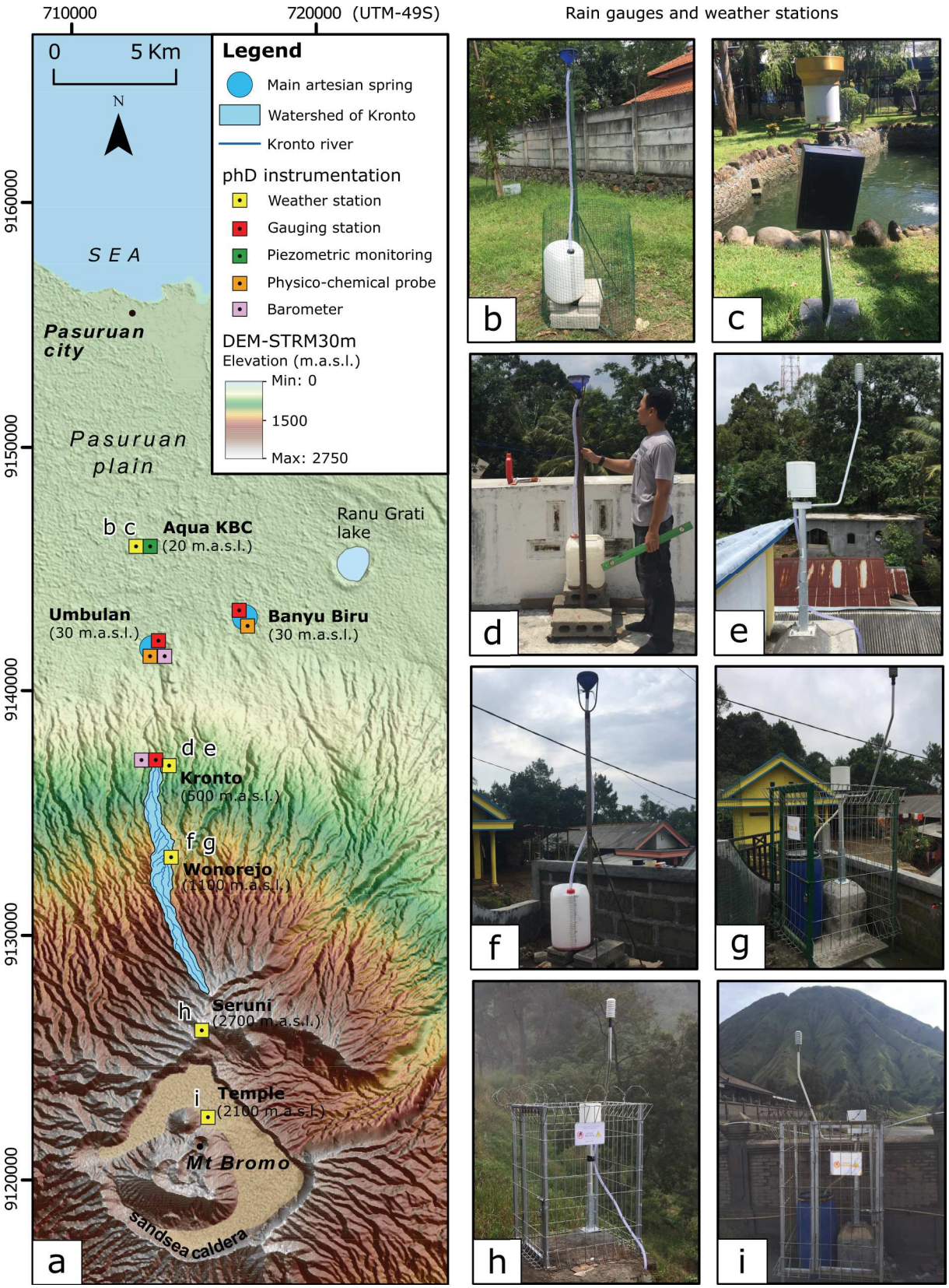

Figure 1. 22. Location of rain gauges and weather stations installed on the northern volcano flank, **b, c.** Aqua Kebon Candi plant, **d, e.** Kronto village, **f, g.** Wonorejo village, **h.** Seruni caldera summit, **i.** Temple in the sand sea caldera.

Probe monitoring

To understand the outflow conditions on the Pasuruan plain, the two main artesian springs were instrumented with gauging stations using a TD-Diver pressure probe (**Figure 1. 23. b, e**). These stations are located respectively at channel B8 and weir 1 of the Umbulan and Banyu Biru springs. To assess the hydrosystem reactivity of such springs, a physico-chemical probe CTD-Diver probe (Conductivity and Temperature) was installed at their main outflow to measure temperature and conductivity variations. This probe is positioned within the main water abstraction works of Umbulan spring and fixed onto the pumping system in basin 1 of the Banyu Biru spring (**Figure 1. 23. c, f**).

Another gauging station was installed in a representative watershed of the northern flank of the volcano (**Figure 1. 23. g**). Indeed, the catchment shows a highly elongated morphology, with a surface area of less than 10 km², a predominantly agroforest-type land use and a perennial river (Kronto river) whose base flow (< 10 L s^{-1}) is mainly supplied, apart from rainfall events, by small gravity springs in upstream.

Monitoring of the hydraulic head of the Pasuruan artesian aquifer was carried out using a piezometer located at Aqua KBC (bottling plant). The piezometer is 70 m deep and allows a visualization of the piezometric head with a transparent tube at the surface (**Figure 1. 23. h**).

Two barometers were installed (at Umbulan and Kronto) to correct the water levels recorded by the TD-Diver probes. Note that the sensors used (CTD, TD, and Barometer) allow continuous measurement with an hourly time step (in Coordinated Universal Time), (**Table 1. 1**).

Additional gauging cross-section measurements (electromagnetic flowmeter - Hydreka) were performed at the Umbulan and Banyu Biru springs and Kronto river to determine the rating curve that allows a continuous discharge measurement. The rating curve of the Kronto river was established for different hydrological periods (dry/wet season), including a flood recorded on 12/02/2018.

Table 1. 2. Monitoring set-up with new instrumentation probes.

Location	**UTM - 49S**			**Probe (VenEssen)**			**Hourly monitoring (UTC)**		
	X	Y	Z	TD diver	CTD diver	Barometer	Pressure	T°C	Conductivity
	(m)	(m)	(m.a.s.l.)	(*installed*)	(*installed*)	(*installed*)	(m)	(°C)	(µS cm^{-1})
Umbulan	713299	9141740	33	*21/04/2017*	*09/05/2017*	*26/04/2017*	yes	yes	yes
Banyu Biru	717072	9143007	33	*26/04/2017*	*17/03/2017*		yes	yes	yes
Aqua piezometer	713209	9145887	17	*17/05/2017*			yes	yes	-
Kronto river	713446	9137185	435	*18/06/2017*		*23/03/2018*	yes	yes	-

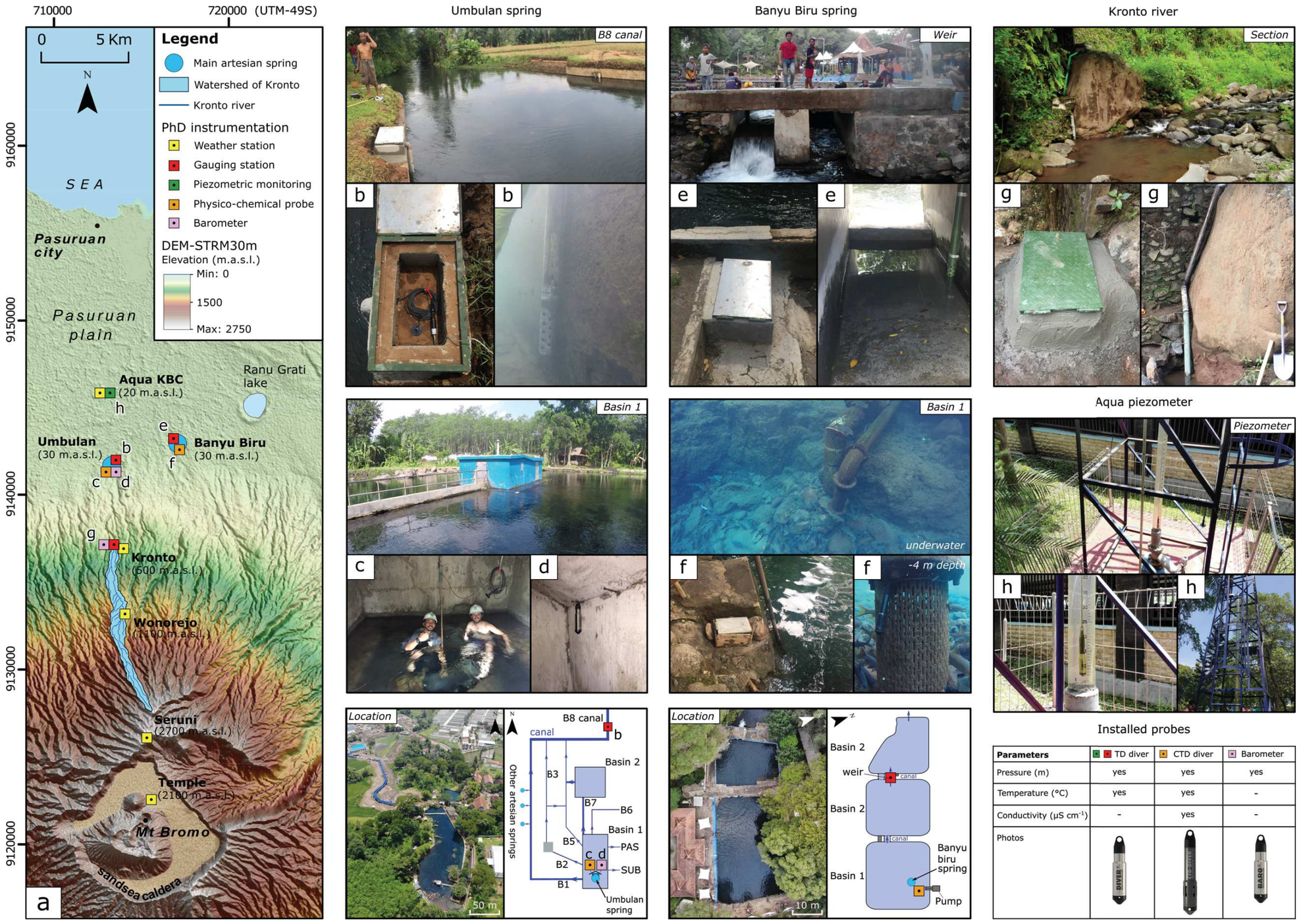

Figure 1. 23. Installation of new probes on the northern volcano flank (**a**) with TD Diver for gauging stations (**b, e, g**) and piezometric artesian well monitoring (**h**), CTD Diver for physico-chemical monitoring of Umbulan and Banyu Biru artesian springs (**c, f**), supplemented by 2 barometers, at Umbulan (33 m.a.s.l.) and Kronto (435 m.a.s.l.) (**d, g**).

Chapter 2



View of the Umbulan artesian spring used for drinking water supply and recreative area by the local population

Chapter 2. Geological and hydrogeological characterization of piedmont artesian springs related to the coastal volcano-sedimentary deposits of Pasuruan, Indonesia

This chapter introduces the concept of artesian volcano-sedimentary aquifers, which are located in the distal parts of volcanic complexes that frequently represent areas with high hydrogeological potential. A multidisciplinary approach is used to define the main lithologies and structures of this type of aquifer, leading to a geological conceptual model for the piedmont area of the volcano and its downstream volcano-sedimentary plain.

The Pasuruan volcano-sedimentary artesian plain to the north of Bromo-Tengger volcano is used here as a study case. The lithology and areal extent of this aquifer are identified as well as the context of the emergence of high-discharge artesian springs in the volcanic piedmont area, such as the Umbulan spring showing a discharge of about 3500 L s^{-1}. This chapter presents the first hydrogeological field data acquired in the study area and provides a scientific basis for the following chapters.

Abstract

Coastal volcano-sedimentary deposits are barely described in the major conceptual models of volcanic hydrogeology (e.g. Hawaiian model). The highly heterogeneous nature of the processes and dynamics of the deposits gives rise to complex structures with a wide range of permeability. In some configurations, these deposits can form an artesian aquifer corresponding to the confined part of the basal aquifer of the volcano. The groundwater of these artesian aquifers is often potable and relatively easily exploitable through artesian springs and wells. This latter type of configuration is found on the Pasuruan coastal plain on the flanks of the Bromo-Tengger volcano in East Java (Indonesia). The aim of this study is to define the lithologies and geometries of the Pasuruan artesian volcano-sedimentary plain. Understanding the geological transition from the volcanic massif towards the volcano-sedimentary plain provides new insights to determine the outflow context of high-discharge artesian springs in volcanic piedmont areas. For that purpose, a multidisciplinary approach was carried out including hydrogeological, geological and geophysical investigations. The interpretation of the results makes it possible to propose a first conceptual geological model of the Pasuruan plain and highlight a probable fault zone at the origin of the outflow context of such important artesian springs.

Keywords: volcano-sedimentary deposits, artesian aquifer, Bromo-Tengger volcano, volcanic piedmont artesian spring

2.1 Introduction

Volcanic formations show a high heterogeneity related to variable depositional processes that are triggered by (1) syn-eruption deposits (directly eruptive) and (2) the inter-eruption deposits (indirectly eruptive). Under tropical climates, weathering processes are intense and heavy rainfall contributes to the remobilization of non-consolidated volcanic formations by stream transport. The degree of consolidation (welding of loose materials), combined with facies variations along the volcano flanks leads to a complex structure, especially within the volcano-sedimentary series which usually border the foot of the volcano (Custodio, 2007).

Despite numerous studies on volcano-sedimentary features (Blyth, 1940; Hildenbrand et al., 2008; Rovida and Tibaldi, 2005; Selles et al., 2015), their structure and geometry in distal areas is still poorly defined, especially regarding the confined aquifer conditions. Indeed, artesian basins related to volcano-sedimentary distal deposits are barely mentioned in the literature; hence, we need to improve the consideration of such basins in the main hydrogeological conceptual models. Many studies have been focused on free-flowing artesian wells (Meinzer, 1928; Nichols et al., 1996; Sun et al., 2015; Sun and Xu, 2014), but special attention should be paid to the outflow context of artesian springs in volcanic piedmont areas.

In the literature, artesian springs are usually referred to as “mound springs” defined as “circular, gypsiferous or calcareous, volcano-like structures fed by point sources of artesian water rising from a confined aquifer” (Roberts and Mitchell, 2019). Artesian mound springs are observed worldwide, such as in the Great Artesian Basin (GAB) of Southern Australia (Mudd, 2000), in the Fedjadj and the Nefzaoua oases in Tunisia (Roberts and Mitchell, 2019), or around playas in the USA (Peter and Mehringer, 1967). However, artesian springs related to volcanic environments are rare. In Kenya, East Africa, Ashley et al., (2002), describe artesian mound springs flowing along a rift-related fracture system near the contact between volcanic bedrock and late Quaternary sediments. In Indonesia, artesian springs seem more frequent and can define “spring belts” probably related to conductive faults (Selles, 2014), which appear at the foot of volcanic massifs (e.g. Umbul Ponggok spring in Klaten, Merapi). These latter springs do not form a circular concretional mounds because of the low mineral contents of the waters, but are usually flowing at the bottom of large pools probably deepened by humans. The cool temperature of the water in these pools allows their recreational use by the local population. Although geological investigations have been performed near these springs (Selles, 2014), the outflow context of artesian volcanic springs is still unclear.

The aim of this study is to define the lithologies and geometries of the volcano-sedimentary deposits of the Pasuruan plain located at the foot of the Bromo-Tengger volcano. The outflow context of the high-discharge artesian springs emerging on this plain (Umbulan and Banyu Biru springs) is investigated in detail using a multidisciplinary approach.

First, hydrogeological investigations allow to make an inventory of springs and wells related to the Bromo-Tengger aquifer system. All these water points are compiled into the first Bromo-Tengger database. Then, key volcanic outcrops are described and combined with analyses of cuttings/core samples from drillings in progress located on the plain. Complementary geophysical investigations are carried out in three main zones near artesian

spring outflows and key outcrops. The results lead to a first geological conceptual model of the Pasuruan plain and provide new insights related to the outflow context of artesian springs.

2.2 Study area

The studied area extends from the northern flank of Bromo-Tengger volcano to the plain of Pasuruan in East Java, covering about 1 000 km² (**Figure 2. 1**). Bromo-Tengger is a Quaternary stratovolcano (< 1.4 Ma) and results from subduction in the Java trench (Mulyadi, 1992). The volcano is mainly composed of basalt-andesite lava flows and pyroclastic deposits, several thousands of metres thick. Other lithologies such as ignimbrites or lahars, related to pyroclastic flows or landslides, respectively, are observed in some places (e.g. Sapikerep valley), (Zaennudin, 1990). At the present day, the northern flank extends towards the Madura strait and leads to a horseshoe-shaped rift zone filled by volcano-sedimentary deposits. The last active vent is Mount Bromo, located in the wide "sand sea" caldera summit of Tengger.

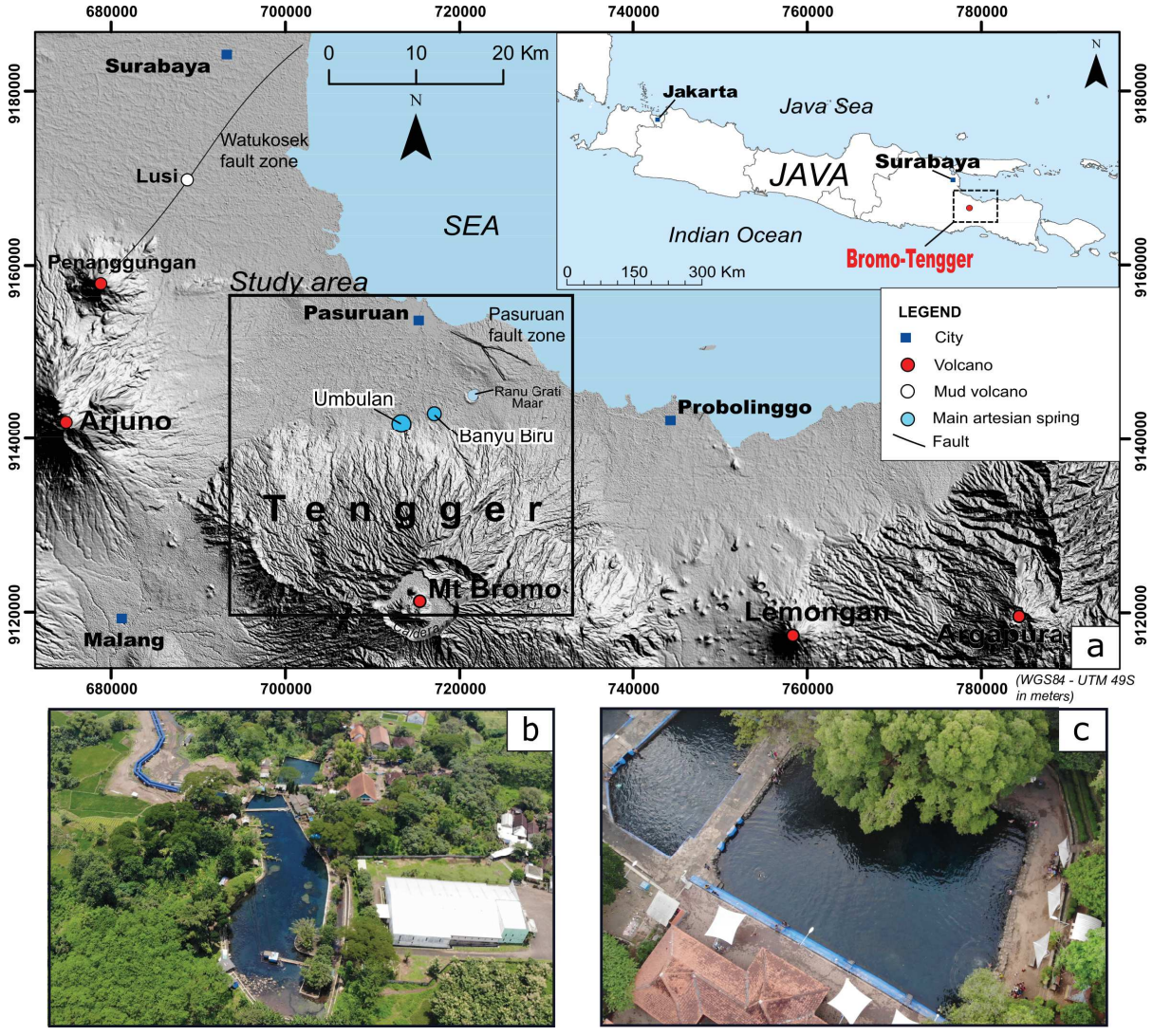

Figure 2. 1. a. Relief map of the North-Eastern part of Java Island (USGS SRTM30 dataset) with location of the studied area. **b.** Drone view of the Umbulan artesian springs. **c.** Drone view of the Banyu Biru artesian spring.

Indeed, Pasuruan is located on the southern flank of the Kendeng anticline basin (Marliyani, 2016). This region corresponds to back-arc region of the Java subduction system in the immediate vicinity of the modern volcanic arc represented by the Bromo-Tengger-Semeru volcanic complex. This region is probably impacted by local subsidence and fault systems. The Pasuruan basin appears to follow a N-S graben structure infilled by about 300 m of recent volcano-sedimentary deposits (Mazzini et al., 2017) and probably bounded in the North by the only active normal E-W fault system identified in the basin (Marliyani et al., 2019), (**Figure 2. 1. a**).

In term of hydrogeology, there is currently scant information regarding the aquifer system of the Bromo-Tengger volcano and the artesian basin of Pasuruan. However, many outflows from wells or springs on the plain are well known by the local population and may suggest an important hydrogeological potential. Recent oral testimonies suggest that more than 600 free-flowing artesian wells are located in the artesian basin of Pasuruan. In 2015, the two main artesian springs of the plain (Umbulan and Bany Biru; **Figure 2. 1. b, c**) provided a discharge of about 3600 and 300 L s^{-1}, respectively (CKNet, 2015). According to villagers, discharge of these springs has decreased during the last few decades in parallel with the development of free-flowing artesian wells.

2.3 Methodology

2.3.1 Groundwater points inventory and database

A large-scale inventory of groundwater points was drawn up during this thesis project (October 2016 - April 2019). The hydrogeological investigations are mostly divided into two main zones:

- On the Bromo-Tengger volcano, especially at locations where springs are supposed to outflow (e.g. deep erosion canyons). Several springs were also inventoried around the volcanic massif near the cities of Malang, Lumajang or Probolinggo.
- On the plain of Pasuruan, where we find the main artesian springs and also a high density of wells.

The groundwater points were inventoried according to the water type nomenclature presented in section 1.5.2. The nomenclature is divided into two groundwater point types: springs and wells (shallow or deep), among which we distinguish (1) gravity springs, (2) artesian springs, (3) dug wells, (4) pump wells and (5) artesian wells.

Supplementary field data were collected for each water point, including the hydrogeological context of outflow, physical-chemical parameters (T°C, EC, pH, O_2), discharge and other measurements related to the well features such as the casing diameter, depth or location of screens (or open hole).

To facilitate the sharing of the groundwater points collected in the field, a database (DB) was created under Access software (from Microsoft Office). The DB was created using the

previous nomenclature of five water point types, which refers to natural (spring) or artificial outflows (wells) that are used, non-used or abandoned.

For each water point, information is classified into six topics corresponding to data tabs accessible from the home menu interface: (1) Water points; (2) Geology/hydrogeology; (3) Field measurements; (4) Water analyses; (5) Location; (6) Documentation.

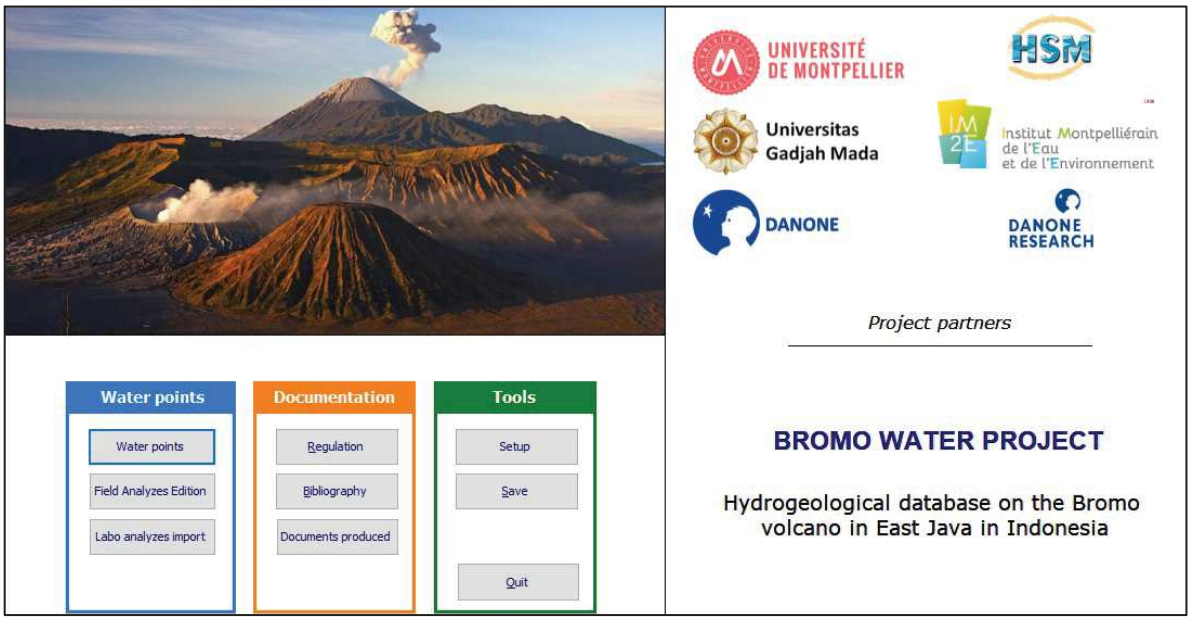

Figure 2. 2. Bromo-Tengger database developed with the Access Microsoft platform.

The contents of these tabs are presented in **Appendix 1**. This database not only offers a way of archiving and organizing the data collected on the field, but it could also allow the sharing of these data in an easy and playful way with all the water resource stakeholders in the study area. In the future, this database could be improved and supplemented for further water management studies.

2.3.2 Geological and drilling surveys

Based on the description of volcaniclastic deposits from the literature, the field geological surveys help characterize the geological structure of the northern part of the Bromo-Tengger volcano and the Pasuruan plain. Several field surveys were performed between May 2016 and March 2017. At the volcano scale, more than 200 observation points were identified. To study the geological transition between the volcanic massif and the volcano-sedimentary plain, we selected 19 key outcrops that highlight the geological and structural context of the Pasuruan plain (red dot in **Figure 2. 3**). Several of these outcrops are described in the following sections as key outcrops required for the geophysical calibrations.

The first step was to identify the facies of the deposits. As volcaniclastic sediments display systematic facies changes, their identification and geological mapping is difficult especially due to the dense vegetation and extreme climatic conditions that do not facilitate observations.

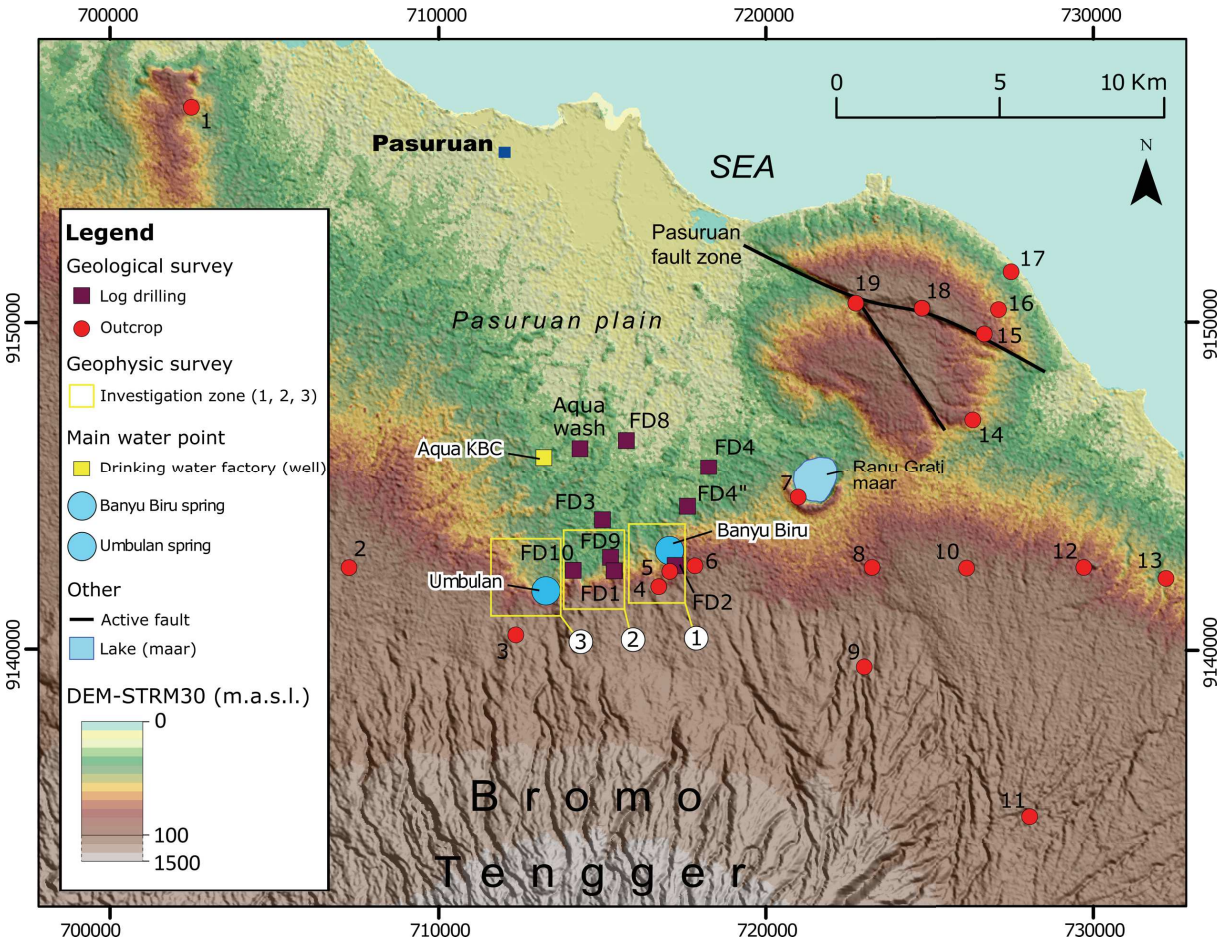

Figure 2. 3. Location map of the geological and geophysical investigations.

The second step was to assist the local drillers during the drilling of the new artesian wells. On the Pasuruan plain, there is a high density of wells drilled without any control or regulation. The drillers have no professional background and most of them do not know the laws relating to the exploitation of groundwater resources in Indonesia. Most of the wells are sunk with the core drill method allowing the collection of cuttings and core samples. A detailed description of the method and equipment is provided in **Figure 2. 4**. Depending on the geological layers traversed during the drilling process (hard or soft materials), a well bore 90 m deep can be drilled in a period varying from two weeks to more than a month. Collapse events inside the open hole are common, so the drillers frequently have to start the drilling process all over again.

In this way, 9 wells (FD1, FD2, FD3 etc., shown as purple squares on **Figure 2. 3**) were surveyed (from October 2016 to March 2017) which allowed the collection of cuttings and core samples to a maximum depth of about 100 m. The compilation of reliable samples provided 9 drill logs with a good spatial distribution on the plain. In addition, a video well logging device was designed and used at different artesian wells to visualize the lithological formations inside wells. The design of the camera device is illustrated in **Appendix 2**.

The last step was to compute outcrop data and drill logs to obtain a global understanding of the architecture of deposits in the distal zone of Pasuruan.

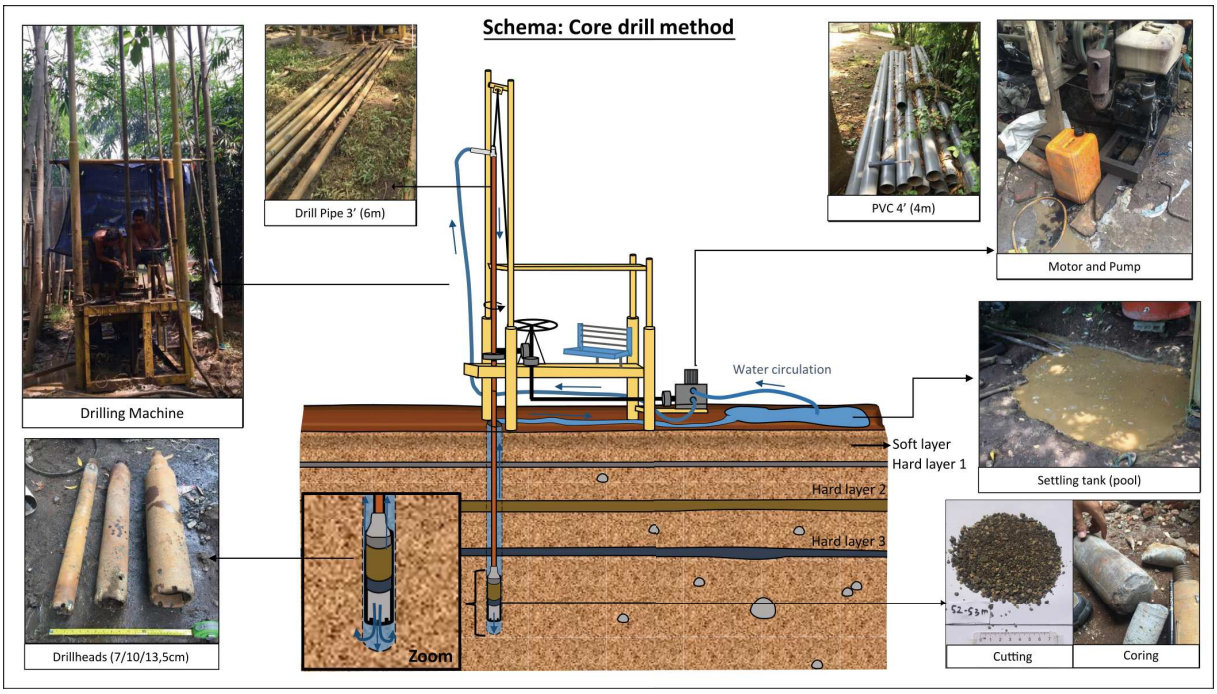

Figure 2. 4. Core drill method applied in the Pasuruan plain.

2.3.3 Geophysical survey

In addition to the geological survey, geophysical investigations using an electrical method (Electrical resistivity tomography, ERT) were performed in the downstream area of the Tengger volcano flank where outcrops are scarce (**Figure 2. 3**). The objectives of this geophysical survey are to define the geological and geomorphological structures related to the outflow context of the main artesian springs (Umbuan and Banyu Biru).

ERT is an indirect ground imaging tool well adapted to hydrogeological issues. This geophysical tool allows non-invasive investigations which are relatively easy to use and which facilitate data processing. It is based on the principle that the distribution of electrical potential in the ground around a current-carrying electrode depends on the electrical resistivity and distribution of the surrounding soils and rocks. The tool allows to measure the electrical resistivity of ground materials. To implement the ERT method, electrodes are hammered into the ground at a constant spacing. A current is transmitted from a logger through two electrodes (A & B), while the passage of this current in the ground creates a potential that is measured with two other electrodes (M & N) (Knödel et al., 2007), (**Figure 2. 5**).

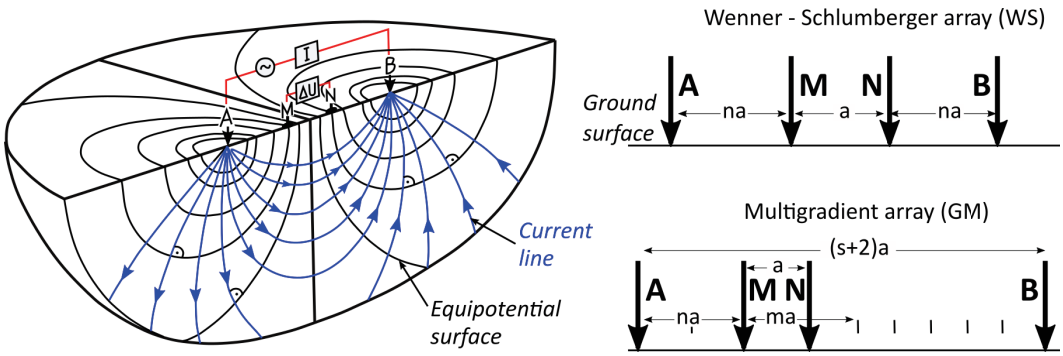

Figure 2. 5. Principle of resistivity measurements with four electrodes (modified after Knödel et al., (2007)) and two arrays configurations presented (WS & GM).

The injection and reception of the current are successively assigned to all the electrodes of the line according to a specific schema related to the array configuration used, such as Wenner-Schlumberger or Multigradient (**Figure 2. 5**). Depending on the position of the electrodes A & B and M & N, the electrical signal is measured at each x and z point. The sum of these measurements provides a profile of 2D electrical values in the {x ; z} plane. The area investigated by the electric field injected into the ground is three-dimensional (hemispherical). However, the results obtained are applied to a plane. To correct for this dimensional transfer, the main assumption in the interpretation of ERT profiles is the absence of lateral variations along the profile. Ohm's law is defined by:

$$R = \frac{U}{I} \tag{2.1}$$

Where R is the resistance (Ohm), U the potential difference (Volt) and I the current intensity (Ampere).
Knowing the U and I values during the injection, R can be inferred. The resistivity ρ (Ohm m^{-1}) of a media is given by:

$$\rho = R \times \frac{S}{L} \tag{2.2}$$

where R is the resistance of the media (Ohm), S the section of the media perpendicular to the current (m^2), and L the length of the media investigated (m). The parameters S and L are defined by the length (known) of the profile and the parameter R is measured by the logger, the electrical signal can then be converted into resistivity. The resistivity profiles thus obtained relate to an apparent resistivity which has to be corrected by a numerical inversion. For inversion of the profiles, the software RES2DINVx64 is classically used to create a two-dimensional (2-D) resistivity model that can be refined depending on the inversion program, noise correction and the scientific issue that needs to be visualized.
Therefore, the ERT tool provides valuable information about the resistivity distribution in the ground, which is directly related to its nature and structure (Audebert, 2015). Resistivity variations can be triggered by factors such as mineralogy, porosity, water occurrence within the materials, the electrical conductivity and temperature of the solutes present (Samouëlian et al., 2005). In volcanic contexts, the use of ERT is challenging because of groundwaters with low

electrical conductivity (usually σ < 150 µS cm^{-1} in volcanic formations without any influence from surrounding active vents) (Custodio, 2007). This groundwater signature hinders the recognition of resistivity contrasts between saturated/unsaturated formations such as observed in volcano-sedimentary deposits.

I – Calibration		
Outcrop		**Drilling log**
L1: Alluvial quarry		FD2 well
L2: Old lava quarry		FD1 well
L11: Aqua factory		Aqua wel
L10: Fresh lava quarry		-
II – Geophysicsinvestigations		
Zone	**Line (n°)**	**Length (m)**
Zone 1	L1	190
	L2	230
	L3	630
	L4	150
	L5	310
	L13	390
	L14	390
Zone 2	L6	540
	L7	470
Zone 3	L8	630
	L9	590
	L12	550
Additional	L10	150
	L11	550
TOTAL	14 lines	5770m

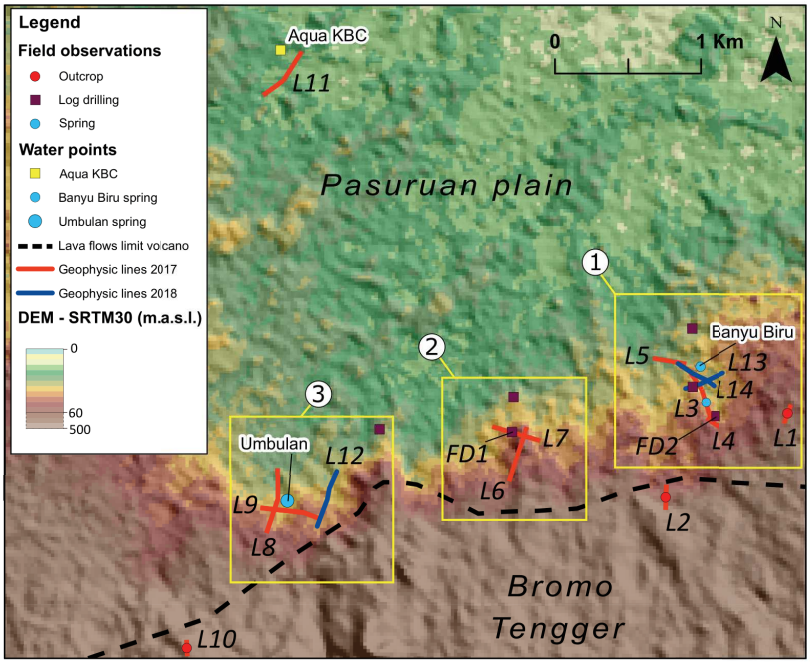

Figure 2. 6. Location map of the geophysical profiles performed in three main investigation zones.

The geophysical investigations were performed in April 2017 and April 2018 (3 weeks of work) with the collaboration of Danone Aqua. The surveys were carried out in 3 main zones judiciously selected to deploy geophysical profiles in the immediate vicinity of the 2 main artesian springs and near key outcrops or well logs. The profiles were performed with the Wenner-Schlumberger and Multigradient array configurations (**Figure 2. 5**). The Wenner-Schlumberger array provides a good depth resolution (Dahlin and Zhou, 2004; Martorana et al., 2017) and is well adapted for vertical soundings, allowing better detection of horizontal layers (Baltassat et al., 2015). The multigradient array provides the best horizontal resolution among the other existing arrays (Dahlin and Zhou, 2006, 2004). A standard inversion was applied.

A total of 14 geophysical lines were operated corresponding to an investigated profile length of 5770 m. For this survey, a SYSCAL PRO system (Iris instruments) was used with a maximum deployment of 8x80m cable length and 64 electrodes spaced at 10 m (i.e. 630 m maximum length) and a maximum depth investigated of about 110 m below surface (L11, 3, 6, 8 ,9). First, a geophysical calibration was performed in two ways:

- Based on the apparent resistivity values obtained from four calibration sites including key outcrops and/or well logs (see **Figure 2. 6**).
- From the field electrical conductivity data measured for each groundwater point on the plain (see Database in section 2.3.1). These electrical conductivity values allow to roughly estimate the resistivity of the aquifer bodies (where ρ = 1/σ, equation 2.2).

The calibration-based resistivity values are used to constrain the interpretations of the further geophysical lines that provide the most reliable hypothesis about the context of artesian spring outflow.

2.4 Results

2.4.1 Groundwater inventory

Up to April 2019, more than 662 water points have been inventoried at the scale of the Bromo-Tengger-Semeru volcanic complex including the Pasuruan plain (**Table 2. 1** and **Figure 2. 7**). The main water points correspond to the artesian well type (red dots), which have attracted a special attention on the Pasuruan plain. The list of dug wells and pump wells inventoried (orange and purple dots) is non-exhaustive, but provides a rough overview of their spatial distribution. All the results for the water points are compiled in the Bromo-Tengger database.

Table 2. 1 Inventory of groundwater points up to April 2019.

Outflow context	Groundwater type (1, 2, 3, 4 ,5)	Notation	Depth (m)	Inventory (number)	North Bromo discharge (L s^{-1})
Spring	1 - Gravity spring	GS	-	54	600
	2 - Artesian spring	AS	-	11	4000
Well	3 - Dug well	DW	2 - 40	114	-
	4 - Pump well	PW	10 - 30	22	-
	5 - Artesian well	AW	30 - 200	461 (+20%)	2400
TOTAL				**662 (+93)**	**≈7000**

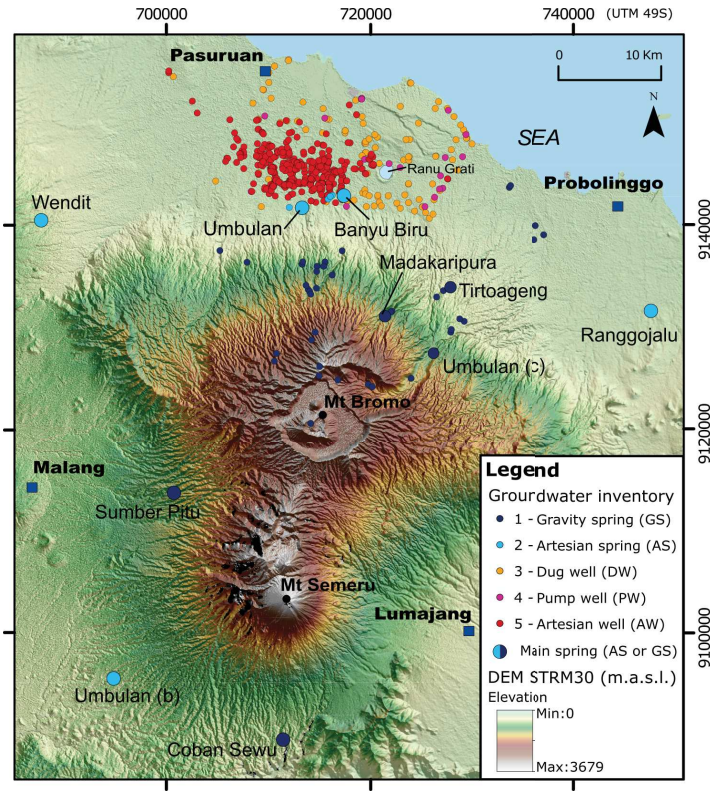

Figure 2. 7. Location map of the inventoried groundwater points

1) There are 54 gravity springs inventoried at the scale of the Bromo-Tengger-Semeru volcanic complex, most of them being found in canyons of the northern flank of Bromo-Tengger (**Figure 2. 7**). These springs are associated with lava flow formations (e.g. Sumber pitu) or in the Sapikerep valley flowing from fractures in ignimbrite deposits (e.g. Umbulan (c)). They correspond mostly to perennial springs with a discharge from 0.1 to more than 1000 L s^{-1}, such as observed at Coban Sewu (**Figure 2. 7**). The total measured discharge of gravity springs on the northern flank of Bromo is about 600 L s^{-1} (**Table 2. 1**).

2) Several artesian springs are located around the Bromo-Tengger-Semeru massif (e.g. Wendit, Umbulan, Banyu Biru, Ranggojalu and Umbulan (b)), corresponding to the main outflows of the volcanic massif (**Figure 2. 7**). Their discharge ranges from 10 to more than 3500 L s^{-1} (e.g. Umbulan). The total outflow measured on the northern flank of Bromo-Tengger is about 4000 L s^{-1}. This value does not include the Wendit and Ranggojalu springs whose outflow context is probably related (or partly) to other volcanic massifs such as the Arjuno and Lamongan volcanoes, respectively.

3) Dug wells are located over the whole Pasuruan area with depths ranging from several metres to more than 30 m, especially near the first relief of Bromo-Tengger where the elevation increases slightly (or in the relief north of Ranu Grati). The total dug well discharge is unknown since it is not continuous. However, it is probably significant considering the density of dug wells in Pasuruan (almost one for each house).

4) Pump wells are mainly located in the eastern paddy field areas (near the Ranu Gati maar), (**Figure 2. 7**). This type of well usually does not exceed 30 m depth. They substitute artesian wells in the East and their discharge observed in the field is frequently higher than 5 L s^{-1}, depending on the strength of the motor pump used. The total discharge of these pump wells is unknown.

5) Inventoried artesian wells (free-flowing artesian wells) are very dense on the Pasuruan plain (461), being mostly located around the paddy fields. They are usually equipped with a simple PVC casing generally extending to no more than 20-30 m depth. They flow continuously out into the environment without any valve control (**Figure 2. 8**). In the villages, artesian wells are classically deeper to ensure a higher discharge, most of them being connected to a local water supply system providing water to each house. An overflow outlet is frequently observed near the well head that avoids water stagnation within the pipes (**Figure 2. 8**). The discharge of artesian wells ranges from 0.1 to more than 35 L s^{-1} depending on the depth, diameter and location. The depth ranges from 40 m (e.g. near Banyu Biru spring) to more than 200 m depth at the extreme west of Pasuruan where elevation increase slightly. There are no longer any artesian wells found near the coast of Pasuruan, or farther east of Ranu Grati lake (**Figure 2. 7**). Considering the average discharge of artesian wells is 4.1 L s^{-1} and that about 20% were omitted from the inventory survey, the total outflow measured in the Pasuruan can be estimated at about 2400 L s^{-1}. However, this first value is purely indicative and does not account for the artesian wells in the west of Pasuruan which have not been inventoried.



Figure 2. 8. Artesian wells inventoried in paddy fields (left, middle) and in a village (right).

A detailed description of the main springs of the Bromo-Tengger-Semeru volcanic complex is given in **Appendix 3**.

2.4.2 Geological survey

Based on the geological survey carried out from the northern flank of the volcano to the Pasuruan plain, six main outcrops in quarries were selected as "key outcrops" that correspond to the main lithologies identified on the volcano-sedimentary plain (see location map in **Figure 2. 3**).

Table 2. 2. Selection of key outcrops from the 2016-2017 geological survey.

Location map	Outcrop n° (see Figure 2. 3)	Name of site	Identified lithology
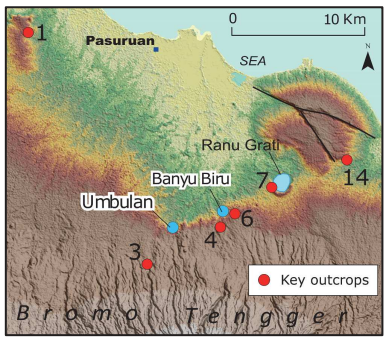	3 and 4	Fresh lava quarry Old lava quarry	Lava flows (weathered or not)
	6	Alluvial quarry	Reworked pyroclastic deposits
	7	Ranu Grati quarry	Phreatomagmatic deposits
	14	Ignimbrite quarry	Ignimbrite deposits
	1	Sedimentary quarry	Carbonates and alluvial deposits

The key outcrops n° 3, 4 and 6 are described below. Descriptions of the other key outcrops are provided in **Appendix 4**.

2.4.2.1 Lava quarries (fresh and weathered)

The fresh lava quarry (key outcrop n° 3) is composed of a massive thick and unweathered lava flow (more than 10 m), slightly fractured, which splits into a lamellar structure (key outcrop n° 3; **Figure 2. 9. a**). This unweathered lava flow type represents the framework of Bromo-Tengger.

In subsurface or at outcrop crop, weathering processes trigger the dismantling of massive lava into blocks showing "onion skin" weathering (key outcrop n° 4; **Figure 2. 9. b)**. The advanced state of erosion of the lava is represented by saprolite formations composed of lava blocks, sand and clay-rich materials (**Figure 2. 9. c**) as observed in granitic contexts. Under tropical climates, intense leaching creates lava boulders (block fields; **Figure 2. 9. d**). These lava blocks (boulders) can be reworked by stream transport during torrential flow.

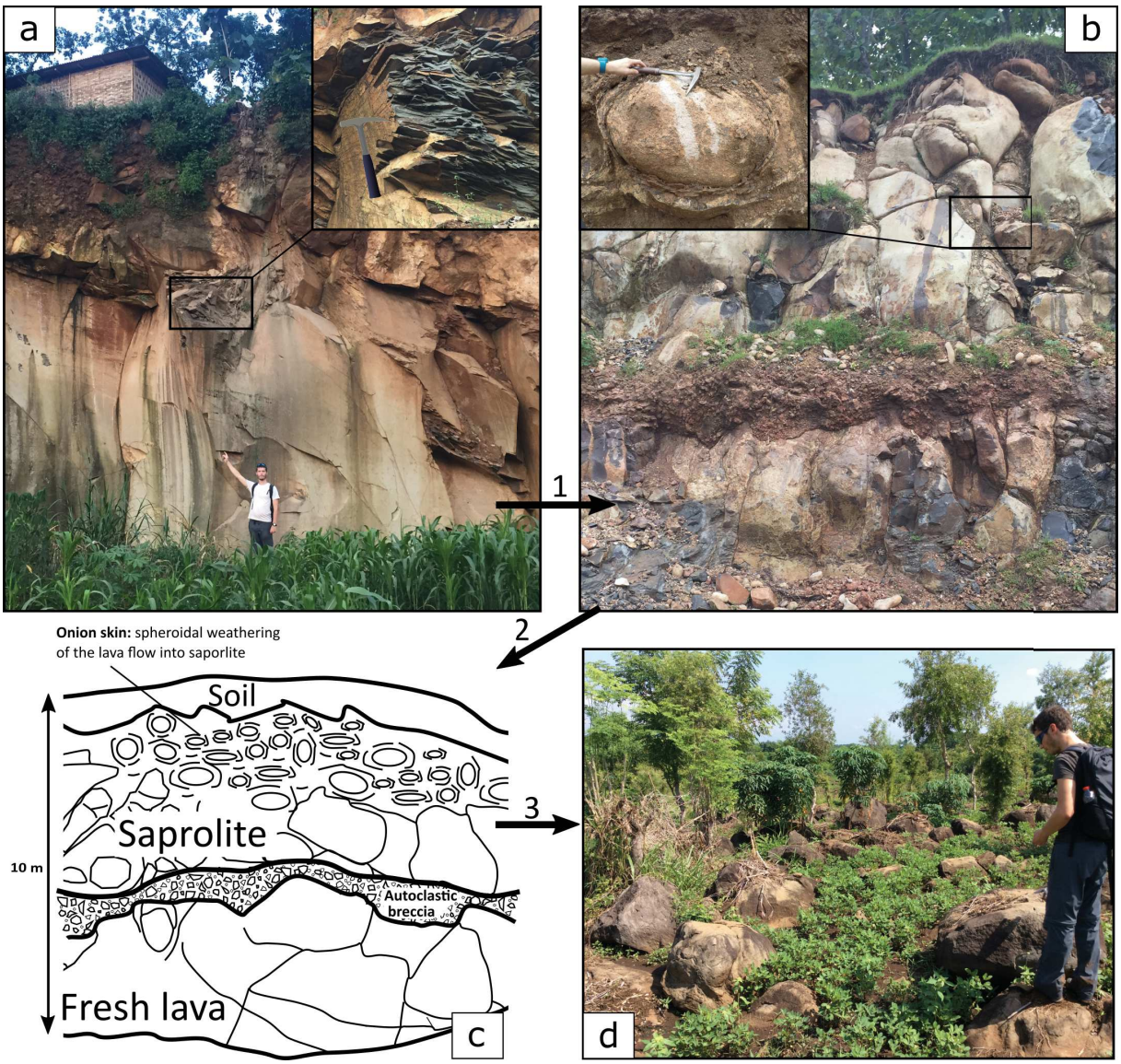

Figure 2. 9. Steps of lava flow weathering with **a.** Massive slightly fractured fresh lava flow (key outcrop n° 3), **b.** Old lava flow with "onion skin" weathering (key outcrop n° 4), **c.** Weathering of lava flow leading to saprolite formation, **d.** Final weathering stage of the top lava flow unit represented by lava boulders (blocks field) in surface.

2.4.2.2 Alluvial quarry

This quarry is entirely representative of a typical volcano-sedimentary series as observed on the Pasuruan plain. The series is mainly composed of reworked pyroclastic deposits, bedded pyroclastic fall and surge deposits as well as alluvial braided and sheetflood pyroclastic deposits (cemented or not). Paleo-channels filled by coarse materials (e.g. rounded blocks) can be observed crossing these latter formations (**Figure 2. 10**). In this quarry, the volcano-sedimentary layer is about 30 m thick, covering lava boulders as described in the previous key outcrops.

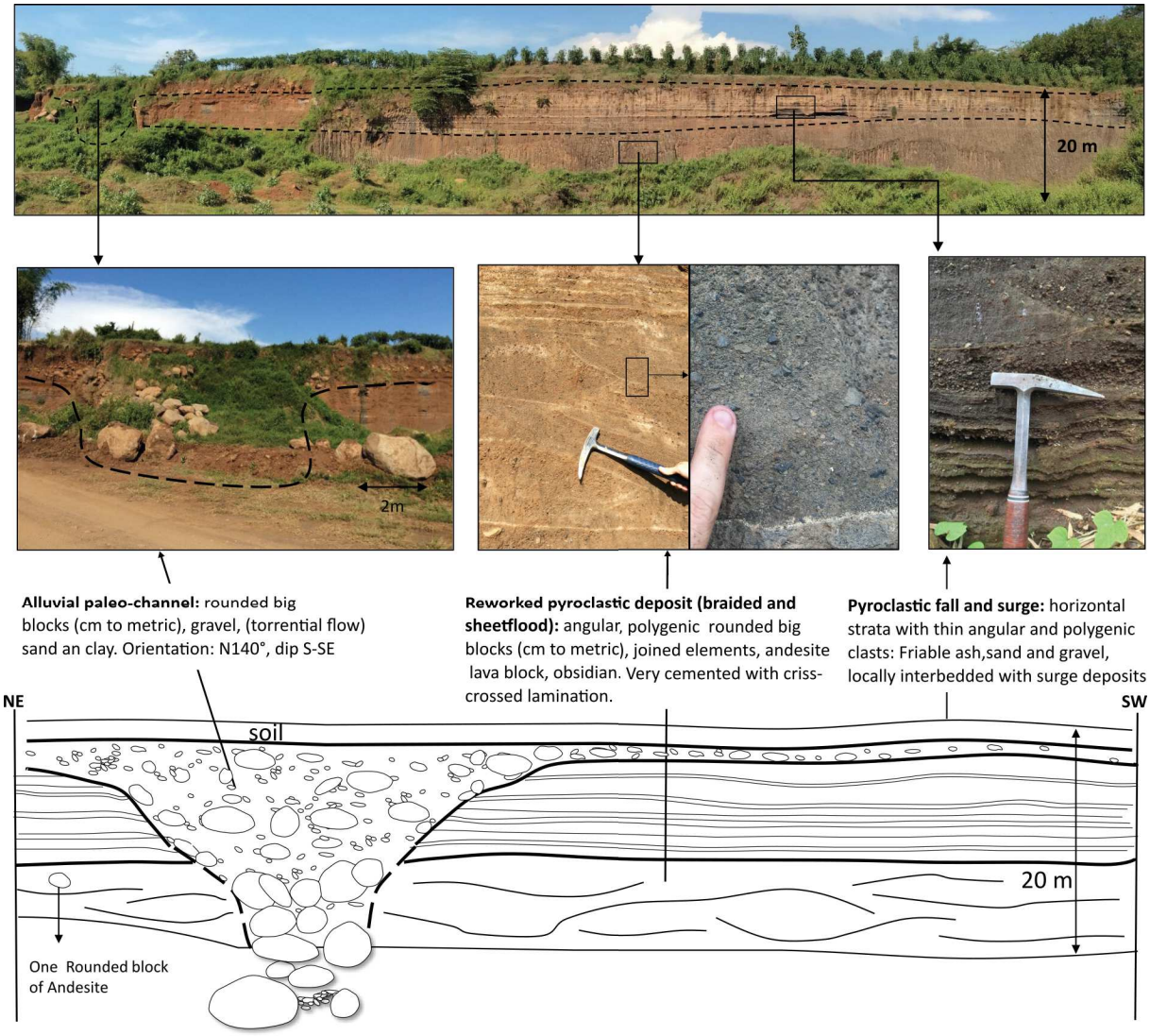

Figure 2. 10. Geological description of the alluvial quarry near Banyu Biru spring.

2.4.2.3 Ranu Grati quarry

This quarry (key outcrop n°7) is composed of alternating phreatomagmatic deposits corresponding to the proximal deposits of a large explosion maar (diameter about 1300 m), including fall deposits, wet/dry surges and explosion breccias (see detailed description in **Appendix 4**). The height of the phreatomagmatic formation is more than 30 m above the surface (probably thicker in the subsurface) and spreads in the form of a tuff ring.

2.4.2.4 Ignimbrite quarry

In the region, ignimbrites are mainly used as of construction blocks since this deposit is very well cemented (see description in **Appendix 4**). At outcrop, ignimbrites are characterized by welded pyroclastic deposits about 10 m thick, composed of pumice, obsidian, and andesite fragments alternating with thin ash layers. Several blocks of andesite and obsidian (cm) are observed within the welded matrix of the ash fall. This unit is successively overlain by fluvial deposits (gravel in an unconsolidated sandy matrix) and weathered lahar deposits composed of polygenic materials with a brown clayey ground-mass.

2.4.2.5 Carbonate-alluvial quarry

This quarry located at the extreme northwestern edge of Pasuruan plain is the only outcrop where carbonate deposits are observed. The outcrop is composed of alternating lahar deposits (poorly weathered), white marly layers (sometimes with travertine and algal concretions) and fluviatile deposits with rounded clasts. This outcrop forms a residual hill of about 30 m high, made up of marine deposits and distal reworked volcanic products (see **Appendix 4**).

2.4.3 Drilling survey

The geological compilation was drawn up by projecting the key outcrops and well logs onto a cross-section of the Pasuruan plain (**Figure 2. 12**). The 19-km-long topographic profile first follows a S-N direction, then changes to SW-NE in order to include the main lithologies and structures of the plain as far as the fault in the northeastern part of Pasuruan. This compilation is supplemented by hydrogeological information such as the flow rate (Q) of artesian springs and wells, along with water inlets identified on the well logs. The electrical conductivity and temperature are also given on some of the wells.
From the geological point of view, we can simplify the lithologies into four main units:

- Lava flows and volcanic breccia unit: the fresh lava flows (unweathered, **Figure 2. 11. a**) are located on the volcano flank, while old lava flows (weathered) are located around the break in slope of the volcano (in grey). These two distinct units frequently alternate with autoclastic breccias (purple) which are generally associated with water inlets ($Q < 1$ L s^{-1}). The Umbulan and Banyu Biru artesian springs are located - at least partly – within the lava flows and volcanic breccia unit.

- Volcanic sand unit: the major aquifer system of Pasuruan, yielding the highest productivities, is composed of medium-coarse grained volcanic sands (**Figure 2. 11. b**), derived from pyroclastic deposits and alluvial remobilization, in yellow. This unit is still found at more than 100 m depth and includes several consolidated layers of pyroclastics (in red; **Figure 2. 11. c**) or lahar/polygenic breccia (in brown; **Figure 2. 11. d**) which are very difficult to correlate with each other. Drilling within these consolidated layer triggers successive water inlets. Their flow progressively increases with depth ($1 < Q << 8$ L s^{-1}), also depending on the well diameter. The well logging video camera allows to visualize the diverse facies of this volcanic sand unit (**Figure 2. 11. e, f, g, h**).

- Pyrcolastics cover unit: pyroclastic materials (fall and reworked) seem to overlie both the lava flows in the south and the volcanic sand in the north. These units, which can be observed in the southern alluvial quarries (key outcrop n°6), cover the Pasuruan plain to a depth of several tens of metres. They are considered to be aquifers or aquitards depending on the granulometry, ranging from ashes to coarse volcanic sand/blocks, and the degree of cementation. This unit probably stores the shallow unconfined aquifer in which the local pump wells or dug wells are drilled.

- Distal deposits unit: around the Pasuruan active fault, deltaic/marine sediments (in blue) are associated with weathered lahar deposits (in pink) and cover a thick series of well-cemented and poorly fractured ignimbrites (in black). This unit is relatively less permeable (more clayey or cemented) than the previous ones. Only a few dug wells are inventoried in this area, all showing a very low productivity.

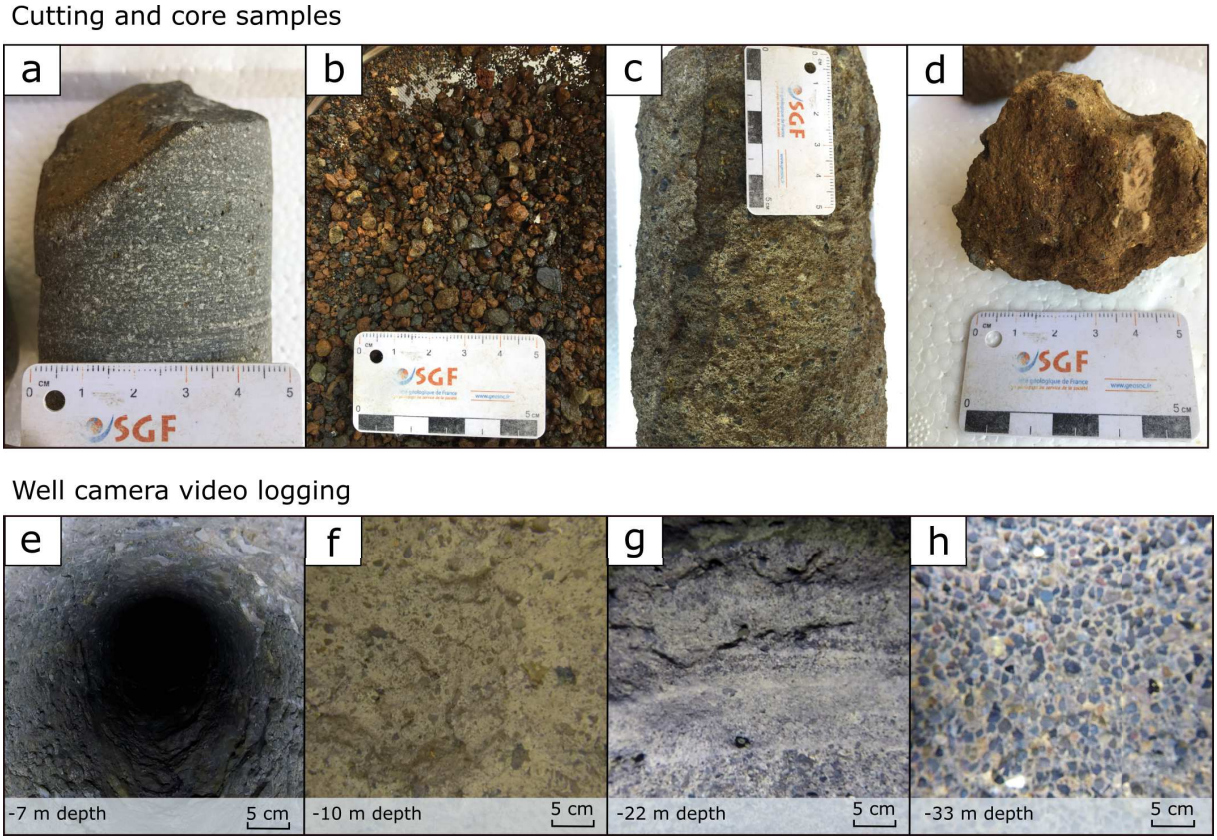

Figure 2. 11. Cores and cutting samples provided from the drilling survey with **a.** andesitic lava core collected at well FD1 at 15 m depth, **b.** Coarse-grained volcanic sand collected at Aqua wash well at 80 m depth, **c.** Cemented pyroclastic deposits, **d.** Clayey and cemented lahar deposits collected at well FD4 at 70 m depth. Well logging video performed in artesian well B33, with **e.** A vertical downhole view, and a horizontal view with different types of cemented pyroclastic deposits (**f, g, h**).

From the hydrogeological point of view, artesian productive inlets are located between 0 and -100 m.a.s.l. (**Figure 2. 12**) depending on the position of the well on the plain. The well discharge is different according to the depth attained, generally increasing with depth. The electrical conductivity and temperature of the groundwater increase northward, from 200 to 400 µS cm^{-1} and from 23 to 26°C, respectively.

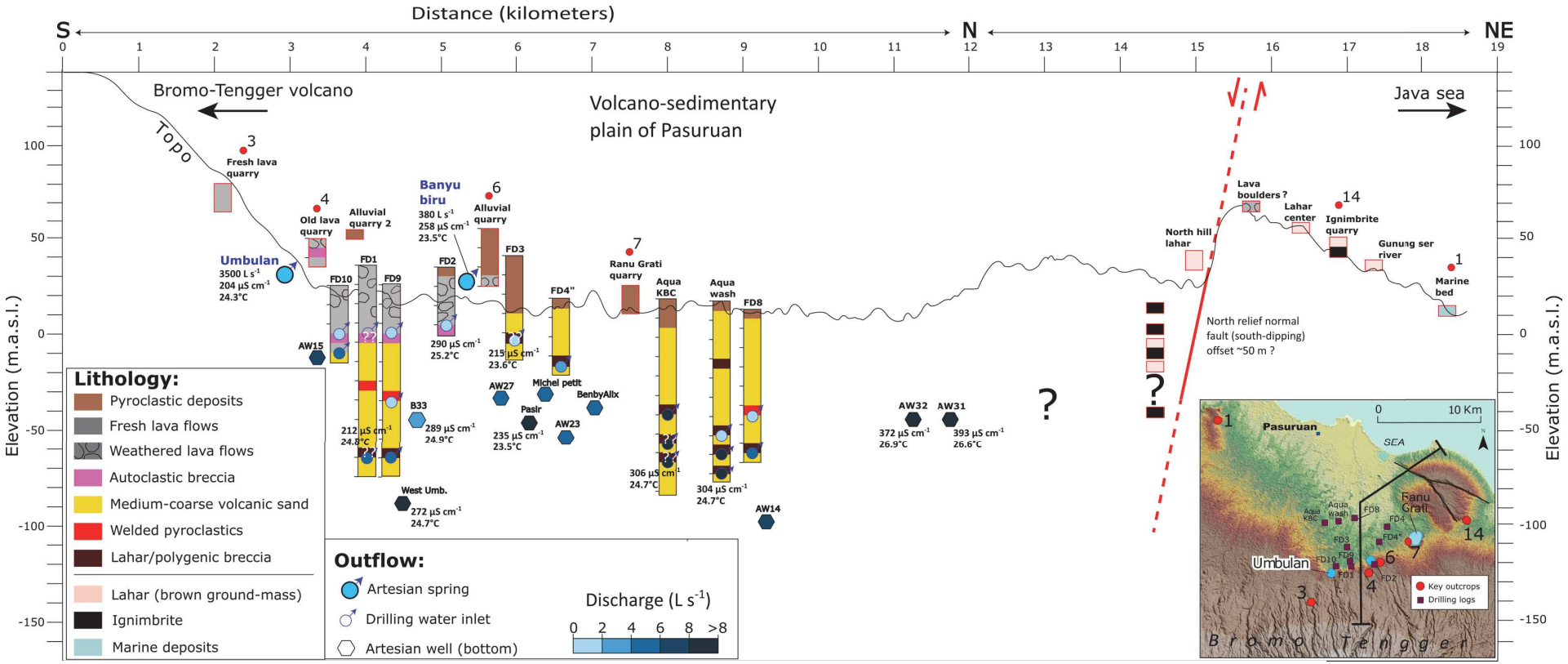

Figure 2. 12. Compilation of geological and hydrogeolgoical data along a S-N-NE cross section of the Pasuruan plain

2.4.4 Geophysical survey

2.4.4.1 Calibration

The geophysical calibration was performed using the lithologies identified from four main outcrops and well logs (geophysics lines 1, 2, 10 and 11) and from the electrical conductivity measured in the field from artesian wells/springs and dug wells, related to the confined and unconfined aquifers of Pasuruan, respectively. The calibration results are presented in **Table 2. 3**. The color coding represents the apparent resistivity in unsaturated conditions for soil, paleo-channels, pyroclastic deposits and un/weathered lava flows. In unsaturated conditions, a color range for the resistivity value is inferred from soil, tuff and volcanic sand materials. From the electrical conductivity measurements, the unconfined aquifer should be represented by values of about 5 to 20 Ω m^{-1}, while the confined aquifer body may reflect 20 to 50 Ω m^{-1}. However, these latter values are purely indicative and do not take into account the additional resistivity of the "store-material".

The geophysical calibration lines and the electrical conductivity measurements are provided in **Appendix 5** and **Appendix 6**, respectively.

a

Lithology calibration	Unsaturated material		Saturated material	
	Resistivity (Ohm m^{-1})		Resistivity (Ohm m^{-1})	
	W-Schlumberger & Multigradiant		W-Schlumberger & Multigradiant	
	interval	Mean	interval	Mean
L1/L11 - soil	20 40 80 120	50		
L1/L11 - Paleo-channel (sand + lava blocks)	160 320	200	60 - 320?	200?
L1 - Pyroclastic deposits	160 320 640 1280	960	10 - 80?	<80?
L2 - Weathered lava flow	40 80 120	80	<40?	20?
L10 - Fresh lava flow	160 320 640 1280	320	/	/
L11 - Soil & tuff	/	/	5 10 20 30	15
L11 - Volcanic sand (lapilli)	/	/	20 40 80	50

b

Aquifer formation calibration					
Resistivity (Ohm m^{-1})	Unconfined: 5 10 20	Confined: 40 80 160 320 640			
Confined aquifer (from artesian wells & springs)					
Electrical conductivity (µS cm^{-1})	400	350	300	250	200
Resistivity (Ohm m^{-1})	25	29	33	40	50
Range color resistivity					
Unconfined aquifer (from dug wells)					
Electrical conductivity (µS cm^{-1})	2000	1500	1000	700	400
Resistivity (Ohm m^{-1})	5	6	10	20	25
Range color resistivity					

Table 2. 3. Results of the resistivity calibration from **a.** key outcrops and well logs and **b.** from electrical conductivity (converted to resistivity value) of the groundwater from artesian springs/wells and dug wells (i.e. confined and unconfined aquifers).

2.4.4.2 Zone 1

Based on the previous calibration and the additional outcrop/well log information identified in the field, it is possible to identify four main resistivity units (**Figure 2. 13. a, b**):

- From 5 to 40 Ω m^{-1} in the sub-surface (mainly in dark blue color): may represent reworked lava boulders and alluvial deposits with sand and rich clay-rich materials (=low resistivity) about 20 m thick. The FD2 well log confirms the existence of such a formation that seems to show a paleo-channel shaped geometry on line 13 (**Figure 2. 13. a**). This unit probably contains an unconfined aquifer which is identified at the surface by the FD2 and Banyu Biru 2 springs;

- From 40 to 120 Ω m^{-1} (mainly in dark green color): may represent weathered lava flows as observed in the old lava quarry on calibration line 2. The massive and unweathered part is represented by the highest resistivity values (in red color), supported by the resistivity values (> 320 Ω m^{-1}) of the fresh lava flows identified on calibration line 10.

- From 120 to 240 Ω m^{-1} (mainly yellow/brown color): may show unsaturated and cemented pyroclastic deposits as observed on calibration line 1. This formation crops out at around Banyu Biru spring (outcrop 1) and covers the bottom of the Banyu Biru basin. The thickness varies from 10 m (near FD2 well) to more than 30 m downstream of the Banyu Biru spring.

- From 20 to 40 Ω m^{-1} (mainly light blue color) on line 5: may represent the confined aquifer developed in the volcanic sand (lapilli-tuff) formations identified on calibration line 11. The resistivity values of this formation match with the electrical conductivity of Banyu Biru water, which is 256 μS cm^{-1} (i.e. ~40 Ω m^{-1}) with a temperature of 23.3°C. The confined aquifer body appears to occur at about 20 m depth in the downstream part of the Banyu Biru spring.

The Banyu Biru artesian spring outflows between lines 5 and 14 (**Figure 2. 13. a**), which seems to correspond to the transition zone between lava flows and volcanic sand units.

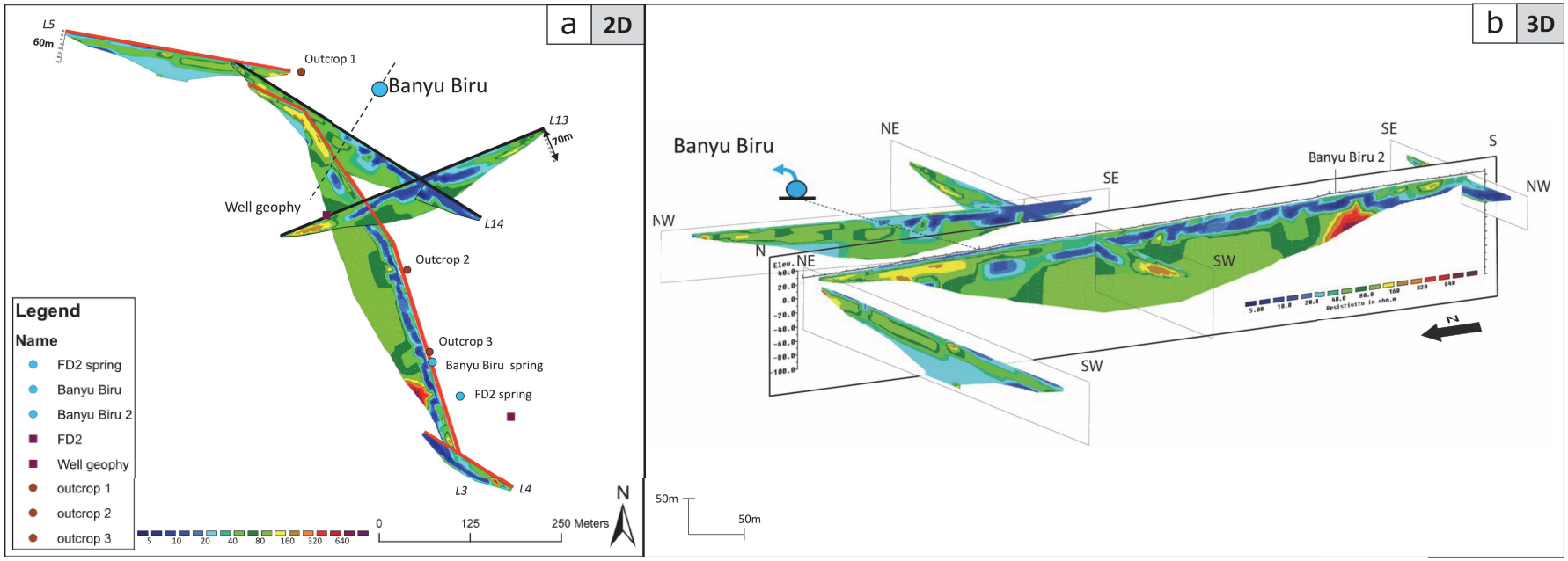

Figure 2. 13. 2D and 3D representation of the geophysical profiles of zone 1 surrounding the Banyu Biru spring.

2.4.4.3 Zone 2

The geophysical profiles (L6 and 7) are supported by supplementary information from the well logs FD1, FD9 (see **Figure 2. 12**) and the outcrop of lava boulders observed in the South (outcrop 1), illustrated in **Figure 2. 14**. **a. b.**

- On profiles L6 and L7, the lava boulders are associated with low resistivity values ranging from 5 to 40 Ω m^{-1} (mainly in dark blue color) in the south of the profile, and are also observed towards the east on profile L7. The boulders may cover a massive and thicker lava formation represented by resistivity values ranging from 120 to 320 Ω m^{-1} (mainly in brown to yellow color).

- Resistivity values ranging from 60 to 80 Ω m^{-1} could correspond to two distinct units: i) weathered lava flows as suggested by calibration line 2 or ii) slightly saturated volcanic sand as suggested by well log FD1, where no lava flows or boulders have been identified from 35 to 110 m depth. The log observations from the FD1 well favor the second hypothesis. Therefore, this new resistivity range (dark green in color) corresponding to slightly saturated volcanic sand leads to reconsider the interpretation of zone 1 where weathered lava flows were initially suggested.

Therefore, this zone is considered as a geological transition zone between old lava flows (visible as field boulders at the surface) and the volcano-sedimentary plain of Pasuruan mainly composed by sandy materials (medium-coarse grained sand). The latter is mixed with lahars and cemented pyroclastic layers which are mostly impervious, thus explaining the origin of the artesian level found at around 80 m depth below surface in well FD1 (**Figure 2. 14**. **a. b**).

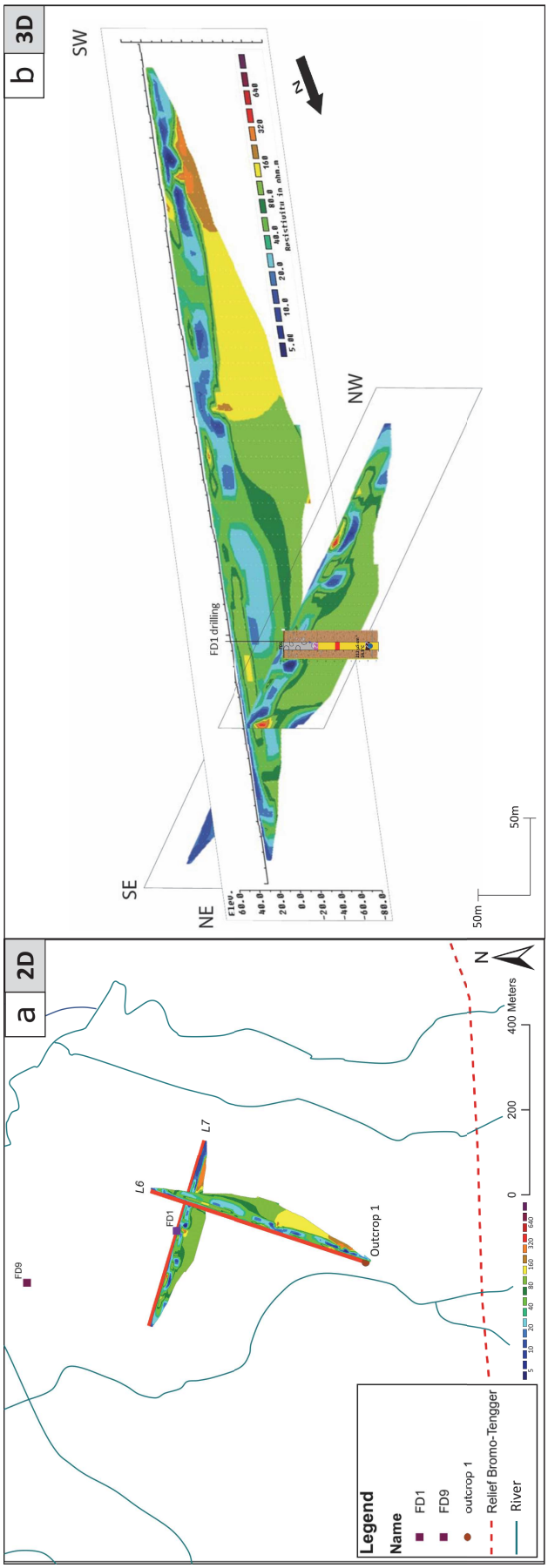

Figure 2. 14. 2D and 3D representation of the geophysical profiles of zone 2 surrounding the FD1 well log.

2.4.4.4 Zone 3

The geophysical profiles L8, L9 and L12 are illustrated in **Figure 2. 15** and supported by field observations from outcrops 1 and 2 and the well log FD10 (see **Figure 2. 12**). The profiles L8, L9 and L12 are composed mainly of:

- Lava boulders mixed with sand in the sub-surface, forming a unit about 20 m thick represented by low resistivity values from 5 to 60 Ω m^{-1} (mainly in light green to dark blue). The difference of resistivity between the southern and northern (green to blue color) part of the profile is probably related to paddy field irrigation that partly saturates the boulder unit in the North of the profile;

- Massive/unweathered lava flows under the boulder unit are represented by high resistivity values ranging from 120 to 1280 Ω m^{-1} (in yellow to purple) as illustrated by calibration line 10. This massive lava reaches more than 110 m depth.

There is no clear evidence of any resistivity contrast at the location of the Umbulan outflow, but it is almost certain that this artesian spring is associated with the massive lava flow unit as observed in well log FD10. In addition, there are no artesian wells in the southern part of Umbulan, which suggests the absence of a confined aquifer between the lava boulders at the surface and the massive lava flows found at depth.

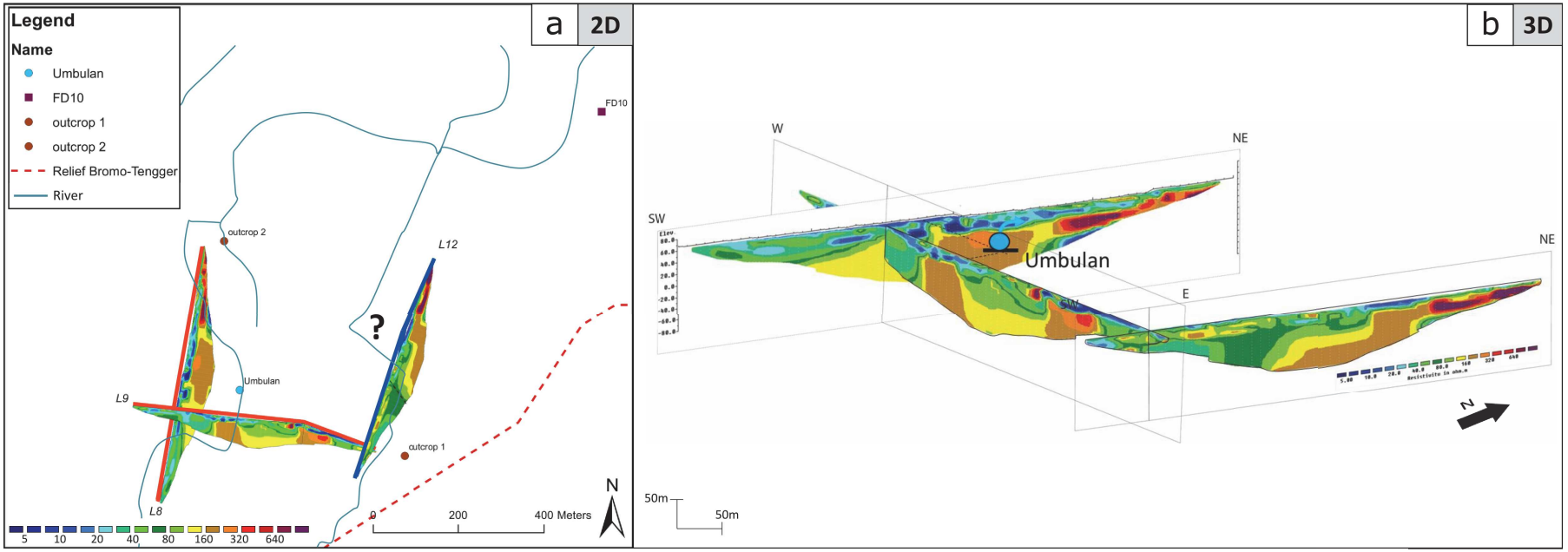

Figure 2. 15. 2D and 3D representation of the geophysical profiles of zone 3 surrounding the Umbulan artesian spring.

2.5 Discussion

2.5.1 Geological and hydrogeological characterization

Based on the new insights from geological, drilling and geophysical surveys, a reservoir conceptual model is proposed here for the Pasuruan plain (**Figure 2. 16**).

The conceptual model simplifies the complex lithologies of this volcano-sedimentary basin into four main units: 1) un/weathered lava flows with intercalated autoclastic breccias, 2) pyroclastic deposits covering the Pasuruan plain, 3) volcanic sands intercalated with consolidated lens (welded pyroclatics or lahars).

The lava boulders identified in previous surveys could be inherited from the distal part of a lava flow, giving rise to outcrops that constitute a preferential weathering zone. Boulders may also have been eroded on the volcano flank, and then transported downstream by rivers and buried in paleo-channels on the plain, as observed at Merapi by Selles, (2014). However, in contrast to observations at Merapi, the boulder formations on the Pasuruan plain are mainly aquitards since the matrix is predominantly composed of clay-rich materials as shown by the low resistivity values acquired during the geophysical survey. Therefore, on the Pasuruan plain, it is rather complicated to consider paleo-channels as being due to a preferential circulation of groundwaters that supplies the artesian wells and springs. In fact, the presence of autoclastic breccias within lava flows allows a preferential groundwater circulation that explains the good productivity of some lava units. The artesian conditions of wells located in the lava zone are probably due to the water circulation in breccias and the presence of a confined aquifer hosted by the underlying volcanic sand.

The confined aquifer of Pasuruan is represented by an artesian multilayered volcano-sedimentary system. The diverse water inlets found at different depths in the same well suggest a complex multilayered configuration constrained by impermeable lenses of cemented layers of pyroclastics or lahars that intersect the volcanic sands aquifer. The age of the volcanic sand formation is not clear in the literature, but according to Miftakhul Fajar and Nogroho (2018), the youngest lava flows outcropping out on the plain could be younger than some of the volcano-sedimentary series.

On the plain, there is an increase in electrical conductivity and temperature of groundwaters towards the north, respectively from 200 to 400 µS cm^{-1} and from 23 to 26°C, suggesting an increase in groundwater flow circulation and transit time to the North. The distribution of artesian wells listed by the hydrogeological inventory seems to indicate that the artesian aquifer is limited to the North of Pasuruan. To explain this distribution, two hypotheses can be proposed, i) the confined aquifer dips northwards, thus preventing wells from reaching the artesian aquifer which is probably too deep (> 200 m), ii) the confined aquifer is bounded by thin coastal and cemented deposits such as those observed in the North-East (lahars, ignimbrites and thin marine/deltaic deposits, mostly impermeable). The ignimbrite deposits in this area are derived from the Sakapura ignimbrite, in relation to the collapse of the Sapikerep valley, whose distal part near the Pasuruan coast is often reworked into lahars or fluviatile deposits (Mulyadi,

1992). These ignimbrite formations are cut by the Ranu Grati maar and their eastward extension may represent the eastern boundary of the artesian aquifer. However, it is important to mention the high productivity of the pump well ($Q > 5$ L s^{-1}) in this area, which could reflect upward leakage to the unconfined aquifer from an underlying artesian aquifer, also explaining the perennial flow of the Ranu Grati lake ($Q > 500$ L s^{-1}). The hydrogeological role of the North-East Pasuruan active fault is not clearly defined, but the normal fault displacement of impermeable layers such as ignimbrites and lahar deposits may favor the hypothesis of an impermeable limit.

The pyroclastic cap (about 10 to 30 m thick) observed over the entire surface of the Pasuruan plain is a semi-permeable formation. Indeed, this formation hosts an unconfined aquifer on the whole Pasuruan plain as suggested by the wide distribution of dug wells. These permeable conditions are probably related to the explosion of the Ranu Grati maar that provided huge quantities of loose pyroclastic fall deposits, which also could have been supplied by the last Bromo-Tengger adventive cones such as Gunung Tinggi and Gunung Pandak located on the volcano flank about 1 km from Umbulan Spring (Zaennudin et al., 1994). This pyroclastic cap can also be impermeable, as observed at the bottom of the Banyu Biru basin, depending on the degree of cementation.

The volcano-sedimentary plain of Pasuruan may be about 300 m thick according to the literature, which describes similar recent alluvial deposits in the Kendeng basin surrounding the Lusi mud volcano located about 40 km north of Pasuruan (Mazzini et al., 2017; Moscariello et al., 2018). In fact, several artesian wells to the west of Pasuruan show a drilling depth of about 200 m that seems to confirm the thickness of the volcano-sedimentary plain. However, the East-West extent of the artesian aquifer is still not clearly defined since artesian wells are still observed near Arjuno volcano in the West and an important artesian spring "Ranggojalu" is located near Probolinggo city (**Figure 2. 7**).

From the convergence of different types of survey method, it is clear that the artesian springs (Umbulan and Bayu Biru) are located in areas with lava flows. Their precise outflow context is discussed in the following section.

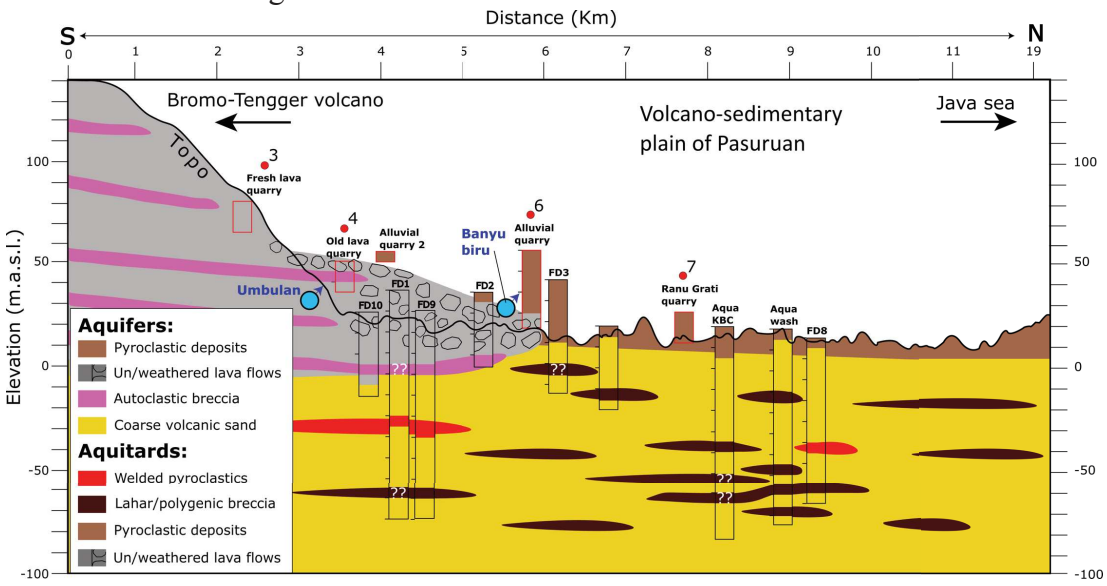

Figure 2. 16. Reservoir conceptual model for the plain of Pasuruan.

2.5.2 Outflow context of artesian springs of volcanic piedmont area

The artesian springs of the Bromo-Tengger piedmont are located on lava formations such as the massive lava flows at Umbulan and lava boulders at the Banyu Biru spring, respectively. The termination of distal lava flows at the foot of the volcano cannot alone explain the existence of such important local artesian springs. In this latter configuration, we would be more likely to observe a high density of artesian springs spreading radially all around the volcano.

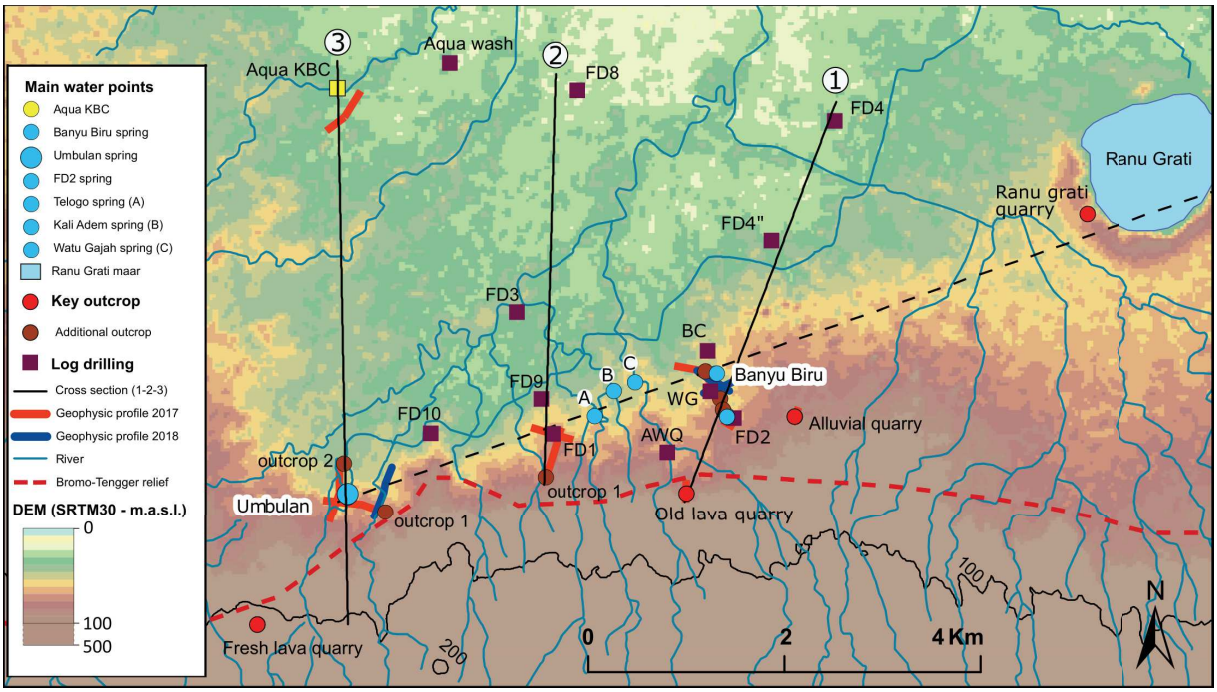

Figure 2. 17. Map showing location of cross-sections on the plain of Pasuruan.

From a hydrogeological point of view, the presence of a SW-NE-trending fault zone seems to be most reliable hypothesis to explain the outflow context of artesian springs. This hypothesis is supported by the following arguments:

1) From the groundwater points inventory, we can identify three new artesian springs with a small discharge (< 20 L s^{-1}) located on the plain between Umbulan and Banyu Biru spring (**Figure 2. 17**). It is interesting to note the perfect alignment between Umbulan, the 3 new artesian springs (A, B, C), Banyu Biru and the Ranu Grati maar. Indeed, the alignment with the Ranu Grati maar is in agreement with a fault zone which has caused a major phreatomagmatic explosion linked to a magmatic intrusion;

2) A drainage network anomaly is clearly visible around the artesian springs (**Figure 2. 17**). The streams are initially oriented N-S down the volcano flank, but suddenly show a change in direction to the North-East. This is particularly visible on the geophysical profiles in zone 3, as presented in **Figure 2. 15. a**;

3) The five topographic cross-sections along the supposed fault show a similar break of slope that could be associated with the fault plane (**Figure 2. 18**);

4) A pre-existing fault system can terminate where another one appears. This is the case of the North Pasuruan active fault (**Figure 2. 18**), which produces geomorphological scars which terminate abruptly where the new identified fault is supposed to extend;

5) The major tectonic structures of East Java are normal (E-W) and strike-slip faults (NE-SW), inherited from the previous geodynamic contexts (Marliyani, 2016; Susilohadi, 1995).

Based on the above arguments, we can consider that a NE-SW strike-slip fault is at the origin of the piedmont artesian springs. Indeed, in volcanic areas, faults are conductive when they traverse welded tuffs, but this is not the case with the non-welded tuffs (Hinds et al., 1999).

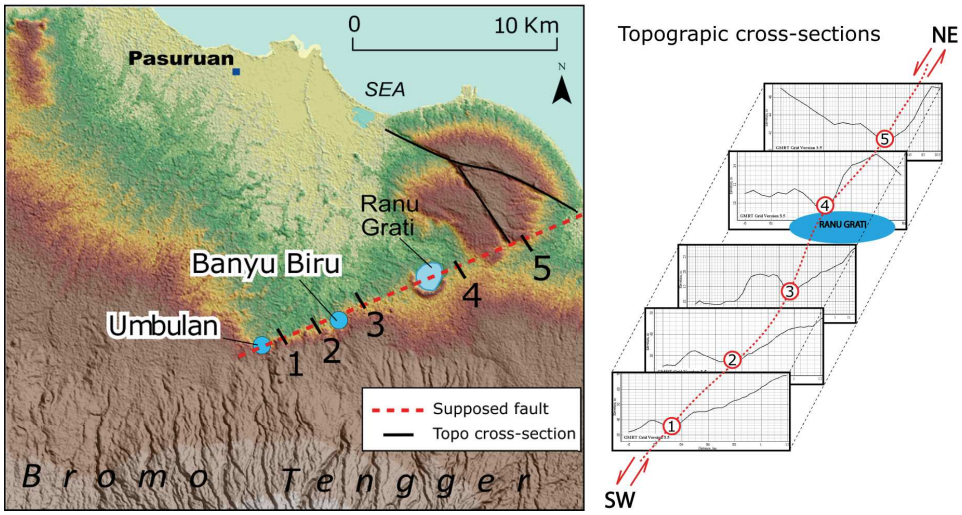

Figure 2. 18. Correlation of five topographic cross-sections along the supposed strike-slip fault on the volcano-sedimentary plain of Pasuruan.

Three cross-sections are based on the projection of data compiled from drilling and geophysical surveys (1, 2 and 3; **Figure 2. 17** and **Figure 2. 18**). This provides a global overview of the geometry of the volcano-sedimentary plain as well as the outflow context of artesian springs.

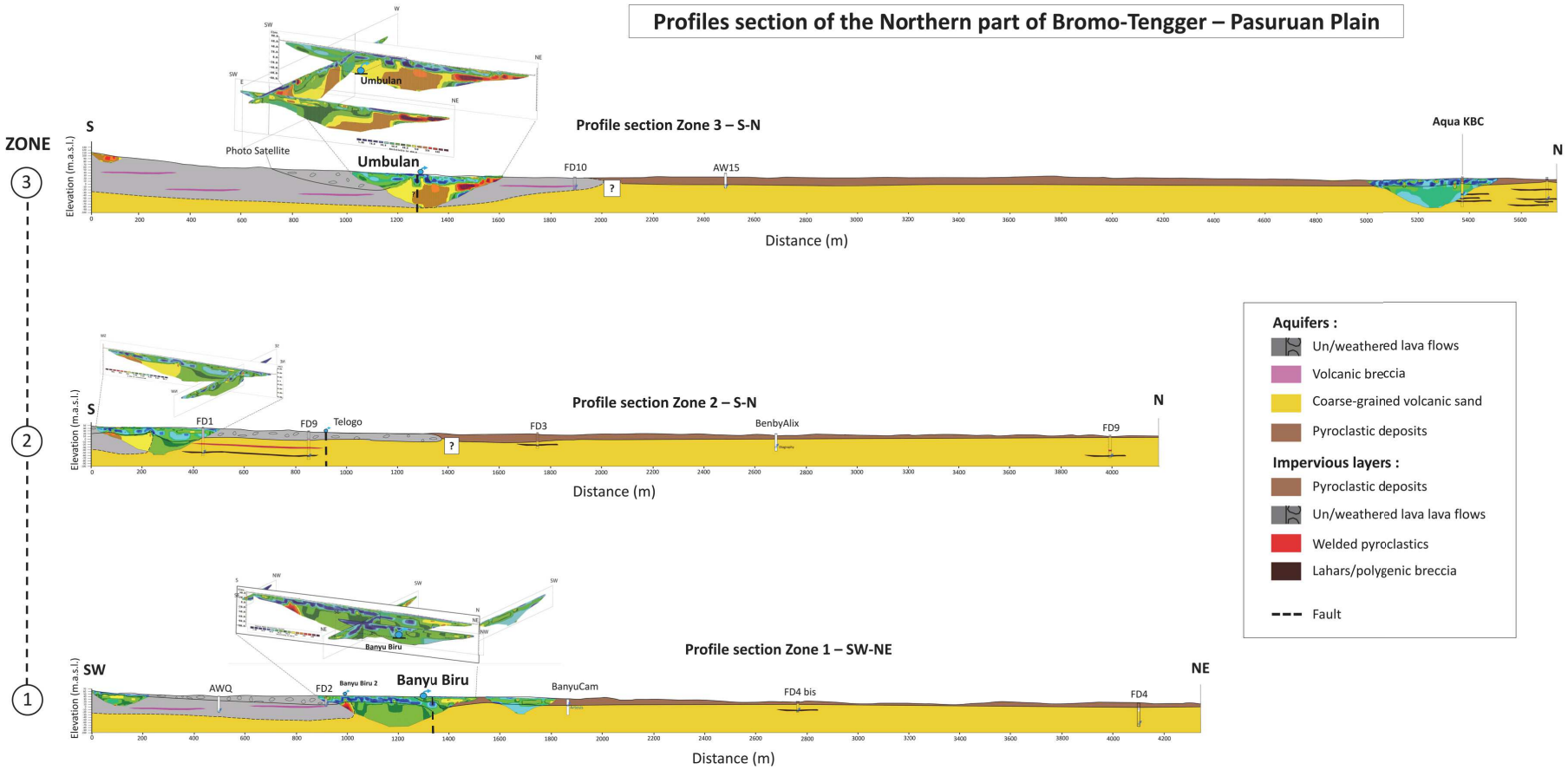

Figure 2. 19. Drilling and geophysical surveys synthesis projected into 3 N-S cross-sections related to the main geophysics zones.

2.5.2.1 Outflow context of the main artesian springs

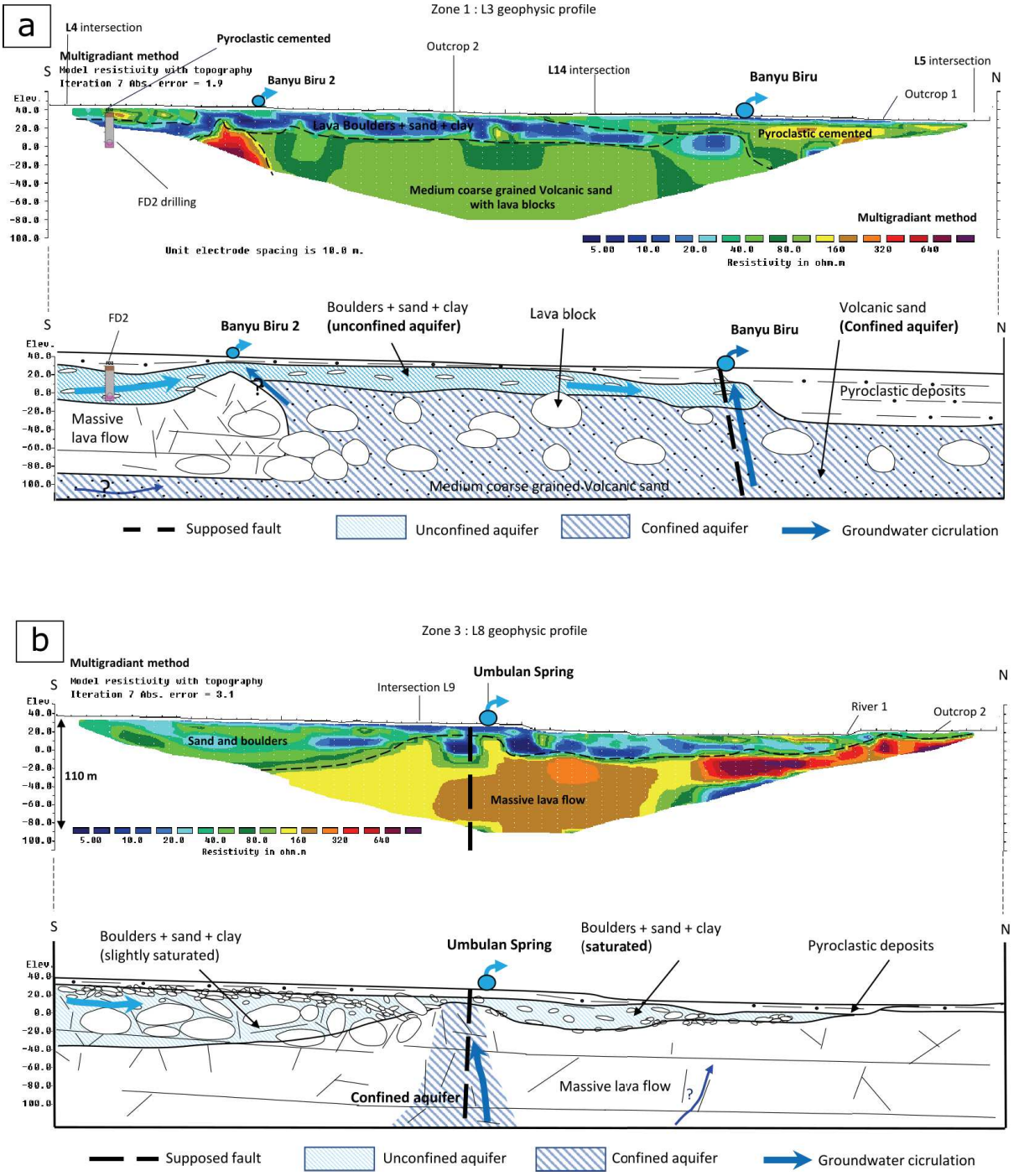

Figure 2. 20. Hydrogeological interpretations of the outflow context of **a.** Umbulan and **b.** Banyu Biru artesian springs.

- **Banyu Biru**

Based on the interpretations shown on **Figure 2. 20. a**, we consider that the groundwater of the Banyu Biru artesian spring (Q≈ 300 L s^{-1}) is related to a fracture zone triggered by the previously identified fault. Indeed, at the outflow location of the spring, the lower resistivity values suggest the existence of a more conductive zone (light green – blue color). The fault probably cuts successively across the cemented pyroclastic deposits and the clayey lava boulders that make up the confining layer of the confined aquifer hosted within the underlain volcanic sand formation. However, it is noted that the sub-surface boulder formation probably hosts an unconfined aquifer as suggested by the presence of a spring (Banyu Biru 2), and the water inlet identified at well FD2. It is not excluded that some upward leakage from the confined aquifer may partly provide groundwater to the unconfined layer. Therefore, the Banyu Biru spring may reflect a mixing of waters from the confined and unconfined aquifers.

- **Umbulan**

The important outflow of Umbulan (Q≈ 3 500 L s^{-1}) is related to the same fault as at Banyu Biru, which allows preferential groundwater circulation through the massive lava flows identified by geophysical survey. In the same way as at Banyu Biru, the boulder formations represent a confining layer and host an unconfined aquifer. The cemented pyroclastic deposits are also visible at the surface over the whole Umbulan area. According to Miftakhul Fajar and Nogroho (2018), the Umbulan outflow could be explained by the presence of dykes associated with tuff ring deposits surrounding the spring. From our field observations, we did not find any ring tuff, but only cemented pyroclastic deposits with a rather homogeneous distribution. However, the existence of a dyke is not inconceivable since such intrusions are generally developed within pre-existing fracture zones triggered by faults as previously suggested. It is noted that other important gravity springs (Q > 500 L s^{-1}) have been identified around the Bromo-Tengger-Semeru complex (e.g. Sumber Pitu and Coban Sewu, **Figure 2. 7**), and also an outflow at a cliff location corresponding to the interface between impermeable paleo-baked formations and porous autoclastic breccias. This type of spring under buried/confining conditions, such as observed in Pasuruan, is intersected by a conductive fault zone and could be representative of the Umbulan spring outflow.

Robust electrical conductivity and temperature data are provided by the continuous physico-chemical monitoring from 2017 to 2019 (**Appendix 7**) of both the Banyu Biru (255 µS cm^{-1} and 23.5°C) and Umbulan springs (215 µS cm^{-1} and 23.3°C). These results suggest a long transit time and a recharge at much higher elevation (Davis, 1999) compared to the mean annual surface temperature in Pasuruan of about 30 °C (BMKG 2018). This last issue is addressed in *Chapter 3*.

2.6 Conclusion

Volcanic formations are heterogeneous and form complex structures, especially on the volcano-sedimentary plains around volcanoes where stream networks trigger intense remobilization and lateral variation of volcanoclastics. A multidisciplinary approach was implemented involving four main field investigations including an inventory of groundwater points at the scale of the whole Bromo-Tengger-Semeru volcanic complex, supplemented by geological, drilling and geophysical surveys carried out on the volcano-sedimentary artesian plain of Pasuruan.

These surveys highlight the main lithologies that extend downstream from the volcanic massif towards the North coast of Pasuruan. The artesian aquifer is mainly hosted within reworked coarse-grained volcanic sands, while cemented layers such as pyroclastic breccias or lahar deposits control a complex multilayered configuration. The last lava flows extending as far as the Pasuruan plain have a key hydrogeological role since they constitute a confining layer composed of weathered lava boulders with sand and clay. Groundwater flow can be enhanced in these lava units due to autoclastic breccias, especially in fracture zones. Additional impermeable lithologies such as unfractured ignimbrites and marine deposits may act as a coastal barrier to groundwater flow from the artesian aquifer. This groundwater flows northwards and is probably bounded by local tectonics in the North and by impervious ignimbrite deposits to the East. However, the western limit is still unknown since artesian wells are observed as far as the foot of the Arjuno volcano. The artesian aquifer reaches an estimated depth of about 300 m and probably supplies more than 7000 L s^{-1} (measured outflow) considering the uncertainties in aquifer boundaries. The whole Pasuruan plain hosts an unconfined aquifer corresponding to a semi-permeable cap of pyroclastics about 30 m thick that supplies groundwater to numerous dug wells used by the Pasuruan population. The extent and relationship of the unconfined aquifer with the underlying artesian aquifer are still not clearly defined but leakage may probably occur.

Finally, the convergence of field observations with geomorphological and hydrogeological analyses support the hypothesis of a conductive fault to explain the outflow context of artesian springs in a volcanic piedmont area.

Chapter 3



View of the Bromo-Tengger caldera with the Mount Bromo smoking in background

Chapter 3. Multidisciplinary study with quantitative analysis of isotopic data for the assessment of recharge and functioning of volcanic aquifers. Case of Bromo-Tengger volcano, Indonesia.

This chapter deals with the recharge processes that occur along stratovolcanoes under tropical climate. This type of volcano is characterized by large facies variation related to sedimentation, remobilization and chemical weathering processes which can even change the hydrodynamical properties of volcanic rocks.

Since decades, hydrogeological conceptual models of volcanic aquifers have been largely improved, especially in volcanic island such as in Hawaii and Canary Islands. Moreover, the hydrogeological conceptual models for andesitic stratovolcano associated to an artesian volcano-sedimentary plain is barely studied. The Bromo-Tengger volcano and the plain of Pasuruan in East java, show this latter configuration and will be use as a study case.

In this context, a multidisciplinary approach is used to identify and better understand the hydrogeological processes at the scale of the Northern volcano's flank. The main results allow defining the recharge distribution and are used to propose a valid hydrogeological conceptual model of the northern flank of the Bromo-Tengger volcano.

This chapter is a research paper that has been published in *Journal of Hydrology: Regional studies* (Toulier et al., 2019).

Journal of Hydrology: Regional Studies 26 (2019) 100634

Contents lists available at ScienceDirect

Journal of Hydrology: Regional Studies

journal homepage: www.elsevier.com/locate/ejrh

Multidisciplinary study with quantitative analysis of isotopic data for the assessment of recharge and functioning of volcanic aquifers: Case of Bromo-Tengger volcano, Indonesia

Alix Toulier[a,*], Benjamin Baud[a], Véronique de Montety[a], Patrick Lachassagne[d], Véronique Leonardi[a], Séverin Pistre[a], Jean-Marie Dautria[b], Heru Hendrayana[c], M. Haris Miftakhul Fajar[c], Azwar Satrya Muhammad[e], Olivier Beon[d], Hervé Jourde[a]

[a] HSM, Univ Montpellier, CNRS, IRD, Montpellier, France
[b] Géosciences Montpellier, Univ Montpellier, CNRS, Montpellier, France
[c] Universitas Gadjah Mada, Geological Engineering Department, Yogyakarta, Indonesia
[d] Water Institute by Evian, Water Resources and Sustainability Division, Danone Waters, Evian-les-Bains, France
[e] Danone Aqua group, Department of Water Resources, Jakarta, Indonesia

Abstract

Study region: The Bromo-Tengger volcanic aquifer system, (East Java, Indonesia).
Study focus: Andesitic volcanic aquifers in Indonesia are an important source of groundwater supply for the population. The artesian flow from high discharge springs facilitates the access for irrigation and drinking water but continuously flowing artesian wells exert an increasing pressure on the groundwater resource. Given the complexity of the volcanic edifice, a multidisciplinary approach including geological, hydrometeorological, hydrochemical and isotopic measurements was performed to characterise the hydrogeological functioning of the volcano's northern flank.
New hydrogeological insights for the region: Two main hydrogeological systems are identified: a system with perched aquifers in the lava flows and pyroclastic complex, supplying low discharge springs or infiltrating to a deep flow system. The latter system is unconfined and provides groundwater to the downstream plain that hosts a confined multi-layer volcano-sedimentary aquifer. The joint implementation of a quantitative isotopic approach and a groundwater budget allows characterising aquifer recharge along the whole volcano flank. It is mainly controlled by the rainfall distribution that peaks around 1200 m elevation. The caldera basin on the top of the volcano has a very limited contribution to recharge. A conceptual hydrogeological model is proposed and compared to the main concepts of volcanic islands. This study is a first step for further scientific and management discussions to implement protection policies on the Bromo-Tengger aquifer system.

Keywords: Hydrogeology, Volcanic aquifer, Artesian system, Recharge, Isotopes, Hydrochemistry, Quantitative analysis.

3.1 Introduction

Worldwide, insular volcanic aquifers are a serious asset for drinking water supply. In such environments, due to the growth of water needs, surface water resources are no longer sufficient, particularly during the dry season. In many cases, groundwater becomes an alternative resource to provide drinking water, such as on Hawaii in the Pacific ocean (Whittier et al., 2010), Jeju Island in Korea (Hamm et al., 2005), Martinique Island in the Caribbean Sea (Vittecoq et al., 2015) or the Canary Islands in the Atlantic ocean (Izquierdo, 2014).

The Indonesian Archipelago is located on the ring of fire (Pambudi, 2018) which is an area of intense seismic and volcanic activity including 400 andesitic volcanoes, of which about 70 are still active. Some of them are known for the emission of the most major Plinian eruptions already having upset global climate, such as the Mont Samalas (Guillet et al., 2017). In this region, volcanoes represent a concentration of significant hazards and natural livelihood for the population. The Mount Bromo-Tengger in the Eastern part of the Java island is one of the most visited andesitic volcanoes in the world (Bromo-Tengger Semeru national park, FAO 1982; Cochrane, 2006). More than a profitable touristic spot, the massif also provides a unique drinking water resource to the local population through groundwater.

Several volcanic springs discharging more than 1000 L s^{-1} are known at the feet of the volcano and are used for irrigation and the population needs, since centuries to millennials. In particular, they partly supply the second biggest city of Indonesia (Surabaya; about 4 million inhabitants, 80 km north of the volcano) and other cities surrounding the volcano such as Probolinggo (east) and Malang (west). They also totally supply the city of Pasuruan (north). The artesian spring of Umbulan is the most important spring of the area, with a current discharge of about 3500 L s^{-1}.

During the last few decades, and mainly since the 80', hundreds of wells were drilled at the feet of the volcano, particularly for paddy fields irrigation. These continuously flowing artesian wells, with a discharge often higher than 15 L s^{-1}, modify the hydrogeological functioning of the aquifer, as highlighted by the significant decrease of the major springs' discharge. The knowledge of the structure, functioning and water budget of the whole hydrogeological system in this area is thus required to ensure the sustainable quantitative management of the aquifer and also to preserve groundwater quality.

The andesitic-type volcanism hydrogeology is much less studied than the basaltic one, and there is a need for the development of hydrogeological conceptual models. Two majors distinctions have been proposed in the literature to describe basaltic-type volcanism hydrogeological systems at the volcano/island scale: (1) the Hawaiian model and (2) the Canary Island model. The Hawaiian model describes a low-lying, basal aquifer with high-level water bodies perched on low permeability layers and impounded by dikes (Ingebritsen and Scholl, 1993). The Canary model describes a continuous aquifer that domes steeply inland, to high elevation, over a low permeability volcanic core (Custodio, 2007; Hemmings et al., 2015b). However, there is now a consensus on considering only one single conceptual model with differences depending on local circumstances and the effects of the volcanic deposits succession, erosion and reshaping due to major landslides (Custodio, *Com. Pers.*, Custodio, 2007; Herrera and Custodio, 2008). This single conceptual model considers only one main

stratified and heterogeneous groundwater body through a combination of a central low permeability volcanic core with a dyke-intrusion network, a more permeable cover and a skirt (or apron) of very transmissive materials in periphery (Custodio, *Com. Pers.*, Custodio et al., 2016; Marrero-Diaz et al., 2015).

Some andesitic geological environments, such as pyroclastic formations, have locally been studied, e.g. Charlier et al. (2011) in the Caribbean or Selles et al. (2015) in Indonesia. However, the hydrogeological functioning of andesitic volcanoes, or composite shield volcanoes such as the Bromo-Tengger, are poorly known. Moreover, the proposed case study can also be considered as an example of the hydrological responses to changing conditions, due to anthropogenic forcings.

There is a real lack of knowledge regarding the hydrogeology of the Bromo-Tengger volcano. Previous studies mostly focused on the volcanology and seismics of the Mount Bromo and its caldera, and some others on the geological architecture of the volcanic edifice (Aiuppa et al., 2015; Bachri et al., 2015; Bani et al., 2013; Gottschämmer and Surono, 2000; Mulyadi, 1992; Van Gerven and Pichler, 1995; Zaennudin et al., 1994). The main aim of this study is thus to identify the structure and hydrogeological functioning of the northern flank of the Bromo-Tengger volcanic edifice. As required for a correct characterization of such complex hydrosystems, a pluridisciplinary approach see for instance (Dewandel et al., 2017; Maréchal et al., 2014; Pryet et al., 2012) has been implemented. Geological, hydroclimatic, hydrochemical and isotopic investigations allow the construction of a robust conceptual model of the Bromo Tengger volcano. In addition, it is also important to adapt existing methodologies, such as isotope hydrology, and to reinforce their robustness into this specific context of humid tropical climate with a wide range of elevations.

The present work is structured as follows. After this Introduction (Section 3.1), the study area is presented in Section 3.2. Section 3.3 details the methodology which combines geological surveys, the implementation of a hydro-climatologic monitoring network, hydrochemistry and isotopes analyses. Section 3.4 focus on the results and interpretations of the gathered data for a better understanding of groundwater circulation. Section 3.5 is devoted to a discussion about the interest of a quantitative isotopic modelling coupled with a hydrological water balance to identify the recharge area of the multilayer aquifer located at the basis of this andesitic volcano and to the set-up of its conceptual hydrogeological model.

3.2 Study area

The study area (**Figure 3. 1**) is approximately 1300 km², and covers the northern flank of the Bromo-Tengger volcano including the highest caldera (Tengger caldera), and the coastal plain of Pasuruan city. While only few springs exist in the southern part of the volcano, the northern part is of great hydrogeological interest due to the numerous high discharge water points (groundwater outflows) known in that area.

3.2.1 Geology

The Bromo-Tengger (BT) mountain is one of the many volcanic edifices in the eastern part of the Java island, Indonesia (**Figure 3. 1 a**). It is a complex andesitic stratovolcano comprising, in its actual caldera, several cones such as the last active Mount Bromo (**Figure 3. 1 b**). The Bromo-Tengger is located in the Bromo-Tengger-Semeru national park and culminates at about 2700 meters above sea level (m.a.s.l.). The inner caldera floor is at about 2100 m.a.s.l..

This volcanic massif began to grow about 1.4 million years ago as a result of the northwards subduction of the Indo-Australian plate beneath the Eurasian plate. This volcano is located in the back arc basin of the Sunda arc (Hamilton, 1988). The different eruptions of the Tengger are mainly classified as VEI 2 as regards the Volcanic Explosivity Index defined by Newhall and Self (1982), that comprises 8 classes. Over time, they produced a succession of a huge accumulation of lava flows and subordinate pyroclastic deposits which constitute the framework of the composite Bromo-Tengger volcano (Thouret, 1999). The recent collapse of the magmatic chamber created a large caldera, 16 km in diameter, with a large collapse in its North-East edge (Sapikerep valley). Widespread ash fall deposits covering the upper flanks of the Tengger are related to phreatomagmatic activity from the intra-caldera complex (Mulyadi, 1992). Erosion by streams forms numerous canyons with very steep slopes which extend radially from the caldera and the volcano slopes to the piedmont areas.

The peripheral zones of the volcano structure, and particularly the Pasuruan north plain, are constituted by volcano-sedimentary deposits (Quaternary in age) such as observed around most big stratovolcano volcanoes in Indonesia (Selles et al., 2015). The thickness of this filling is more than 300 m according to the stratigraphy proposed for the Lusi mud volcano (Mazzini et al., 2017) located about 40 km North from the Pasuruan plain (**Figure 3. 1 a**).

This volcano-sedimentary series exhibits a South-North graded bedding. It comprises all the transition terms between proximal volcanic series, such as lava flows, pyroclastic falls and flows, lahars, reworked volcanic formations and more distal volcano-sedimentary deposits that are progressively more clayey towards the North. Fine clayey sediments constitute the first tens of meters below ground surface of this volcano-sedimentary series.

If many studies focused on the geology and geomorphology of the Tengger Caldera (**Figure 3. 1 b**), there is still an important lack of knowledge concerning the fault system of the Tengger edifice and the detailed structure of the peripheral sectors such as the north Pasuruan plain. The major tectonic structures of East Java are normal (E-W) and strike-slip (NE-SW) faults, inherited from the subduction context (Marliyani, 2016; Susilohadi, 1995). Some authors describe the caldera structure and the caldera-bounding faults of different type of volcanoes (Cabusson, 2012; Cole et al., 2005). In particular, for the Tengger, the northeast margin of the Tengger caldera (Fig. 1 a) is linear, suggesting a control by a NW-SE trending fault (Newhall and Dzurisin, 1988). Additionally, Neumann van Padang (1951) suggested the existence of two subtle alignments of vents within the caldera: NNE-SSW and E-W. No other fault system is described on the Tengger in the literature. However, the Watukosek fault system (**Figure 3. 1 a**) associated to the Arjuno Welirang volcanic complex described by Moscariello et al (2017) could be extrapolated to similar regional NE-SW fault systems responsible of the alignment of the Semeru, Bromo and the piercement structure illustrated by the Ranu Grati maar in the Pasuruan plain. The North Pasuruan fault zone surveyed by Marliyani (2016) suggests that the Pasuruan plain is structured by a South-North graben.

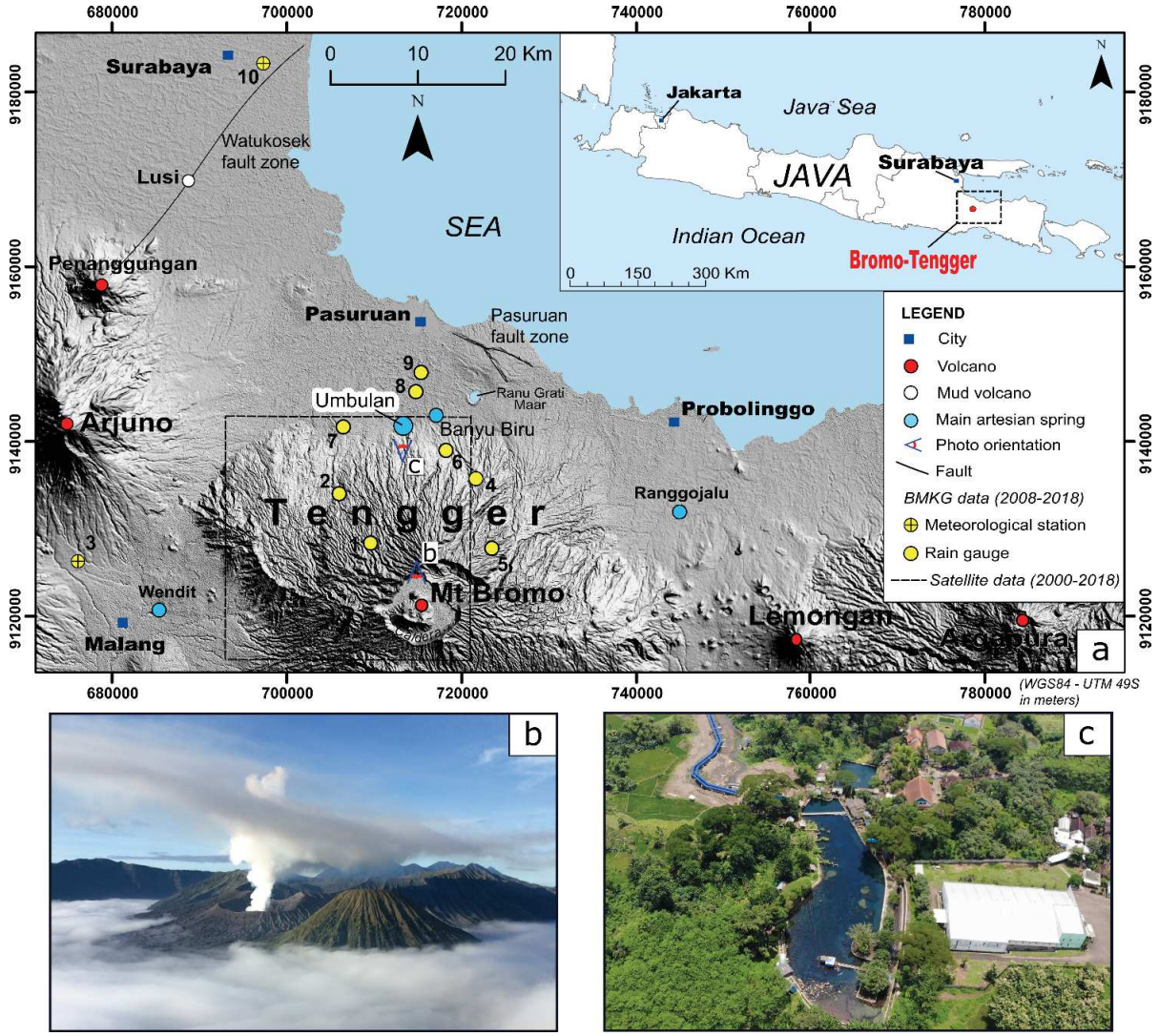

Figure 3. 1. a Relief map of the North-Eastern part of the Java Island (USGS SRTM30 dataset) with the location of the studied artesian springs, among which Umbulan, and the main volcanoes active vents. The major active faults systems (Watukosek and Pasuruan) and the meteorological stations from BMKG are indicated, and completed by the satellite data provided by the Tropical Rainfall Measuring Mission (TRMM) (3b42v7; Zone: 25x25 km). **b** The Tengger caldera, seen from Mt Penanjakan at 2700masl. Mt Bromo still active on the left. **c** South-North view of the Umbulan artesian spring with the new adduction pipe that supplies the Surabaya city with drinking water (drone view). The main spring outflow is located in the southern part of the basin in the catchwork visible on the photo.

3.2.2 Climate

According to Badan Meteorologi, Klimatologi dan Geofisika of Malang (BMKG, 2018), East Java is characterised by a humid tropical climate with two distinct seasons: a wet season from November to April and a dry season from May to October. The East Java mean annual rainfall is about 1500 mm at sea level, with about 140 rainy days a year (BPS-Statistics Indonesia, 2017). For the Bromo-Tengger area, the precipitation recorded for the 2008-2018 period is ranging from 1290 to 2400 mm $year^{-1}$, respectively for the station 9 and 5 (BMKG, 2018), (**Figure 3. 2 a, b**). The mean interannual precipitation estimated on the basis of 6 rain gauges (n° 1, 2, 4, 5, 6, 7; **Figure 3. 1 a**) regularly located on the northern flank of Bromo-Tengger is about 2000 mm $year^{-1}$, with a maximum amount of rainfall from December to February (**Figure 3. 2 a, b**). Unfortunately, BMKG data are not precise enough to map rainfall on the Tengger volcano because of numerous and long gaps observed in data for all rain gauges. In such steep topographic environment, the rainfall usually increases from the coastal low elevation areas to the inland highest areas, but also depends on the wind orientation. From the Surabaya and Malang stations data, the annual average wind direction is about N150° (NW-SE), with a mean velocity of about 5 km h^{-1} and the annual average humidity is 76 %. The 2008-2018 annual average temperature shows a minimum temperature of 18.3°C for Malang (580 m.a.s.l.) and a maximum temperature of 32.1 °C for Surabaya (10 m.a.s.l.).

The mean interannual precipitation estimated by the TRMM satellite data (Kummerow et al., 1998) for the hydrological years 2000 to 2018 (**Figure 3. 2 c**) is 2123 mm $year^{-1}$. There is no significant precipitation trend observed during the last 18 years for annual rainfall as well as for rainfall during wet and dry seasons. The two last hydrological years (2017-2018) have rainfall very near the average, and can both be considered as representative “mean” hydrological years. In addition, the 2017 and 2018 rainfall amount measured during the rainy season is near the average rainfall amount of the rainy season.

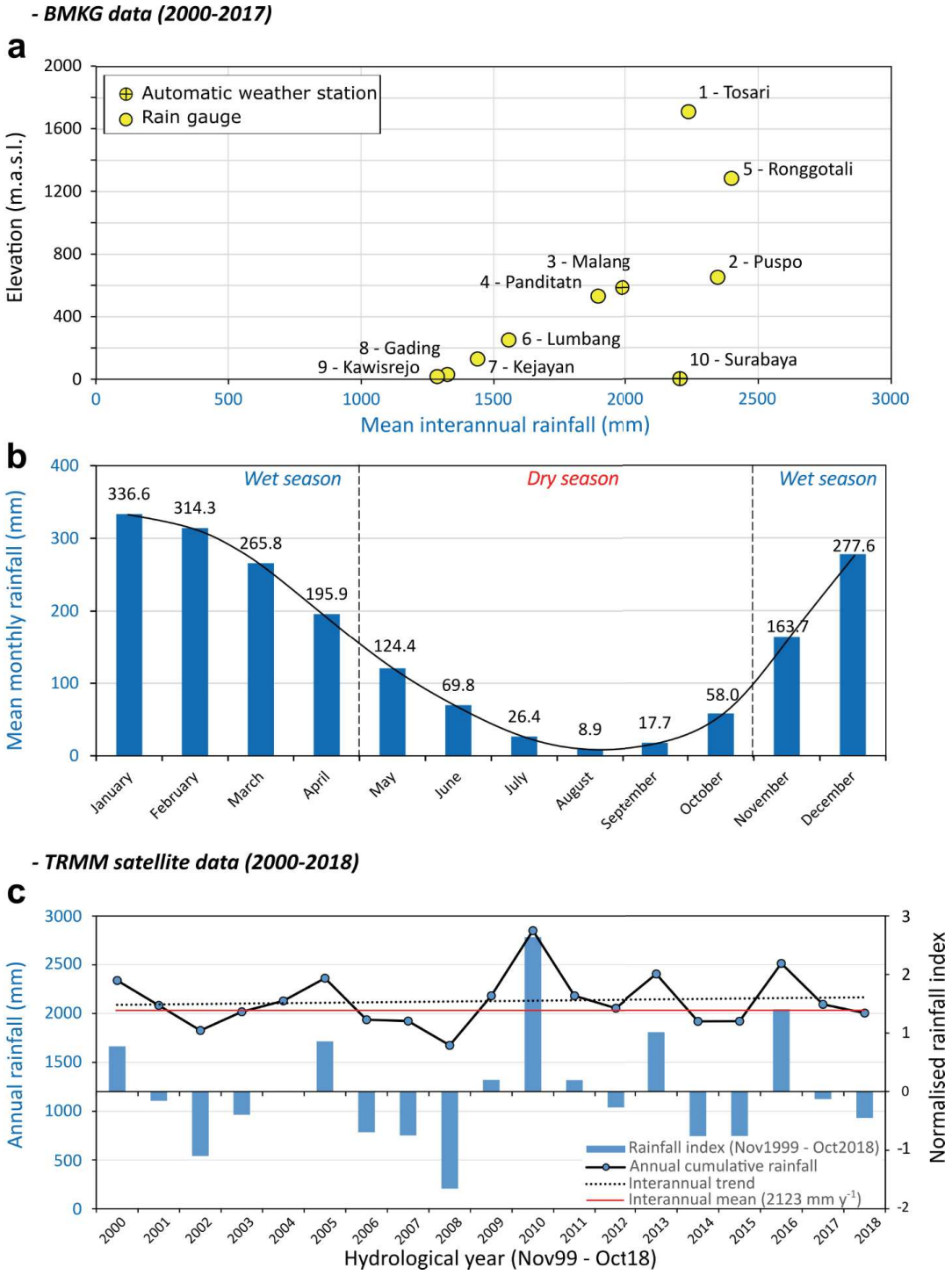

Figure 3. 2. a Mean interannual rainfall at 10 rainfall stations, as a function of their elevation (m.a.s.l.) (data from BMKG of Malang city); the location of each rainfall station is reported on Fig. 1 a. **b** Mean monthly precipitation for the 10 rain gauges. **c** Normalised rainfall index (i) and annual cumulative rainfall from 2000 to 2017 hydrological years, estimated from the TRMM data (3b42v7, 2011). The index is given by the equation: $i = (P_i - P_{mean})/\sigma$ where P_i = annual cumulative rainfall, P_{mean} = mean interannual rainfall and σ = standard deviation of the total annual cumulate rainfall.

3.2.3 Hydrogeology

In continental context, the structure of volcanic aquifers is mainly governed by the opposition between an impermeable substratum (often non-volcanic), and overlying volcanic formations generally permeable (see for instance Bourlier et al. (2005) or Rouquet et al. (2012)). In insular volcanic context, two main manifestations of a single conceptual hydrogeological model are described in the literature, at the volcanic edifice scale or even at the whole island scale: (1) a low-lying basal aquifer linked to inland dike-impounded and perched aquifers such as in the island of Oahu in Hawaii (Nichols et al., 1996; Peterson, 1972); (2) a continuous basal aquifer extending far inland and at rather high elevation which is well detailed in the Canary Islands (Custodio, 2007). These hydrogeological models were developed for basaltic volcanism (hot spots, transform faults, etc. geodynamical context) and are still improved by the hydrogeological community, especially regarding the key role of the volcanic core with dike network acting as barriers or as water conducting features through the fissures associated (Herrera and Custodio, 2008). Recent studies show a more complex reality, and the need for higher resolution hydrogeological studies, even in basaltic context (Join et al., 2005; Lachassagne et al., 2014).

Moreover, andesitic-type volcanism exhibits different hydrogeological patterns than the basaltic one and still need to be better characterized (Charlier et al., 2011; Hemmings et al., 2015b). In such andesitic context, the volcanic formations have often more various lithologies than in basaltic context, with lavas, but also pyroclastic formations, and volcano-detritic series, such as lahars and debris flows. For instance, the hydrogeological role of the extensive ignimbrite deposits frequently found in andesitic context is still poorly understood and may enable the presence of more than a single groundwater system. The andesitic volcanic formations are also often older, with several volcanic and erosion phases, and the associated weathering processes and paleosurfaces. It generates multiple superimposed or juxtaposed hydrogeological units with various hydrogeological relationships. Furthermore, the high relief of volcanoes favours erosion and the associated presence of deep canyons may also laterally limit the extension of the hydrogeological units. In the Merapi volcano (Indonesia), a dominant pyroclastic and volcano-detritic volcano, groundwater flow pathways are described to be related to the volcanic infilling of ancient paleovalley systems, locally comprising lava flows, which act as a preferential underground drainage networks (Selles et al., 2015).

The volcanic context of the Tengger strato-volcano is rather different as lava flows (mainly basic andesite), extensively present on most of the northern slope, gradually disappear to the upper reach of the North plain, where the volcano-sedimentary series appear. Only a few gravity springs with discharge of a few L s^{-1} are known on the flank of the volcano. In contrast, important artesian springs outflow from the upper part of the volcano-sedimentary series of the Northern Plain, such as Umbulan ($Q \approx 3500$ L s^{-1}) and Banyu Biru ($Q \approx 300$ L s^{-1}) springs, which are used for irrigation and drinking water supply in the Pasuruan plain (**Figure 3. 1 a**). An artesian spring (or well) is defined as a groundwater outflow which occurs through some fissure or other opening features (lithological heterogeneity, fault, intrusive bodies, or drilling for a well) in the confining bed that overlies the confined aquifer (definititon modified from UNESCO, 2012).

The plain is also characterized by hundreds of artesian wells drilled in the volcano-sedimentary formation, near or downstream the springs, for agricultural or domestic uses. Their depth varies between 30 and 120 m, and their discharge often reaches several L s^{-1}. The geometry and lateral extent of the confining units responsible of artesianism are not known but some authors present the Pasuruan plain as an "extensive and productive aquifer system of moderate transmissivity and with piezometric head near or above the land surface" (Soekardi Puspowardoyo, 1985).

There is no information about hydrothermal activity on the northern flank of the Bromo-Tengger. In addition, the water temperature measured in artesian wells of the volcano-sedimentary plain is about 23°C which indicates a negative thermal anomaly in comparison with the local mean annual air temperature of about 30°C. Then, the low temperature of the groundwater suggests a recharge at "high" elevation. The hydrogeological functioning of the 40 km^2 endorheic basin at the summit of the volcano (Tengger sea sand caldera) is also unknown.

3.3 Methodology

The comprehension of the structure and hydrogeological functioning of complex systems requires a multidisciplinary approach; in fact, each method provides some clues of the hydrosystem which can only be considered as reliable insights when they converge. Complementary methods were then applied: geological study, implementation of a hydro-climatologic monitoring network, hydrochemistry and isotopes analyses. Results of these investigations and analyses, described here below, allow delineating the recharge area and conceptualizing the aquifer structure and its functioning.

3.3.1 Geological study

A multi-scale geological field work has been conducted to gather complementary data.

- First, the main geomorphological structures of the Bromo-Tengger massif were characterized using Arcgis and Google Earth tools. An hill shade map of the SRTM30m at a resolution of one arc-second (Farr et al., 2007) was elaborated and compared to the different existing geological maps (Mulyadi, 1992; Santosa et al., 1992; Zaennudin et al., 1994).

- Second, a 5 months geological fieldwork was performed to both observe lithological features in areas where information was missing, and verify geological descriptions and limits of the existing maps. On the northern flank of the volcano, this work was mainly carried out in canyons where most of the outcrops are located. Stratigraphic logs and geological data were collected from about 250 outcropping sites, then analyzed to

corroborate and sometimes correct information from the existing geological maps. On the volcano sedimentary plain of Pasuruan, the existing geological description was completed by the geological logging of seven wells (34 to 103 m deep) on the basis of the cuttings and cores collected during drilling (see *chapter 2*, **Figure 2. 12**).

3.3.2 Monitoring network for recharge assessment

3.3.2.1 Hydro-climatological monitoring

The rainfall and temperature pattern of the Bromo volcano were characterized using 4 meteorological stations (CIMEL RTU station) installed along a North-South transect at different elevations: Kronto - 535 m.a.s.l., Wonorejo - 1158 m.a.s.l., Temple - 2154 m.a.s.l. and Seruni - 2681 m.a.s.l. (**Figure 3. 3**).

Hourly temperature and rainfall measurements were recorded over one year from 1/04/2017 to 31/03/2018. This period is part of 2017 and 2018 hydrological years considered as mean hydrological years (see section 3.2.2). Rainfall was collected for isotope analysis and cumulated rainfall assessment in a 200 L water tank, initially filled with 1 L of motor oil to avoid evaporation. The final volume of water in this tank was measured at the end of the monitoring period to check the good calibration of the CIMEL rain gauges. In addition, the Aqua Factory meteo station located in the Pasuruan plain (Aqua - 17 m.a.s.l.), that records daily rainfall, was also used.

A 5.8 km² representative surface watershed was monitored to estimate the water budget of the study area. This watershed ranges from 435 m.a.s.l. at the Kronto river gauging station to 2615 m.a.s.l.. Stream water level was measured with a 0.5 cmH_2O precision pressure probe, during the hydrological year stemming from 01/11/2017 to 31/10/2018. A rating curve was built using 5 manual discharge gaugings ranging between 2.5 and 60 L s^{-1}, and completed by the discharge estimated during a peak flood (about 1500 L s^{-1}) from a velocity estimate performed with a floating object (a bottle), and the known section of the stream.

Water points on the volcano flank and in the plain (springs, wells, dugwells) were inventoried and stored in a database. Discharge measurements of the main artesian springs and the artesian wells were also realized.

3.3.2.2 Analysis of climatic and hydrological data

The monitoring results were used to characterize the spatial rainfall and temperature distributions along the northern flank of the volcano.
Based on the Thornthwaite method (Thornthwaite, 1948), the aquifer recharge was computed as follows:

$$Re = R - (RET + R_{off} + \Delta S) = ER - R_{off} - \Delta S \quad (3.1)$$

where:
Re: recharge (mm)
R: rainfall (mm)
RET: real evapotranspiration or also known as actual evapotranspiration (AET) (mm)
R_{off}*: runoff (mm)*
ΔS*: variation in soil moisture storage (mm)*
ER: effective rainfall (=R - RET) (mm)

The potential and the real evapotranspiration (PET and RET) were calculated for each meteorological stations at a Monthly time step, considering a 100 mm maximum soil moisture storage, initialized at 100 mm in April 2017 (end of the rainy season), (Ponce and Shetty, 1995). Then, effective rainfall (ER) was computed monthly as ER = R – RET.

The water budget parameters (R, RET, ΔS) come from the 01/04/2017 to 31/03/2018 monitoring period. The runoff was estimated from the watershed of Kronto.

3.3.2.3 Hydrochemical and isotopic measurements

During 4 sampling campaigns including dry and wet season (May-June 2016, November 2016, May- June 2017 and March-June 2018), with sampling elevation ranging from 13 to 2700 masl, were collected:

- i) 31 groundwater samples (artesian wells, artesian and gravity springs),
- ii) 1 surface water sample from a lake (Maar),
- iii) 4 rainwater samples from meteorological stations.
-

Details of the sampling points are given in **Table 3. 1** and plotted in **Figure 3. 3**.

On the northern flank of the Bromo-Tengger, the 17 groundwater samples were mainly collected from “gravity springs” such as inter lava flows springs**.** In the volcano sedimentary plain, the 14 water samples were collected from artesian springs and artesian wells. For each groundwater sample, physico-chemical measurements (Electrical Conductivity (EC), pH, Temperature, Dissolved Oxygen) were recorded in the field using a multiparameter probe HACH HQ40D and completed by spring/well discharge measurements.

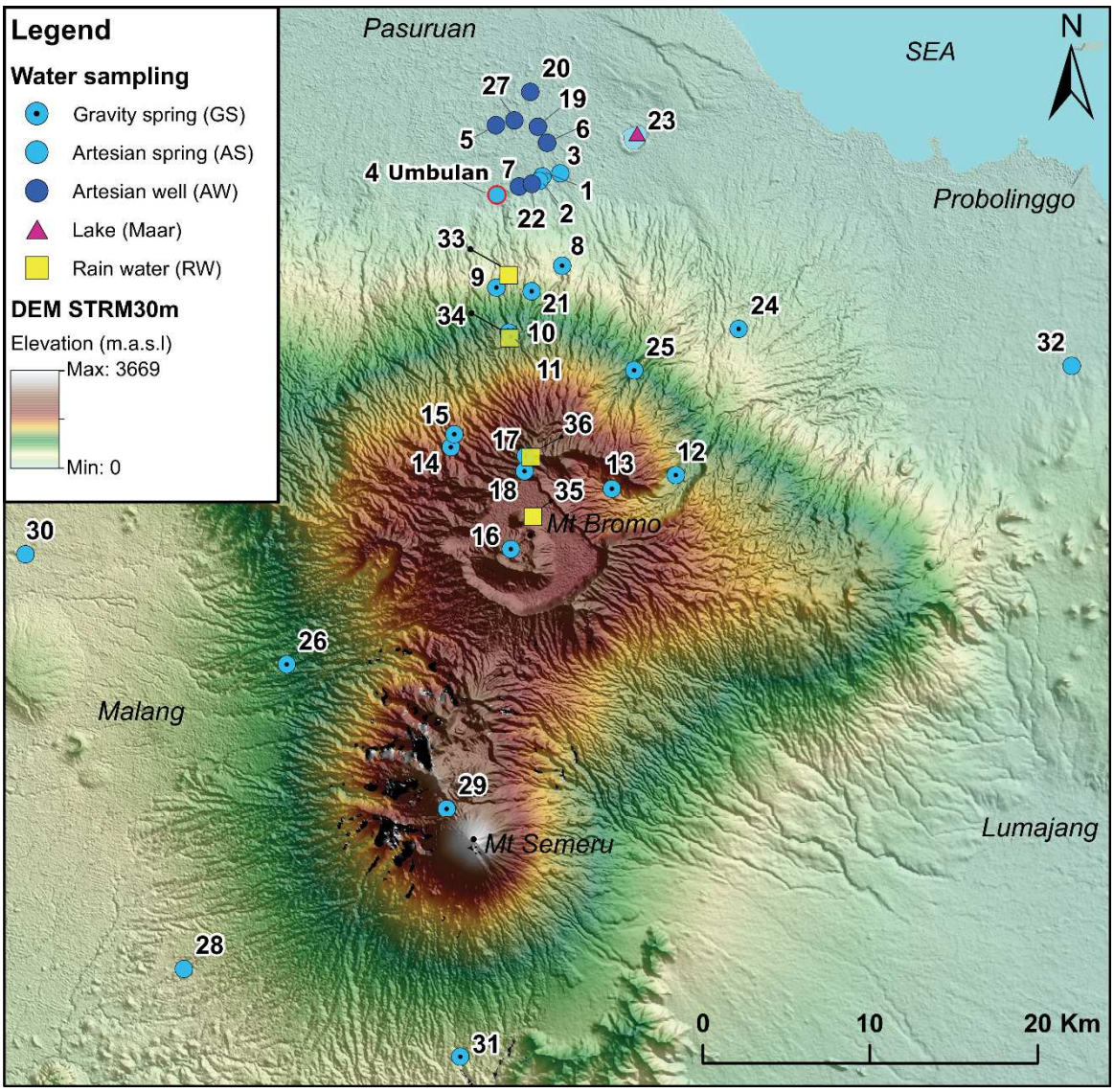

Figure 3. 3. Location of the sampling sites on the Bromo-Tengger-Semeru area plotted on a DEM (STRM30m). The sampling points are divided in 5 types: 1) Gravity springs, 2) Artesian springs, 3) Artesian wells, 4) Ranu Grati lake (Maar) and (5) Rainwater from raingauges.

Anion and alkalinity were collected in HDEP bottles of 10 ml and 50 ml respectively, and stored without air bubbles. Water isotopes were collected in 10 ml amber glass bottles also avoiding entrapped air bubbles. Samples for cation and traces analysis were collected in acid washed 20 ml vials and the samples were preserved by acidifying to pH 2 with concentrated trace grade $HNO3^{-}$. Each vial was previously rinsed 3 times with the water being sampled. Anion, cation and trace elements were filtrated using a 0,22 µm Millipore filter. Samples were kept refrigerated prior to analyses.

Alkalinity was determined in the field by titration with HCL (0,1M) using a manual Titrator Hach. The other analyses were performed in Hydrosciences laboratory, University of Montpellier. Anions were analyzed by ionic chromatography using a IC1000 Dionex. Cations and traces were analysed with an ICP-MS iCAP Q Thermo-Fisher. The analytical error for major elements is below 5% and below 0.1% for traces elements. Stable isotopes ($\delta^{18}O$, δD) were analysed at LAMA laboratory using an Isoprime mass spectrometer with an accuracy of

±0.08‰ for $\delta^{18}O$ and of ±0.8‰ for δD. The isotopic data are reported in the conventional delta (‰) notation as a deviation from the Vienna Standard Mean Ocean Water (VSMOW).

Comparison of the stable isotopic compositions of groundwater and rain water at different altitudes is defined as an efficient and approved scientific tools for evaluating recharge area from complex hydrogeological systems (Gat, 1996; Jones et al., 2000). This method has been successfully performed for many volcanic Islands (Heilweil et al., 2009; Hildenbrand et al., 2005; Prada et al., 2016). However, the monthly rainfall sampling required for establishing altitudinal isotopic gradient (Gonfiantini et al., 2001) is challenging to perform in volcanic regions with difficult access due to dense vegetation and high slope, and has some drawbacks.

As no local isotopic monitoring exists on the study area, we first determined an altitudinal gradient of water isotopes using small local springs ($Q < 1$ L s^{-1}) called "integrative springs", located along the northern flank of the volcano. These integrative springs are characterised by small watershed (< 0,5 km²) and short flowpaths between recharge and discharge locations. The geomorphology confirmed the limited extension of their watershed such as "Seruni" (n°17; table 2) located in a small thalweg at less than 100 m from the volcano summit or "Little spring of Tosari" (n° 14; table 2) located under a high cliff, and no relationship with stream water infiltrated upstream. In addition, these springs show significantly stable physicochemical parameters and water isotopes suggesting a local aquifer, nevertheless sufficiently developed to smooth rain events and seasonal variations. Local anthropogenic impacts or volcanic activity dry deposits influence some of these springs, in accordance with the land use of their inferred recharge area, also confirming a local recharge. This methodology has been successfully applied on volcanic context such as in Guatemala (Mulligan et al., 2011). The isotopic value of the integrative springs was used to calculate a local meteoric water line referred as the Bromo Spring Water Line (BSWL).

The stable isotopes of rain water were also sampled at the end of March 2018, after one full year of cumulated rainfall storage, at each meteorological station (Fig. 3 and section 3.2.1). These samples allowed to establish a local meteoric water line (BMWL, Bromo Meteoric Water Line) calculated as a first approximation with the PWLSR precipitation weighted method (Hughes and Crawford, 2012). Due to uncomplete rainfall collection at Aqua station, we estimated water isotope values in the plain using the GNIP station of Jakarta (IAEA, 1961) determined for the same coast and elevation than Aqua station (IAEA 1962-1998; 8 m.a.s.l.; $\delta D‰ = 7{,}47\ \delta^{18}O + 7{,}99$). The BMWL is then compared to the global meteoric water line (GMWL) defined by Craig (1961), (GMWL; $\delta D‰ = 8\ \delta^{18}O + 10$) and validated by the local meteoric water line (LMWL) based on GNIP of Jakarta.

3.3.3 Quantitative estimation of stable isotopes signature for recharge area delineation

To delineate the recharge area of the aquifer, we assume that the isotopic signature of the main spring (Umbulan) is representative of the isotopic signature of the "basal" volcano-sedimentary aquifer, which is confirmed by isotopic sampling in the plain. The methodology developed in this paper combines the use of:

A. the stable isotopes data: outflow at the main spring on the one hand, and local meteoric water line built from the integrative springs (BSWL) on the other hand;
B. the total groundwater outflow measured from the aquifer (see section 3.3.2.1.), and elevation-dependent groundwater recharge computation.

The interest of a 2D quantitative modeling developed in this paper, as compared with a simple 1D approach, allows (1) to take into account the conical shape of the volcano, and (2) to accordingly compute a recharge function (leading to the water budget) that depends not only on the elevation, but also on the shape of the volcano, which is a key point to constrain the results. These geometrical characteristics (shape) and recharge function (more precisely effective rainfall = f(elevation and shape of the volcano) are considered as fixed entry parameters, as well as the isotopic data. The infiltration rate on the contributing slices is also considered as a fixed parameter (based on hydrological measurements). Then, the only adjusted parameters are the contributing slices (which elevation for the recharge area), and the surface area of the whole recharge area. Geological and hydrogeological arguments are used to validate and ensure the reliability of the results.

Of course, such a methodology provides theoretically a non-unique solution. However, constraining a maximum of parameters from other independent methods/approaches, and using other information, such as geology and hydrogeology, helps identify the most probable one(s).

The methodology comprises 5 steps (**Figure 3. 4**).

STEPS 1 to 3 correspond to the preparation of the data base then of the model, STEPS 4 and 5 to its calibration to delineate the aquifer recharge area. Computations were performed with MSExcel.

- ***STEP 1***: Discretization of the maximum lateral and vertical extension of the potential recharge area of the aquifer:
  (i) dividing all the northern flank of the volcano into 100 m range of elevation "slices".
  The number of slices "*n*" is defined as:

$$n = \sum_{(i)} Slice(i) \quad (3.2)$$

  Where:
  i = 0 to n, and each slice mean elevation is M_h (i).

  (ii) using morphological information to laterally (West-East) limit the extension of the recharge area.
  This step enables to compute a first distribution of surface area for each slice, that may be refined later during the modeling process. The potential recharge surface area "S_{total}" is computed as follows:

$$S_{total} = \sum_{(i)} S(i) \quad (3.3)$$

  Where:
  S(i): the surface of slice i (km²) enabling aquifer recharge

- ***STEP2***: Recharge was computed for each slice along the same range of elevation by interpolating the results (R, RET from water budget section 3.3.2.2 obtained at the 5 meteorological stations of the northern flank of the volcano), and infiltration rate. The recharge of each slice $Re(i)$ is given by:

$$Re(i) = ER(i) \times C_{inf} \times S(i) \quad (3.4)$$

  from which the total estimated inflow to the aquifer is inferred:

$$Q_{total} = \sum_{(i)} Re(i) \quad (3.5)$$

  Where:
  ER: the effective rainfall of the slice i (mm y^{-1})
  C_{inf}: the coefficient of infiltration of the effective rainfall, initially fixed at 100% for each slice (%)

- ***STEP 3***: the $\delta^{18}O$ recharge signal for each slice was derived from the BSWL and used as an input in the model. The $\delta^{18}O$ recharge signal for each slice $\delta^{18}O_{rec}(i)$ is given by:

$$\delta^{18}O_{rec}(i) = \delta^{18}O_{rec}(i=0) + grad\ (BSWL/100m) \times Mh(i) \quad (3.6)$$

Where:
$\delta^{18}O_{rec}(i = 0)$: $\delta^{18}O$ input of the slice 0 m.a.s.l.
grad (BSWL/100m): $\delta^{18}O$ gradient (Bromo Spring Water Line, BSWL).

Then, the $\delta^{18}O$ contribution of each slice is given by:

$$\delta^{18}O_{cont}(i) = \frac{Re(i) \times \delta^{18}O_{rec}(i)}{Q_{total}} \quad (3.7)$$

- ***STEP 4****:* First calibration phase of the model. Here, the objective is to define the elevation slices where recharge can occur with the objective to obtain the $\delta^{18}O$ composition measured at the spring/aquifer. Calibration is performed first from the altitudinal distribution of Re imposed from *STEP 2 and* 3.

The computed $\delta^{18}O$ composition of the aquifer ($\delta^{18}O_{total}$) is calculated from:

$$\delta^{18}O_{total} = \sum_{(i)} \delta^{18}O_{cont}(i) \quad (3.8)$$

Based on geological or hydrogeological information (ex: low permeability layers, runoff, etc.), the coefficient of infiltration (C_{inf}) applied on each slice (see equation 3.4) can be adjusted to fit with the observed $\delta^{18}O$ composition of the aquifer/spring (**A.**).

- ***STEP 5***: Second phase of the model calibration: calibration of the width of the total recharge area, and then of the total surface of the recharge area. The West-East width of the recharge area is adjusted to fit with the total outflow measured from the aquifer (**B.**).

The calibration process can be iterative, particularly between STEPS 4 and 5.
Finally, sensitivity analyses are performed to estimate the accuracy of the calibration.

The outputs of this process are mainly the altitudinal and lateral delineation of the recharge area, and the spatial distribution of the recharge within this area.

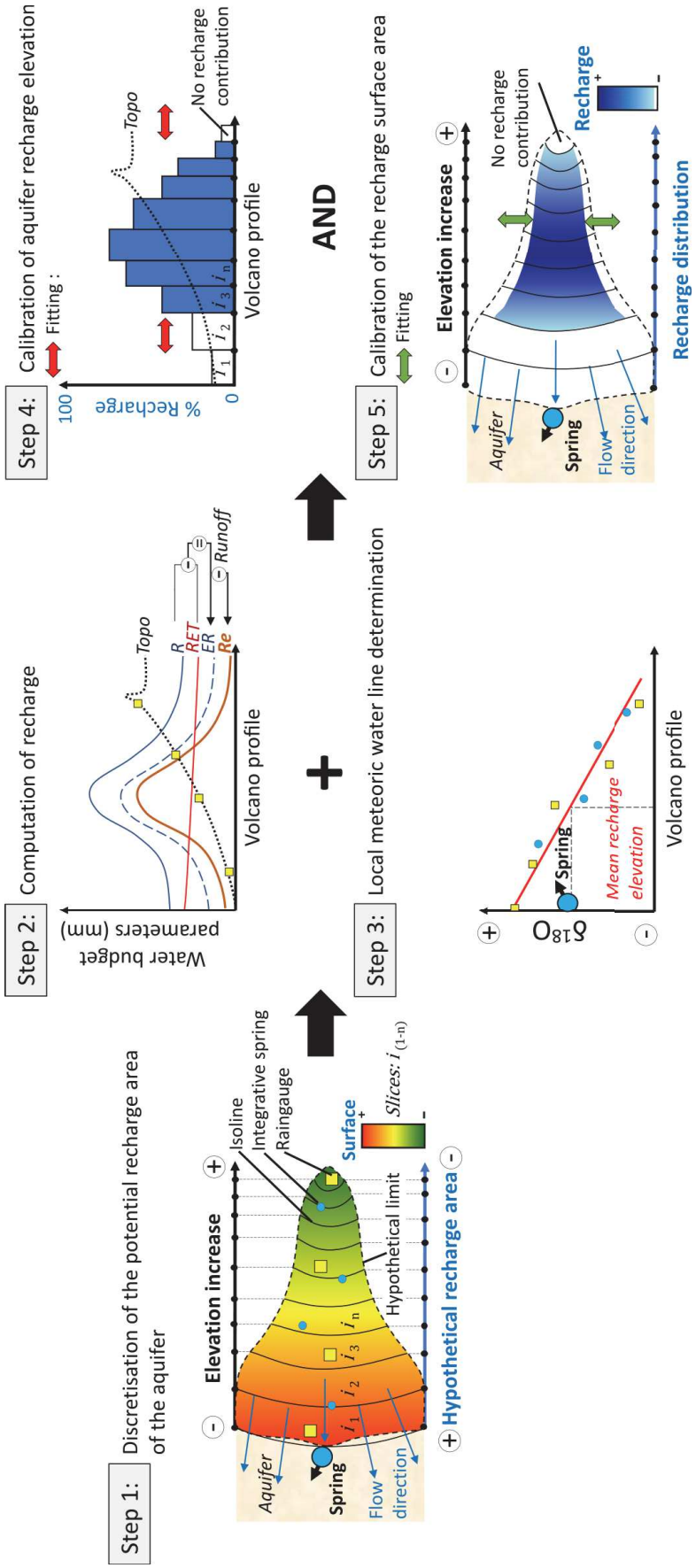

Figure 3. 4. Quantitative modeling method for recharge area delineation of the Bromo-Tengger hydrogeological system.

3.4 Results and interpretations

3.4.1 Geological synthesis and hydrogeological implications

The existing geological maps (Mulyadi, 1992; Santosa et al., 1992; Zaennudin et al., 1994) have been compiled and completed with field observations (**Figure 3. 5 a**).

The northern flank of the Bromo-Tengger volcanic edifice appear to be mostly composed of a thick series of calc-alkaline lava flows, mostly andesitic and unweathered. These formations outcrop in the medial zone, from 60 to 1500 m.a.s.l. (and are referenced as Olf, BRI, Klf, Nkj on **Figure 3. 5 a**). Some lava flows series are more than 50m thick. Cooked paleosoils, locally covered by autobreccia of limited thickness (2-3 m max) are interstratified within the lava flows series. The upstream part of the volcano (current proximal zone), ranging from 1500 to 2700 m.a.s.l., is covered by pyroclastic materials (Wjph, Njp) mainly constituted from fall deposits (ash, lapilli) sometimes crisscrossed by lava flows. These fall deposits are unconsolidated and are deeply incised by canyons from the hydrographic network. A few slope deposits are identified at the outlet of some large valleys (Madakaripura and Sapiekerep); they are composed of lahars, pyroclastic flows and ignimbrites (Mulyadi, 1992) spread towards the North (SUig, NM).

In term of geomorphology, the volcanic edifice is scarred by 4 main super structures:

- the Sand sea caldera (SS) of the Bromo-Tengger summit with the Tengger caldera wall unit (TDK),
- the deep Sapikerep valley (Nap), located East of the volcano, related to the Bromo-Tengger caldera collapse,
- the Madakaripura valley (SM, NM) due to the Ngadisari caldera collapse,
- the old caldera of Nongkojajar (Nkj) bordering the west side of the volcanic edifice.

Our observations enable to complete the geological map as follows, with the black dotted line units in **Figure 3. 5 a**:

- the pyroclastic deposits ejected by the Ranu Grati maar explosions (RG) encircle this 120 m deep volcanic lake;
- the north hill of Pasuruan (Hng) is composed of pyroclastic deposits, lahars and possibly ignimbrites. This relief may be the distal part of the Sapikerep fan deposit (SUig);
- more than 100 m thick lahars deposits were mainly identified in the downstream part of the Madakaripura valley (SM and NM);
- adventive cones (Cinder cones; AC) seem to correspond to the last lava outflows: Gunung Tinggi and Pandak, South-East of Umbulan spring;
- the western limit of the “old lava flows” (Olf) has been extended, and is now in contact with the Nongkojajar unit (Nkj);
- a SW-NE inferred fault may explain the artesian springs alignment (Umbulan, Banyu Biru, Telogo, Kali Sukun, respectively n°4, 2, 1, 3, on **Figure 3. 3**) with the Ranu Grati Lake.

In the distal zone of the volcano (Pasuruan plain), 7 drillings (red dots on **Figure 3. 5 b**, **Figure 2. 12**) enabled the identification of a superficial first unit, ranging from 0 to 30 m deep, mainly composed of weathered volcanic tuffs mixed with fluvial deposits characterized by their clayey and cinder matrix. Several cores at about 30 m deep were collected and show consolidated and clayey pyroclastic materials probably from lahars or ignimbrites deposits. The lateral variation of these materials is difficult to precise but the thickness of each unit is about 10 m. The clayey formations described in this first unit surely confine the underlying main aquifer. The second unit (top deeper than 30-40 m deep) is composed of reworked volcanoclastics (ash and lapilli materials) with ripples marks, intersected by paleochannels filled with alluvial, laharic and polygenic conglomerates mostly consolidated. This deep unit is probably contemporaneous and interstratified (at its southern limit) with the lava flows but, as these formations are difficult to drill with the local engines, there is no drilling data in the transition zone. The volcano-sedimentary series thickness is still unknown but some deep artesian wells may be more than 200 m deep (from farmers oral testimonies). No artesian deep wells have been inventoried in the northern part of the plain (in the surroundings of the Pasuruan city). The distal zone of the stratovolcano is surely characterized by fine deltaic sediments, such as silts and clays, carried along the hydrographic network (Selles et al., 2015). This surely explains the northern ending-up of the aquifer.

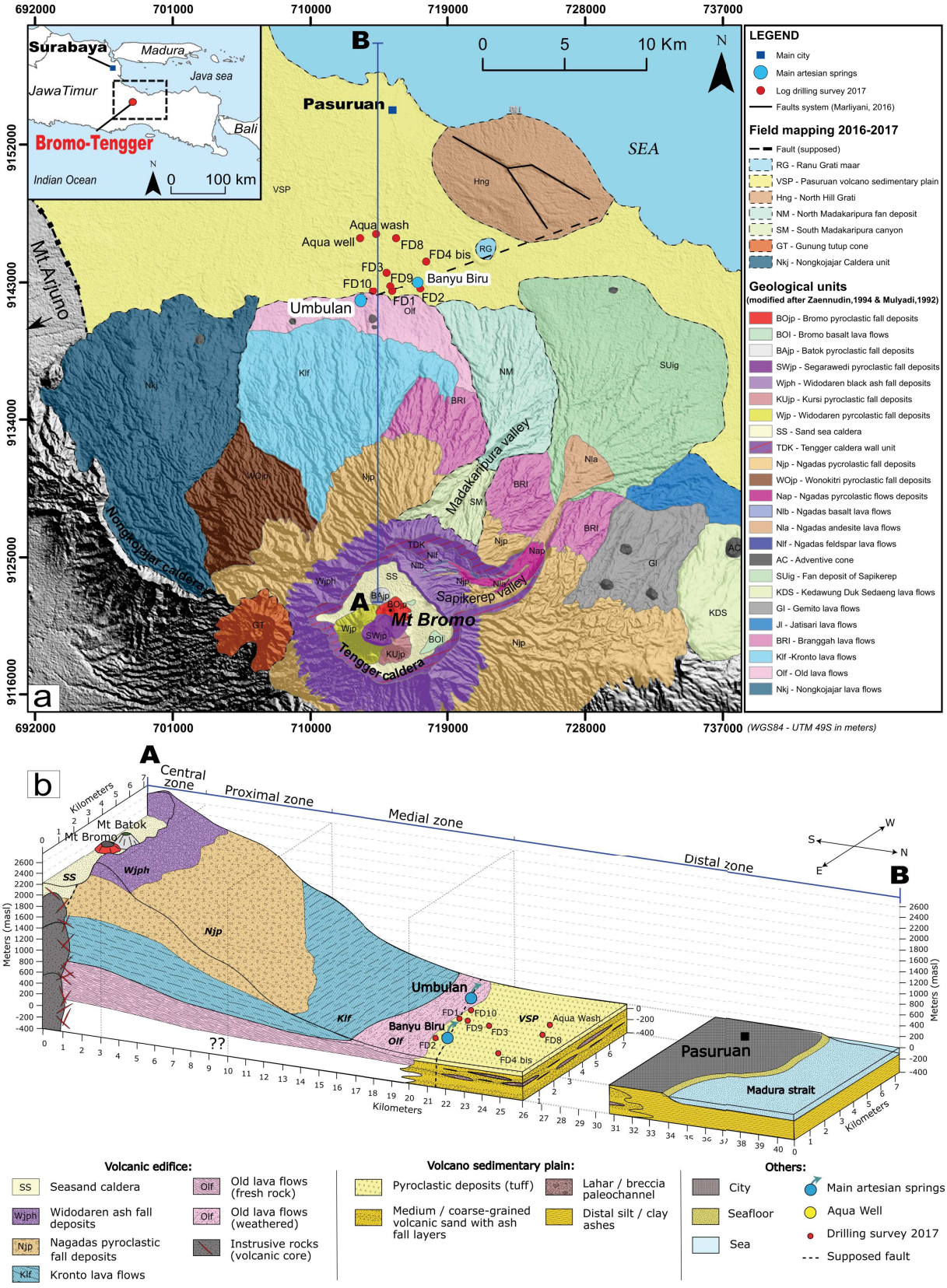

Figure 3. 5 a Geological map of the Northern flank of the Bromo Tengger, modified after Mulyadi, (1992); Santosa et al., (1992); Zaennudin et al., (1994). **b** Schematic geological cross section of the Northern flank of the Bromo Tengger from the Caldera summit (A) to the north coast of Pasuruan (B). Detailed drilling logs are provided in chapter 2, **Figure 2. 12**.

3.4.1.1 Hydrogeological implications

From this complex geological structure, we propose a simplified hydrogeological structure composed by 5 main hydrogeological units, from the volcano summit to the North coast:

- the central zone, constituted by the sand sea caldera (SS), is filled mostly by dark sand, with a high porosity. This large endorheic zone, with no permanent steam network, probably hosts an unconfined aquifer of unknown thickness, which outlets and relationships with other aquifers are unknown;
- in the proximal zone of the edifice, the thickness of the pyroclastic complex is difficult to estimate. However, the inner caldera rim outcrops (TDK) indicate that it could be several hundred meters thick. It may overlay the lava flows complex described just below. A few low discharge springs were identified in this formation, at the favour of layers of lower permeability (e.g. Seruni spring, **Table 3. 1**). This formation apparently exhibits a high interstices porosity and permeability;
- the medial zone is occupied by the mostly unweathered lava flow complex (LFC, with chronologically Nkj, Olf, klf, BRI…). It constitutes a huge geological unit. Springs and rivers discharge observations show that, at the exception of the Olf lava flow unit, which exhibits a weathering profile, the LFC can be considered as homogeneous as a whole. This is demonstrated by the fact that only a few low discharge (a few L s^{-1}) inter lava flows springs have been identified indicating few perched and local aquifers. Most of these inter lava springs flow out from clinker layers in contact with cooked paleosoils (red layers) acting as local impermeable layers. Hydrogeological surveys along the streams during the dry season show their low specific discharge (as compared to the efficient rainfall), and no measurable discharge increase along the stream was observed. It suggests that, beyond these small springs, streams do not drain significant aquifers, nor loss significant amount of water, this later process being surely due to stream siltation. In addition, few adventives cones (AC) have been observed on the medial zone and may provide a laterally continuous, low permeability and high density materials, according to Kereszturi and Nmeth (2012);
- In the distal zone of the volcano, the "slope deposits" (NM, SUig, Hng) most probably have a low permeability because of their clayey content;
- in the volcano-sedimentary plain ("distal zone"), the main hydrogeological feature is the confined aquifer which provides groundwater to the artesian springs and wells. According to the geological logs realized during the drilling survey, the confined aquifer is multi-layered. It is confined by a more than 10 m thick confining unit.

461 artesian wells were inventoried in the plain with an average discharge of 4.1 L s^{-1}. Considering the density of well on the field (≈6 well km^{-2}), we assume that 20% of the wells have not been inventoried. A maximum of about 600 wells is then estimated, corresponding to 2400 L s^{-1} flowing out in the plain. All the artesian springs show a total discharge of about 4000 L s^{-1} (**Table 3. 1**). Assuming a mean hydraulic head difference of about 5 m between the multi-layered confined aquifer and the unconfined aquifer and a confining unit of about 10 m

thickness with an hydraulic conductivity of 10^{-8} m s^{-1} (Breuer et al., 2000; Charlier et al., 2011), this gives a mean leakage of about 5 L s^{-1} km^2. For the whole volcano-sedimentary plain where artesianism is known (about 150 km^2), it results in a discharge of about 750 L s^{-1} due to "natural" leakage through the upper confining unit. The first roughly estimation of the total outflow from the Pasuruan aquifer system would thus be about 7000 L s^{-1}.

3.4.2 Hydro-climatological monitoring of the northern flank of the Bromo-Tengger

The new meteorological data are in agreement with the duration of the dry and wet seasons in this area: from May to October and from November to April, respectively (**Figure 3.6. a**). The minimum of the dry season occurred on August with only 3 mm of rainfall at the Temple station, and no rainfall at all at the other stations. The wet season peak occurred in February 2018 with a maximum rainfall value of 668 mm at Kronto. During both seasons, the Kronto and Wonorejo stations show higher rainfall than Aqua on one hand, but also than Seruni and Temple that are however at a higher elevation. On the basis of all data, 9 to 21% of annual rainfall occurs during the dry season while 79 to 91% of rainfall is recorded during the wet season.

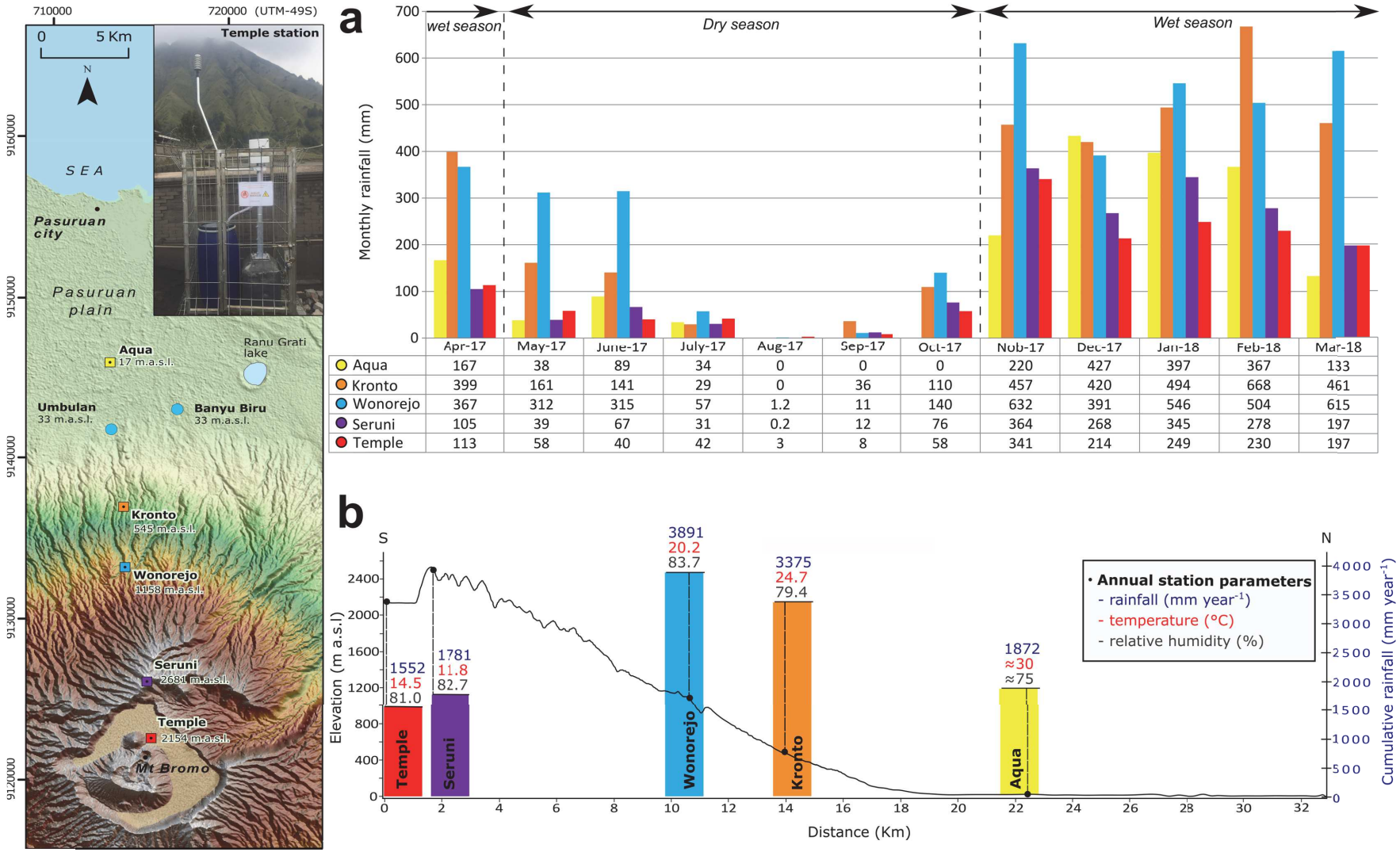

Figure 3. 6. a Monthly rainfall monitored at the 5 meteorological stations installed during this research along the Northern flank of Bromo-Tenger. **b** Annual rainfall, mean annual temperature and relative humidity for each meteorological station. The Aqua temperature and humidity have been inferred from the temperature altitudinal

An important altitudinal gradient of rainfall is observed on the volcano's flank, from Aqua station (≈20 m.a.s.l.) in the plain, to Wonorejo station (≈1100 m.a.s.l.) with annual rainfall of 1878 mm and 3891 mm, respectively (**Figure 3. 6. b**). Upstream, rainfall decreases from Wonorejo to Seruni (≈2700 m.a.s.l.) and to Temple (≈2100 m.a.s.l.), with annual rainfall of 1781 and 1552 mm, respectively. Studies about altitudinal gradient of precipitation on high tropical or equatorial mountains also show a decrease of rainfall beyond a certain elevation, such as in Hawaii (Scholl et al., 1996; Scholl et al., 2002), or in the Martinique French West Indies island (Vittecoq et al., 2010). The air mass reaching the volcano's summit are cooler, however they are impoverished in vapor. Based on these studies and our data, the most realistic precipitation pattern was drawn, with a peak at an elevation of about 1200 m a.s.l. (**Figure 3. 7. b**).

An altitudinal gradient of temperature of about -0.6°C/100 m was assessed, with a mean annual temperature of about 30°C in the plain to 11.8°C in the caldera, which is consistent with the known temperature gradient on volcanoes in such tropical environment (Selles, 2014). No significant gradient is observed for the relative humidity, ranging from 75% in the plain to 83.3% in Wonorejo station. However, cloud and fog accumulation are frequently observed below Seruni (2700 m.a.s.l.), indicating a condensation layer below this elevation. The interception of wind-blown droplets of water by the vegetation, commonly called cloud water interception (CWI), or fog drip, is likely to increase rainfall height. In the Santa Cruz Island of the Galapagos (Ecuador), the fog drip is negligible at 400 m.a.s.l., but represents more than 20% of incident rainfall at about 650 m.a.s.l. and directly contributes to groundwater recharge (Pryet et al., 2012). This parameter can thus be a significative part of the recharge, as also identified on La Gomera (Canary Island) where it represents more than 700 mm y^{-1} according to the fog drip calculation models (Izquierdo, 2014). On the Bromo-Tengger, except some field observations, there is no measurement allowing to quantify fog drip.

As a summary, these first results indicate a precipitation pattern controlled by orographic effects occurring on the Northern flank of the volcano, under the influence of the dominant NW-SE winds. The rainfall thus increases to a maximum value at about 1200 m.a.s.l. elevation and decreases beyond.

3.4.2.1 Results of the climatic and hydrological analyses

The computation of the water budget at each meteorological station allows to plot the Rainfall, RET and ER as function of the elevation (**Figure 3. 7 a, b, c**). From April 2017 to March 2018, the recharge rate was also estimated on the representative Kronto watershed (**Figure 3. 7 a**). All results are compiled in the table from **Figure 3. 7 c**.

- PET & RET: similarly to the temperature, the potential evapotranspiration (PET) and the real evapotranspiration (RET) continually decrease from the plain to the volcano summit with, for example, a RET of about 1460 mm in the Pasuruan plain, and about 620 mm at Seruni. These RET results are consistent with the GLEAM satellite data (Martens et al., 2017) with a

difference of less than 6% (**Figure 3. 1**) (1153 mm y^{-1} for the mean GLEAM interannual RET from November 1980 to October 2017 and 1223 mm computed on our site for April 2017 to March 2018).
The effective rainfall (ER) is very concomitant with the rainfall (R) variation because of the RET absolute value (much lower than R, at the exception of the lower part of the volcano) and the RET distribution along the flank of the volcano. Nevertheless, the "impact" of RET is maximum at low elevation where ER is finally rather low (about 600 mm at an elevation of 50 m.a.s.l.). Then, ER increases steeply, to reach a maximum of 3100 mm also at about 1200 m.a.s.l.. At higher elevation, ER steeply decreases with 1300 mm only on the top of the volcano's flank and 900 mm in the inner caldera.

- Re: during the period Nov-17 to Oct-18, the discharge of the Kronto representative watershed is only about 7% of the rainfall (9.5% of the effective rainfall). These data suggest that aquifer recharge is about 66% of the rainfall, and about 90.5% of the effective rainfall (**Figure 3. 7 c**). This result is consistent with the geological observations (cf. section 3.4.1) that did not identify impermeable rocks on this experimental watershed, nor on the whole flank of the Bromo volcano. Similar results were found in tropical and andesitic (pyroclastics) context in Guadeloupe (French West Indies) where the aquifer recharge was estimated at about 85% of the annual effective rainfall (Charlier et al., 2011). This recharge rate is an average infiltration rate on the whole representative watershed (450 to 2600 m.a.s.l.) as the hydrological and hydrogeological field observations did not enable to identify any preferential recharge area.

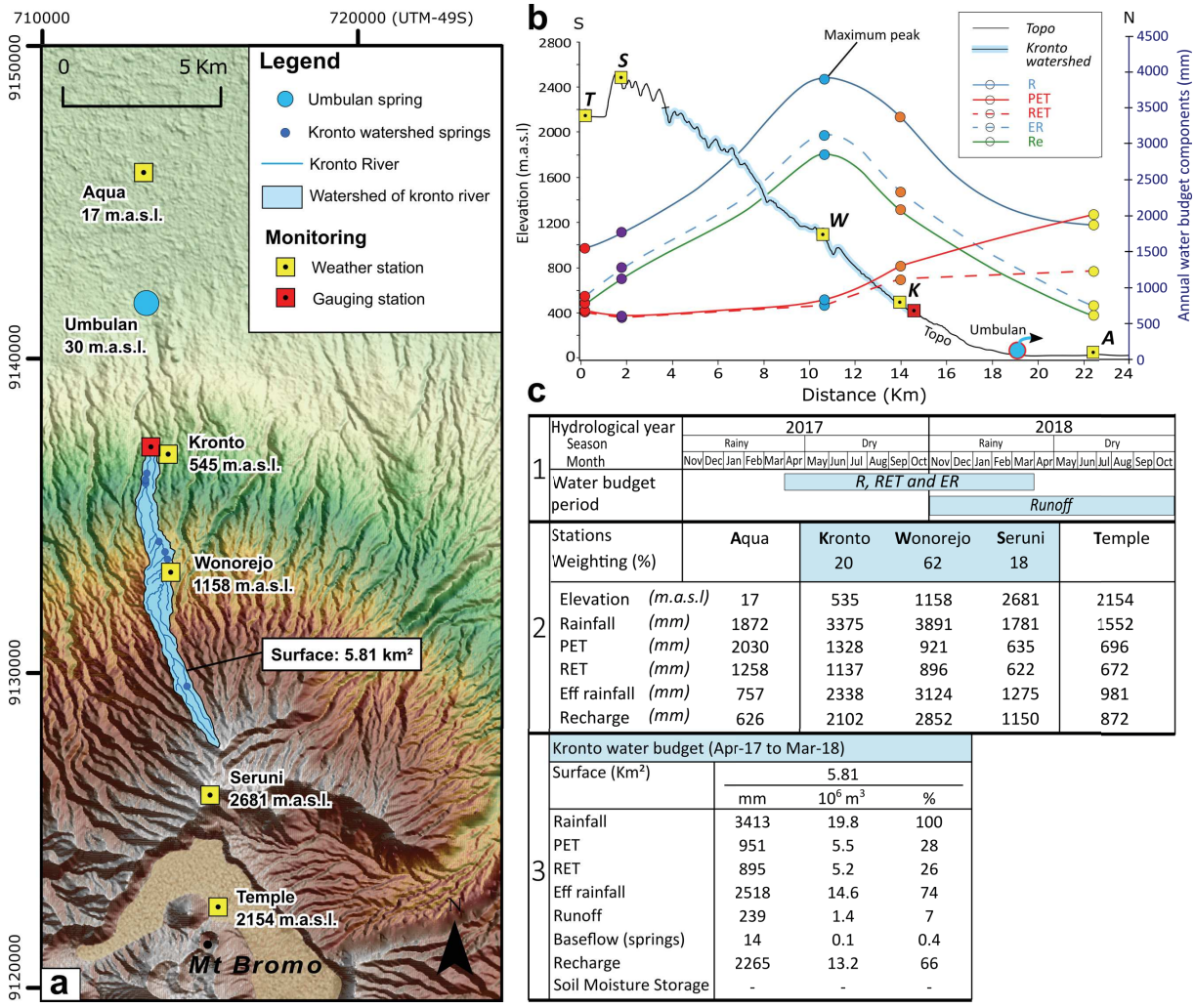

c

1

Hydrological year	2017	2018
Season	Rainy / Dry	Rainy / Dry
Month	Nov Dec Jan Feb Mar Apr May Jun Jul Aug Sep Oct	Nov Dec Jan Feb Mar Apr May Jun Jul Aug Sep Oct
Water budget period	*R, RET and ER*	*Runoff*

2

Stations		Aqua	Kronto	Wonorejo	Seruni	Temple
Weighting (%)			20	62	18	
Elevation	*(m.a.s.l)*	17	535	1158	2681	2154
Rainfall	*(mm)*	1872	3375	3891	1781	1552
PET	*(mm)*	2030	1328	921	635	696
RET	*(mm)*	1258	1137	896	622	672
Eff rainfall	*(mm)*	757	2338	3124	1275	981
Recharge	*(mm)*	626	2102	2852	1150	872

3

Kronto water budget (Apr-17 to Mar-18)			
Surface (Km²)	5.81		
	mm	10^6 m³	%
Rainfall	3413	19.8	100
PET	951	5.5	28
RET	895	5.2	26
Eff rainfall	2518	14.6	74
Runoff	239	1.4	7
Baseflow (springs)	14	0.1	0.4
Recharge	2265	13.2	66
Soil Moisture Storage	-	-	-

Figure 3. 7. a Location map of the Kronto river representative watershed and the monitoring network. **b** water budget parameter. **c** Tables of results: 1) periods for each type of computation, 2) water budget computations at each meteorological station 3) Kronto watershed water budget.

3.4.3 Hydrochemistry

Field parameters and laboratory analyses, including major ions and stable isotopes ($\delta^{18}O$, δD) of groundwater samples from gravity springs, artesian springs and artesian wells are reported on **Table 3. 1** and **3.2** and their location is plotted on **Figure 3. 3**.

Electrical conductivity (EC) of groundwater ranges from 109 to 671 µS cm^{-1}. In the plain, artesian wells and springs show relatively homogeneous conductivity values (ranging from 202 to 353 µS cm^{-1} and 203 to 381 µS cm^{-1} respectively). Gravity springs located on the flank of the volcano show a large range of conductivity (from 109 to 671 µS cm^{-1}) and the highest values but no correlation was found between the conductivity and the location of the spring as high conductivity is mostly linked to anthropogenic impacts on each small watershed. In contrast, an increase of conductivity towards the North was found for artesian springs and wells located in the plain due to water-rock interactions.

The mean temperature of the water samples is 22.6°C ± 3.6°C. Groundwater temperature is well correlated with the elevation of the spring. The water temperature increases as the elevation decreases, with a minimal temperature of 12.5°C at 2700 m.a.s.l. (Seruni spring, n°17) and a maximal temperature of 26.2°C in the plain for the deep artesian well 20 (150 m deep). The main spring of the system, Umbulan, has an intermediate temperature of 23.5°C. Temperatures of the artesian wells and springs in the plain are not at the equilibrium with the mean local air temperature (about 30°C) indicating a recharge at a higher elevation.

For all groundwater samples, dominant cations are Ca and Mg (**Figure 3. 8 a**, **Table 3. 1**), in good agreement with the andesitic bedrock composition. Three dominant anions (HCO_3^-, SO_4^{2-}, Cl^-) were found depending on the groundwater samples. Based on the dominant anions and the relative Ca vs Mg concentration of water, three groups of groundwater were identified. They are also related to various elevations (**Figure 3. 8 a**):

- In the plain, water samples of artesian springs and wells are dominated by CaMg-HCO_3- water type (**Figure 3. 8 a**).
- On the flank of the volcano, gravity springs located higher than 1000 m.a.s.l. (Volcanic & anthropogenic group; **Figure 3. 8 a**) belong to CaMg-Cl or CaMg-SO_4 water type. The high values of Cl^- and NO_3^- occur in the vicinity of villages or crop fields and indicate anthropic contaminations (e.g. Banyu Ngisor n°15, **Table 3. 1**). The highest SO_4^{2-} contents were found in springs close to the top of the volcano at elevation ranging between 1700 and 2700 m.a.s.l. where volcanic sulphur deposits occur. They indicate the influence of the volcanic activity (e.g. Widodaren, n°16).
- A last group show an intermediate composition between the volcanic-anthropogenic type and the main basal aquifer type.

Groundwater samples from intermediate and artesian plain groups show a continuous geochemical evolution through an increase of Ca/Mg towards the North (**Figure 3. 8 b**), with the distance from the volcano. The conductivity increase and Mg^{2+} enrichment in the volcano-sedimentary plain, may result from an increase of residence time triggered by an intensive water-rock interaction with clayey formations (Paternoster et al., 2010). The weathering of the

volcano-sedimentary formations allows the dissolution of Mg -rich minerals like Olivine ($(Mg,Fe)_2SiO_4$) and Pyroxene ($X^+Y^-(SiO_3)_2$). This dissolution together with the North-South groundwater flow direction explains the Mg^+ trend observed on artesian wells towards the North (**Figure 3. 8 b**). This relatively linear Mg enrichment for these 2 groups is well correlated with the electric conductivity and water temperature increases. This spatial evolution of water chemistry suggests that gravity springs at low elevation and artesian wells/springs belong to the same lithological and hydrogeological system with groundwater aging as it flows towards the North. Gravity springs result from perched aquifers. Direct recharge, leaking water from these perched aquifers and surface water directly infiltrating to the main basal aquifer supply the multi-layered aquifer feeding the artesian springs and wells. As a consequence, common recharge processes can be considered for the artesian springs/wells and gravity springs of low elevation. The gravity springs above 1700 m.a.s.l. do not exactly show the same evolution as they are also influenced by different processes, and notably deposits issuing from the active volcanic vents. Regarding the Ca^{2+} increase observed on these springs, it may correspond to water rock interaction at the surface of clay-minerals within the pyroclastic complex.

No anthropogenic and volcanic chemical components are significantly observed in the plain system. This suggest a limited contribution from the highest part of the volcano to the recharge of the main basal aquifer (SO_4) and confirm the limited extension of agricultural activities compared to the total recharge area of the aquifer (dilution effect).

Two wells (n°7 and 22) follow the same Ca/Mg ratio trend. They are located between Umbulan and Banyu Biru springs and aligned on the supposed SW-NE fault (**Figure 3. 5**) which could explain a shorter transit time led by this fault.

The Ranu Grati maar could be a natural outflow from the same type of aquifer(s), at least as regards lithology, but with longer water/rock interactions.

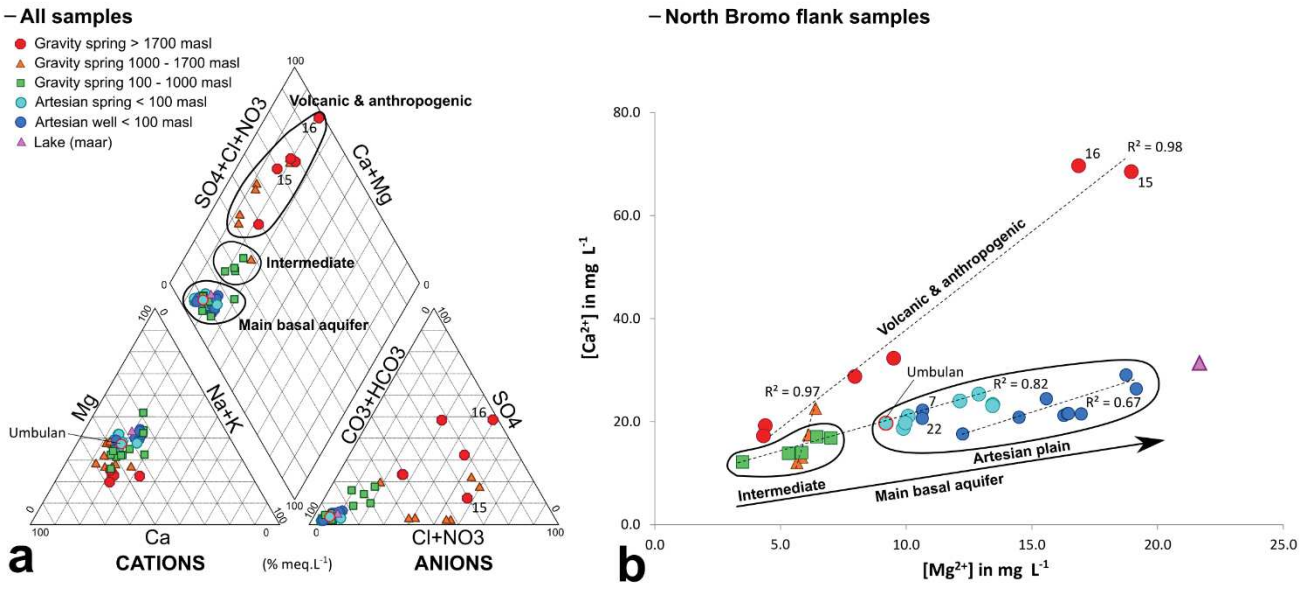

Figure 3. 8. a Piper diagram of major ions analysed in springs, wells and lake. **b** Binary plot $[Ca^{2+}]$ vs $[Mg^{2+}]$ for same groundwater samples.

Table 3. 1. Hydrochemical and isotopic results. Samplings and water analyses were repeated for some locations (b and c letters). *NA:* not available; *BDL:* below detection limit.

No.	Water point name	Type	Location	WG84 UTM Zone 49S Long (m)	Lat (m)	Elev. (m.a.s.l.)	Well depth (m)	Discharge (L s^{-1})
1	Kali Sukun	Artesian spring	Sruwi	716014	9142825	26	-	<10
2	Telogo	Artesian spring	Sruwi	715819	9142568	31	-	10
3	Banyu Biru	Artesian spring	Banyu Biru	717071	9143017	33	-	380
4	Umbulan	Artesian spring	Umbulan	713303	9141735	33	-	3500
5	Aqua well	Artesian well	Keboncandi	713239	9145886	13	100	40
6	Bandaran well	Artesian well	Bandaran	716299	9144839	40	100	7.5
7	Small artesian well Sruwi	Artesian well	Sruwi	714614	9142240	50	NA	<0.01
8	Sumber Lumbang	Gravity spring	Cukurguling	717194	9137517	384	-	1
9	Sumber Gondang 1	Gravity spring	Kronto	713273	9136210	551	-	2
10	Danyang (Wonorejo)	Gravity spring	Wonorejo	714011	9133531	1060	-	<0.5
*11	Sumber Tengah	Gravity spring	Wonorejo	714114	9133282	1144	-	0.1
12	Posong Tepis-Tesa Sapikerep	Gravity spring	Sapikerep valley	723956	9125054	1261	-	<1
13	Kendil	Gravity spring	Ngadas	720153	9124239	1753	-	>1
*14	Little-Spring-Tosari	Gravity spring	Tosari	710563	9126720	1810	-	>1
*15	Banyu Ngisor	Gravity spring	Wonokitri	710763	9127493	1860	-	<0.01
16	Widodaren Caldera	Gravity spring	Widodaren	714129	9120656	2200	-	<0.5
*17	Seruni	Gravity spring	Seruni	715008	9126199	2700	-	<1
18	Séruni 2	Gravity spring	Cemoro Lawang	714943	9125300	2675	-	0.5
19	Borehole 7	Artesian well	Gading	715751	9145789	22	80	12
20	Borehole 54	Artesian well	Pandan Rejo	715293	9147863	18	125	4
21	Kali Pancur 3	Gravity spring	Pancur	715374	9135997	672	-	1
22	FD1	Artesian well	sruwi	715390	9142385	20	110	2
23	Ranu Grati	Lake (Maar)	Grati	721646	9145382	17	-	NA
24	Tirtoageng	Gravity spring	Sapikerep valley	727707	9133759	356	-	<20
25	Madakaripura	Gravity spring	Sapikerep valley	721478	9131294	850	-	200
26	Sumber Pitu	Gravity spring	Malang	700778	9113788	870	-	1000
27	Community drill 96m	Artesian well	Winongan	714339	9146170	15	96	15
28	Umbulan Malang	Artesian spring	Malang	694643	9095612	465	-	100
29	Kalimati	Gravity spring	Kalimati	710306	9105189	2700	-	1
30	Wendit Malang	Artesian spring	Malang	684528	9120348	478	-	300
31	Coban sewu	Gravity spring	Lumajang	711117	9089737	526	-	100
32	Ranggojalu	Artesian spring	Probolinggo	747589	9131545	61	-	3200
33	Kronto station	Rain water	Kronto	713990	9136958	545	-	-
34	Wonorejo station	Rain water	Wonorejo	714071	9133211	1158	-	-
35	Temple station	Rain water	Caldera bromo	715445	9122585	2154	-	-
36	Seruni station	Rain water	Seruni	715323	9126121	2681	-	-

Table 3. 1. Hydrochemical and isotopic results. Samplings and water analyses were repeated for some locations (b and c letters). (-): not available;

No.	Water point name	Elevation (m.a.s.l.)	Type	Date	pH	EC ($\mu S.cm^{-1}$)	T (°C)	O_2 ($mg.L^{-1}$)	HCO_3^- ($mg.L^{-1}$)	Ca^{2+}	Mg^{2+}	K^+	Na^+	Cl^-	SO_4^{2-}	NO_3^-	Ionic Balance (%)	$\delta^{18}O$ (‰)	δD (‰)
1	Kali Sukun	26	AS	13/06/2016	7.0	264	24.0	6.5	135.9	24.0	12.1	2.7	7.5	2.5	3.0	2.4	4	-7.37	-44.2
2	Telogo	31	AS	13/06/2016	7.3	204	23.7	7.3	119.3	21.0	10.1	2.2	6.5	2.7	3.0	3.3	2	-7.46	-44.8
3	Banyu Biru	33	AS	13/06/2016	7.0	258	25.6	7.0	152.5	25.3	12.9	2.4	7.4	1.7	2.3	3.5	1	-7.08	-41.5
	b	33	AS	23/11/2016	7.2	253	24.0	6.4	160.5	23.3	13.4	2.1	7.4	1.7	2.4	4.0	-3	-7.08	-40.7
	c	33	AS	15/05/2017	6.4	257	23.8	6.4	153.6	23.1	13.4	2.4	7.5	2.1	2.3	3.6	-1	-7.14	-41.4
4	Umbulan	33	AS	11/05/2016	6.9	205	23.5	6.9	100.0	19.7	9.2	2.7	7.0	2.3	3.2	4.7	7	-7.32	-42.8
	b	33	AS	23/11/2016	7.2	208	23.5	7.3	137.1	18.7	9.9	2.4	7.3	2.2	3.3	5.4	-7	-7.15	-42.2
	c	33	AS	17/05/2017	6.9	217	23.4	6.9	122.6	19.7	10.0	2.7	7.4	2.5	3.1	5.1	-1	-7.28	-42.7
5	Aqua well	17	AW	15/05/2016	7.1	306	25.0	6.4	137.8	20.9	14.5	5.2	11.5	6.1	8.1	6.4	3	-6.96	-40.6
	b	17	AW	23/11/2016	7.2	310	24.6	6.5	176.4	21.5	17.0	5.2	13.1	6.5	8.4	7.5	-3	-7.00	-39.9
	c	17	AW	11/12/2017	7.1	316	24.9	6.4	162.7	22.1	14.6	5.4	12.0	7.0	7.7	7.0	-3	-6.96	-41.7
6	Bandaran well	17	AW	13/06/2016	6.9	230	24.8	8.0	131.3	17.6	12.2	4.8	10.7	3.0	4.3	3.8	2	-7.31	-43.3
7	Small art well Sruwi	17	AW	13/06/2016	7.0	203	25.0	7.2	121.5	22.2	10.6	2.1	6.8	2.3	2.8	3.4	4	-7.44	-43.8
8	Sumber Lumbang	384	GS	22/05/2016	7.8	148	25.1	7.8	97.6	13.9	5.3	0.3	5.9	1.1	1.8	6.9	-12	-6.93	-42.0
	b	384	GS	24/11/2016	7.7	147	25.6	7.9	89.4	14.0	5.8	0.3	7.1	1.1	2.0	5.6	-4	-6.98	-39.6
9	Sumber Gondang 1	551	GS	11/06/2016	6.3	158	25.0	7.3	88.6	17.1	6.4	1.0	5.6	0.9	1.7	6.9	1	-7.18	-42.7
	b	551	GS	24/11/2016	7.4	164	24.0	7.9	96.9	16.9	7.0	0.9	5.8	1.0	1.9	7.0	-2	-7.21	-41.9
10	Danyang (Wonorejo)	1060	GS	11/06/2016	6.6	192	22.2	7.6	55.9	22.6	6.4	0.8	4.9	10.0	2.1	24.2	7	-7.43	-44.1
	b	1060	GS	24/11/2016	7.4	173	22.0	7.6	62.5	17.5	6.1	0.6	4.8	10.0	2.1	24.4	-4	-7.44	-41.8
*11	Sumber Tengah	1144	GS	11/06/2016	6.6	132	22.2	7.5	31.2	13.1	5.8	0.4	3.3	9.8	1.1	24.7	3	-7.47	-45.8
	b	1144	GS	24/11/2016	7.0	136	22.0	7.4	35.7	12.0	5.7	0.3	3.4	10.4	1.1	26.2	-4	-7.52	-44.1
12	Posong Tepis	1261	GS	07/06/2016	6.3	192	22.4	5.3	67.8	17.8	6.2	4.5	9.5	5.6	16.4	11.1	4	-7.26	-44.9
13	Kendil	1753	GS	10/06/2016	7.0	462	18.4	7.8	61.2	47.2	15.0	10.2	15.2	12.2	42.6	118.3	4	-8.17	-53.3
*14	Little-Spring-Tosari	1810	GS	06/06/2016	6.7	305	18.0	7.6	38.1	32.3	9.5	5.7	10.0	11.9	21.9	79.3	5	-8.58	-54.3
*15	Banyu Ngisor	1860	GS	06/06/2016	6.6	610	19.7	7.1	103.9	68.5	19.0	6.0	19.5	39.2	31.9	128.6	4	-8.85	-57.6
16	Widodaren Caldera	2200	GS	14/05/2016	5.6	671	17.9	7.0	7.4	69.7	16.9	11.6	23.8	104.4	138.6	0.0	2	-8.61	-55.8
*17	Seruni	2700	GS	14/05/2016	7.5	170	12.5	7.2	46.0	19.2	4.4	3.2	6.8	12.2	16.4	2.2	7	-10.49	-68.1
	b	2700	GS	01/12/2016	7.0	170	12.6	7.3	19.9	17.2	4.3	2.7	6.5	18.1	23.3	11.4	2	-10.40	-66.7
18	Seruni 2	2675	GS	09/06/2016	6.7	275	15.7	7.1	33.4	28.8	8.0	3.4	9.7	24.6	55.8	0.5	4	-10.17	-66.9
19	Borehole 7	22	AW	27/06/2016	6.7	297	26.0	5.8	166.5	24.5	15.6	6.0	12.6	5.6	8.0	5.5	1	-7.00	-42.1
	b	22	AW	23/11/2016	7.3	296	25.1	5.9	191.3	21.3	16.3	5.1	12.9	5.8	8.1	6.0	-7	-6.91	-39.7
20	Borehole 54	18	AW	27/06/2016	7.3	353	26.2	3.8	207.2	29.1	18.7	7.9	17.0	7.1	9.4	3.1	1	-7.15	-42.2

	b	18	AW	23/11/2016	7.4	361	25.6	3.9	210.0	26.4	19.1	6.5	16.9	7.3	9.9	4.2	-2	-7.19	-40.6
21	Kali Pancur 3	672	GS	27/06/2016	6.0	109	24.6	2.9	61.2	12.2	3.5	0.9	4.5	0.6	1.4	1.5	2	-7.03	-42.4
22	FD1	20	AW	23/11/2016	7.5	212	24.8	7.5	139.6	20.7	10.6	1.8	6.7	1.6	2.3	4.3	-4	-7.35	-41.8
23	Ranu Grati	17	LAKE	18/05/2017	8.8	470	25.2	13.9	144.4	31.4	21.7	6.6	14.6	8.8	6.3	0.0	2	-4.96	-33.7
24	Tirtoageng	356	GS	27/04/2017	6.2	479	24.5	5.0	203.5	37.6	30.5	10.2	25.2	25.0	43.5	12.5	5	-7.83	-47.9
	b	356	GS	19/05/2017	6.2	573	24.1	5.3	228.2	33.8	25.4	8.7	21.5	20.8	35.5	12.4	-4	-8.05	-51.0
25	Madakaripura	850	GS	19/05/2017	6.9	114	20.9	8.1	98.2	13.6	5.6	2.1	5.5	2.5	4.7	3.2	-12	-7.71	-46.3
26	Sumber Pitu	870	GS	12/06/2017	7.1	628	20.6	7.3	312.9	39.2	42.6	9.8	24.5	18.6	52.3	5.7	0	-8.95	-56.4
27	Community Drill 96m	15	AW	27/05/2017	7.0	304	24.7	6.1	148.8	21.6	16.4	5.6	12.7	6.3	8.0	5.6	4	-6.98	-40.2
	b-78m	15	AW	22/05/2017	7.1	318	24.3	5.4	148.4	21.6	16.5	5.6	12.7	6.1	8.0	5.5	5	-7.08	-41.0
28	Umbulan Malang	465	AS	11/04/2017	6.7	200	20.9	7.1	105.1	15.9	8.2	3.4	12.0	8.1	9.3	4.0	-4	-7.50	-42.4
29	Kalimati	2700	GS	28/04/2017	6.6	-	-	-	71.5	9.9	3.0	2.6	6.7	1.5	3.3	0.8	-9	-10.83	-68.8
30	Wendit Malang	478	AS	11/04/2017	6.3	327	25.0	5.4	139.8	27.4	13.6	5.2	13.4	8.2	15.5	25.0	-1	-6.65	-39.5
31	Coban sewu	526	GS	11/04/2017	7.8	359	22.6	8.4	241.7	26.1	20.1	5.8	18.3	5.0	9.5	2.6	-6	-6.76	-39.1
32	Ranggojalu	61	AS	10/04/2017	6.8	381	26.5	6.1	215.3	29.9	17.7	5.7	18.1	12.7	5.4	6.5	-3	-6.55	-37.0
33	Kronto station	535	RAIN	27/03/2018	-	-	-	-	-	-	-	-	-	-	-	-	-	-7.44	-45.6
34	Wonorejo station	1158	RAIN	27/03/2018	-	-	-	-	-	-	-	-	-	-	-	-	-	-7.97	-48.1
35	Seruni Station	2681	RAIN	30/03/2018	-	-	-	-	-	-	-	-	-	-	-	-	-	-11.83	-78.6
36	Temple station	2154	RAIN	30/03/2018	-	-	-	-	-	-	-	-	-	-	-	-	-	-10.45	-70.1

3.4.4 Isotopic composition of groundwater and rainfall

Water isotopes signatures of groundwater, surface water and precipitation are reported in the **Table 3. 1** and plotted in **Figure 3. 9 a**.

The four rain gauges, from 545 to 2681 m.a.s.l., have sampled one full year of annual cumulated rainfall (April 1st 2017 – March 2018). They show a large range of variation from -7.5 to -11.8‰ for $\delta^{18}O$ and from -45.8 to -78.6‰ for δD. The observed $\delta^{18}O$ altitude gradient for rainfall is consistent with to a Rayleigh adiabatic condensation process. The isotopic signature of groundwater samples (**Figure 3. 9 b**) shows a similar range of variation (-6.6 to -10.8‰ for $\delta^{18}O$ and from -37 to -68.8‰ for δD), for an elevation of sampling locations ranging from about 20 to 2700 m.a.s.l.. In the main artesian system of the plain (springs and wells), the range of variation is narrower with variations ranging from -6.91 to -7.46‰ for $\delta^{18}O$ and from -39.70 to -44.75‰ for δD, strongly suggesting a common recharge area. The surface water sample (Ranu Grati lake, n° 23), shows the lowest $\delta^{18}O$ value and the highest δD (-4.9 and -33.7‰ respectively).

Most of the groundwater samples align above the global meteoric water line (GMWL) and the local meteoric water line (LMWL) calculated from the GNIP station of Jakarta (IAEA, 1961). These results show that rainwater composition undergoes the local topographic effects of the volcano. The sample from surface water (Ranu Grati Lake) falls below the LMWL (**Figure 3. 9 b**). This position indicates an evaporation process in good agreement with the stagnation of the lake water and the high temperature in the plain (about 30 °C).

To consider the local topographic effect on rainwater, the Bromo meteoric water line was calculated (BMWL; **Figure 3. 9 b**) from the four rain gauges of the area and the GNIP station of Jakarta (with weighted mean respectively -5.63 and -36.10‰ for $\delta^{18}O$ and δD). The BMWL equation is:

$$\delta D‰ = 7.23\ \delta^{18}O + 7.53 \quad (3.9)$$

In addition, four “integrative springs” (n°11, 14 ,15 and 17; black crosses, **Figure 3. 9**) selected for their short groundwater flow paths and no relationships with nearby stream water were used as proxies for precipitation to calculate the Bromo spring water line (BSWL), given by the equation:

$$\delta D‰ = 7.71\ \delta^{18}O + 12.37 \quad (3.10)$$

The elevation effect is clearly visible for the Northern flank of the Bromo-Tengger (**Figure 3. 9 c**) with a $\delta^{18}O$ and δD decrease as elevation increases. The Widodaren spring n°16, located at 2200 m.a.s.l., in the inner caldera, does not follow this trend. Its $\delta^{18}O$ signature is similar to the one of the springs from the Northern flank of the Bromo-Tengger, located at about 1800 m.a.s.l elevation. The difference may be explained by the impact of the local volcanic steam from the active vent of Mt Bromo, that probably emits an enriched $\delta^{18}O$.

There is a good correlation between the isotopic composition of the 4 elevations classes of groundwater samples (**Figure 3. 9**) and the precipitation defined by a gradient of -0.19‰

$\delta^{18}O$/100 m from the BSWL and by a gradient -0.23‰ $\delta^{18}O$/100m from BMWL. These gradient values are of the same order of magnitude than those found for other volcanoes in Indonesia such as Merapi (-0.29‰ $\delta^{18}O$/100 m; (Selles, 2014)), or the Vulture volcano in Italy (-0.17‰ $\delta^{18}O$/100 m; (Parisi et al., 2011)).

Nevertheless, a shift is observed between BMWL and BSWL. This shift cannot be solely explained by the isotopic inter-annual variation; 1962 to 1998 data from the GNIP station of Jakarta show only a seasonal difference of 0.58 ‰ $\delta^{18}O$. But the fog drip observed from about 2000 m.a.s.l. on the Bromo-Tengger (section 3.4.2) may represent a water input to the aquifer which has to be taken into account and may explain this shift. According to (Scholl et al., 2002), fog samples have isotopic signatures enriched by as much as 3‰ in $\delta^{18}O$ and 21‰ in δD compared to volume-weighted average precipitation at the same elevation. Our field observations comfort this hypothesis as the highest part of the volcano is covered by cloud layers, and fog drip from the trees was observed near Seruni rain gauge and spring. This enrichment cannot be observed on the rain isotopic results because rain gauges are located on a clear and open area to avoid fog drip or other quantitative artefact from vegetation, but they are registered by the springs. As elevation decreases, the fog drip effect decreases, reducing the shift between the two lines (BMWL and BSWL).

As a consequence, the BSWL is more representative of the recharge of the aquifer. The $\delta^{18}O$ altitudinal gradient from integrative springs was thus used to infer recharge elevation for the artesian springs and wells (**Figure 3. 9 c**). The apparent mean recharge elevation of the all artesian springs and wells is from about 700 to 1300 m.a.s.l., +/-150 m if one considers analytical uncertainty (**Figure 3. 9 c**).

The artesian springs and wells (< 100 m.a.s.l.) seem to have the same isotopic signature than the gravity springs below 1300 m.a.s.l., (green square and orange triangle, **Figure 3. 9**). Careful hydrogeological interpretation shows that “orange triangle springs” have a small-sized recharge area and can also be considered as “integrative” springs whereas “green square springs” have a large recharge area and are probably influenced by stream infiltration or connected perched aquifers. Stream infiltration is the most relevant explanation as recharge elevation inferred from these springs’ isotopic signature is consistent with the elevation range of streams surface watersheds near the springs. These data cannot be used to draw the BSWL.

The highest springs on the northern flank with the lowest isotopic values suggest that they are (i) disconnected from the downstream groundwater and the artesian plain or (ii) represented a low contribution to the recharge of the main basal aquifer.

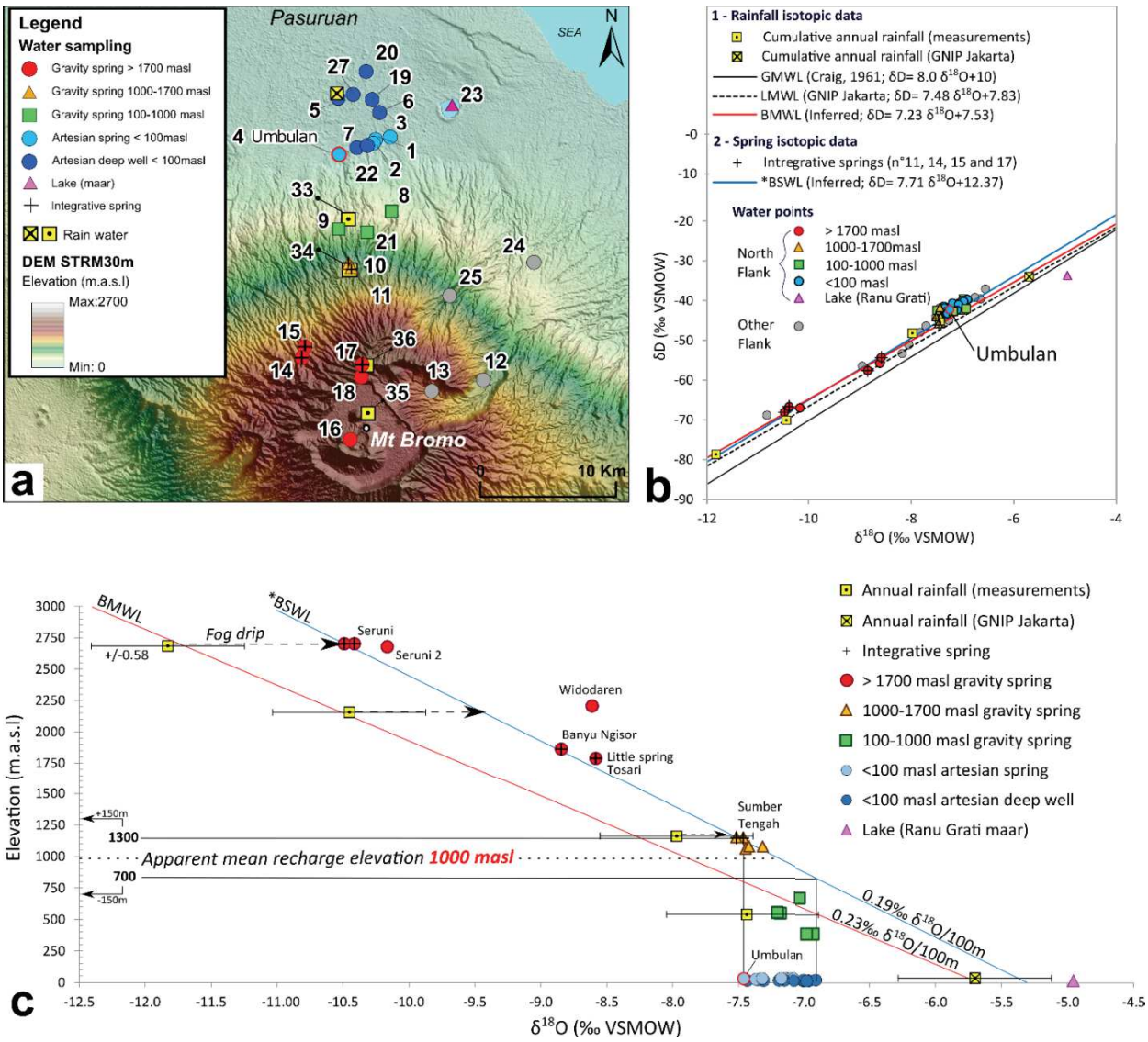

Figure 3. 9. a Location map of the water sampled on the Northern flank of the Bromo-Tengger, **b.** $\delta D/\delta^{18}O$ graph, **c.** $\delta^{18}O$/elevation graph.

3.4.5 Quantitative modeling of groundwater isotopic signature

- **Step I**: discretisation of the potential recharge area (refer to **Figure 3. 4** for methodology)

The whole northern flank of the Bromo-Tengger was discretized into 29 slices of 100 m elevation interval (**Figure 3. 10**). The median elevation of each slice is ranging from 50 m.a.s.l. (1st slice) to 2750 m.a.s.l. (28th slice). A 29th slice considers the half surface of the Tengger caldera with an elevation of 2150 m.a.s.l.. The total surface considered (potential recharge area) is 540.8 km². The first slice was considered without any potential recharge due to the cover of the low permeability volcano-sedimentary confining unit and the upwards piezometric gradient; it was thus not taken into account. This slice constitutes the northern limit of the potential recharge area. The western and eastern limits of the potential recharge area are delineated on the basis of geomorphological arguments (Nongkojajar caldera rim to the West and Sapikerep valley to the East) while the southern limit is bounded by the volcano's summit and the half of the Tengger caldera.
The lowest slices exhibit the largest surface areas (44.7 km² for the lowest slice). Surface areas progressively decrease when elevation increases, at the exception of the 29th slice which is larger since it comprises the half of the Tengger caldera (20 km²).

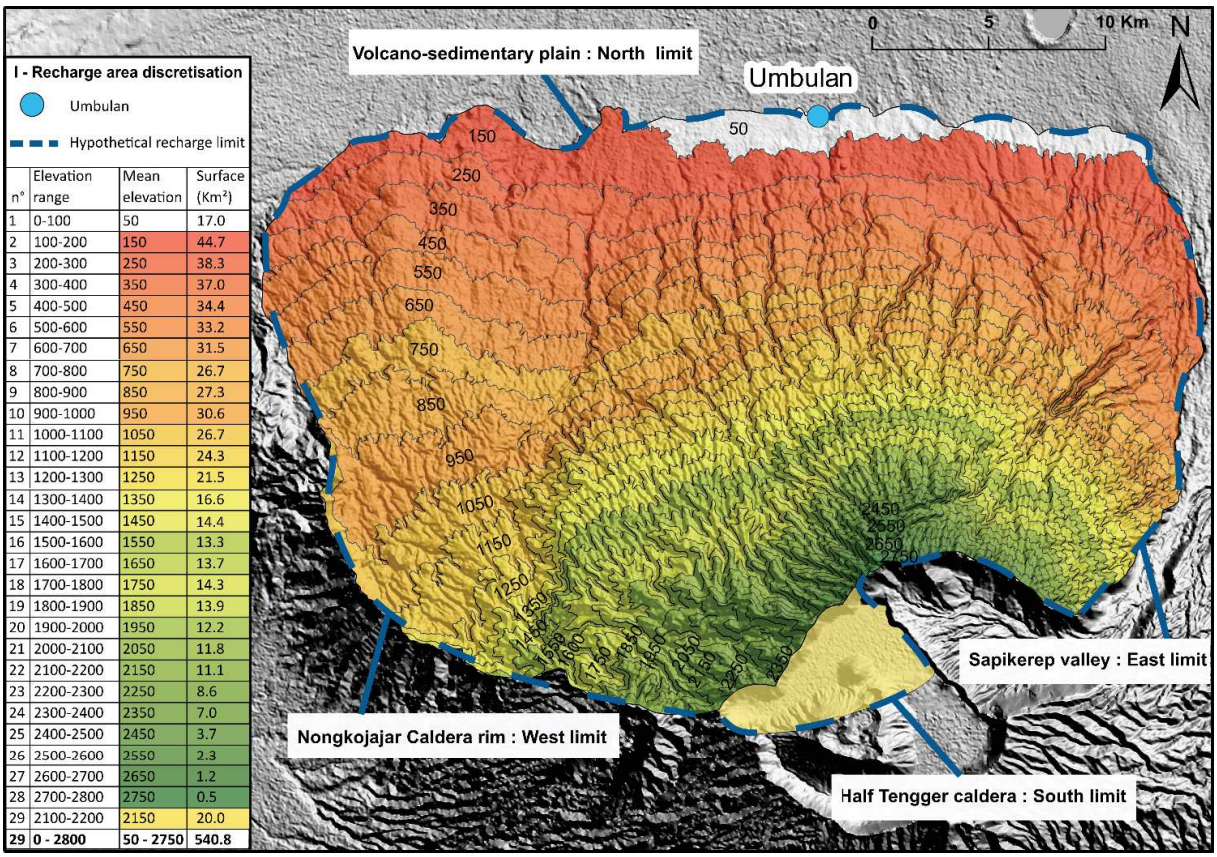

n°	Elevation range	Mean elevation	Surface (Km²)
1	0-100	50	17.0
2	100-200	150	44.7
3	200-300	250	38.3
4	300-400	350	37.0
5	400-500	450	34.4
6	500-600	550	33.2
7	600-700	650	31.5
8	700-800	750	26.7
9	800-900	850	27.3
10	900-1000	950	30.6
11	1000-1100	1050	26.7
12	1100-1200	1150	24.3
13	1200-1300	1250	21.5
14	1300-1400	1350	16.6
15	1400-1500	1450	14.4
16	1500-1600	1550	13.3
17	1600-1700	1650	13.7
18	1700-1800	1750	14.3
19	1800-1900	1850	13.9
20	1900-2000	1950	12.2
21	2000-2100	2050	11.8
22	2100-2200	2150	11.1
23	2200-2300	2250	8.6
24	2300-2400	2350	7.0
25	2400-2500	2450	3.7
26	2500-2600	2550	2.3
27	2600-2700	2650	1.2
28	2700-2800	2750	0.5
29	2100-2200	2150	20.0
29	**0 - 2800**	**50 - 2750**	**540.8**

Figure 3. 10. Discretization of the aquifer potential recharge surface area.

- **Steps 2 and 3**: Potential recharge computation

Figure 3. 11 reports the results from the water budget and recharge computation presented at section 3.4.2.1. (**Figure 3. 7 b**) (ordinate axis) as a function of the elevation of each considered slice (abscissa axis), as well as the $\delta^{18}O$ recharge line (BSWL) selected at section 3.4.4. At this step of the process, recharge is still a "potential recharge" as it does not account for the isotopic composition of the water from the aquifer (here the Umbulan spring) nor for the total outflow (outflow = recharge) from the volcanic aquifer (see steps 4 and 5).

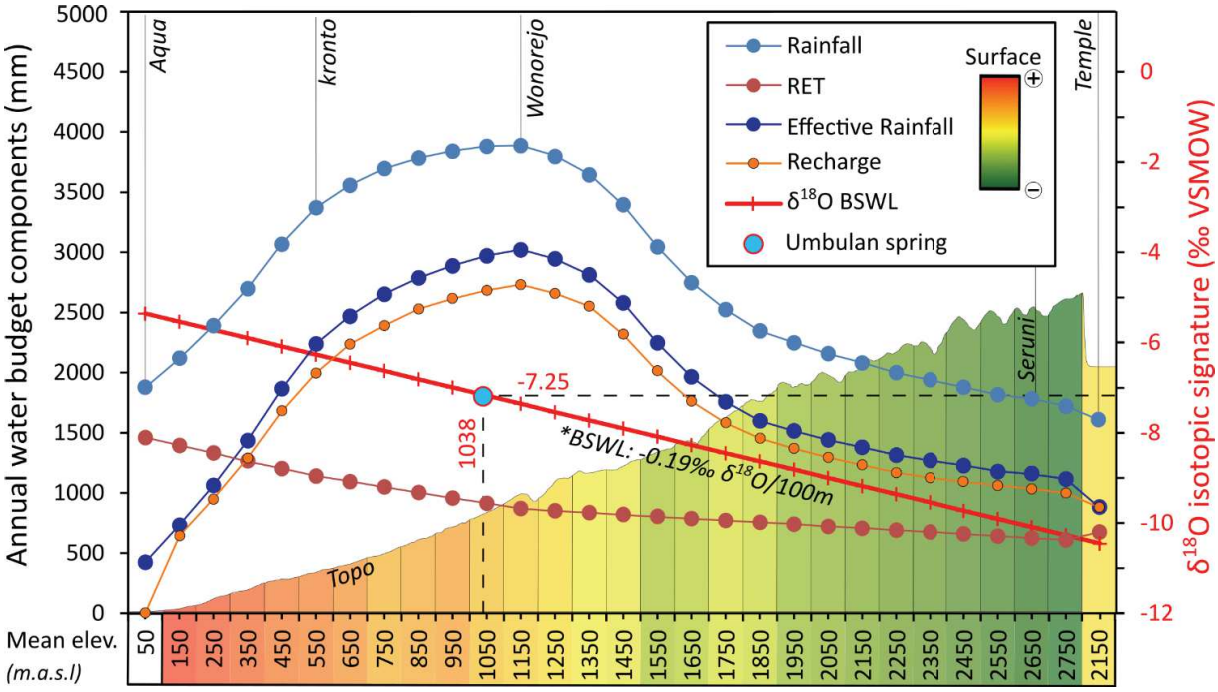

Figure 3. 11. Computed annual water budget components (R, RET and ER), potential recharge (Re) and $\delta^{18}O$ gradient (BSWL) as a function of the elevation. The isotopic signature of the recharge in the caldera is provided by the Temple meteorological station at 2150 m mean elevation.

- **Steps 4 and 5**: recharge area calibration:

The main outputs from step 3, with recharge = 90.5% of effective rainfall except for the slice of the sea of sand caldera where 100% of effective rainfall is considered to infiltrate (i.e. C_{inf}= 90,5% as runoff = 9.5%, see section 3.4.2.1.), are the following:

- $\delta^{18}O$ signature of the whole recharge ($\delta^{18}O_{total}$) = -7.25‰, to be compared with the average Umbulan spring signature = -7.25‰ (standard deviation = 0.07‰), (section 3.4.4.) which is used to perform the recharge computations;

- total estimated outflow/recharge (Q_{total}) = 31 000 $L.s^{-1}$, to be compared with the total outflow measured in the plain of 7 000 L s^{-1} (section 3.4.2.1).

At this stage, without any calibration, the computed isotopic composition (-7.25‰) is already perfectly fitting to the one of the Umbulan spring (-7.25‰). This result comforts the hypothesis that the recharge occurs along most of the northern flank of the Bromo-Tengger volcano. The computed outflow is much higher than the observed one; the surface of the recharge area thus

must be significantly reduced (laterally), by a factor of about 4.4. Then, the recharge distribution (on each slice) is available (Step 4) and illustrated in **Figure 3. 12**.

Finally, the step 5 calibration was performed to proportionally reduce the surface area of each slice in order to adjust to the measured outflow. The proportionality coefficient is 4.43 (31 000/7 000). Then, the total computed recharge area may finally be about 122 km^2.

These results show that most of the northern flank of the Bromo-Tengger may contribute to the recharge of the artesian aquifer. Consequently, the recharge pattern is strongly influenced (i) by the recharge vs elevation relationships, and (ii) by the morphology of the northern flank of the volcano (smaller surfaces at high elevation than at the lower ones due to the shape of the volcano). The limited contribution of the lowest elevation area of the volcano to aquifer recharge is supported by geological evidences: the cover of the lower area by low permeability sediments that confine the artesian aquifer below the about 50 m.a.s.l. elevation line (**Figure 3. 5 a, b** and **Figure 3. 10**), and the observed weathering profile developed at the surface of the "Olf" old lava flows (**Figure 3. 5 a, b**). Moreover, in this area rainfall minus Real Evapotranspiration is at minimum (**Figure 3. 11**).
This first estimation also shows that the eastern and western morphological limits chosen at step 1 are far away from the "real" limits of the recharge area.

As a consequence of this recharge pattern, about 80% of the recharge occurs within an elevation range of 150 and 1450 m.a.s.l., around the R, ER and Re peak (**Figure 3. 12**). This result is consistent with the hydrochemistry and isotopic results suggesting a limited contribution of the highest part of the volcano. The irregular shape of the recharge values between 750 and 1050 m.a.s.l. is strictly related to the corresponding slices surface area which are locally less or larger in the western part of the potential recharge area (see Step 1). These variations have then no real physical signification and an average 7 to 8% recharge contribution must be considered. The computed average recharge elevation (computed with the BSWL isotopic line) is 1038 m.a.s.l.. However, this value is purely indicative as was demonstrated by the current computations.

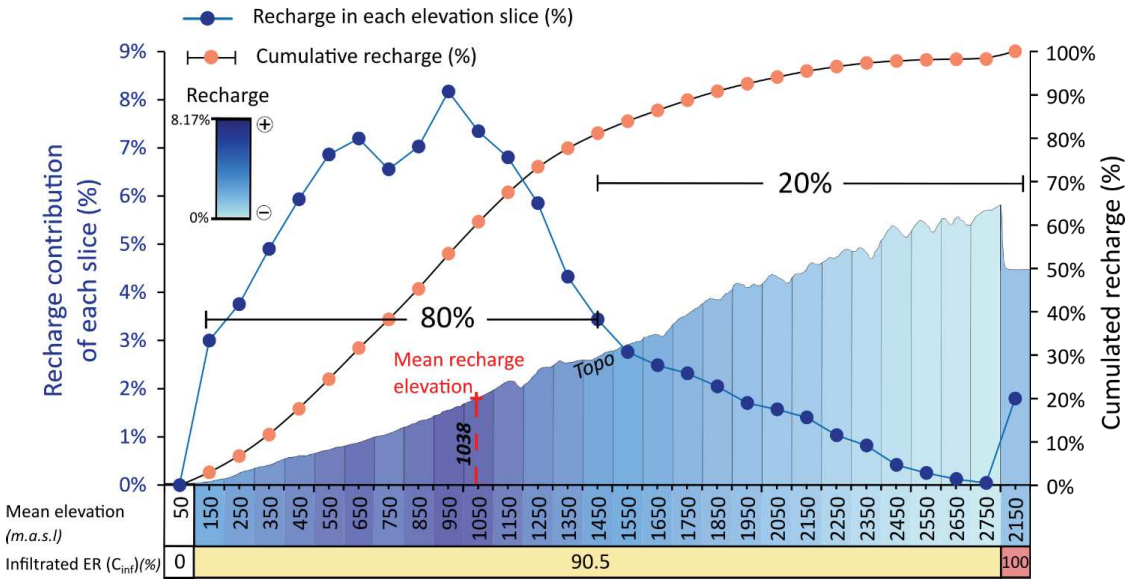

Figure 3. 12. Recharge distribution vs elevation.

3.4.5.1 Sensitivity analysis

As said above, the quantitative modeling is mainly controlled by the recharge pattern and the recharge surface area distribution along the volcano's flank.

The sensitivity analysis (**Table 3. 2**) shows that not considering the contribution of the caldera has a significant impact on the aquifer's computed isotopic signature (-7.19‰ vs -7.25‰, all other parameters being the same as described above), but no significant impact on the aquifer's water budget (6870 L s^{-1} vs 7000 L s^{-1}). It then requires to modify the calibration through reducing the recharge at lower elevation (no recharge in the 0 – 200 m.a.s.l. slices, 76% recharge rather than 90.5% in the 200 – 300 m.a.s.l. slice). Conversely, if the whole caldera surface (40 km²) is considered, it requires enabling aquifer recharge to occur much lower than the 100 m threshold (even below sea level), which is impossible.

This sensitivity analysis shows that this approach is not precise enough to really demonstrate that the caldera is contributing to the aquifer recharge, but the probability is high. On the other hand, the contribution of the whole caldera is rather inconceivable according to isotopic data.

Table 3. 2. Results of the sensitivity analysis. The reference scenario is based on recharge in half of the caldera and satisfying (1) the $\delta^{18}O$ measured at Umbulan spring and (2) the outflow measured in the plain. In comparison with the reference scenario, various adjustments are tested (1). no contribution of the caldera or full caldera and (2). +/- 15% of rainfall).

	Reference scenario		**Sensitivity analysis**							
			Caldera contribution				**Rainfall variation**			
Parameters	**Half caldera 20 km²**		**No caldera**		**Full caldera 40 km²**		**-15%**		**15%**	
(1) $\delta^{18}O$ *(‰)*	-7.25		-7.19		-7.31		-7.28		-7.23	
							Recalibration			
Recharge slice (%)	*0%*	*0-100m*	*0%*	*0-200m*	*90.5%*	*<0m*	*0%*	*0-100m*	*0%*	*0-100m*
distribution	*90.5%*	*100-2800m*	*76%*	*200-300m*	*90.5%*	*0-2800m*	*90.5%*	*100-2800m*	*60%*	*100-200m*
fitting the C_{inf}			*90.5%*	*300-2800m*	*100%*	*full caldera*	*52%*	*half caldera*	*90.5%*	*200-2800m*
			0%	*half caldera*					*100%*	*half caldera*

A rainfall variation on all slices, for instance of +/- 15%, has a significant impact on the results. As efficient rainfall, and then recharge, does not evolve linearly with rainfall, a 15% decrease of rainfall logically yields a decrease of the aquifer recharge (7000 to 5420 L s^{-1}). It triggers also a shift of the computed isotopic signature (from -7.25 to -7.28‰) as the recharge is smaller mainly at the lowest elevations, which also correspond to the largest potential recharge area for the aquifer. Recalibration of the model requires only to decrease the contribution of the half caldera with a recharge of 52% of effective rainfall. Conversely, increasing rainfall by 15% only requires to reduce the recharge in the lowest 100 – 200 m.a.s.l. slice of the model to 60% of effective rainfall (against 90.5%). Again, similarly to the previous sensitivity test, this result shows the limits of this approach which precision is not enough to precisely determine the upper and lower limits of the recharge area.

Logically, a similar change in the recharge rate along all the volcano's flank has no impact on the isotopic signature of the recharging water, but only on the required recharge surface area. The calibration carried out and the sensitivity analysis clearly shows that the recharge surely occurs along most of the volcano's flank. Furthermore, as there is neither geological nor hydrogeological change along the flank of the volcano, the recharge pattern is mainly controlled by the effective rainfall distribution and the morphology of the volcano (surface area distribution vs elevation).

3.5 Discussion and implications for the conceptual hydrogeological model

3.5.1 Hydrogeological structure and functioning

The hydrogeological structure of the northern flank of the volcano comprises two main geological units:

- (i) an upstream volcanic geological unit mostly composed of pyroclastic and lava flow series (PC and LFC). Despite the geological complexity of these formations, this volcanic unit hydrogeologically appears as homogeneous and permeable at the scale of the whole northern flank of the volcano. The pyroclastic formations display an interstice porosity whereas the lavas exhibit both an interstice porosity (clinker layers) and a cooling fractures porosity. These hydrogeological formations host an unconfined aquifer, similar to a "basal aquifer" described in other shield volcanoes such as in Hawaii and parts of Reunion Island, where piezometric level is very deep and covered by a thick vadose zone. Local aquifers perched on ash layers and cooked paleo-soil formations feed a few low discharge springs (inter and under lava springs (Naud, 1971)) on the flank of the volcano. Isotopic results confirm the small extension of their hydrogeological catchment (about 0.5 km^2 on average). If these local impervious layers are leaking, these perched aquifers also partly recharge the basal aquifer. This volcanic hydrogeological unit is limited to the south by the Tengger caldera summit. West and East the geological limits of the studied aquifer where not precisely identified; the results of the study shows that they are much less far than the Nongkojajar caldera rim and the Sapikarep valley.

- (ii) a downstream volcano-sedimentary unit composed of volcanic coarse sand (interstratified reworked ashfall, lahar, tuff) bounded to the North by distal clayey deposits. The superficial part of the plain is composed of shallow unconfined aquifer described as low permeability volcanic tuff intercalated with permeable fluvial deposits. The runoff coming from the rivers flank provides water to the shallow aquifer. The confining unit identified around 30 m deep probably explains the presence of artesian aquifer in the plain. This aquifer also comprises ash fall deposits and consolidated breccia mostly impermeable, which provide it the characteristics of a multilayer confined aquifer system. This aquifer is in continuity with the upstream volcanic basal aquifer. The hydrochemistry results (notably Ca/Mg) demonstrate a groundwater flowing and aging towards the North. A SW-NE fault system could explain the alignment of high discharge artesian springs (Umbulan) and maar. The other main outflow from this aquifer is due to human activities in the plain with about 600 artesian wells.

The transition between the upstream volcanic hydrogeological unit and the downstream volcano-sedimentary hydrogeological unit is rather well constrained spatially from field geological observations, and also from the southern limit of the artesian wells. It is however not well described in terms of geological structure. The detailed characterization of this transition zone would require modern drilling techniques, which are not available among the local drillers, and geophysical measurements. However, this knowledge is not of prime interest for the understanding of the aquifer's functioning neither for its management.

3.5.2 Recharge distribution and hydrogeological balance

The recharge occurs on the whole northern flank of the volcano within the andesite lava flows series and the pyroclastic complex (LFC and PC) However, hydrochemical and isotopic results suggest a low contribution of the highest volcano part (> 1700 m.a.s.l.) and an apparent mean recharge elevation of about 1000 m.a.s.l.. The Bromo spring water line (*BSWL) inferred from integrative springs is a cost-effective robust way to characterize the isotopic gradient on the volcano. Such measurements enable to avoid artefacts such as seasonal rainfall selection (Blavoux et al., 2013), and to account for fog drip observed on the Bromo-Tengger. There are still some questions regarding the proportion of recharge input from fog drip, that was not explicitly quantitatively computed at this stage of the research. Complex interception models, such as the Rutter-Type, (Rutter et al., 1972) could be used to better quantify it, or even working on the shift between this BSWL and the rainfall line (BMWL).

Lower than expected groundwater temperatures in the plain (between 23 and 25°C, whereas the expected shallow local groundwater temperature should be about 30°C) qualitatively confirm that recharge occurs at high elevation. Based on this quantitative modeling of groundwater isotopic content, 80% of the recharge occurs between 150 and 1450 m.a.s.l.. The recharge is mainly controlled by the rainfall spatial distribution, itself strongly impacted by seasonal and elevation effect. The rainfall reaches 4000 mm $year^{-1}$ at 1200 m.a.s.l. with 79 to 91% of which occurring during the wet season. The low precipitations recorded on the highest volcano part associated by the $\delta^{18}O$ impoverished values excludes the Tengger caldera as being the main recharge zone but it is quite sure that it contributes to the recharge. An additional hypothesis is to consider the Tengger caldera with a North-East groundwater flow circulation supplying gravity springs along the Sapikerep collapse valley. The Sapikerep collapse formations may represent a preferential drainage network in agreement with other large landslides of deep erosion in volcanic context, as is the case in Tenerife Island (Marrero-Diaz et al., 2015). This could be confirmed/infirmed by isotopic measurements at these springs.

In 2018, the outflow measured from the studied hydrogeological system occur within the volcano-sedimentary unit and is about 7000 L s^{-1}. The artesian springs constitute a large part of this outflow (about 60%), the rest is mostly flowing out from the artesian wells. A water budget estimation on a representative watershed indicates an effective rainfall infiltration of about 90.5% (i.e. 66% of rainfall). Based on the previous quantitative insights, recharge surface area on the northern volcano flank is estimated to about 120 km^2. However, the lateral extension of the recharge area should be precised to enable the real delineation of the recharge area. Other tracers than water isotopes could be used.

3.5.3 Towards a conceptual hydrogeological model

The new insights previously described enable to build a robust hydrogeological conceptual model of the northern flank of the Bromo-Tengger (**Figure 3. 13 a, b**), inferred from a high-resolution and multidisciplinary approach.

The hydrogeological observations performed on the Bromo-Tengger volcano can be compared with the main volcanic hydrogeological conceptual model illustrated by the Hawaiian (Ingebritsen and Scholl, 1993) and the Canarian manifestations (Custodio, 2007; Hemmings et al., 2015a). The high permeability apron, the presence of perched aquifers and the related thick vadose zone of the Bromo-Tengger show many similarities with the Oahu island in Hawaii (Nichols et al., 1996), additionally with the presence of an artesian basin such as in Honolulu. However, in the proximal zone of the Bromo-Tengger, there is no clear indication whether a volcanic core exists or not. Neither highly altered rocks nor dike clusters have been observed on the field, but this may be due to the lack of deep erosion incisions in this part of the volcano. On the basis of the andesitic-volcano architecture described in Indonesia such as in Merapi (Selles et al., 2015), we may assume an inner structure with a volcanic core but probably occupying a low to middle elevation because of the absence of gravity springs at high elevation, enabling a thick unsaturated zone (Cruz-Fuentes et al., 2014; Herrera and Custodio, 2008). The main differences between the Bromo-Tengger and the conceptual model of basaltic islands are:

- the presence of ignimbrite deposits (Sapikerep valley and North Ranu Grati), maybe playing an important role within the confining layers;
- a more complex volcanic architecture of the Tengger edifice induced by separated or partially overlapping, with a wide spectrum of different cumulative structures such as the calderas.

3.5.4 Perspectives

Now that a hydrogeological conceptual model is proposed, it opens-up perspectives for a complete deterministic 3D modeling of this complex hydrosystem, necessary to set-up quantitative management scenarios of this groundwater resource. Complementary field investigations with a piezometric survey in the plain will notably precise the West-East extension of the downstream aquifer. Modeling of $\delta^{18}O$ from the recharge area to and within the downstream aquifer may enable explaining the slight spatial $\delta^{18}O$ variations observed in the plain. Then, precise the aquifer recharge area, especially to identify the eventual hydrogeological role of the Nongkojajar caldera. The study of the other flanks of the volcano may provide a thorough understanding of the global hydrogeology of the Bromo-Tengger. Groundwater age dating is scheduled and will provide precious residence time data, necessary to prevent some pollution impacts, such as those induced by anthropogenic pressures on the northern flank of the volcano.

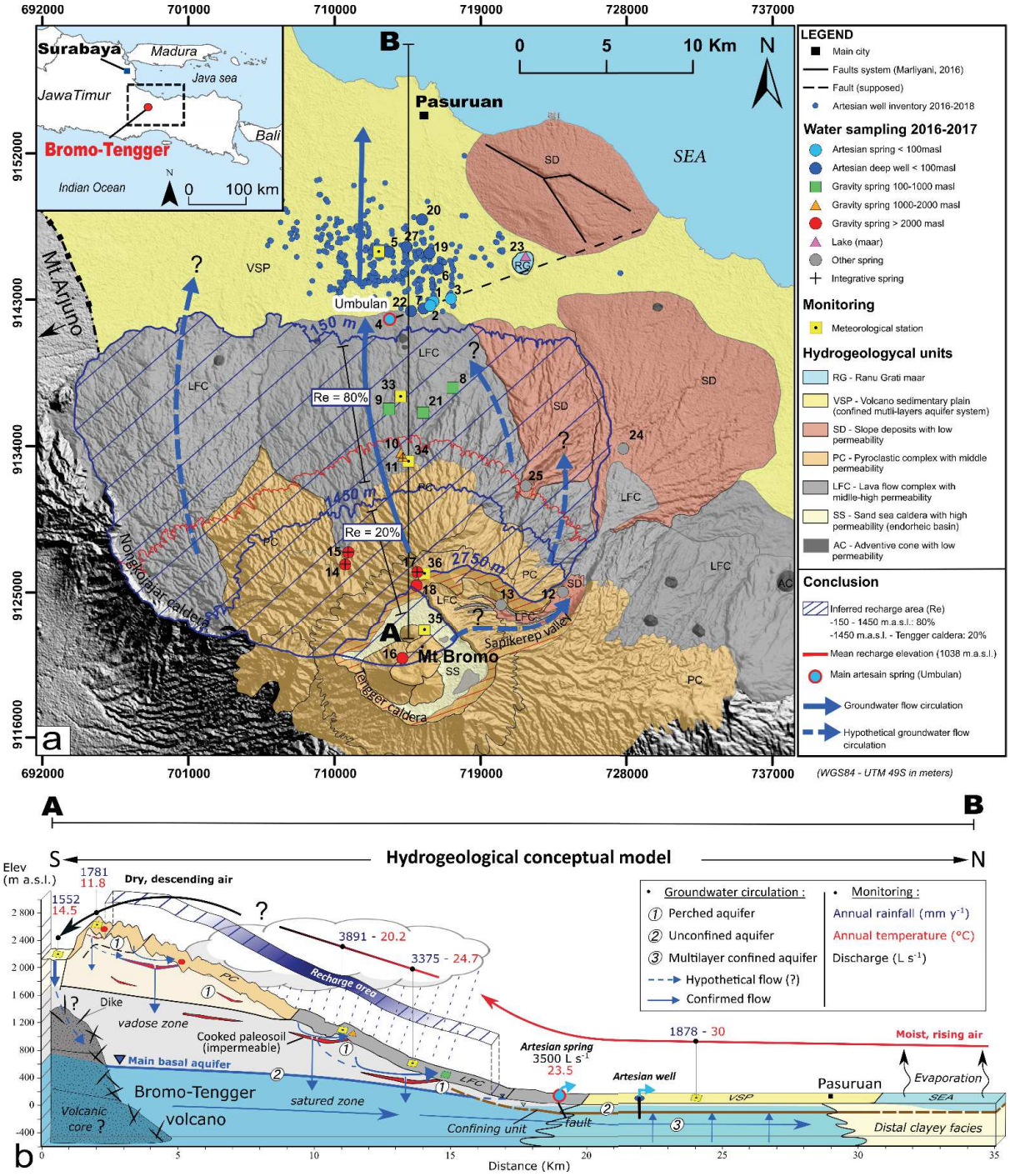

Figure 3. 13. Hydrogeological conceptual model of the northern part of Bromo-Tengger volcano with **a.** The location map showing the main hydrogeological units, the main recharge area (whole flank), the groundwater samples plotted according four elevation groups and types. Arrow with full and dashed black line show respectively the groundwater flow circulation identified or assumed. **b.** Schematic N-S cross section of northern volcano flank showing the groundwater flow paths according to the identified recharge locations and the atmospheric circulation features from the sea to the Tengger caldera summit.

3.6 Conclusion

This multidisciplinary study comprising geological, hydrometeorological monitoring, hydrochemical and isotopic approaches, together with a simple quantitative modeling of groundwater isotopic content allowed designing the hydrogeological structure and functioning of a complex andesitic system such as the Bromo-Tengger volcano. Only a combination of results, each obtained from one discipline, allows to build a robust conceptual model of the Bromo-Tengger.

On this volcano, two main hydrogeological systems are identified:

- the upstream host aquifer rock is composed of an andesite lava flows series topped with a pyroclastic series. These formations, geologically complex in details, appear as homogeneous and permeable at the volcano scale. They host a basal aquifer and a few perched aquifers, the latest being characterised by low discharge gravity springs. The basal aquifer supplies the volcano-sedimentary aquifer from the plain;
- the downstream part is characterised by a multilayer volcano sedimentary confined aquifer. It gives rise to high discharge artesian springs (such as Umbulan) and numerous artesian wells.

The realistic modeling of groundwater isotopic content, supported by isotopic data and the water budget of the northern flank of the Bromo-Tengger, shows that the recharge occurs along the whole northern flank of the volcano. It is mostly controlled by orographic effects that trigger the rainfall spatial distribution. As a consequence of this recharge pattern, about 80% of the recharge occurs within an elevation range of 150 and 1450 m.a.s.l., around the R, ER and Re peak. The contribution of the Tengger caldera to recharge is then limited.

The insights presented here provide first valid hydrogeological constraints for further 3D numerical modeling to assess the response of the aquifer to anthropogenic and climate changes, on the basis of various simulation scenarios.

3.6.1 Acknowledgements

This research was carried out in the frame of a PhD research part of the Rejoso Kita project which is co-realized by Danone AQUA, International Centre for Research in Agroforestry (ICRAF), Social investment of Indonesia (SII) and CKNet foundation, with the financial support of Danone Aqua and Danone Ecosystem Indonesia. Scientific and logistic supports from Gadjah Mada University is gratefully acknowledged. We thank the Montpellier (France) LAMA and Hydrosciences laboratories for the chemical and isotopic analyses of water samples. The authors gratefully acknowledge the partnership and authorizations provided by the Ministry of Research, Technology and Higher Education of Indonesia (RISTEKDIKTI) and the Bromo Tengger Semeru National Park (TNBTS) for the free access to the Tengger caldera zone. Assistance from Mas Kevin, Mas Yuda and Mas Ahmad during field measurements were very appreciated while logistic support delivered from Jean Luc Bonjour has facilitated this research. We also warmly thank the Editor-in-Chief, Patrick Willems, as well as the 3 reviewers, E. Custodio and two anonymous, for their constructive comments that helped improving this paper.

Chapter 4



View of the caldera “Segara Anak Lake” of the Rinjani volcano in Lombok Island with the last active cone “Barujari” in center.

Chapter 4. A cost-effective methodology to estimate aquifer transmissivity and hydraulic head from free-flowing artesian wells. Case study of Bromo-Tengger volcano-sedimentary aquifer

The hydrodynamic characterization of volcanic aquifers has been the scientific purpose of many studies using different pumping tests methods in massive formations such as lava flows, cemented deposits including ignimbrites or unconsolidated materials related to pyroclastic fall deposits. However, the hydrodynamic characterization of volcano-sedimentary deposits in a distal position away from the volcano is scarcely addressed in the literature.

Due to the natural artesian conditions in the volcano-sedimentary plain of Pasuruan, the pumping tests involve allowing the groundwater to flow freely without pumping. The simple measurement of discharge and pressure head at the artesian well may provide data from which the hydraulic properties can be estimated.

In this context, a new free-flowing artesian well device was designed and applied at the scale of the Pasuruan artesian plain. The results allow us to determine the hydrodynamic properties and piezometric head at the well location. Analysis of the results contributes to a better understanding of groundwater flow circulation across the volcano-sedimentary plain and will provide hydrodynamic data to implement further numerical modeling.

This chapter presents a research paper that will be submitted soon in *Hydrogeology Journal.*

Alix Toulier[a*], Patrick Lachassagne[b], Hervé Jourde[a]

[a]*HSM, Univ Montpellier, CNRS, IRD, Montpellier, France*
[b] *Water Institute by Evian, Water Resources and Sustainability Division, Danone Waters, Evian-les-Bains, France*

Abstract

Artesian systems offer important possibilities for drinking water supply by providing a groundwater resource that is easily abstracted without any installation of pumps (e.g. the Great Artesian Basin in Australia, the Table Mountain Group aquifer in South Africa or the Honolulu artesian basin on Oahu Island in Hawaii). In such aquifers, the estimation of hydrodynamic properties is challenging since the hydraulic head is higher than the ground surface, thus allowing free-flowing springs and wells. Accordingly, hydraulic tests on flowing artesian wells are particularly hard to perform. This paper describes a low-cost, easy to reproduce and adaptable device that can be used to perform hydraulic tests on free-flowing artesian wells.
Flow rate and continuous pressure measurements at the well allow to estimate the piezometric head and transmissivity of the aquifer with the Cooper-Jacob approximation, taking into account the Houpeurt-Pouchan method. Using GPS measurements at each well head, a piezometric map of the artesian aquifer can then be produced. This hydraulic test device is applied on the volcano-sedimentary artesian plain of the Bromo-Tengger volcano (Indonesia). The measurements were carried out at about twenty artesian wells in May 2018 to visualize the transmissivity distribution and identify the preferential groundwater flow paths. A large-scale deployment of this method could improve the understanding of the hydrogeology of other regional artesian basins.

Keywords: Free-flowing artesian well, hydraulic test device, recovery test, transmissivity, piezometry, volcano-sedimentary aquifer, Bromo-Tengger volcano.

4.1 Introduction

Artesian conditions start to develop where the hydraulic head from a confined aquifer is higher than the topographic surface, allowing the free-flow of groundwater through artesian wells (and/or springs). Large artesian systems, such as the Great artesian basin in Australia (Habermehl, 2001), or smaller systems such as volcano-sedimentary aquifers in Indonesia (Toulier et al., 2019), are of great interest insofar as the groundwater withdrawal does not involve any pump installations and power supply costs. This is important in developing countries, notably where groundwater is used by low-income farmers (Toulier et al., 2019). Moreover, these aquifers often provide very high-quality groundwater (in terms of microbiology and anthropogenic contaminants) due to the confined conditions.

Confined aquifers have been surveyed and studied in several places around the world for a very long time, at least as early as the 19th century, notably the water wells drilled in the "Artois" region of the Paris Basin (France) from which the term "artesian" is derived (Margat et al., 2013). Several studies, some including hydraulic tests, have demonstrated the elasticity and deformation properties of water-bearing layers in artesian aquifers (Meinzer, 1928; Thompson, 1929). Other studies have pointed out the complexity of such layers regarding the transmission of pressure changes (Legette and Taylor, 1934; Versluys, 1930) and the rate of spreading of the depression cone (Lohman, 1965). However, hydrodynamic studies of artesian systems are mostly focused on only a few flowing artesian wells (e.g. the Table Mountain Group aquifer in South Africa (Lin, 2007), the Honolulu artesian basin in Hawaii (Nichols et al., 1996) or the Dakota artesian basin in the USA (Meinzer and Herbert, 1925). A better understanding of such aquifer systems needs a basin-scale hydrogeological characterization that requires the implementation of low-cost and easy to implement devices and methods, to be able to perform measurements on numerous free-flowing wells over a short period of time, notably during piezometric surveys.

Since the 1960s, several such devices have been designed, including such as the photographic method with a camera and manometer for water-level monitoring (Wyrick and Floyd, 1961). A more accurate device was proposed by Oberlander and Almy (1979), using an ultrasonic flowmeter. Recently, a device was designed by Sun and Xu (2014), integrating an ultrasonic flowmeter and pressure transmitter, EC and pH probes, all with connections to a data logger requiring an external power supply. Despite the progress in such device, their use remains complex and laborious in remote location lacking a power supply, or even not accessible by car, for instance in agricultural areas with paddy fields.

This study proposes (i) a simple device and method, both cost-effective and easy to implement, without any need of external power supply, and (ii) a data interpretation methodology, to estimate the transmissivity and to compute the piezometric head of free-flowing artesian wells. This methodology aims to access the piezometric head in the confined aquifer, eliminating the local impact (drawdown cone) of the free flowing artesian well in question.

This method is applied to the artesian volcano-sedimentary aquifer of Pasuruan, located at the foot of the Bromo-Tengger volcano (Indonesia). Additionally, differential GPS measurements are carried out to enable piezometric mapping of the artesian basin. The results

of transmissivity and piezometric head at free-flowing artesian wells enable to understand the functioning of the aquifer and will serve as input data for a further aquifer numerical modeling. The advantages and limitations of using the device, along with the interpretation methodology are discussed at the end of this article.

4.2 Methodology

4.2.1 Basic concepts concerning artesian aquifers

The aim of the device and the associated implementation method is to perform measurements that can be used to estimate: (i) the hydraulic head h in the aquifer, (**Figure 4. 1**); (ii) the transmissivity of the aquifer.
As a reminder:

The hydraulic head (h) is defined according to the Bernoulli theorem, as follows:

$$h = \frac{u^2}{2.g} + \frac{P}{\rho.g} + z \tag{4.1}$$

where:

h: piezometric head of the aquifer (m)
u: fluid velocity (m s^{-1})
P: water pressure at the measurement location (kPa), i.e. not taking account of atmospheric pressure
ρ: volumetric mass of water (10^3 $kg.m^{-3}$)
g: acceleration due to gravity (9.81 $m.s^{-2}$)
z: elevation above a given datum (m)

In porous media, the fluid velocity is very slow, allowing to ignore the kinetic energy term ($\frac{u^2}{2.g}$), so the hydraulic head (h) can be simplified by the piezometric head (H) given by the following equation (de Marsily, 1986):

$$H = \frac{P}{\rho.g} + z \tag{4.2}$$

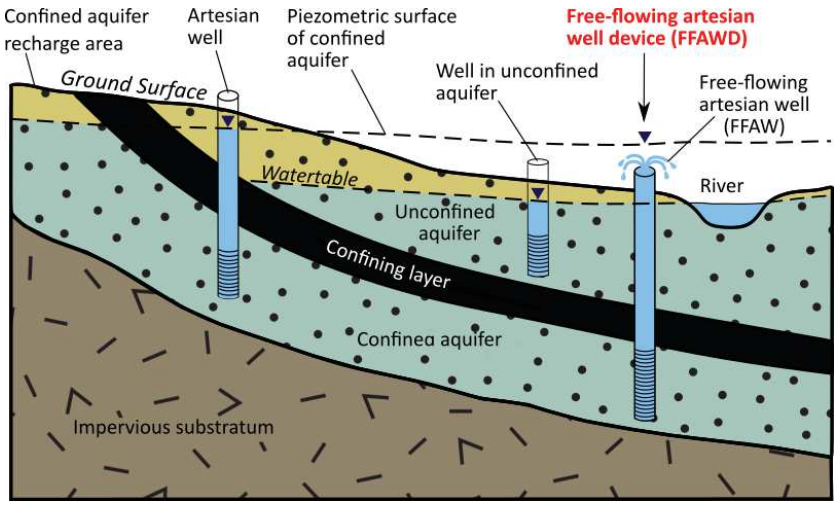

Figure 4. 1. Conceptual model and technical terms for confined and unconfined aquifers (modified from Chen et al., (2017)).

A Free-Flowing Artesian Well (FFAW) has a piezometric head H that is higher than the topographic surface or, rather, higher than the top of the well head. However, an artesian well is not necessary flowing at the surface (UNESCO, 2012) as illustrated in **Figure 4. 1**. In the following parts of this article, the device that we developed here will be referred to as a "Free-Flowing Artesian Well Device" (FFAWD).

4.2.2 Design of the free-flowing artesian well device (FFAWD)

The principle of the measurement method is to install the device on the well head (**Figure 4. 2. a**), allowing the pressure to increase inside the device until it reaches an equilibrium for a given piezometric head. The device is built up as follows, from bottom to top:

- A PVC tube whose base diameter can be changed in the field to adapt to the well head diameter. It can also be equipped with an elbow tube in case the outlet of the free-flowing well is not vertical. This first tube comprises a smaller tube which is fixed inside to install and secure the pressure probe. The pressure probe is easy to extract from the device, to download data when the measurement process is over, and also easy to reinsert.

- A T tube whose horizontal outlet is equipped with a valve.

- The vertical outlet of the T tube is equipped with a transparent acrylic graduated pipe, open at the top, which allows observation of the water level during the test. Its length is open at its top. Its length can be adjusted by adding tube sections to adapt the H. The top of this pipe is equipped with an elbow to redirect the water flow if H is higher than the measuring device, to avoid wetting the technicians;

In this study, we used a "VanEssen TD-Diver" pressure probe for water levels ranging from 0 to 10 m, with a +/- 0.5 cm and a resolution of 0.06 cm. The pressure was recorded at 1 s intervals. The PVC and acrylic pipes are about 100 mm in diameter (4 inches). Up to 6 m long Acrylic/PVC tubes were connected to each other to measure high piezometric heads. Only the

last tube is composed of a 2 m transparent acrylic pipe. A maximum water level of 8 m was measured with this device.

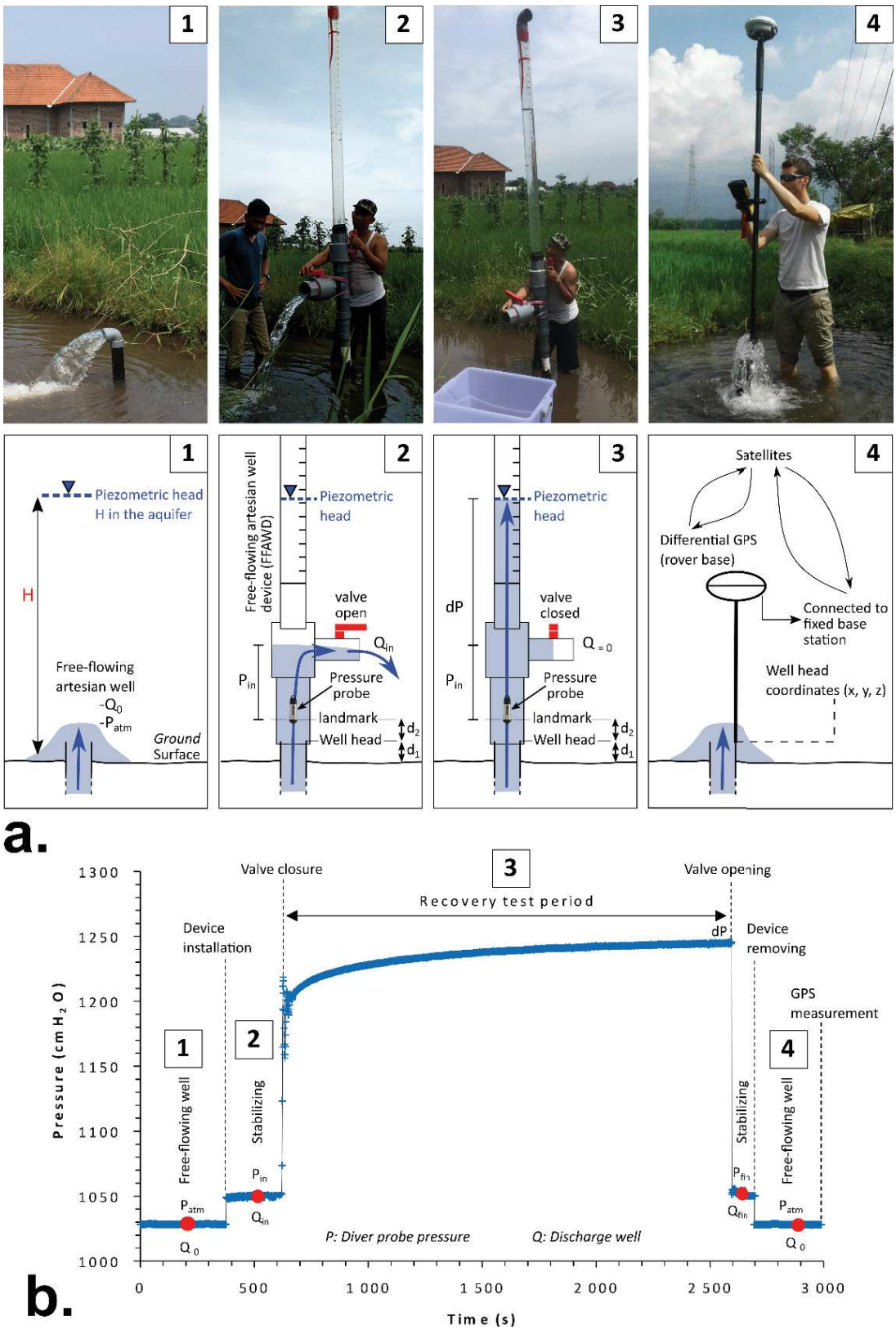

Figure 4. 2. **a.** Description of the free-flowing artesian well device (FFAWD) and measurement protocol, **b.** Typical pressure data set recorded by the probe over time during the test of well n°8. The characteristics of free-flowing well n°8 shown here are described in **Table 4. 1**.

4.2.3 Measurement procedures

1) Selection of free-flowing artesian wells: first, it is important to select reliable flowing artesian wells without any leakage between the casing and the ground surface, since grouting can be of poor quality or non-existent in wells owned by farmers with modest means such as in Pasuruan. The wells with a concrete base, satisfactory grouting and a well head in good condition (no corrosion or breaking) were selected in priority. It is also recommended to select wells with a vertical, open and straight pipe long enough to connect the device. Wells with a well head diameter less than 3 inches are not recommended as they are not strong enough for the device and may break during the test. A prior manual discharge measurement (Q_0) allows a rough estimate of the number of PVC tubes required for the hydraulic test. Of course, the selected wells should meet the purpose of the study: for instance, a homogeneous spatial distribution to ensure an accurate piezometric map, or locations chosen to characterize the hydrodynamic properties (T) of various lithological units.

2) Discharge measurement: Measurement of the "steady" discharge of the free-flowing well (Q_0). Fitting an elbow on the vertical pipe may improve the accuracy of the flow measurement, even if it may slightly reduce the discharge (slight increase of the piezometric head). The discharge measurement is performed manually with a bucket or any other graduated collection container (a bucket of 140 L was used in this study).

3) Device installation:
    a. The setting up and calibration of the pressure probe is carried out before placing it inside the device.
    b. The device is installed on the well head with the valve open (**Figure 4. 2 a.**).
    c. After a few minutes of flow stabilization (that can be regularly measured), when there are changes in piezometric head related to installation of the device (P_{in}), discharge measurements are performed to estimate the "initial" well discharge (Q_{in}).
    d. The height parameters of the device are measured: height from ground surface to well head (d_1) and from the well head to the exact position of the pressure sensor measurement (d_2).

4) "Recovery test":
    a. The valve is closed (**Figure 4. 2 a.**), which induces a rapid rise of the water level/pressure in the tube. The transformation of kinetic energy (water flowing up in the well tube at a significant velocity) into potential energy may cause some pressure fluctuations during the first few seconds after closure of the valve, as described further below. Then, the valve must not be closed too suddenly (closing duration: 2 to 3 s). The time at which the valve is closed must be noted. Nevertheless, it is also monitored by the pressure probe.

b. A "recovery period" of about 30 min is recommended during which the pressure build-up (dP) is monitored with the sensor until pseudo-stabilization of H. The choice of duration of this period is discussed in the following sections.
c. Then the valve is re-opened and the discharge (Q_{fin}) is measured (as well as the time of the measurements).
d. Then the device is removed, and the discharge (Q_0) is measured (as well as the time of the measurements).

The **Figure 4. 2. b,** shows a typical pressure graph obtained during this procedure.

5) GPS measurements: a differential GPS Trimble R6 is used to measure the precise coordinates (x, y, z) of the well head (or any other fixed landmark), based on the satellite signals received both at the rover and base stations (Parkinson and Spilker, 1996). The geoid height is corrected considering the gradient of the local geoid (Kasenda et al., 2011). Then, the ellipsoid height measurements are converted into metres above sea level (m.a.s.l.) using a digital elevation model (USGS SRTM30 dataset). With the differential GPS used here, the relative precision in z elevation between each well is about +/-10 cm.

4.2.4 Hydrodynamic response analysis

Under such artesian conditions, the "aquifer test" is divided into three main phases (Sun and Xu, 2014), **Figure 4. 3**:

(i) The adjusting period (Sun and Xu, 2014): during which the well is drilled, with a discharge until the aquifer is reached. Once the top of the aquifer is drilled, the well discharge increases rapidly while the piezometric head is imposed to well head elevation ($t_0 \sim t_1$);
(ii) the free-flowing period: it follows rapid opening of the well that triggers a decrease in discharge; in contrast to Sun and Xu, (2014), the wells in our study were drilled several months or years before the test, without any well closure period, so the free-flowing period was long enough to reach a steady state. The discharge can be considered as steady, and the piezometric head at the well is considered as stabilized ($t_1 \sim t_3$);
(iii) the recovery period: closure of the well as described in section 4.2.3. allows the pressure to increase inside the device, until it reaches an equilibrium for a given piezometric head (no further increase in discharge). In the vicinity of the well, the piezometric head in the aquifer also increases ($t_3 \sim t_4$);
(iv) After re-opening of the well and removal of the device, the well returns to its previous test conditions ($t_4 \sim t_\infty$).

Each phase described above may enable to compute aquifer hydrodynamic parameters of the aquifer through different interpretation methods, but the longer duration of two phases (the free-flowing and the recovery period) are considered to yield more robust results. The decrease of

well discharge during the free-flowing period can be interpreted by a conventional method developed by Jacob and Lohman, (1952), Hantush (1959) and Glover, (1987). A simple approximation for the free-flowing well problem was provided by Swamee et al. (2002) using an error minimizing method to compute the discharge and production volume. Recently, the diagnostic plot method using the reciprocal rate derivative was adapted for the free-flowing test period Sun et al. (2015). This phase is inappropriate in our study because the well discharge has been stabilized for a long time.

If the well is closed (again) after completion of a free-flowing period, the recovery test period (measurement of piezometric head) in transient state can be interpreted with the classical "Horner" recovery method in transient state (de Marsily, 1986), taking into account notably the duration of the free-flowing period (see also Vuković and Soro, 1992).

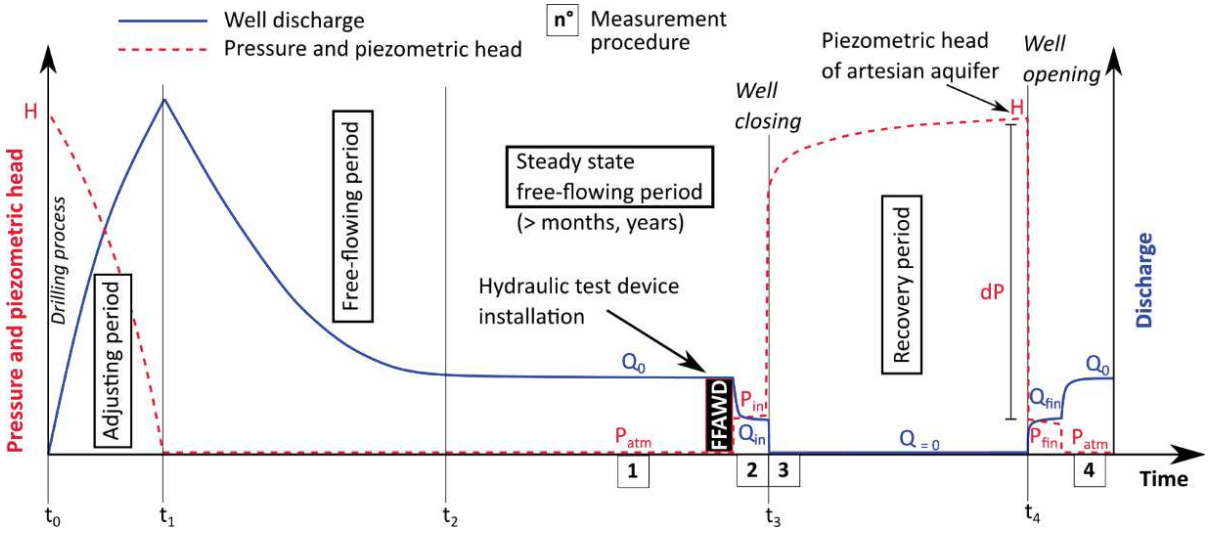

Figure 4. 3. Schematic evolution of well discharge, piezometric head in the confined aquifer, and pressure measured with a probe installed at the top of the well head (or in our device). Modified after Sun and Xu (2014).

In this study, we will only surveyed "old" wells in steady free-flowing state (without any continuous discharge measurement since their drilling). The steady state attained before free-flowing is stopped by the device, which allow to use the Houpeurt-Pouchan transient state recovery method. "Then, the recovery curve is interpreted as a drawdown curve with the help of Jacob's or Theis's method" (de Marsily, 1986).

Such a "recovery" test is usually not sensitive to well losses (Willmann et al., 2007) and can be easily interpreted with the Cooper-Jacob's transient solution, as provided by the software AQTESOLV (Duffield and Court, 2007). The Cooper-Jacob (1946) method, has already been successfully used in other confined aquifers (Jacob, 1947, 1940; Jacob and Lohman, 1952; Merritt, 1995; Wyrick and Floyd, 1961) but never applied at the artesian basin-scale.

For each free-flowing artesian well, we consider a single well test assuming a confined aquifer model, with a vertical and full penetration well, taking in account the discharge rate (Q_{in}) and the radius of the well (5 cm here). This interpretation method is valid for fully

developed unscreened wells (Wyrick and Floyd, 1961) and it is assumed that the artesian aquifer is homogeneous, isotropic and of infinite areal extent.

To avoid any artefacts, it is first necessary to distinguish the well-bore storage effect, called the "post production effect" under recovery conditions which occurs during the early stage of the test. During that period, it is impossible to estimate the transmissivity of the aquifer. For each well, information given by the derivative curve from Bourdet et al. (1983) is compared with a numerical estimation provided by equation (4.3) (Forkasiewicz, 1972), that computes the duration of the "post-production effect" (Ungemach et al., 1968).

$$t = \frac{25.rd^2}{T} \tag{4.3}$$

where:

T: duration of the post-production effect (s)
rd: radius of the tube device (m)
T: transmissivity ($m^2 s^{-1}$)

Then, recovery tests were interpreted for 16 free-flowing artesian wells, considering a constant derivative period of 1 log-cycle to obtain a reliable estimate of the transmissivity (Renard, 2005). **Table 4. 1** reports the transmissivity results and duration of the post-production.

4.2.5 Computation of the piezometric head at free-flowing well

In this study, the recovery period rarely exceeded 30 minutes, to avoid affecting the population's access to water supply for an excessive duration, and also to keep a reasonable duration for the test. Moreover, not all recovery tests performed during this field campaign had the same duration. In addition, recovery was not completed during most tests, and the piezometric head continued to increase significantly.

It is thus important to choose an appropriate recovery duration to be considered for the computation of the piezometric head in the aquifer. Indeed, the magnitude and duration of this recovery is theoretically influenced by i) the discharge of the artesian well prior to the recovery period and ii) the hydrodynamic properties of the aquifer in the vicinity of the well (**Figure 4. 4**). Therefore, it is necessary to extrapolate the recovery data in a homogeneous way for all tested wells in order to compare all the results taken together and thus produce a representative piezometric map devoid of most of the local influence of each free flowing well. In other words, the objective is to obtain a similar recovery for all the tested wells.

Since our research objective was to produce a "regional" piezometric map, we consider a recovery with a residual drawdown of about 1 m. In this case, we can assum that the obtained piezometric surface is underestimated by about 1 m (**Figure 4. 4**).

For this purpose, we consider a confined aquifer whose boundaries N-S limits are about 10 km apart from North to South and about 20 km apart from East to West (this is related to the geometry of the studied aquifer; see section 4.3. and **Figure 4. 5**), with a storage coefficient (S) of 10^{-4}, representative of a confined volcano-sedimentary aquifer (Nichols et al., 1996). We consider a radius of 0.1 m for all wells (r_p), as all wells are equipped with similar pipes. The methodology used to compute the piezometric head comprises three main steps:

1) Computation of the steady-state piezometric drawdown in a free-flowing well "i", having a discharge "Q_i", drilled a long time previously in an aquifer of local transmissivity "T_i".

   a) We use the Dupuit formula for the radius of influence (R_i) of a well with a specified piezometric head (equation 4.4) (de Marsily, 1986).

$$R_i = 1.61\sqrt{\frac{T\,t_i}{S}} \tag{4.4}$$

   From this formula, we derive t_i (equation 4.5).

$$t_i = \left(\frac{R_i}{1.61}\right)^2 \frac{S}{T} \tag{4.5}$$

   Considering the minimum and maximum transmissivity values computed for all wells (from $4.01.10^{-4}$ to $4.32.10^{-2}$ m² s^{-1}, see **Table 4. 1**), and the maximum distance from a well to the boundaries of the aquifer (R_i= 20 km), t_i is always less than 2 years (0.01 and 1.2 years, respectively). Therefore, since all wells were drilled several years ago, we can consider that their drawdown has reached a steady state.

   b) From the Dupuit formula for a captive aquifer (equation 4.6; (de Marsily, 1986)), the drawdown for an artesian well under free-flowing conditions is computed from its respective discharge Q_i and transmissivity Ti, with R_i = 20 km.

$$s_{steady} = Q\,\frac{\ln\left(\frac{Ri}{rp}\right)}{2\,\pi\,T_i} \tag{4.6}$$

2) Computation of the residual drawdown during recovery. To compute a unique residual drawdown equal to 1 m for all wells, Jacob's transient flow formulation (equation 4.7, (De Marsily, 1986)) is used to compute the time "t_{res}" required to recover the above s_{steady} drawdown minus 1 m (equation 4.8).

$$s_{transient} = \frac{2.3\,Q}{4\,\pi\,t\,res}\,log\left(\frac{2.25\,T\,t\,res}{rp^2 S}\right) \tag{4.7}$$

$$At\ t_{res} = \left(s_{steady} - s_{transient}\right) = 1m \tag{4.8}$$

Then, t_{res} is computed for each well which enables to determine, from the observed data, the "H_i" value for well i (piezometric head). In some wells, it is necessary to extrapolate the drawdown over times much longer than the observed 30 minutes whereas. In other wells, the interpolation must be sought within the observed data set (**Appendix 8**). For a computed t_{res} < 0.1 s, the piezometric head value is extrapolated to 1 s.

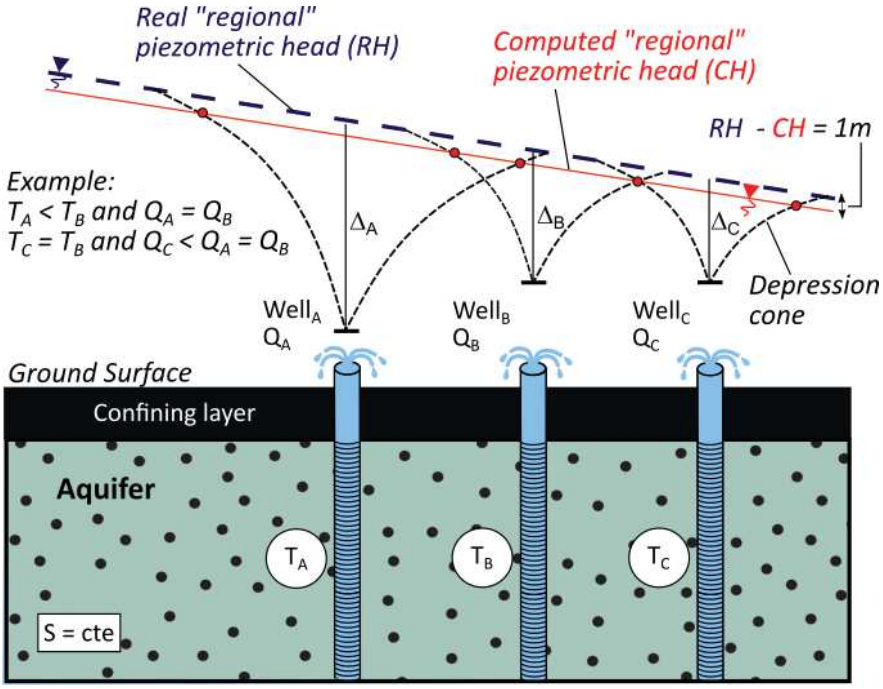

Figure 4. 4. Methodology applied to correct the piezometric head measurements from the recovery tests considering an example of three free-flowing artesian wells with different hydrodynamic parameters.

4.2.6 Piezometric mapping

This recovery times computation leads to coherent set of piezometric heads for all flowing wells, and enables to draw a piezometric map. As a result, the piezometric heads used for piezometric mapping are divided into two types according to their quality (**Table 4. 1**):

-H1: a valid and reliable value is obtained from the above methodology, with a theoretical s_{res} of about 1 m.
-H2: inaccurate value without any continuous pressure data (which prevents computation of T_i).

The kriging method produces smooth surfaces contour and generates a good overall presentation (Brochu, 2003). It is employed here to produce maps of the piezometric head, transmissivity and hydraulic conductivity of the artesian basin of Pasuruan (with a spherical variogram). Coupled with the hydraulic conductivity results, the piezometric map is used to determine the direction, velocity and transit time of the groundwater flow (Berenbrock, 1993; Knapp, 1988).

4.3 Description of the study site

The study area encompasses the artesian basin of Pasuruan covering about 200 km², located the in the north of the Bromo-Tengger volcano in East Java (Indonesia; **Figure 4. 5**). A detailed description of the aquifer conceptual model is provided by Toulier et al. (2019). The Bromo-Tengger volcanic massif is Quaternary in age and mainly composed of lava flows and pyroclastic deposits, several thousands of metres thick. These deposits host an unconfined aquifer. Downstream, these volcanic formations progressively pass into a volcano-sedimentary complex that hosts the studied confined aquifer. This confined aquifer system comprises three main units with, from bottom to top:

- (i) From more than 200 m (deepest wells) to about 40 m below ground surface (b.g.s.): the confined volcano-sedimentary aquifer, which is supplied by the unconfined volcanic aquifer from the northern flank of the volcano. This confined aquifer lies on an unknown substratum.

- (ii) A 10 - 30 m thick clayey pyroclastic unit forming a confining layer;

- (iii) Locally, an unconfined superficial aquifer of medium to low permeability.

In 2018, more than 600 free-flowing artesian wells, drilled over the last 25 years, continuously abstracted (24h/24) about 2400 L s^{-1} from the confined aquifer, mainly for paddy field irrigation. The discharge of the free-flowing wells ranges between 0.5 and 35 L.s^{-1}, with an average of 4.1 L s^{-1}. In 2018, the two main artesian springs of the plain (Umbulan and Banyu Biru; **Figure 4. 5**), provided a discharge of about 3600 and 300 L s^{-1}, respectively. Their discharge has decreased greatly during the last few decades in parallel with the development of the free-flowing wells.
Among all the artesian water points, 33 were selected for applying the device and developing the methodology presented here. This water points comprise:

- 30 artesian wells (including 2 non-flowing artesian wells) with 16 recovery test interpretations;

- 2 main artesian springs;

- 1 lake supplied by the confined aquifer.

All the measurements were performed over a short period of time, from May to June 2018, to obtain a synchronous piezometric map. **Table 4. 1** reports the characteristics of the free-flowing wells, springs and lake, along with the results obtained.

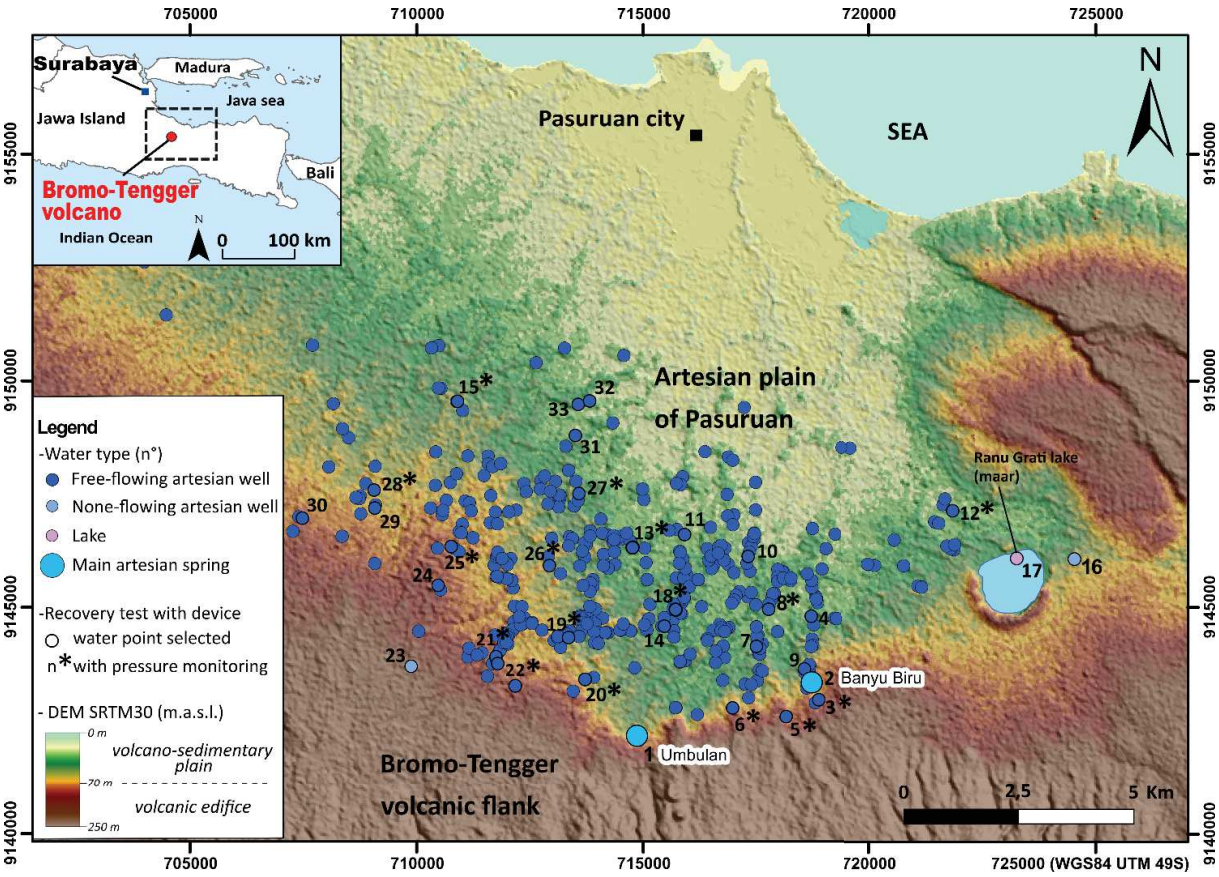

Figure 4. 5. Location map of the Pasuruan artesian basin in East Java (Indonesia) with description of water types, showing water points selected for recovery tests with or without continuous pressure monitoring or not. The map and location data are provided in UTM zone 49S coordinates, using the WGS84 datum.

4.4 Results

4.4.1 Computation of hydrodynamic parameters

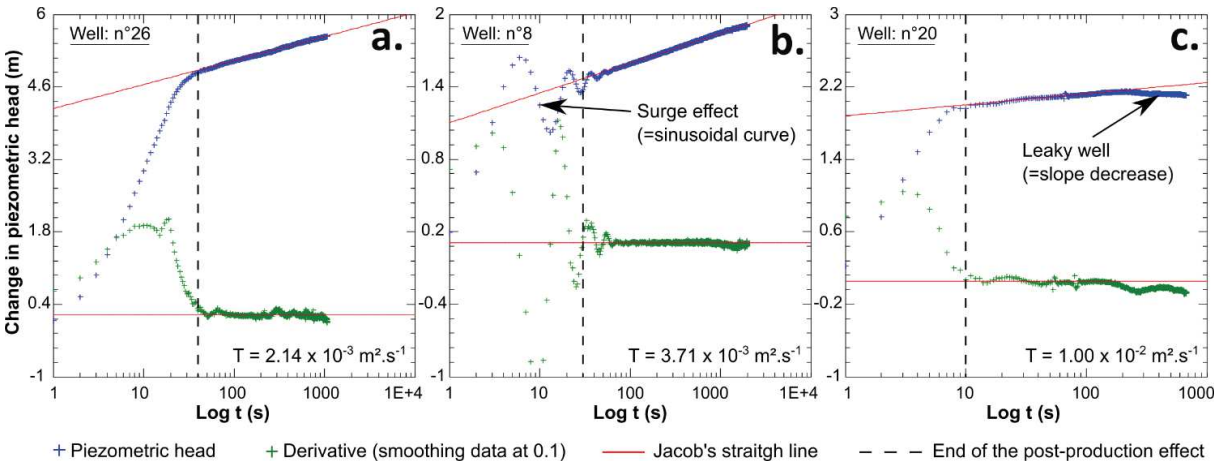

Figure 4. 6. Representative piezometric head data recorded during the tests, sorted into three categories: **a.** Recovery curve without any visible influence, except for post-production effects, **b.** Recovery curve influenced by surge effect during the first ten seconds of the test (=sinusoidal curve) and **c.** Recovery curve influenced by leaky well or internal leakage from the aquifer itself. All the recovery test periods are interpreted with the Cooper-Jacob solution.

The recovery parameters for 16 artesian wells are reported in **Table 4. 1**. The semi-log recovery curves (**Figure 4. 6**) all show a post-production effect followed by a period of recovery of piezometric head corresponding to the aquifer response. Overall, three types of curves can be distinguished:

(i) Ideal recovery (**a.**): the entire recovery does not seem to be disturbed by any external effects (except post-production). The inflection point of the drawdown curve after the post-production effect is followed by a second phase of constant recovery over time (confined aquifer without any limit or leak). The slope of the line is steady after the end of post-production. The end of the post-production effect corresponds to the end of the hump in the derivative curve. It is visually delimited by the vertical black dotted line on **Figure 4. 6**.

(ii) Recovery with surge (**b.**): the beginning of the recovery is impacted by a water hammer effect due to the rapid closure of the well, which causes a sudden change in water velocity in the well (down to zero). The corresponding kinetic energy is converted into piezometric head (Vasquez, 2010) and triggers sinusoidal fluctuations. This can mask the inflection point of the curve at the end of the post-production phasecbut does not affect the critical part of the curve (Wyrick and Floyd, 1961).

(iii) Recovery with leaks (**c.**): the inflection point of the post-production phase remains clearly visible. After a first phase of constant recovery, it is influenced by leaks in the well or, less probably, from the aquifer itself. This leak effect reduces the slope of the curve. The unaffected part of the curve (here between 10 and 100 s) should be used to compute the transmissivity.

Some recovery curves can combine the three types presented here.

A compilation of the recovery test results shows that:

- The post-production duration ranges from a few seconds to 180 s depending on the well (30 s on average). A comparison of the durations of the post-production effect, computed from Eq. 4.3. and graphically determined, shows no significant discrepancies. Only well n°18 shows an inconsistent result but the transmissivity value used in Eq. 4.3 is probably overestimated as suggested by the leak effect (type c.) considered for this well (**Figure 4. 7**). This post production effect is well understood and computed.

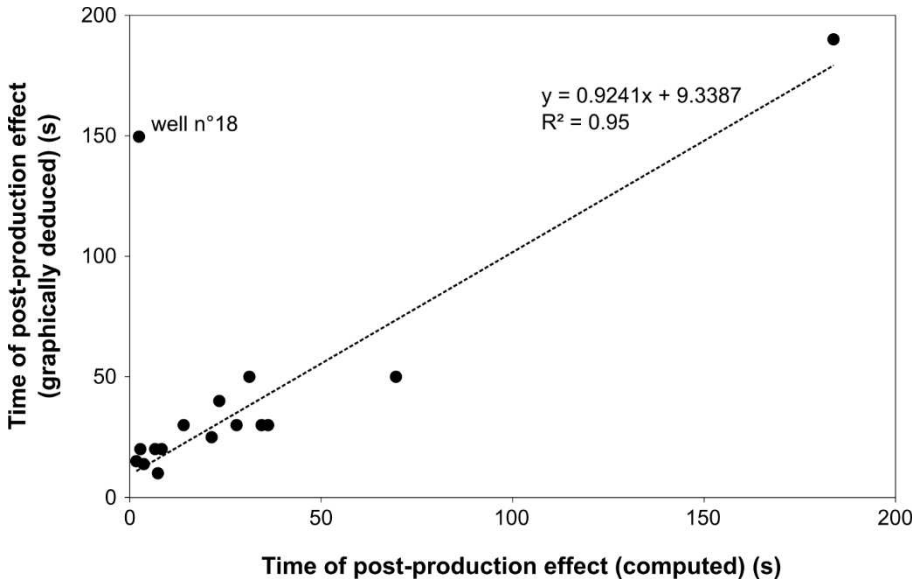

Figure 4. 7. Comparison of the duration of the post-production effect between computed values (formula from Forkasiewicz, (1972)) and values graphically determined from the derivative curve.

- The constant log-log derivative curves at long duration (e.g. between 80 to 1000s in **Figure 4. 6. a.**) confirm that the response of the aquifer well follows the Cooper-Jacob straight line. A two-dimensional infinite acting radial flow model (IARF) can be assumed, describing a flow converging towards the circular cylinder of the well (Renard et al., 2009).

- The transmissivity results ranging from 10^{-2} to 10^{-4} m² s^{-1}, with an average value of 10^{-3} m² s^{-1}.

Table 4. 1. Characteristics of Artesian water points and results obtained. The piezometric data refer to 4 types: artesian springs (AS), non-flowing artesian well (NFAW), free-flowing artesian well (FFAW) and surface water (LAKE).

Water point description							Recovery test results						GPS - Piezometric head results			
No.	Name	Type	X (m)	Y (m)	Depth below ground surface	Casing diam. out	Flow Qin	Recovery duration (t3 ~ t4)	Water level above ground surface	T	Post production effect Computed	Measured	Recovery type (Fig.4.6)	Ground level	Piezometric level (t4)	Corrected piezo level	Classification
			(UTM49S)	(UTM49S)	(b.g.s)	(mm)	(L s^{-1})	(s)	(m.a.g.s.)	(m^2 s^{-1})	(s)	(s)	(a,b,c)	(m.a.s.l.)	(m.a.s.l.)	(m.a.s.l.)	H1 reliable H2 inaccurate
1	Umbulan	AS	713304	9141736			3500.0		Surface water					31.95	32.10		2
2	Banyu Biru	AS	717072	9143018			350.0		Surface water					29.43	28.47		2
3	FD2	FFAW	717239	9142550	32	904	0.2	2999	0.99	3.10×10^{-3}	23.4	40	a	37.36	38.35	38.33	1
4	Truck	FFAW	717107	9144385	50	1146	8.0		> 2.85					19.86	22.71		2
5	AWQ	FFAW	716558	9142195	60	904	0.9	2093	0.74	8.83×10^{-3}	8.4	20	b	39.83	40.57	40.51	1
6	FD1	FFAW	715390	9142385	103	904	1.9	1903	3.72	1.06×10^{-3}	69.5	50	b	38.22	41.93	41.95	1
7	Pasir Well	FFAW	715907	9143728	40	1146	8.6	< 300	3.14					19.61	22.75		2
8	BenbyAlix	FFAW	716175	9144539	63	773	4.8	1973	2.46	3.45×10^{-3}	21.4	25	b	17.18	19.64	19.51	1
9	BanyuCam	FFAW	716969	9143232	66	1146	6.0	< 30	3.56					29.32	32.88		2
10	F8	FFAW	715723	9145698	40	904	10.0	< 60	7.47					15.86	23.33		2
11	Aqua Wash	FFAW	714339	9146170	96	1400	15.0		> 5.2					16.54	21.74		2
12	AW6	FFAW	720216	9146694	120	621	0.1	1924	1.85	4.01×10^{-4}	183.8	190	a	16.02	17.87	17.67	1
13	Aqua Piezo	FFAW	713213	9145881	70	904	12.7	25397	3.48	1.11×10^{-2}	6.6	20	b	19.61	23.09	22.71	1
14	AW24	FFAW	713888	9144172	60	904	4.8	< 300	3.98					22.52	26.50		2
15	AW2	FFAW	709387	9149073	93	1146	6.0	2097	6.02	2.64×10^{-3}	27.9	30	a	24.61	30.63	31.02	1
16	P13	NFAW	722866	9145631	30	1146			-2.54					28.95	26.41		1
17	Ranu Grati	LAKE	721382	9145180	120				Surface water					23.30	22.88		2
18	Michel	FFAW	714150	9144515	38	904	6.0	1420	3.68	2.91×10^{-2}	2.5	150	c	22.36	26.04	25.94	1
19	AW27	FFAW	711747	9143939	60	904	4.3	1878	5.77	2.36×10^{-3}	31.3	50	a	32.63	38.40	38.28	1
20	AW15	FFAW	712173	9142980	52	1146	6.7	679	2.86	1.00×10^{-2}	7.4	10	c	37.72	40.58	39.88	1
21	B33	FFAW	710227	9143490	88	1146	2.1	610	1.13	4.05×10^{-2}	1.8	15	b	44.90	46.03	46.01	1
22	West Umb	FFAW	710267	9143352	133	1146	18.2	2129	5.08	4.32×10^{-2}	1.7	15	c	44.29	49.37	49.33	1
23	AW16	NFAW	708369	9143299	140	1146			-6.74					66.20	59.46		1
24	AW21	FFAW	708963	9145059	129	1146	3.2	1800	0.96					46.60	47.56		2
25	AW74	FFAW	709306	9145872	79	1146	3.1	1935	3.03	2.04×10^{-3}	36.1	30	c	36.26	39.29	39.47	1
26	AW23	FFAW	711390	9145489	83	1146	5.2	1069	6.12	2.14×10^{-3}	34.4	30	a	31.61	37.73	38.52	1
27	AW14	FFAW	711972	9147092	60	1146	8.0	225	2.12	2.62×10^{-2}	2.8	20	b	22.16	24.28	24.18	1
28	B23	FFAW	707564	9147142	81	1146	11.2	2097	5.5	5.24×10^{-3}	14.1	30	b	36.96	42.46	42.57	1
29	B19	FFAW	707594	9146821	150	904	35.0	< 60	7.26					37.88	45.14		2
30	AW33	FFAW	705998	9146529	200	904	12.7	< 60	7.69					44.48	52.17		2
31	Pylone	FFAW	711954	9148334	100	1146	10.0		> 5.15					17.08	22.23		2
32	Grogol 1	FFAW	712270	9149088	60	1146	12.0	< 60	> 8.8					15.07	23.87		2
33	Grogol 2	FFAW	712021	9149008	60	1146	15.5	< 60	> 8.5					16.25	24.75		2

4.4.2 Piezometric head computation

A compilation of the piezometric heads for the 33 water points surveyed here is provided in **Table 4. 1**and illustrated in **Figure 4. 7**. The piezometric head homogenization method explained in section 4.2.5 is applied to the 16 artesian wells that comprise a monitored recovery test. Details of the calculations are provided in **Appendix 9**.

1) Interpolation: 8 wells reach a residual drawdown of 1 m for a "t_{res}" recovery duration of less than 1s (interpolation of Jacob's line to 1 s). This interpolation modifies the piezometric head at the end of the test, leading to decrease ranging from 2 to 20 cm (wells n°3 and 12, respectively). Low t_{res} values correspond to wells with a high transmissivity and/or low discharge, which also show a small slope on the semi-log curve. For these wells, the corrections are all relatively small.

2) Extrapolation: the piezometric heads of the 8 other wells are “extrapolated” (or interpolated in a few cases) for "t_{res}" durations comprised between 27 and 47 000 s, (wells n°70 and 26, respectively). The extrapolation modifies the observed piezometric head at the end of the test from -37 to +79 cm, (wells n°13 and n°26).

The piezometric heads range from 17 to 59 m.a.s.l. (**Figure 4. 7**) and can be divided into 2 types:

- H1 (reliable value): 16 piezometric heads reached a residual drawdown of 1m through extrapolation or interpolation. Therefore, the values are considered as reliable with the exception of wells n°18, 20, 22 and 27. Despite their correction, these latter wells show influence of leaks during the recovery test. As a precaution, these wells are not included in the type (H1). Measurements performed at non-flowing artesian wells are considered as reliable (H1) as they are probably in a steady state without pumping;

- H2 (inaccurate value): 19 piezometric heads are considered as underestimated insofar as leaks are observed (e.g. well n°7), or as simply imprecise without any continuous pressure monitoring. Thus, it is impossible to extrapolate/interpolate these points for the calculation of the residual drawdown of 1 m. The water surface measured at artesian springs and in the lake are also considered as leading to an underestimation of piezometric heads.

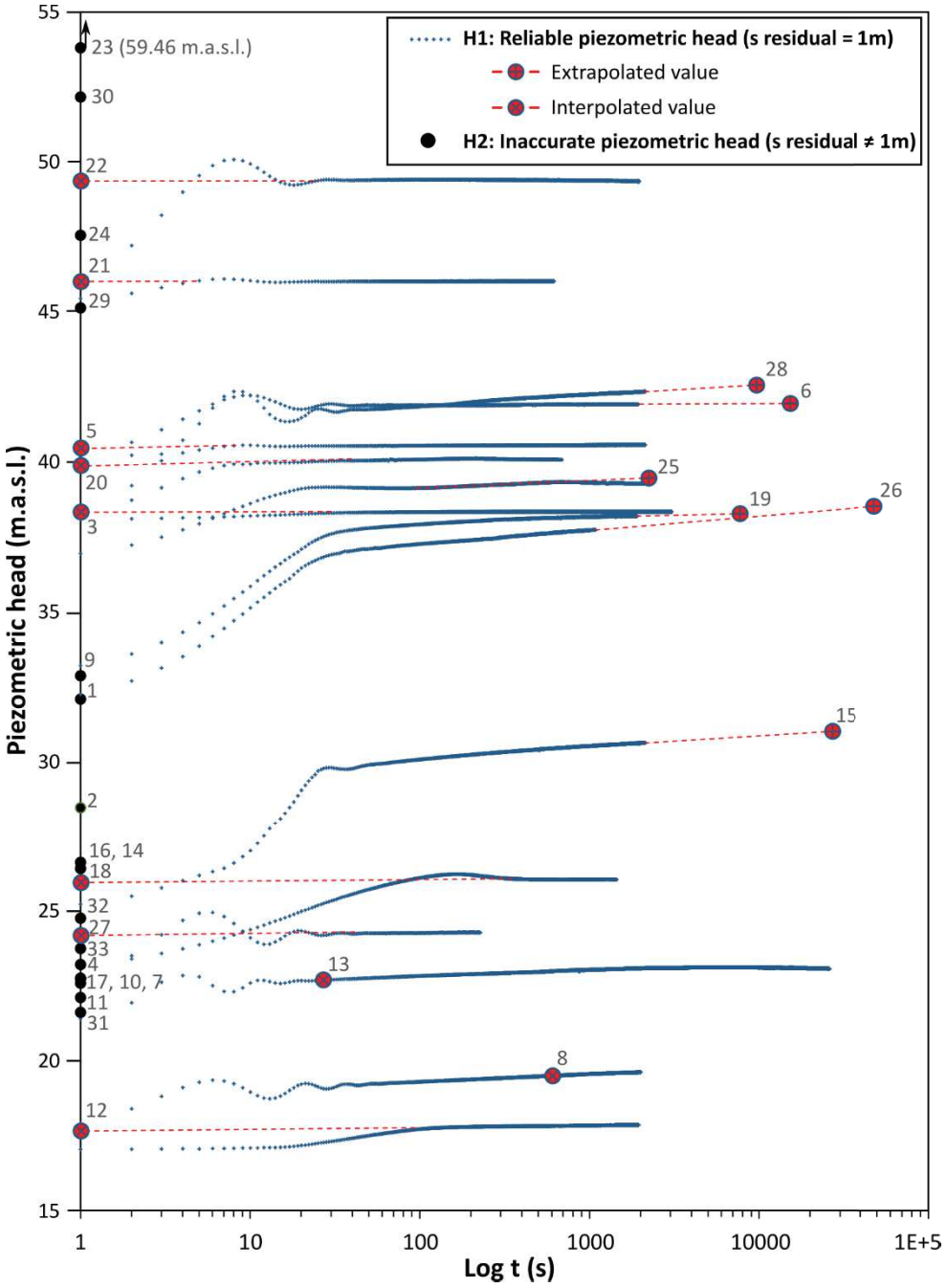

Figure 4. 8. Compilation of the 33 piezometric head values classified into 2 types: H1: reliable value (extrapolated or interpolated); H2: inaccurate value without any continuous pressure measurements.

Overall, the distribution of piezometric heads (**Figure 4. 7** and **Figure 4. 8**) can be divided into two groups:

- Group on the piedmonts: with high heads (> 36 m.a.s.l.) measured in wells mainly located near the foot of the volcano (e. g. well n° 6, 20, 24, etc.).
- Group on the plain: with lower heads (< 30 m.a.s.l.) measured in wells mainly located in the volcano-sedimentary plain. With the exception of artesian springs (n° 1 and 2), well n° 9 is present in the piezometric transition zone included in both identified groups.

4.4.3 Piezometric mapping

A piezometric map can be drawn up from the piezometric head data presented above (**Figure 4. 9. a**). This kriging does not take account of the piezometric heads of artesian springs considered as being highly underestimated. Indeed, taking these heads into account would cause an overestimated cone of depression at each spring, which would skew the surrounding piezometric contour.

The piezometric map:

- confirms that the flow comes from the volcanic aquifer (Bromo-Tengger volcano), and is relatively parallel to the topography in the upstream part of the studied area (between 45-60 m.a.s.l.);

- that groundwater flow has a main SW-NE direction in the West sector and N-S in the East sector. In the central part of the area, groundwater flow is influenced by free-flowing of the artesian springs whose piezometric head should be about 44 m.a.s.l. for Umbulan and 35 m.a.s.l. for Banyu Biru, as derived from the isopiezes extrapolation;

- enables to compute hydraulic gradients that range from 0.01 in the South to 0.001 in the North;

More subtly, groundwater flows are also influenced by the discharge of the 600 free-flowing wells, with a gradient that decreases downstream due to the decrease flow within the aquifer as a result of the outflows. Areas with probably underestimated piezometric head (red dot (H2), **Figure 4. 9. a**), particularly visible in the central part, should be carefully interpreted as they may cause nugget effects (e. g. well 11).

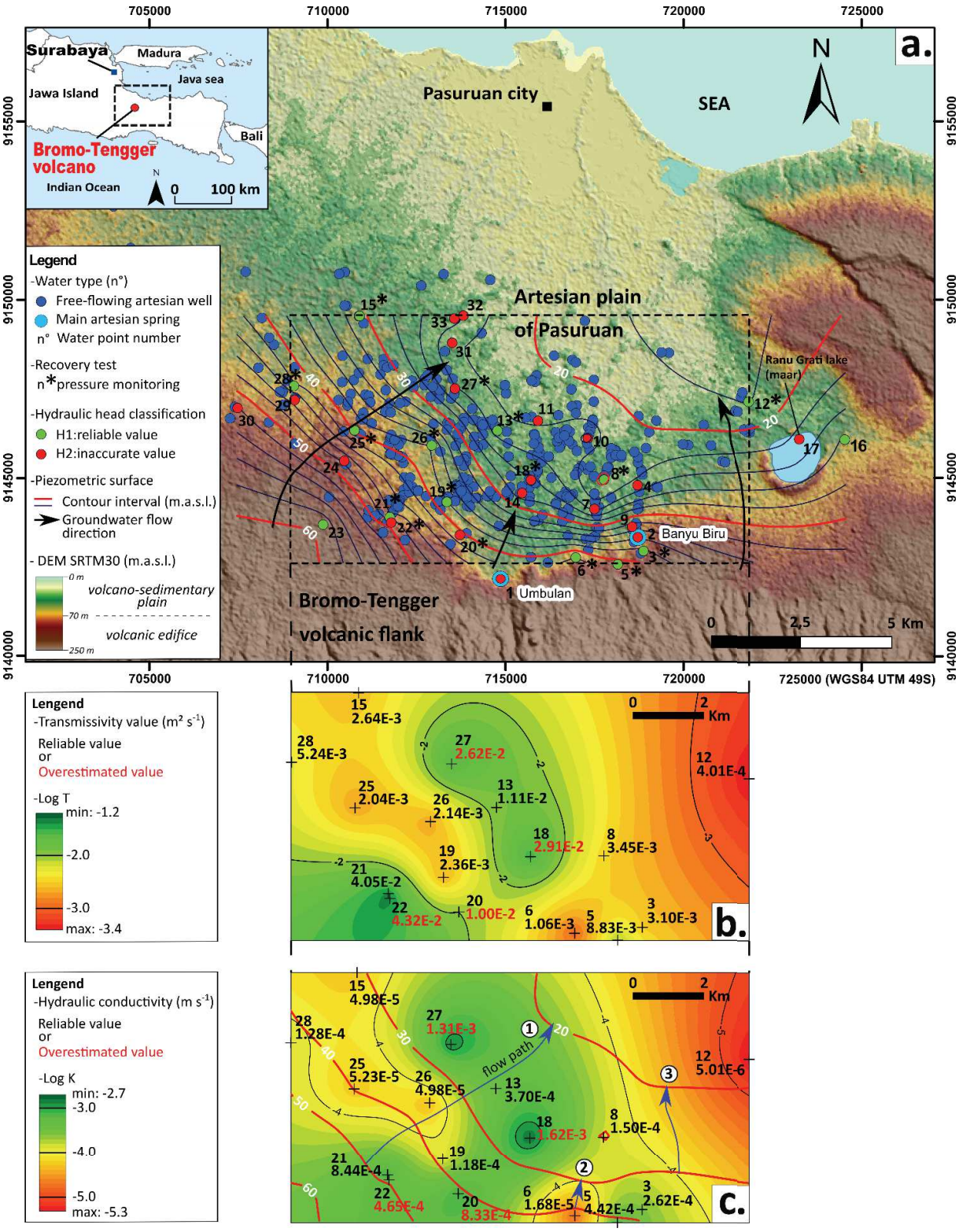

Figure 4. 9. **a.** Piezometric map of the Pasuruan artesian basin in East Java (Indonesia). The map and the location data are provided in UTM zone 49S coordinates, using the WGS84 datum. **b.** Transmissivity map of the artesian aquifer basin (=confined aquifer) using ordinary kriging from the recovery test results. **c.** Map of hydraulic conductivity derived from the piezometric map and different selected groundwater flow paths.

4.4.4 Evaluation of groundwater transit time

A kriging map of the transmissivity (Log T) of the Pasuruan artesian basin was produced (**Figure 4. 9. b**) using the transmissivity results obtained through interpretation of the 16 recovery tests (see section 4.4.1, **Table 4. 1**). At the scale of the artesian basin, the transmissivity is about 10^{-3} m² s^{-1} (yellow-orange colour), but with a variation observed in the South-West as well as in the centre of the plain (green colour). This transmissivity anomaly should be interpreted with caution considering the probable overestimation of the values for wells n° 18, 20, 22, 27 which tightly constrain this kriging (red letter, **Figure 4. 9. b, c**). However, reliable measurements made in wells n°21 and 13 appear to confirm the presence of these more highly transmissive zones. On the contrary, the northeast sector shows a lower T value of 10^{-4} m² s^{-1}, as obtained for well n° 12.

A distribution map of the hydraulic conductivity (Log K) is presented in **Figure 4. 9. c**. For each well, we consider an aquifer of thickness e = (depth - 40m), corresponding to the part of the well that reaches the confined aquifer. For wells with a depth of less than 40m (wells n°3 and 18), we consider: e = (depth - 20m), values also supported by field data indicate that artesian conditions start at a depth of about 20m. The compilation of hydraulic conductivity results indicates values between 10^{-3} and 10^{-6} m s^{-1} with an average of 10^{-4} m s^{-1}. The heterogeneity of hydraulic conductivities is similar to the transmissivity anomaly outlined earlier. Nugget effects are also visible at wells showing an overestimated transmissivity, so the hydraulic conductivity is probably also overestimated (well n° 27 and 18).

Using the distribution of piezometric data on the transmissivity map, three flow lines (flow path 1, 2 and 3 in **Figure 4. 9. c**) were selected near reliable well measurements. These flow paths have different hydraulic gradients and hydraulic conductivities in their vicinity, allowing a first estimate of the flow velocity ranges (Darcy's law) in order to calculate transit times within the artesian plain. We assume an average effective porosity of 0.3 for reworked volcano-sedimentary deposits according to results in the literature (Custodio, 2004; Flint and Selker, 2003; Selles et al., 2015; Singhal and Gupta, 2010; Winograd, 1971). Based on the Darcy's law, the kinematic velocity of water is given by the equation:

$$u = \frac{K\Delta h}{neL} \tag{4.9}$$

where
u: kinematic velocity (m s^{-1})
K: hydraulic conductivity (m s^{-1})
Δh/L: hydraulic gradient along a flow line
n_e: effective porosity

Then, the water transit time is obtained by:

$$t = \frac{L}{u} \tag{4.10}$$

The results for the three selected flow paths are summarized in **Table 4. 2**.

Table 4. 2. Kinematic velocity and groundwater transit time results for each selected flow path (1, 2 and 3), located in **Figure 4. 9. c**.

Parameters	Symbol	Units	Groundwater flow paths selected		
			1	**2**	**3**
Hydraulic conductivity	K	(m s^{-1})	$1.18.10^{-4}$	$4.42.10^{-4}$	$1.34.10^{-4}$
Effective Porosity	n_e	(-)	0.3	0.3	0.3
Hydraulic gradient	$\Delta h/L$	(-)	0.003	0.012	0.004
Kinematic velocity	u	(m s^{-1})	$1.18.10^{-6}$	$1.82.10^{-5}$	$1.78.10^{-6}$
Horizontal distance	L	(m)	6658	810	2498
Transit time	t	(y)	170	1	44
		(y km^{-1})	25	2	18

The kinematic velocity is ranging from 10^{-5} to 10^{-6} m s^{-1}, depending on the hydraulic gradient which is different from West to East (i.e. 0.003, 0.012 and 0.004 for the flow paths 1, 2 and 3, respectively). Depending on the calculated kinematic velocity and the horizontal distance considered, the water transit time ranges from 2 to 25 years per kilometre suggesting good water circulation within the confined aquifer. These transit times should be interpreted carefully, especially in areas where kriging is poorly constrained. The transit time calculated in flow path 1 is probably the most realistic according to the number of nearby wells available for the kriging interpolation.

4.5 Discussion

4.5.1 Device

The device developed in the framework of this research shows the following advantages:

- Easy to build (PVC pipe and valve available everywhere in the world) and low cost less than 100€, pressure sensor not included);
- Very fast to install on variable diameter/discharge wells (<10 min.) and easy to deploy in the field by 2 operators. It is much less convenient if the operator is alone;
- No external power supply required;
- The visibility of water within the transparent pipe during measurements is important to reassure the local population that the water is "still there", even if the well ceases to flow during the test;
- The monitored data are accurate and reliable.

The following shortcomings of the device could be resolved in the future:

- Beyond 8m of hydraulic head above ground surface, the tubes (4 x 2 m) become unstable and a supplementary shoring system is necessary. A lightweight telescopic scaffolding as used in civil engineering could effectively stabilize the tubes;
- Non-monitoring of the discharge prevents the estimation of the storage coefficient (S) usually inferred from the recovery period. Applying an integrated ultrasonic flowmeter with a lithium battery to the control valve should easily solved this issue as well as other integrated probes (ex: CTD Diver) may provide additional physico-chemical parameters during the hydraulic test (EC, T°C, pH, etc.).

4.5.2 Method of measurement

First, the method using several PVC pipes (keeping a water free surface) was preferred to the method involving closure of the artesian well. From our experience, the water pressure makes it difficult to completely close the well. For instance, the free-flowing artesian well device (FFAWD) developed here is hard to maintain in place under such a high-pressure head (> 6 m) and requires an additional fixing system. It is noted that even with the FFAWD, if the grouting well is not totally impervious (casing too short or in poor condition), a leak between well casing and the country rock may appear during the recovery test as observed for wells n° 9, 14, 20 and 27 (**Table 4. 1**, recovery type **c**). Another type of leak may occur inside the aquifer itself, especially in open-hole wells where two water-bearing formations have different hydraulic heads, such as in a multi-layered system classically found in volcano-sedimentary plain (Selles, 2014). Thus, the selection of free-flowing artesian wells with a good visual aspect is a priority before applying the device on large scale. A concrete base at well site is a good indication that the well is probably less liable to leak, although this is not always the case.

As regards the duration of measurements, a recovery period of 30 min is appropriate for the following reasons:

- (i) it does not cut off water access to the local population for an excessive period (e.g. paddy field irrigation or domestic use);
- (ii) most of the artesian wells with different configurations (transmissivity, discharge, depth, etc.) already plot on a constant straight line on the drawdown curve, allowing to easily interpolate or extrapolate the piezometric head value if necessary.

4.5.3 Data interpretation

Recovery test: The interpretation of recovery tests by the Cooper-Jacob method yields consistent transmissivity results, ranging over 1 to 2 orders of magnitude (from 10^{-2} to 10^{-4} m^2 s^{-1}) which seems to be representative of wells in homogeneous and isotropic media. Transmissivity is probably overestimated for some wells influenced by leak, with values of about 10^{-2} m^2 s^{-1}, but analysis of the Bourdet derivative allow to avoid possible skew related to (1) post-production effects (≈ well bore storage) and (2) leaks related to the well casing or the aquifer itself, by applying the Cooper-Jacob straight line on a constant derivative period.

The discharge used to calculate the transmissivity (Q_{in}), corresponding to the discharge before closing the valve of the device, does not significantly influence the transmissivity. As the discharge Q_{in} is about 2 to 6% lower than Q_0 (depending on the PVC connections fitted), the range of variation does not induce any significant change in the calculated transmissivity. However, it is important to bear in mind that the transmissivity calculated at the well represents the local transmissivity, which is usually slightly lower than the regional transmissivity (Willmann et al., 2007).

The piezometric head correction: allows a rigorous comparison of piezometric heads by ensuring a common accuracy based on a residual drawdown (here 1 m). However, in our case study, this correction only slightly modifies the results (79 cm maximum for some wells) and does not change the regional piezometry that is considered as realistic. In addition, this correction method is based on the validity of Jacob's straight line. In the case of a leaky well, the slope of the curve may be underestimated and thus the calculated transmissivity may be overestimated. Therefore, since the calculation of the residual drawdown is based on an overestimated transmissivity value, it can be assumed that the time required for a targeted residual drawdown will also be underestimated. As a precaution, it is therefore preferable to consider this type of situation (leaky well) as leading to inaccurate piezometric head measurements. It can also be noted that extrapolation over very long periods (>10^6 s) could have the disadvantage of increasing the discrepancies between piezometric head measurements carried out without any continuous pressure recording; some of these measurement periods are less than one minute. Other continuously flowing artesian wells in the vicinity may influence the investigated wells, but this effect is difficult to evaluate in the absence of continuous piezometric records at the scale of the plain.

In the case of springs or lakes, the piezometric measurement corresponds only to the surface water level. This level evidently leads to an under-estimation of the piezometric head triggered by the flow of irrigation canals.

4.5.4 Case study

The device developed in this study was applied to the whole artesian volcano-sedimentary plain of Pasuruan during the May-June 2018 period (dry season). This case study provides a better hydrodynamic knowledge of the area:

(i) The calculated transmissivities (from 10^{-2} to 10^{-4} m^2 s^{-1}) are relatively high and representative of a porous medium with good groundwater flow conditions. In comparison with a similar context, the deep multi-layered confined aquifer at the foot of Merapi volcano (Indonesia) shows a transmissivity of about 10^{-3} m^2 s^{-1} (Selles, 2014). The volcanic formations in the aquifer system of Bruneau in Idaho (USA) yield transmissivities ranging from 10^{-1} to 10^{-4} m^2 s^{-1} as estimated by different methods (Berenbrock, 1993). Conversely, volcanic hard rock aquifers such as those composed of dyke-free lava flows on the island of Oahu (Hawaii) yield values of about 10^{-6} m^2 s^{-1} (Hunt, 1996), while basaltic lava flows on Gran Canaria (Spain) yield values of about 10^{-4} m^2 s^{-1} (Singhal and Gupta, 2010). It should be noted that the pressure instrumentation at a nearby well can be used to determine the storage coefficient S from the calculated transmissivity value.

(ii) The average hydraulic conductivity estimated at 10^{-4} m s^{-1} is high and consistent with other volcano-sedimentary contexts (Hunt, 1996; Singhal and Gupta, 2010). However, the hydraulic conductivity anomalies observed here (**Figure 4. 9. b, c**) are significant and seem to reflect a lithological heterogeneity within the plain itself controlled by the stratigraphic relationships and areal extent of the layers penetrated by the wells (Gingerich, 1999). A multi-layered aquifer system associated with a preferential drainage axis could also explain this heterogeneity.

(iii) In terms of piezometry, the groundwater flows northward from the northern flank of the volcano through the volcanic-rock aquifer to the volcano-sedimentary aquifer, with a main flow direction from Southwest to Northeast across the plain. The old caldera of Nongkojajar located on the northwestern flank of Bromo-Tengger could act as a preferential infiltration zone and thus allow flow in the plain from the southwest to the northeast as illustrated by the piezometry. The transmissivity anomaly identified here could be associated with the presence of more permeable materials produced by the collapse of this caldera.

(iv) In terms of hydraulic gradient, the most reliable flow path (n°1) indicates a low hydraulic gradient of about 0.001 and a transit time of about 25 y km^{-1}, suggesting an extensive discharge zone with permeable materials. By comparison, the volcanic aquifer system in the Bruneau area (Idaho) shows similar hydraulic gradients with

an average of about 0.003 (Berenbrock, 1993) where numerous artesian wells are present. Similar low hydraulic gradient are also reported in volcanic coastal areas such as in La Réunion and Grande Comore Islands (Join et al., 2016).

(v) The large areal extent of the depression cone developed around the free-flowing artesian well on the Pasuruan plain may reflect a long-term water-level decline due to withdrawals. If the number of free-flowing wells (about 30 new wells every year) continues to increase, the confined aquifer pressure may decrease dramatically leading to the end of the artesian conditions in the Pasuruan region. This scenario was observed in Honolulu artesian basin (Ohua Island in Hawaii), where the hydraulic head decreased by a few metres between 1880 and 1913, stopping the natural outflow of many artesian wells as well as reducing the discharge of the main submarine springs (Pearl Harbor springs). Furthermore, laws have been enacted to prevent the waste of artesian water and facilitate the restoration of predevelopment conditions in the Honolul artesian basin (Campbell, 1913; Wentworth, 1951). Similar regulations, such as involving the control of discharge using valve systems installed on artesian wells, may contribute to reducing the waste of water from the Bromo-Tengger aquifer system.

4.6 Conclusion

A low-cost hydraulic test device for free-flowing artesian wellw was designed and applied at the scale of the artesian basin of Pasuruan (Indonesia). The pressure data captured by the device allows to estimate the hydrodynamic properties (T and K) from recovery tests results interpreted by the Cooper-Jacob method. A recovery period of about 30 min is sufficient to homogenize the piezometric head values by using a correction method (interpolation or extrapolation) based on a common residual drawdown.

At the scale of the Pasuruan artesian basin, a hydrodynamic survey using the hydraulic test device allows to improve the hydrogeological knowledge of the aquifer system of the Bromo-Tengger volcano:

- The volcano-sedimentary confined aquifer is permeable ($K \approx 10^{-4}$ m s^{-1}) and shows a local hydraulic conductivity anomaly probably triggered by more permeable volcanic materials that were probably deposited following the collapse of the Nongkojajar caldera.
- The main groundwater flow direction from Southwest to Northeast is consistent with the previous hypothesis of a preferential groundwater flow path related to the Nongkojajar caldera. From the low hydraulic gradient (≈0.001) of the artesian basin, a water transit time is inferred from 2 to 25 y km^{-1}. This value reflect the good water flow circulation, clearly influenced by the depression cone developed due to the withdrawals from numerous free-flowing artesian wells. Groundwater abstraction from these artesian wells still remains a major regional issue since no regulations have been enacted to prevent wasting of groundwater.

The device and the methodology used for the estimation of the transmissivity and piezometric head presented here would be usefully applied in other artesian basins. The hydrodynamic parameters inferred from this case study may directly serve as input data for further numerical flow simulations.

4.6.1 Acknowledgements

This research was carried out as part of a PhD thesis in the framework of the Rejoso Kita project, which is co-directed by Danone AQUA, the International Centre for Research in Agroforestry (ICRAF), the Social investment of Indonesia (SII) and the CKNet foundation, with the financial support of the Danone Ecosystem Fund Indonesia. Scientific and logistic support from Gadjah Mada University is gratefully acknowledged. We also thank the University of Gadjah Mada for logistic support. The authors gratefully acknowledge the partnership and authorizations provided by the Ministry of Research, Technology and Higher Education of Indonesia (RISTEKDIKTI) and the Bromo Tengger Semeru National Park (TNBTS). Dr M.S.N. Carpenter post-edited the English style and grammar.

Chapter 5



View of the Coban Sewu springs in Lumajang (South of the Mount Semeru)

Chapter 5. Validation of the hydrogeological conceptual model through numerical modeling coupled with age dating analyses.

In the previous chapters, a combination of multi-disciplinary approaches allows to propose a conceptual model of the groundwater circulation in an andesitic stratovolcano, using as an example the northern flank of the Bromo-Tengger volcano with its downstream artesian volcano-sedimentary plain. To validate this conceptual model and better quantify the groundwater circulation, new hydrogeological data acquired between 2016 and 2019 are used to calibrate a first numerical model aimed at simulating groundwater flow that is representative of present-day hydrogeological functioning.

In this perspective, a 3D steady-state groundwater flow model is built of the northern flank of the Bromo-Tengger volcano and downstream volcano-sedimentary plain. Two steady-state groundwater flow scenarios are simulated to assess: 1) the present-day (2018) groundwater flow circulation, with the impact of abstraction from free-flowing artesian wells, and 2) the natural groundwater flow conditions before exploitation of the artesian aquifer, without abstraction of groundwater from free-flowing wells.

Complementary age dating analyses were performed and compared with the results (hydraulic head and velocity field) of the 1st steady flow model, allowing to determine the groundwater residence time in the artesian plain. Finally, we discuss the most reliable flow model with respect to the hydrogeological conceptual model.
This 3D model should not be considered merely as a tool for groundwater management, but rather a first step for further scientific investigations of the Bromo-Tengger aquifer system, which will help implement management and protection policies

Abstract

Understanding groundwater continuity between the inland and coastal domains of volcanic massifs is particularly challenging, especially when the coastal zone is represented by a multilayered and artesian volcano-sedimentary system. In such artesian conditions, free-flowing artesian wells (FFAW) allow the groundwater to flow freely without pumping. Without any flow control or regulation, areas with a high density of FFAWs can disturb the natural flow conditions of the artesian system. In this study, 3D numerical modeling is used to indirectly infer the groundwater flow conditions with and without groundwater abstraction at wells, and verify the consistency of the hydrogeological conceptual model for the northern flank of the Bromo-Tengger volcano. Simulation results are based on the outflows and hydraulic heads measured on the Pasuruan artesian plain, while the upland recharge rate is based on hydroclimatic data analysis performed for the year 2017-2018. Age dating analyses carried out on waters from the plain of Pasuruan allow to propose a conceptual flow model in agreement with the observed age distribution.

Results of the numerical model are in agreement with the conceptual model, which considers a low-lying basal aquifer in the volcanic edifice and artesian conditions on the plain. There has been a significant change in flow patterns due to groundwater abstraction from the Bromo-Tengger aquifer on the volcano-sedimentary plain. Age dating analyses lead to consider two distinct flow systems, which are related to the piedmont areas and the volcano-sedimentary plain of Pasuruan. Groundwater residence times obtained from ^{14}C analyses on water samples from the plain are discussed in relation to a potential input of deep volcanic CO_2 that could trigger an overestimation of the groundwater age.

Keywords: Groundwater modeling, age dating analyses, Bromo-Tengger volcano, artesian volcano-sedimentary aquifer.

5.1 Introduction

Most of the scientific issues in volcanic hydrogeology are focused on defining conceptual groundwater models for inland aquifers (Izquierdo, 2014). These conceptual models can be divided into two hydrogeological sub-domains: mountainous volcanic massifs (inland terrains) and coastal zones (Join et al., 2016). The hydraulic continuity between the deeper inland aquifers and coastal aquifers is still poorly understood especially in island-arc volcanic areas such as in Java (Indonesia) where volcanic distal deposits frequently make up a complex multilayered volcano-sedimentary aquifer with artesian conditions (Toulier et al., 2019).

A common feature of volcanic massifs is the presence of a main basal aquifer with an unconfined water table, which is mainly recharged by heavy precipitation under tropical climates. The water table elevation is predominantly controlled by infiltration, permeability, and to a lesser extent, by topography, basal heat flow and thermal conductivity (Forster and Smith, 1988). Depending on the origin and the geometry of the volcanic edifice, the basal aquifer has a gentle slope and remains at low elevation (Hawaiian conceptual model) or is located several hundreds of metres above sea level (Canarian conceptual model). Numerical modelling can help to explain the highly contrasted configurations of such basal aquifers.

During the last few decades, many volcanic aquifer systems have been modeled such as the Mosteisros Basin on Fogo Island in the Cape Verde archipelago (Heilweil et al., 2012), the young ocean-island volcano of Piton de la Fournaise (La Réunion), (Join et al., 2016; Violette et al., 1997), Santa Cruz Island (Galapagos) with special attention paid to salt water intrusion (Pryet, 2011), the sedimentary volcanic aquifer of La Aldea valley (Grand Canaria Island), (Cruz-Fuentes et al., 2014) and the eastern flank of the Merapi volcano (Indonesia) (Selles, 2014). To be relevant, numerical models should integrate all the geological and hydrogeological data at the aquifer scale and must be based on a meaningful conceptual model of the system (Machard de Gramont et al., 2010).

Since 1980s, there has been a growing awareness of the groundwater issue regarding the sustainability and mismanagement of the resource in the Bromo-Tengger aquifer system. This numerical modeling is motivated by indications of a decrease of artesian conditions of the Pasuruan plain related to the increased number of free-flowing artesian wells. A steady-state numerical model of the regional groundwater flow was developed to validate the conceptual model and improve understanding of the groundwater circulation and water budget of the Bromo-Tengger aquifer system. This model quantitatively integrates the new hydrogeological data presented in this thesis. The geometry and groundwater outflows of the aquifer system are derived from the new geological and hydrogeological results outlined in *Chapter 2*, while the hydrogeological conceptual model and recharge rates are based on *Chapter 3*. Some hydrodynamic parameters are provided by the hydrodynamic analysis of the Pasuruan plain developed in *Chapter 4* and the remaining parameters are inferred from the literature.

For this purpose, a 3D model is implemented that encompasses the whole northern flank of the Bromo-Tengger volcano extending to the artesian volcano-sedimentary plain of Pasuruan. Groundwater flow is simulated under present-day conditions of exploitation, as well as without exploitation, to assess the impact of abstraction from artesian wells. The age dating of waters sampled at artesian springs and wells allows to discuss the most reliable flow model.

5.2 Methodology

5.2.1 Theoretical background

The numerical modeling approach presented in this study is based on the governing equations of flow and mass transport. The dimensionless groundwater flow in response to pressure gradient can be expressed by the following equation:

$$\vec{\nabla}.\left(\overline{\overline{K}}.\vec{\nabla}\mathrm{h}\right) = S_S\,.\frac{\partial h}{\partial t} + q \qquad (5.1)$$

Where, h is the hydraulic head (L), S_S the specific storage coefficient (L^{-1}), q a source term corresponding to the withdrawal of fluid flow (or injection if negative) per unit volume in the considered media (T^{-1}), and $\overline{\overline{K}}$ the permeability tensor (L. T^{-1}), while $\vec{\nabla}$ is the nabla operator applied to a vector field $\left(\frac{\partial}{\partial x};\frac{\partial}{\partial y};\frac{\partial}{\partial z}\right)$.

The fundamental transport equation accounting for advection, kinematic dispersion and molecular diffusion is combined with the flow equation (5.1), giving the following equation:

$$\vec{\nabla}.\left(\overline{\overline{D}}.\,\vec{\nabla}\mathrm{C} - \mathrm{C}.\vec{\mathrm{v}}\right) = \mathrm{n}\,.\frac{\partial C}{\partial t} + \mathrm{c} \qquad (5.2)$$

Where, $\overline{\overline{D}}$ is the dispersion tensor that includes the dispersity and the diffusion coefficient (L^2. T^{-1}), C the mass concentration (Mole. L^{-3}), c the source term corresponding to the extracted (or injected if negative) mass of tracer (Mole. L^{-3}. T^{-1}), $\vec{\mathrm{v}}$ the Darcy velocity (L. T^{-1}), and n the total porosity.

5.2.2 Model design

To build a groundwater flow model for such a complex volcanic system, we needed to know i) the geometry of the internal structure of both the northern flank of the volcano and the downstream volcano-sedimentary plain, ii) the distribution of the recharge and iii) the spatial distribution of hydrodynamic properties of the different layers of the aquifer. This numerical model accounts for:

1) The results of *Chapter 2* concerning the identification of aquifer formations and their respective geometries on the northern flank of the volcano and the downstream volcano-sedimentary plain of Pasuruan;
2) The estimated groundwater outflow inferred from the inventory of groundwater points (2016-2018) presented in *Chapter 2*;
3) The hydro-climatological dataset acquired from the new meteorological monitoring network installed during this PhD, to define the inflow conditions such as the spatial distribution of recharge presented in *Chapter 3*;

4) The hydrodynamic properties and current piezometric head conditions, provided by the investigations on the volcano-sedimentary plain in 2018 (*Chapter 4*).
5) Estimate of hydraulic and physical parameters necessary for the simulations, provided by the literature review in *Chapter 1*.

The groundwater flow is numerically modelled using the FEFLOW software (Diersch, 2014). Finite element numerical methods are used for spatial and temporal discretization of the differential equations (5.1 and 5.2). 3D simulations are firstly performed in saturated and steady-state flow situations. The boundary conditions are implemented as input of the simulations within the 3D model according to the new hydrogeological information (recharge, outflows, etc.). In the following model, we do not take account of saline water intrusion that could occur near the Pasuruan coastline, since this phenomenon is beyond the scope of this modeling. Considering the high uncertainty about groundwater flowpaths near the Tengger caldera and the rather low estimated recharge contribution (< 2% of the total recharge, see *Chapter 3*, section 3.4.5) from this caldera, this aspect is not considered in the model.

5.2.2.1 Model geometry

First, the outer boundaries of the domain are defined considering three simplified hydrogeological units of the Bromo-Tengger system (**Figure 5. 1. a, b**):

1) The volcanic edifice: we consider its geomorphological limits as corresponding to the caldera rim of Nongkojajar (West), the Tengger caldera (South) as well as the deep valley of Sapikerep bordering the eastern part of the domain. These boundaries can be considered as the maximum extension of the hydrogeological system of the volcanic edifice;

2) The volcano-sedimentary plain: East-West limits are based on flow lines inferred from the new piezometric map drawn up in May 2018, while the North limit is represented by the northward extent of free-flowing artesian wells, i.e. probably corresponding to the northern limit of the artesian aquifer system due to distal clayey facies (for more details, see previous section 2.5.1);

3) A confining unit: for simplification, the confining condition of the Pasuruan plain is represented by a single continuous layer that corresponds to a confining unit on the plain and the low-permeability lava boulders on the volcano flank that crop out as far as an elevation of about 200 m.a.s.l.

A 2D areal finite-element mesh was first created based on the studied domain using FEFLOW (**Figure 5. 1. b),** with progressive discretization extending from the volcanic edifice (mesh elements 1000 m) to the volcano-sedimentary plain, where refining was applied to the nodes corresponding to each artesian well (mesh elements < 1 m). The Delaunay criteria were

respected for each triangular prismatic mesh element. The domain covers a surface area of 711 km² with approximatively 313 500 elements and 156 900 nodes.

Then, the whole domain was vertically discretized into 6 slices corresponding to 5 distinctive layers (**Figure 5. 1. c)**. The top surface of the model (Slice 1) corresponds to ground level, represented by the Digital Elevation Model (SRTM30m) applied to the study area. The following slices 2, 3, 4 and 5 were based on Slice 1 minus 30, 40, 70 and 100 m depth, respectively, while the last slice 6 was horizontally fixed at -300 m.a.s.l. (**Figure 5. 1. d)** considered as the potential limit depth of the volcano-sedimentary units (see section 2.5.1). The confining unit corresponds to the single layer 2 that successively covers the plain and part of the volcanic edifice. As shown in **Figure 5. 1. c,** a single layer can represent different hydrogeological units over the model domain (e.g. layer 1).

The results of the vertical discretization lead to a 3D numerical model grid ranging from -300 to 2750 m.a.s.l., comprising about 1 567 000 elements, 941 400 nodes and a total volume of about 720 km^3.

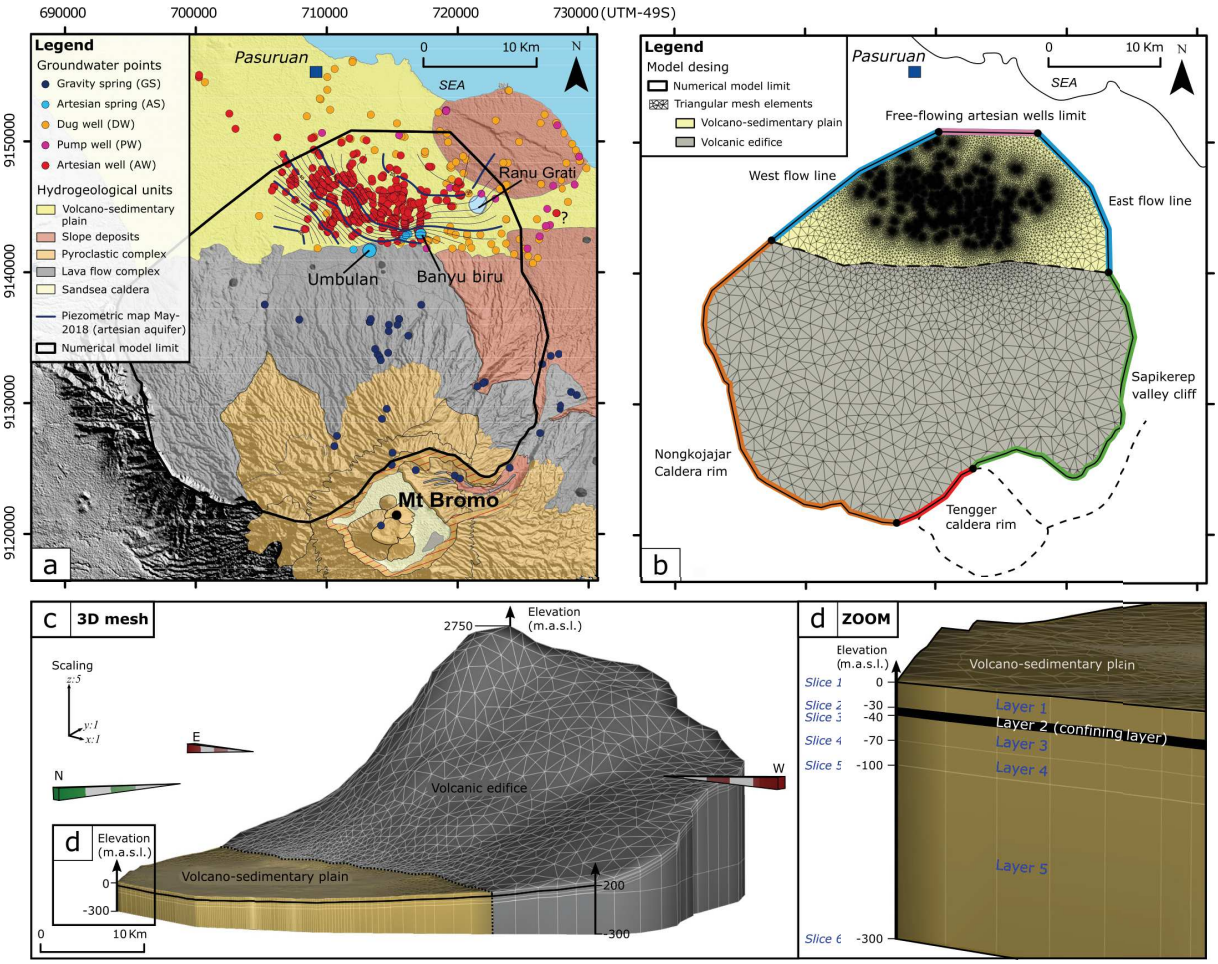

Figure 5. 1. Design of model for the northern flank of the Bromo-Tengger volcano with **a.** the outer limit of the domain that consider geomorphological and hydrogeological limits, **b.** 2D areal finite element mesh with the distinctive volcanic edifice and the volcano-sedimentary plain of Pasuruan from which the nodes of the artesian wells are refined. **c.** Vertical discretization of the 2D mesh considering 5 layers (6 slices) ranging from the surface to -300 m.a.s.l. over the model domain. **d.** Discretization of the volcano-sedimentary unit with a confining unit located in layer 2 (10 m thick).

5.2.2.2 Hydraulic conductivity of the hydrogeological units

The initial hydraulic conductivities for each unit are summarized in **Table 5. 1** and illustrated in **Figure 5. 2. a, b**.
We distinguish the three following hydrogeological units:

- The K value of the volcanic edifice is inferred from the literature concerning andesitic volcanoes (see section *Chapter 1*, section 1.3.2.6), indicating that we can consider a single hydrogeological unit composed of lava flows alternating with pyroclastic deposits of permeability K ≈ 1.10^{-6} m s^{-1} (*Layer 1 to 5*);

- The volcano-sedimentary plain can be divided into 2 subdomains:
  - The deep volcano-sedimentary plain that hosts the confined aquifer (artesian). The K value of this subdomain is based on the kriging map obtained in *Chapter 4* (see section 4.4.3) using data from the new hydraulic test device. The values range from 10^{-3} to 10^{-6} m s^{-1} with an average of 10^{-4} m s^{-1} (*Layer 3 to 5*).
  - The shallow volcano-sedimentary plain that hosts locally an unconfined aquifer. The K value of this 2nd subdomain is based on values estimated for volcano-sedimentary deposits (Selles, 2014), which also corresponds to the average estimate hydraulic conductivity of the deep confined aquifer: K ≈ 1.10^{-4} m s^{-1} (*Layer 1*);

- The hydraulic conductivity of the confining unit is fixed at K ≈ 1.10^{-7} m s^{-1}. This unit corresponds to welded pyroclastic deposits on the plain and lava boulders in the volcanic edifice. It makes up a layer 10 m thick with low permeability but which is sufficiently conductive to allow upward leakage that probably occurs towards the unconfined aquifers (*Layer 2*).

Table 5. 1. Initial hydraulic conductivity values of the model domain

Hydrogeological unit	**Aquifer**	**Discretization**	**Hydraulic conductivity**
		Layer (*1 to 5*)	K ($m\ s^{-1}$)
Volcanic edifice	Basal aquifer (Perched – unconfined)	*1 to 5*	1.10^{-6}
Volcano-sedimentary plain	Shallow (unconfined)	*1*	1.10^{-4}
	Deep (confined)	*3 to 5*	1.10^{-3} to 10^{-6}
Confining unit	Aquitard	*2*	1.10^{-7}

Despite the frequently mentioned anisotropy of volcanic rocks (Singhal and Gupta, 2010), especially with regard to volcanic massifs (lava flows with pyroclastic layers), we consider a k_h/k_v ratio of 1 can be used for all layers as a first and reliable modeling approach.

5.2.2.3 Boundary conditions and recharge

Boundary conditions of the model are summarized in **Table 5. 2** and illustrated in **Figure 5. 2. c**. The flow boundary conditions are represented by:

1) The basal slice of the model (*slice 6* at -300 m.a.s.l.) is defined as a no-flow boundary as well as all layers along the outer boundary of the domain.

2) Based on the groundwater points inventory presented in *Chapter 2*, (section 2.4), all the free-flowing artesian wells are implemented in the model through individual nodes on the volcano-sedimentary plain. The individual discharges of these wells are implemented to represent the real spatial distribution of the outflow values. For that purpose, a boundary condition of the 4th kind (single well) was assigned to each well node on *slices 3* and *5* (i.e. from 40 to 100 m depth from surface). The total discharge of this type of well is 2.4 m^3 s^{-1}, with some of them being used as observation wells to calibrate hydraulic head simulations, since this value was measured using the new hydraulic test device described in *Chapter 4*. Other types of well such as pump and dug wells are not implemented in this model since the water abstraction rate within the shallow unconfined aquifer remains unknown and irrelevant for the purpose of this modeling focused on artesian conditions.

3) A hydraulic head boundary condition of the 1st kind (Dirichlet) with a seepage constraint was imposed at the artesian spring locations (Umbulan and Banyu Biru). A specified head boundary condition was set at 33 m.a.s.l. at the respective node on *slice 3* (under the confining unit) that corresponds to the spring outflow elevation obtained from the digital elevation model (STRM30). This specified head value is supposed to provide the total current spring discharge of 4 m^3 s^{-1}, as presented in *Chapter 2*, (section 2.4). It should be noted that gravity springs that flow in the upper part of the volcanic edifice are not considered in this model since the outflowing water may infiltrate again along the flanks of the volcano.

4) A flow constraint condition of the 2nd kind (Neumann) was assigned along the outer boundary of *layer 1*, but only for the unconfined part of the volcano-sedimentary plain. This flow constraint is used to condition upward leakage from the deep aquifer to the unconfined aquifer. The total flow value is initially fixed at 0.75 m^3 s^{-1}, as suggested from the first rough estimation of "natural" leakage through the upper confining unit (see *Chapter 3,* section 3.4.1.1). We also assign a flow constraint of 0.45 m^3 s^{-1} to the Ranu Grati lake in *slice 3*, which corresponds to gauging measurements performed in canals in May 2018 during the dry season (i.e. probably the minimum outflow). Indeed,

we assume that most of the Ranu Grati discharge is provided by the artesian aquifer because of the great depth of the lake (> 120 m depth in centre).

The recharge distribution along the northern flank of the volcano, as developed in *Chapter 3* (section 3.4.5), is used here to specify the recharge over the model surface (Slice 1) (**Figure 5. 2. d)**. As a reminder, the recharge distribution is based on the assumption that 90.5% of the effective rainfall infiltrates over an area ranging from 2 750 to 100 m.a.s.l. (Toulier et al., 2019). The recharge rate on the plain is not considered here since the modeling is focused on the confining aquifer, under conditions where the confining unit prevents the infiltration of rainwater from the surface. Then, the recharge value from the plain to the volcano summit is initially set in the range from 0 to 2 737 mm.

Table 5. 2. Boundary conditions in the model domain.

Boundary conditions	**Elements**	**Slices**	**Nodes**	**Values**		
		(1 to 6)	(number)	Hydraulic head (m.a.s.l.)	Discharge (m^3 s^{-1})	Recharge (mm y^{-1})
No flow	Basal and outer model boundary	1 to 6				
Flow well	Free-flowing artesian wells	3 and 5	461 x 2		2.4	
Specified head (+ seepage)	Artesian springs	3	2	33	(4)	
Flow constraint	Confining unit leakage (outer boundary on volcano-sedimentary plain)	1 to 2			0.75	
	Ranu Grati lake	3			0.45	
Recharge	Surface model (0 to 2750 m.a.s.l.)	1				0 to 2737

(.) *expected discharge*

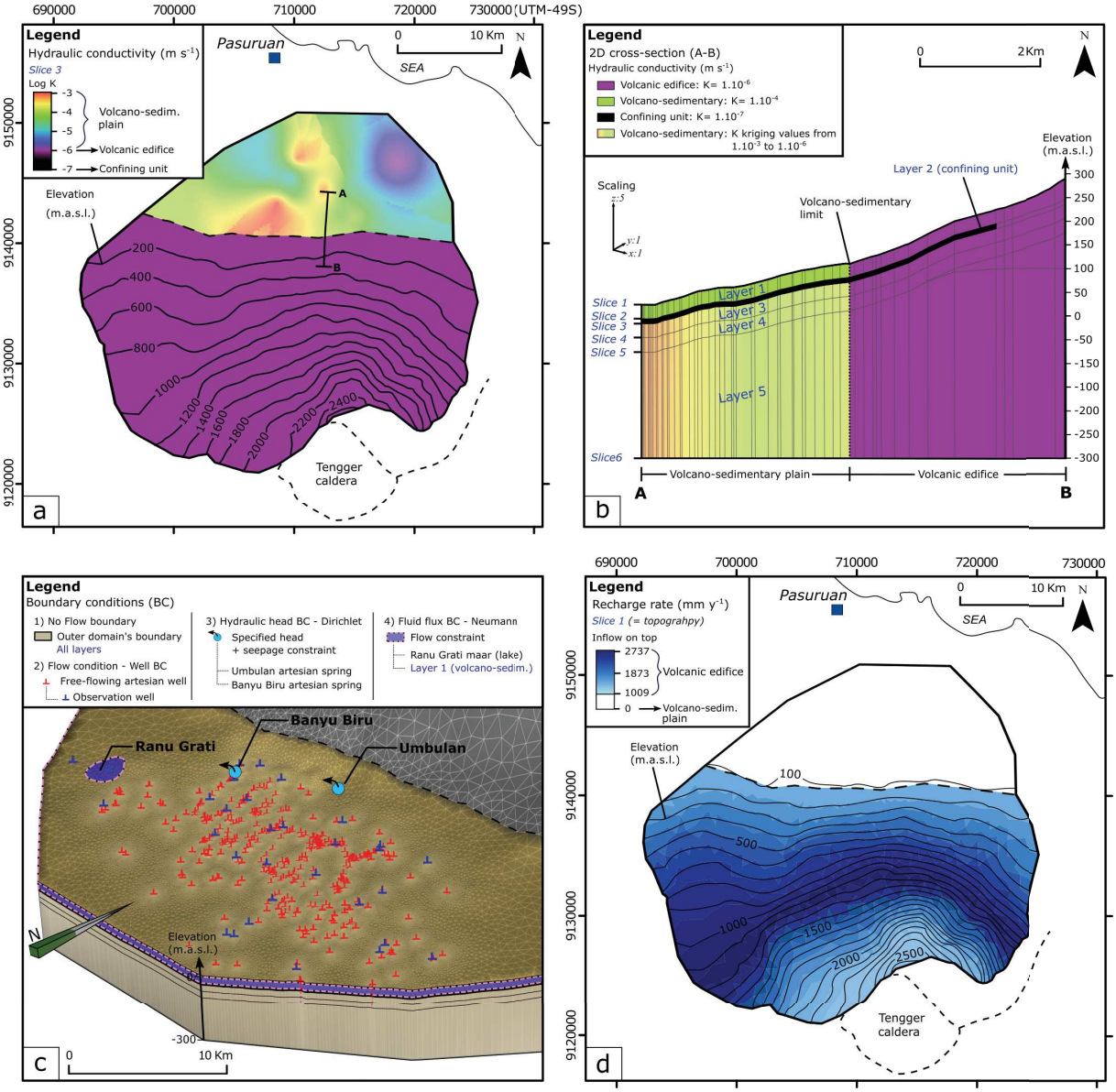

Figure 5. 2. a. hydraulic conductivity of slice 3 over the model domain, **b.** cross-section (A-B) between the volcano-sedimentary plain and the volcanic edifice, illustrating the K values of the five model layers. **c.** description of the boundary conditions applied over the model domain. **d.** recharge distribution applied to slice 1 (ground surface).

5.2.3 Modeling strategy

Present-day flow condition (2018): to model the groundwater flow circulation in the model domain, the following variables are adjusted with the model to provide a representative "steady state" of the artesian conditions in 2018:

1) The piezometric level based on measurements at observation wells;
2) The artesian spring discharge (continuously measured at Umbulan and Banyu Biru);
3) The upward leakage through the upper part of the confining unit;
4) The extent of the artesian area;
5) The direction and magnitude of groundwater fluxes;
6) To a lesser extent, the initial recharge rate and hydraulic parameters of certain layers.

Natural flow condition (1980): based on this first model calibration (2018), the model was run without free-flowing artesian wells as a first approach to establish natural conditions and estimate the impact of such continuous outflow over the years.

The results are discussed with regard to the first estimate of groundwater velocities presented in *Chapter 4* (section 4.4.4) and compared to the age dating analysis described in the following part.

5.2.3.1 Numerical model calibration parameters

There are very limited hydrogeological data related to the pre-development state of the Bromo-Tengger aquifer system, before the start of drilling of the free-flowing artesian wells. From oral testimonies of the local population, the drilling of wells started in the 1980s and the discharge of the main Umbulan spring was about 5 m^3 s^{-1} during this period. Additional calibration datasets were acquired during this thesis work to validate this assumption, and are used to calibrate the steady-state numerical model:

1) Hydraulic head: 33 piezometric level measurements in May-2018 from artesian water points described in *Chapter 4* (section 4.4.2) are used to guide the model calibration.

2) Artesian spring discharge: the mean discharges provided by continuous monitoring at the Umbulan and Banyu Biru springs are, respectively, about 3.5 and 0.2 m^3 s^{-1} in 2018 (**Figure 5. 3**). This trend appears to confirm the expected discharge of Umbulan in 1980. Supplementary results obtained from the instrumentation set up during the thesis work are provided in **Appendix 7**.

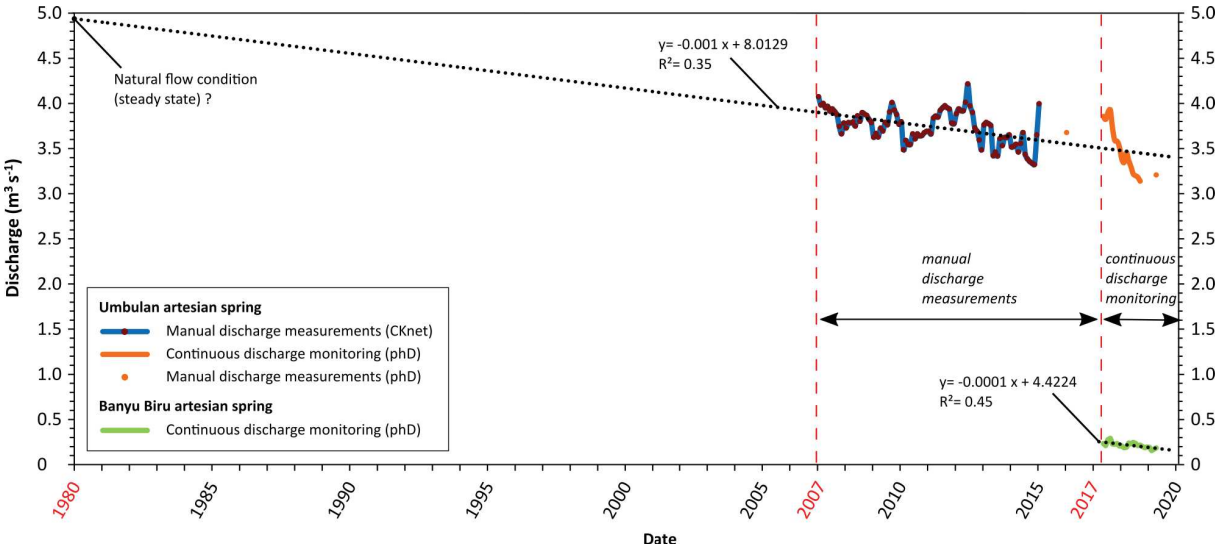

Figure 5. 3. Compilation of discharge data (literature and PhD monitoring) for Umbulan and Banyu Biru artesian springs.

The calibration was carried out by trial-and-error simulation to obtain the best fit between simulated and observed heads and discharges. More than 50 simulation tests were performed. The calibration performance is quantified by calculating the root-mean-square error (RMSE), the correlation coefficient (r) and the scaled RMSE. The combination of a small RMSE and high r indicates a satisfactory model calibration. The scaled RMSE is classically considered as valid if the value is below the threshold of 5% (Anderson and Woessner, (1992)).

5.2.4 Age dating sampling

To specify the groundwater age distribution within the Pasuruan volcano-sedimentary plain, a water dating campaign was carried out in June 2018 during the dry season, including 13 sampling points: 10 free-flowing artesian wells, the two main artesian springs of the area (Umbulan and Banyu Biru) and a shallow pump well (PW13). The selection of these water points is based not only on their spatial distribution but also sampling feasibility and accessibility.

The location and type of samples collected are summarized in **Figure 5. 4**. Samples were used for hydrogeochemical analyses (major and minor elements), isotopic analyses ($^{14}C/^{13}C$, ^{3}H) and dissolved gases analysis (CFCs, SF_6 and noble gases).

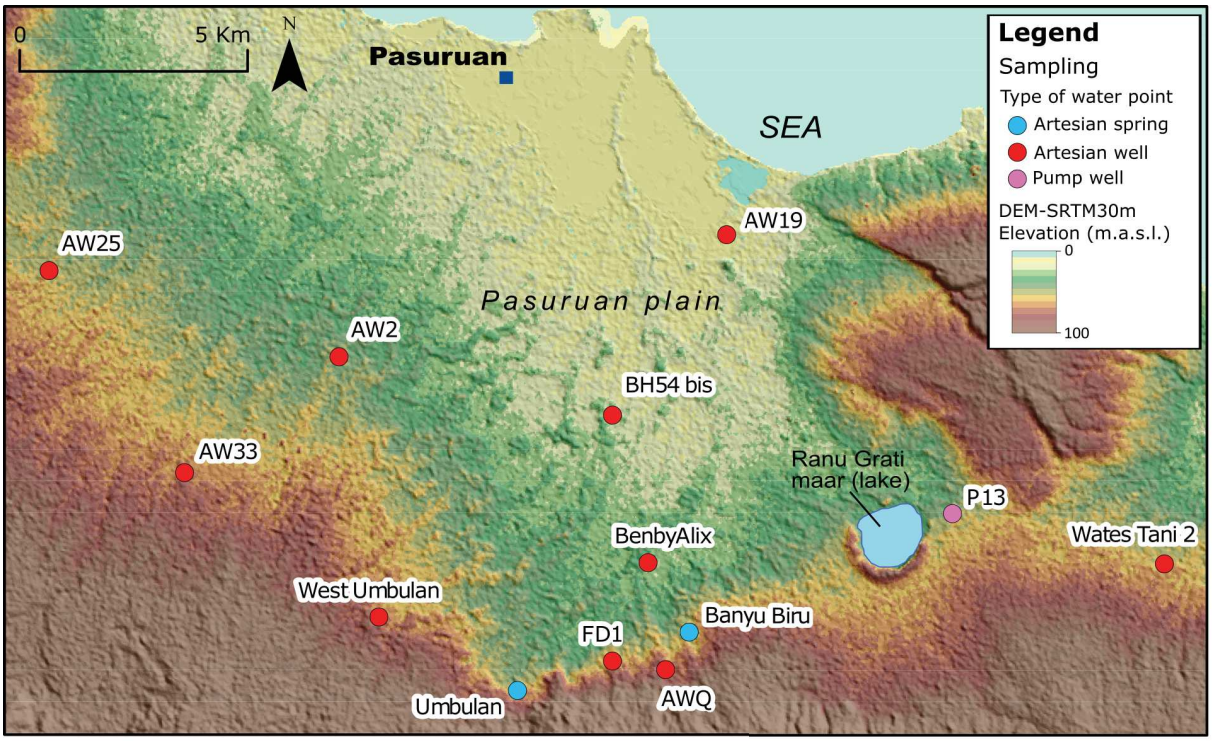

n°	Name	Type	Date	X	Y	Depth	Type of sampling				
				(UTM-49S)		(m)	Mai/Min/$\delta^{18}O$-^{2}H *Hydrosciences Lab*	CFCs-SF6	Noble Gas *Condate Lab*	$^{14}C/^{13}C$ *EIL Lab*	^{3}H *EMMAH Lab*
1	Banyu Biru	Artesian spring	*05/06/18*	717072	9143018	-	yes	yes	yes	yes	yes
2	P13	Pump well	*05/06/18*	722866	9145631	30	yes	yes	yes	yes	yes
3	AW19	Artesian well	*05/06/18*	717897	9151752	16	yes	/	/	/	yes
4	Wates Tani 2	Artesian well	*05/06/18*	727508	9144531	?	yes	yes	yes	yes	yes
5	BH54 bis	Artesian well	*05/06/18*	715394	9147792	>100	yes	yes	yes	yes	yes
6	AWQ	Artesian well	*04/06/18*	716558	9142195	60	yes	/	/	/	yes
7	FD1	Artesian well	*04/06/18*	715390	9142385	110	yes	yes	yes	yes	yes
8	BenbyAlix	Artesian well	*05/06/18*	716175	9144539	63	yes	/	/	/	yes
9	Umbulan	Artesian spring	*04/06/18*	713304	9141736	-	yes	yes	yes	yes	yes
10	AW2	Artesian well	*06/06/18*	709387	9149073	93	yes	yes	yes	yes	yes
11	West Umbulan	Artesian well	*06/06/18*	710267	9143352	133	yes	yes	yes	yes	yes
12	AW33	Artesian well	*06/06/18*	705998	9146529	200	yes	yes	/	yes	yes
13	AW25	Artesian well	*06/06/18*	703028	9150964	>100	yes	yes	yes	yes	yes

Figure 5. 4. Location map with the water point features of the age dating sampling in 2018.

5.2.4.1 Theoretical background and sampling protocol

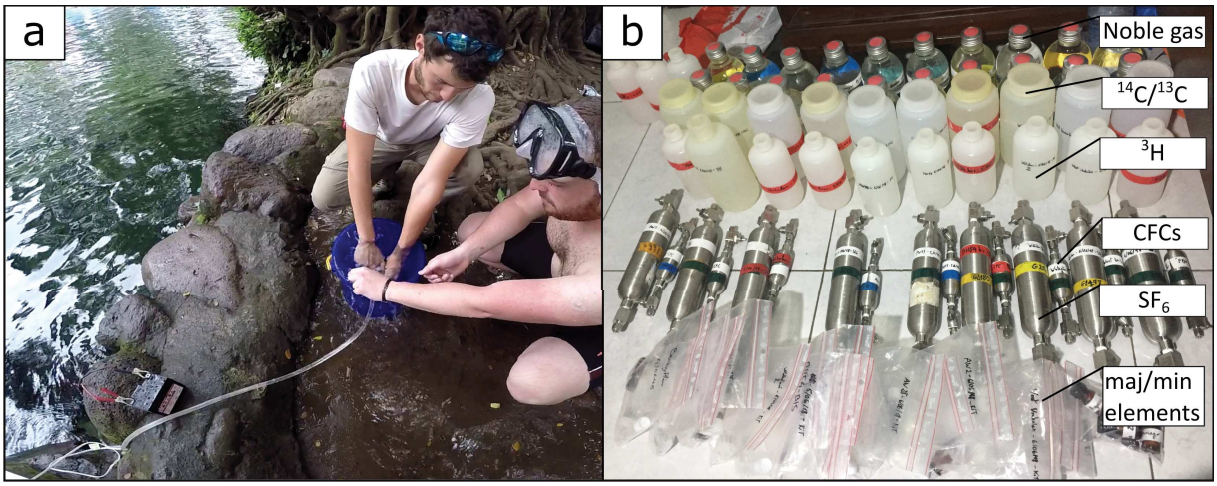

Figure 5. 5. a. Sampling process for noble gas collection using glass bottle and immerged pump at the Banyu Biru spring outflow (- 4m depth underwater). **b.** Sampling kits used for groundwater age dating analyses.

- Minor and major elements (anions, cations).

The theory and sampling method for the analysis of major and minor elements is presented in *Chapter 3*, (section 3.3.2.3). Therefore, it is not explained again here. Major and minor elements were conditioned in the field for analyses back in the laboratory, while alkalinity measurements was carried out in the field to determine the $HCO3^-$ concentrations in each water sample (**Figure 5. 5. b**). Laboratory analyses were carried out in France at the Hydrosciences Montpellier laboratory (UMR 5569) using an IC1000 Dionex ion chromatography system (anions) and a Thermo-Fisher Scientific™ iCAP™ Q ICP-MS analyzer.

- Tritium (^3H)

Tritium is an isotope of hydrogen with a half-life of 12.32 years that can be used to estimate groundwater residence times ranging from years to decades (Clark and Fritz, 1997; Freeze and Cherry, 1979). Tritium is produced naturally in the upper atmosphere by the interaction of nitrogen and oxygen with cosmic rays that generates cosmogenic isotopes of ^3H. ^3H activities are measured in tritium units (TU) and, due to its short half-life, ^3H is commonly used for localizing recent recharge occurrence and quantifying recent recharge rates (Cartwright et al., 2017). A major amount of ^3H was produced during the atmospheric testing of nuclear weapons in the 1950s and 1960s, inducing a strong increase in the ^3H activity of rainfall. Because most atmospheric nuclear tests took place in the northern hemisphere, ^3H activities in the northern hemisphere are much higher than in the southern hemisphere (e.g. 6000 TU at Ottawa vs. 60 TU at Melbourne; IAEA 2017).

At the present-day, the decay of high ^3H spikes and their dispersion makes it more difficult to identify the remnant bomb-pulse peak in groundwater systems, especially in the southern

hemisphere, where the ^{3}H activities of remnant bomb pulse waters are now below the values measured in modern rainfall (Morgenstern et al., 2010). The groundwater residence times may currently be estimated from time series measurements or by assuming that the ^{3}H activities are from one side of the bomb-peak (Cartwright et al., 2017).

Modern rainfall ^{3}H activities in the mid latitudes of the southern hemisphere are < 3 TU (IAEA, 2008), and groundwater ^{3}H activities may be substantially lower. The ^{3}H atmospheric values compiled from the GNIP stations of Jakarta (Indonesia) and Quezon (Philippines) (IAEA 2017) cover the period from 1962 to 2010 (**Figure 5. 6. a**). This ^{3}H dataset is used here to guide the age interpretation of the groundwater samples from Pasuruan. In this study, we use the ^{3}H tracer only as a qualitative indication of the relative groundwater age in terms of being recharged prior or post atomic bomb tests.

Groundwater sampling for ^{3}H analysis was performed without air bubbles in 1 L Nalgene bottles (**Figure 5. 5. b**). The analyses were carried out at the Mediterranean Environment Analysis and Agro-Hydrosystems Modelling Laboratory (EMMAH UMR 1114 INRA-UAPV) in Avignon (France) by counting after electrolytic enrichment of water (low level liquid scintillation). The results are expressed in tritium units (TU).

- Radiocarbon (^{14}C and $\delta\,^{13}C$)

Since the half-life of ^{14}C is 5730 years, measurement of the activity of this nuclide in Dissolved Inorganic Carbon (DIC) allows the dating of groundwater over long periods (Clark and Fritz, 1997). It is possible to determine the age of the groundwater based on the radioactive decay of ^{14}C incorporated into the system during recharge and assuming the evolution of this nuclide within a closed system (Kendall and McDonnell, 1998). ^{14}C activity is expressed as a percentage of modern carbon (pmc), which corresponds to the level of ^{14}C in the atmosphere in 1950, (i.e. 100 pmc). Nuclear tests in the 1950s and 1960s introduced significant amounts of ^{14}C (> 180 pmc) into the atmosphere, thus allowing to assume that groundwaters with ^{14}C activities greater than 100 pmc have been recharged between 1950 and today (Freeze and Cherry, 1979). The calculated ages are expressed in BP (before present), where the age reference is 1950.

During infiltration, water dissolves ^{14}C carbon present in the soil (in the form of CO_2 from the soil and plants). This fraction of dissolved inorganic ^{14}C undergoes radioactive decay without coming into contact with the atmosphere in the saturated zone (closed system), thus allowing to estimate the "apparent age" of the groundwater. However, the abundance of dissolved inorganic ^{14}C in the groundwater can be modified by groundwater interactions with other carbon sources, such as carbonate rocks or deep volcanic CO_2 from geothermal activity (Clark and Fritz, 1997; Singhal and Gupta, 2010). Values of $\delta^{13}C$ DIC are used to identify carbon sources other than soil CO_2 and assess their impact on the abundance of ^{14}C in groundwater (mixtures). The $\delta^{13}C$ value is based on the ratio of stable carbon isotopes ($^{13}C/^{12}C$) and normalized to the international VPDB (Vienna Pee Dee Belemnite) reference. The isotopic composition of $\delta^{13}C$ is representative of the carbon sources that interact with groundwater. Therefore, $\delta^{13}C$ is a good indicator for identifying and quantifying water-rock interactions.

There are several processes that can introduce old ^{14}C-free carbon into groundwater,

including the dissolution of carbonate minerals, isotopic exchange with carbonates, oxidation of old organic matter and input of CO_2 from volcanic gases. These processes can lead to a decrease of the ^{14}C activity in groundwater, which induces an artificial overestimate in the age of the groundwater (Cartwright et al., 2017). However, as these processes are mainly related to marine carbonate rocks, they are assumed to be less important in volcanic contexts (Custodio, 2004). Nevertheless, before interpretation of the results, we check for the potential influence of water-rock interactions and the presence of deep volcanic CO_2, that could lead to an overestimation of the estimated age. The uncorrected 14C age results are given as an indication of whether the water is old or "modern". The results are then discussed considering the evolution $\delta^{13}C$ and other dating tracers.

The waters for the analysis of ^{14}C and $\delta^{13}C$ were sampled in 1.5 L Nalgene bottles (**Figure 5. 5. a**) without air bubbles. The analyses were performed by the Environmental Isotope Laboratory (EIL) of the University of Waterloo (Canada) using the Accelerator Mass Spectrometry (AMS) method. By convention, negative activity is denoted as "Modern".

- Dissolved gases (CFCs and SF_6)

The common chlorofluorocarbons (CFCs) including CFC-11, CFC-12 and CFC-113, are a suite of anthropogenic halogenated alkanes developed in the 1930s and used as aerosols, coolants and solvents (Cartwright et al., 2017). Due to their impact on ozone concentrations in the atmosphere, the use of CFCs has been progressively banned by both developed (2000) and developing countries (2010) under the Montreal Protocol (Plummer et al., 2000).

Since the 1940s, the atmospheric concentration of CFCs has increased and stabilized, but only started to decline in the late 1990s (**Figure 5. 6. c**). Because the ratios between the CFCs are different today from those observed during the 1980s and 1990s, when atmospheric CFC concentrations were increasing, it is still possible to use CFCs to determine groundwater residence times and recharge rates. Current estimates of the atmospheric lifetimes of CFC-11, CFC-12, and CFC-113 are 45 ± 7, 87 ± 17, and 100 ± 32 years (Volk et al., 1997). The long residence times result in uniform distributions of atmospheric CFCs in both the northern and southern hemispheres. Due to initial source-term concentrations at different dates, CFC-11, CFC-12 and CC-113 can be used to date groundwaters from 1947, 1941 and 1955, respectively, for flow without any mixing (Plummer et al., 2000). The principle of the method is to convert the dissolved gas concentration measured in groundwater into atmospheric partial pressure using Henry's Law. This equivalent partial pressure is then compared with existing atmospheric records to infer the date of recharge. Since the dissolution coefficient (K_H) depends on temperature, salinity and pressure, this methodology is dependent on recharge conditions. (Appelo and Postma, 2004; Cartwright et al., 2017). Several processes can affect the estimation of the gas age: such as excess air (entrapment of air contained in the unsaturated zone during variations of piezometric level), temperature conditions affecting the solubility of gases but also microbial activity (degradation) and adsorption (IAEA, 2008; Plummer et al., 2000). The recharge temperature and excess air can be characterized from the noble gases dissolved in water, thus explaining the systematic sampling.

Sulphur hexafluoride (SF_6) is a chemically inert gas used in industrial applications, primarily as an electrical insulator (Cartwright et al., 2017). Anthropogenic activity results in SF_6

emissions to the atmosphere, where this gas remains largely unaffected by degradation processes. The measurement of SF_6 is based on the same principle as the CFCs. The homogeneous distribution of SF_6 in the atmosphere and its long residence time allows to use this gas to estimate groundwater mean residence time up to approximately 60 years under flow conditions without mixing (Appelo and Postma, 2004; Kendall and McDonnell, 1998); SF_6 is considered as a good tracer for dating water from 1970 onwards (**Figure 5. 6. c**). However, SF_6 can be naturally present in groundwaters, particularly in aquifers composed of volcanic rocks associated with hydrothermal fluxes (Healy and Scanlon, 2010; Koh et al., 2007). In such cases, SF_6 can be of limited use for estimating mean residence times (Busenberg and Plummer, 2008).

The age distribution and mean age of samples are generally presented according to four main conceptual models that represent different configurations of groundwater flow from an inlet (recharge area) to an outlet (a well or spring) of the aquifer. These models are represented mathematically as transit-time distribution functions or exit-age distribution functions [g(t)] (Małoszewski and Zuber, 1982) and are classically distinguished (Jurgens et al., 2012) as follows:

- Piston flow model (PFM): assumes a tracer travels from the inlet position (recharge area) to the outlet position (a well or spring, for example) without hydrodynamic dispersion or mixing.

- Exponential mixing model (EMM): considers homogeneous unconfined aquifers of constant thickness receiving uniform recharge that triggers vertical stratification of groundwater age, which increases logarithmically from zero at the water table to ages that approach infinity at the base of the aquifer.

- Exponential piston-flow model (EPM): used to describe an aquifer that has two segments of flow in series: a segment of exponential flow followed by a segment of piston-flow.

- Dispersion model (DM): is based on a solution to a one-dimensional advection dispersion equation for a semi-infinite medium with instantaneous injection and detection of the tracer in the fluid flux.

Binary mixing models (BMM) can be created by combining the previous models.

The groundwater samples were collected without air bubbles under pressure, using hermetically closed steel vials (**Figure 5. 5. b**) to avoid contamination by atmospheric contact. In the same way, noble gases were sampled without air bubbles in hermetically sealed 0.5 L glass vials (**Figure 5. 5. a, b**) with a replicate for each water point. The analyses were performed by the Condate platform of UMR 6118 - Géosciences Rennes (France) using Gas chromatography with electron-capture detection (GC-ECD) for CFCs and SF_6, and with a TCD detector for noble gases (μGC-TCD). The results are expressed in pptv for CFCs and SF_6 and in mol/L for noble gases.

All groundwater samples (for hydrogeochemical, isotopic and dissolved gases analysis) were kept cold for a few weeks in Indonesia before shipping to their respective laboratories.

Groundwater mean residence times obtained from this multi-tracer study are compared with the first estimated transit times for the Pasuruan plain presented in *Chapter 4* (section 4.4.4). This comparison of ages estimated by different methods helps to support the discussion aimed at identifying the most realistic conceptual model (PFM, EMM, and EPM) at the scale of the Bromo-Tengger aquifer.

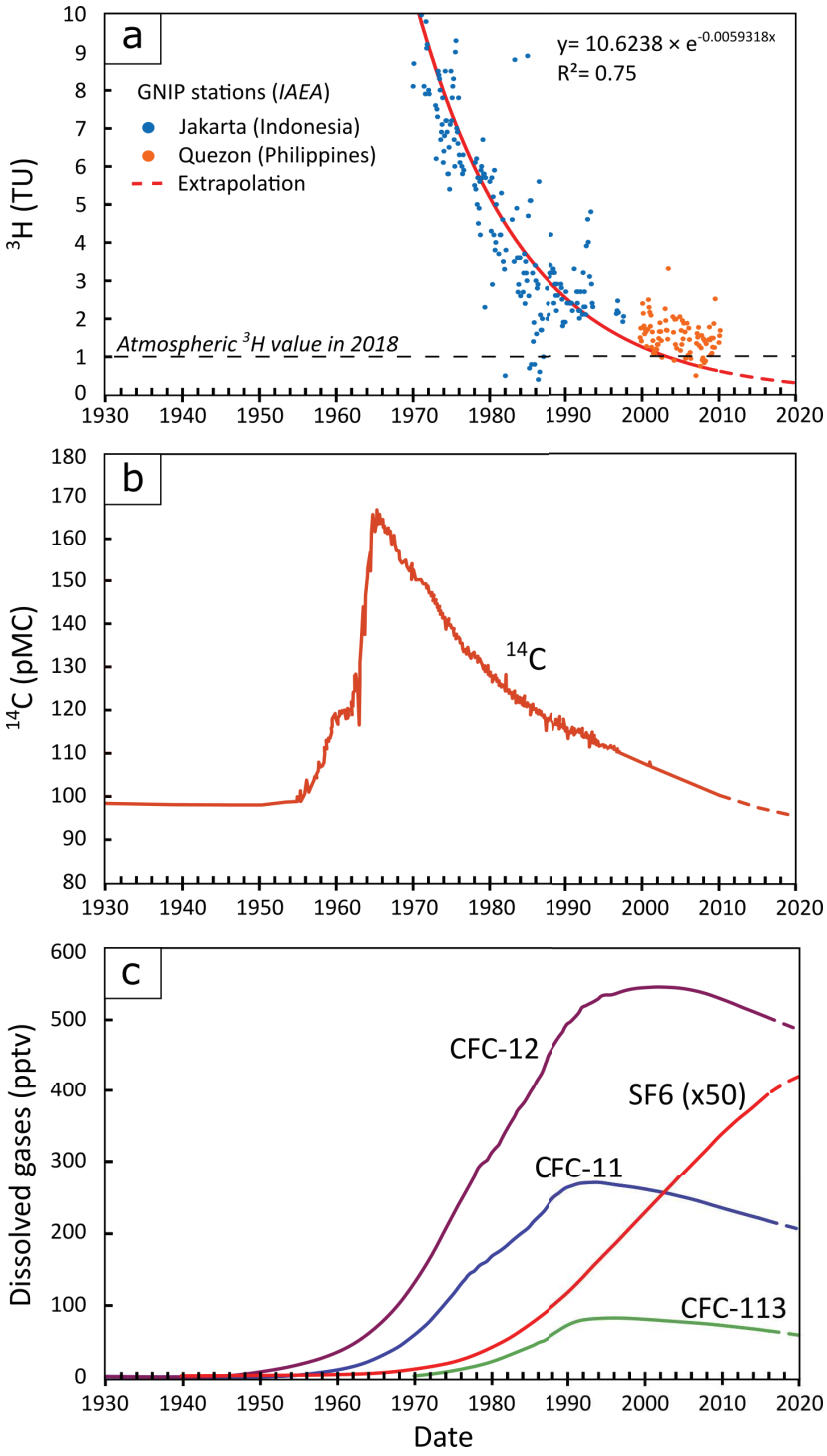

Figure 5. 6. Variation of atmospheric concentrations of the different tracers used to estimate groundwater age, interpolated to 2020. **a.** ^{3}H atmospheric concentrations provided by the GNIP stations at Quezon (Philippines) and Jakarta (Indonesia), (IAEA, 2017). **b.** ^{14}C atmospheric concentrations (IAEA, 2017) and **c.** atmospheric concentrations of dissolved gases (USGS, 2018).

5.3 Results

5.3.1 Groundwater flow modeling

5.3.1.1 Model calibration

More than 50 trial-and-error steady state flow simulations were performed to obtain the best calibration between simulated and measured heads and discharges.
During the calibration process, several parameters were tested such as the hydraulic conductivity of the geological layers, the specified head imposed at the artesian springs, the flow constraint of leakage of the confining unit as well as the recharge rate at the scale of the volcano.
The results are presented in **Figure 5. 7** and illustrated in **Figure 5. 8**.

Calibration (n° 53)	RMSE (m)	Correlation coefficient (r)	Scaled RMSE (%)
Hydraulic head of the Pasuruan plain	6.2	0.84	14.76

Calibration (n° 53)	Specified head (m.a.s.l.)	Simulated discharge (m^3 s^{-1})
Umbulan spring	32.10	2.206 (70% of measured)
Banyu Biru spring	28.47	0.224 (100% of meaured)

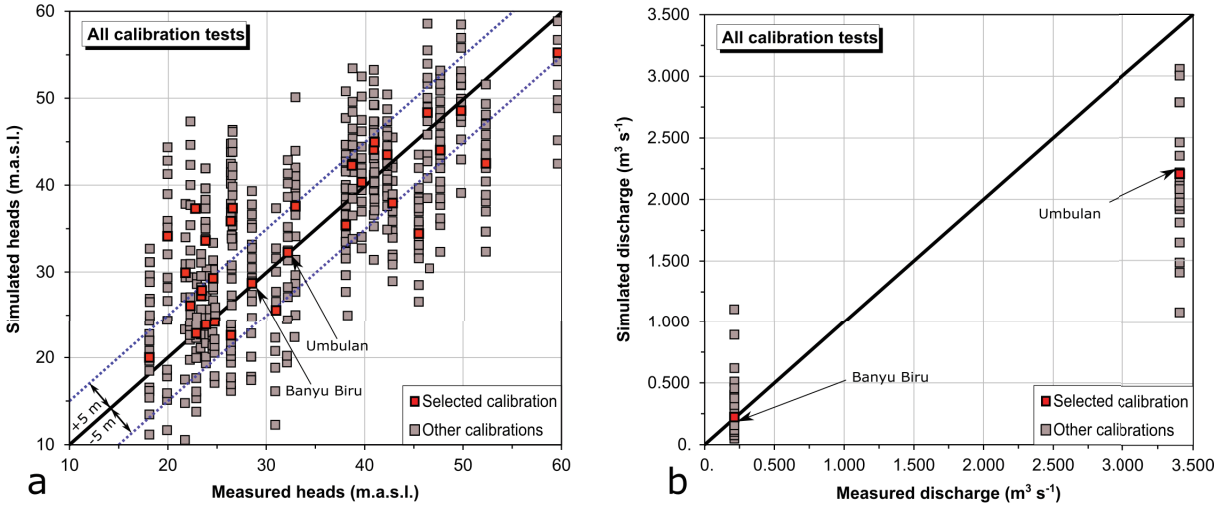

Figure 5. 7. Calibration performance of the groundwater flow model in the Pasuruan plain zone with **a.** the hydraulic head calibration results and **b.** the spring's discharge calibration results

Calibration n° 53 was selected as the one that best represents the steady-state model in 2018. For this purpose, the distributed recharge at the volcano scale was reduced by a factor of 1.68 (18.445 m^3 s^{-1}), representing 60% of the initial recharge based on the maximum limits of the system (see *Chapter 3*, section 3.4.5) The leakage of the confining unit is adjusted so the simulated hydraulic head fits the observed values. These adjustments are discussed further below in this chapter. The calibration results are assessed according to the following criteria:

- The hydraulic heads of the Pasuruan plain (**Figure 5. 7. a**) are considered as correctly simulated for a confidence interval of +/- 5 m of measured head (blue line). This confidence interval corresponds to about 12% of the upstream to downstream hydraulic head variation (42 m) across the volcano-sedimentary plain. We find a RMSE of 6.2 m

and a high correlation coefficient (0.84). The SRME is estimated at about 15%. The calibration tends to overestimate the simulated heads in the central part of the Pasuruan plain where artesian wells are denser. Besides, several simulated heads are under-estimated in the south-western part of the study area where artesian wells are deeper. The highest residual error is about 14 m in the south-western part.

The water level measured in the Umbulan basin and Banyu Biru spring are used to define a specified head of respectively 32.10 and 28.47 m.a.s.l. Based on these values, calibration n° 53 allows to simulate a discharge of about 2.2 $m^3 s^{-1}$ at Umbulan spring (i.e. 70% of measured discharge) and 0.224 $m^3 s^{-1}$ (100 % of measured discharge) at Banyu Biru spring

5.3.1.2 Present-day flow conditions (in 2018)

Figure 5. 8 shows the results of the first steady-state groundwater flow model aimed at simulating the actual (2018) groundwater flow circulation, along with the impact of abstraction from free-flowing wells. For this model, the imposed groundwater abstraction rate corresponds to the value estimated in 2018 (2.4 $m^3 s^{-1}$), as provided by the artesian wells inventory. A 2D map view of slice 3 showing the hydraulic head distribution is illustrated in **Figure 5. 8. a**. **The** details of the water budget are reported in **Figure 5. 8. b**. A 2D vertical cross-section with the piezometric level and a conceptual representation of the water budget is shown in **Figure 5. 8. c**. The results are presented according to the following criteria:

- Conceptual direction (**Figure 5. 8. a**): the simulated heads are in agreement with the SW-NE flow direction based on the piezometric map drawn up in *Chapter* 4. The gradient on the plain is relatively weak (e.g. ≈ 0.001 in the West) while there is a stronger gradient (≈ 0.01) towards the central part of the volcano. This gradient decreases towards the North. The groundwater flows seem slightly influenced by the discharge at Umbulan, as expressed by a small depression cone.

- Piezometric level (**Figure 5. 8. c**): the piezometric level over a wide part of the volcano flanks remains rather low (≈ 400 m.a.s.l.), leading to the formation of an unsaturated zone more than 1000 m thick. Hydraulic heads in the downstream part are higher than the topographic level, which is consistent with the extent of the artesian area across the volcano-sedimentary plain.

- Magnitude of groundwater fluxes (**Figure 5. 8. b, c**): based on the calibrated recharge rate (18.445 $m^3 s^{-1}$) applied on the northern flank of the volcano, the total outflow is divided into:
  - 13% from artesian springs
  - 3% from the Ranu Grati maar
  - 61% through upward leakage from the confining unit to the unconfined aquifer
  - 10% flowing within the unconfined aquifer due to infiltration downstream from the volcano flanks

- 13% from the free-flowing artesian wells.

This water budget does not consider infiltration from rainfall on the plain or re-infiltration of outflows from the artesian wells.

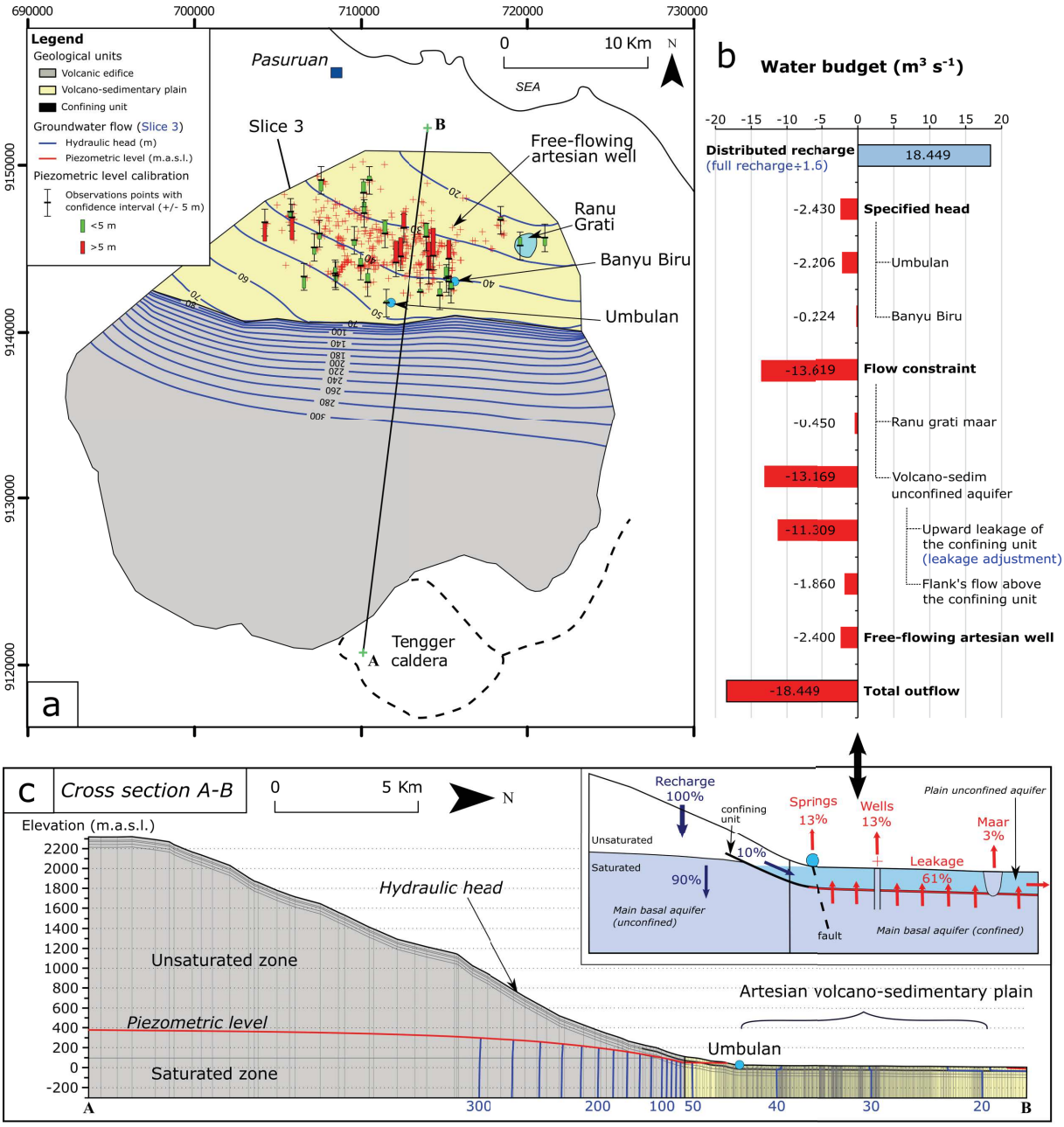

Figure 5. 8. a. 2D map view (slice 3) of the model in steady state in 2018, **b.** water budget results and **c.** 2D vertical cross-section of the model along the conceptual schema of the water budget.

Supplementary results are provided in **Appendix 10**, which presents the distribution of hydraulic head in the top layer. The results are consistent with the shallow unconfined aquifer observed on the plain, where the hydraulic heads are almost coincident with the topography.

5.3.1.3 Natural flow conditions (in 1980)

A second steady state simulation was run as a first approach to define the pre-development artesian conditions. This simulation is based on the previous calibrated steady state (2018) but without free-flowing artesian well as expected in 1980. The expected discharge in Umbulan spring is supposed to reach about 5 m^3 s^{-1}, according the discharge trend previously presented in **Fig 5. 3**. The natural flow condition model is illustrated below in **Figure 5. 9**.

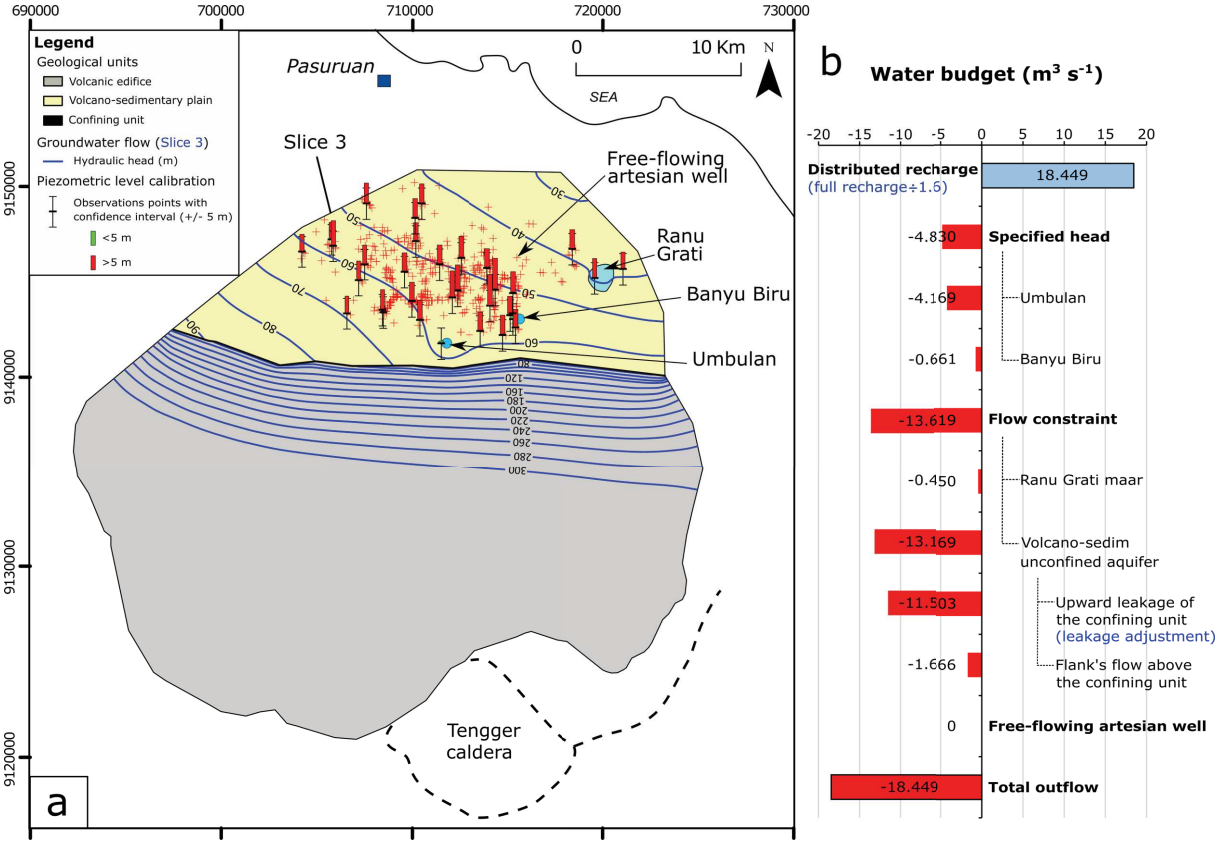

Figure 5. 9. Natural flow conditions model in 1980 with **a.** the hydraulic head distribution in slice 3, **b.** the associated water budget.

The model results show that the hydraulic heads display the same pattern as in 2018, but with higher values. On the plain, the heads are about 15 m higher and no significant change is visible within the volcanic massif. The simulated discharge at Umbulan reaches 4.2 m^3 s^{-1}, which corresponds to 86% of the expected discharge estimated at 4.9 m^3 s^{-1} in 1980 (**Figure 5. 3**). The Banyu Biru spring reaches a discharge of 0.661 m^3 s^{-1}, which corresponds to about 200% of the initial discharge measured in 2018. a large depression cone is visible surrounding Umbulan spring, consistent with the higher discharge rate. Another much smaller cone is observed at Ranu Grati.

In terms of water budget, except for the spring discharge, all the other flow rates are the same. It is noted that the upward leakage increases slightly to 0.194 m^3 s^{-1}.

5.3.2 Groundwater age dating results

5.3.2.1 Radioactive isotopes

The isotopic results of ^{3}H and $^{14}C/^{13}C$ are reported in **Figure 5. 11** and hydrochemical results are summarized in **Appendix 12**.

- Tritium concentrations:

Tritium concentrations are below the limits of detection in most of the water samples from the volcano-sedimentary plain of Pasuruan (**Figure 5. 11**). This may indicate infiltration before atomic tests (pre-1950). However, several artesian wells (FD1, BenbyAlix, West Umbulan) and artesian spring (Umbulan) located in the piedmont area show tritium concentrations ranging from 0.6 to 0.9, which is about the expected level of current atmospheric concentrations (< 1 TU; **Figure 5. 6. a**). These results can be explained by two hypotheses:

1) Groundwater infiltrated prior to the 1950s atomic tests. The measured ^{3}H values thus indicate the background level of the aquifer.

2) Groundwater either comes from a recent recharge with a short transit time or reflects a signal with a memory effect related to infiltration after atomic tests (post-1950).

At this stage, the use of tritium concentrations alone is not discriminant enough to characterize the groundwater residence time.

- $^{14}C/^{13}C$ concentrations:

The ^{14}C activity renormalized to -25‰ using provided $\delta^{13}C$ values is ranging from 71 to 110 pmC (**Figure 5. 11**). As a first approach, no specific ^{14}C correction is applied since there is no predominant source of carbon in this volcanic context and there is no identifiable influence from marine carbonate rocks (negative saturation index of HCO_3^-; **Appendix 12**). In addition, no hydrothermal influence can be identified on the water chemistry related to deep volcanic CO_2 (negative saturation index of CO_2; **Appendix 12**). There is no clear increase in hydrothermal signature associated with sulphur or chlorides, in agreement with the absence of hot springs in the study area. Accordingly, we observe:

- The inferred mean age ranges from “modern” for three groundwater points in the piedmont area (Umbulan, FD1 and Banyu Biru), to about 2 800 years BP (BH54 bis) for the groundwater points located on the volcano-sedimentary plain of Pasuruan. The mean groundwater age increases progressively from the piedmont area towards the North of the Pasuruan plain, which is consistent with the flow directions indicated by the piezometric map.

- East of the plain (P13 and Wates Tani 2), the mean groundwater ages are young (184 and 365 years BP, respectively) and do not correspond to the groundwater age distribution of the remaining study area.

- The $\delta^{13}C$ values progressively increase northward across the plain, from -19‰ (Umbulan) to -14‰ (BH54 bis), while ^{14}C decreases from 108 to 84 pmC for the same

points (**Figure 5. 10. a, b.**). The extrapolation of the trend between the values of $\delta^{13}C$ versus ^{14}C (**Figure 5. 10. c**), allows to define the end-member that influences the C isotopes in the system. The $\delta^{13}C$ value -2.5‰ found for 14C= 0 pmC could correspond to the input of magmatic CO_2. This value is consistent with $\delta^{13}C$ values for high-temperature volcanic gases in subduction zone settings (Genereux et al., 2009) such as in Indonesia, where values are generally around -3‰ (Poorter et al., 1991). This magmatic CO_2 input is discussed further below in this Chapter.

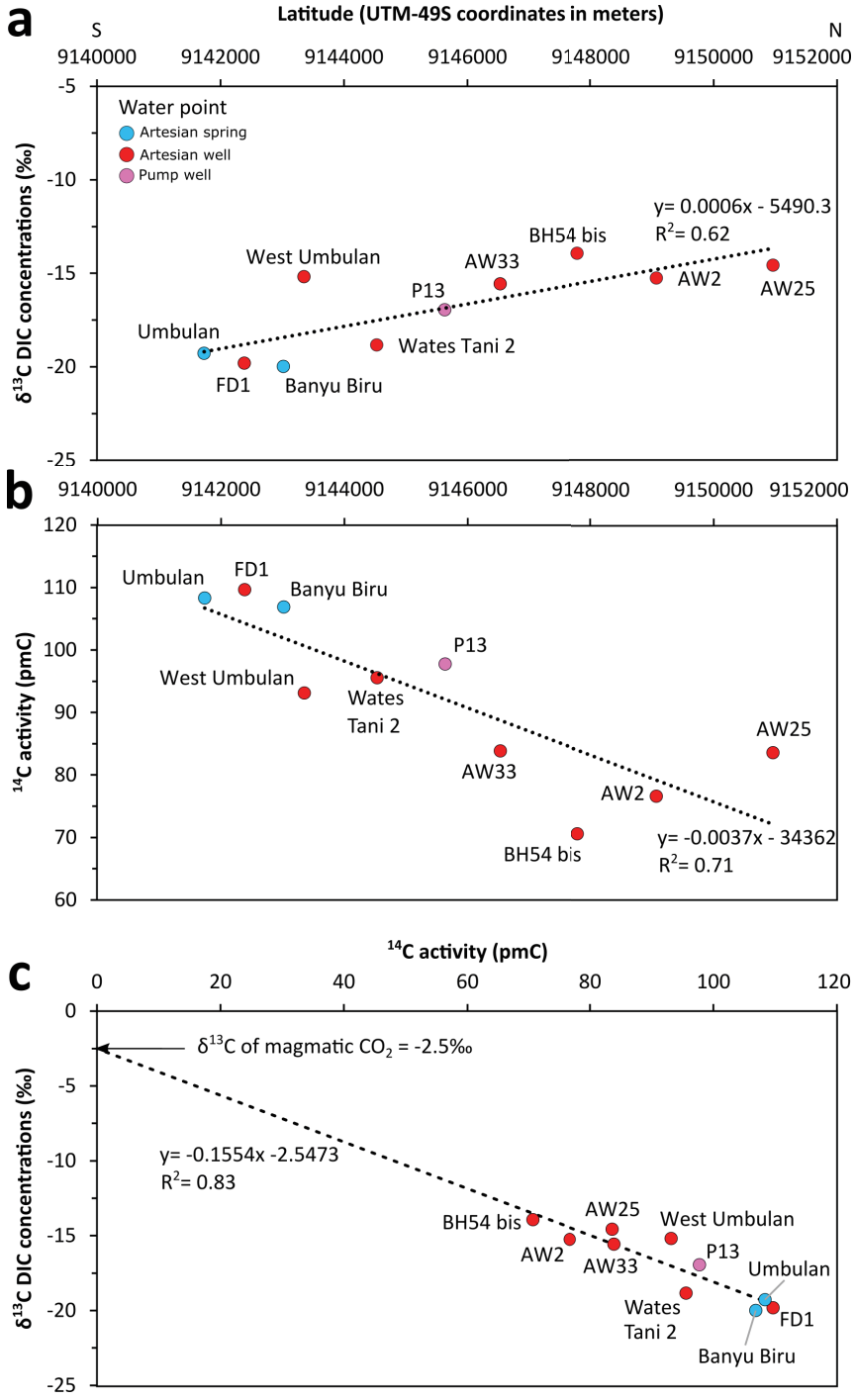

Figure 5. 10. a Values of $\delta^{13}C$ versus latitude, **b.** Values of ^{14}C versus latitude and c. Values of $\delta^{13}C$ versus ^{14}C. The intercept at $^{14}C = 0$ provides an estimate of the $\delta^{13}C$ of magmatic CO_2 (-2.5%).

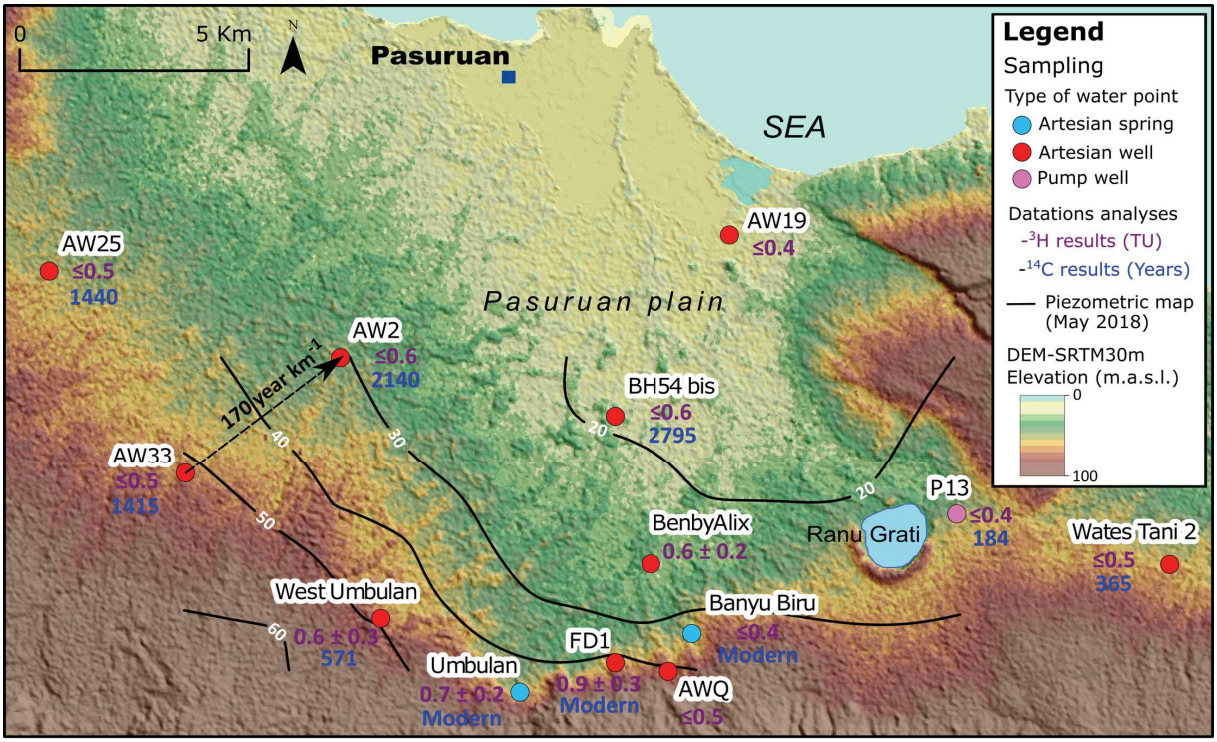

n°	Name	Type	Depth	Datation results - Radioactive isotopes					
				^{3}H	$\delta^{13}C$ DIC	^{14}C		Renormalized Age	
		(AS, PW, AW)	(m)	(UT)	*PDB ± 0.2‰*	pmC	±	year BP	±
1	Banyu Biru	Artesian spring	-	≤0.4	-19.99	106.86	0.32	Modern	-
2	P13	Pump well	30	≤0.4	-16.95	97.73	0.30	184	25
3	AW19	Artesian well	16	≤0.4	-	-	-	-	-
4	Wates Tani 2	Artesian well	?	≤0.5	-18.84	95.56	0.35	365	30
5	BH54 bis	Artesian well	>100	≤0.6	-13.94	70.61	0.26	2795	29
6	AWQ	Artesian well	60	≤0.5	-	-	-	-	-
7	FD1	Artesian well	110	0.9 ± 0.3	-19.81	109.64	0.31	Modern	-
8	BenbyAlix	Artesian well	63	0.6 ± 0.2	-	-	-	-	-
9	Umbulan	Artesian spring	-	0.7 ± 0.2	-19.28	108.32	0.34	Modern	-
10	AW2	Artesian well	93	≤0.6	-15.26	76.61	0.26	2140	27
11	West Umbulan	Artesian well	133	0.6 ± 0.3	-15.19	93.14	0.28	571	24
12	AW33	Artesian well	200	≤0.5	-15.56	*83.85*	0.29	1415	28
13	AW25	Artesian well	>100	≤0.5	-14.58	83.59	0.30	1440	29

Figure 5. 11. Tritium and ^{14}C dating results for the plain of Pasuruan

5.3.2.2 Dissolved gases

The results indicate significant concentrations of CFCs and SF_6, with the following values (**Figure 5. 12**):

- SF_6 ranging from 1 and 3 pptv
- CFC-12 ranging from 80 and 360 pptv
- CFC-11 ranging from 20 and 230 pptv
- CFC-113 ranging from 10 and 50 pptv.

As the groundwater point FD1 yields anomalous values of SF_6, CFC-12, CFC-11 (> maximum atmospheric concentrations), it is not used for the interpretation. In the same way, we do not consider the groundwater point PW13 that shows an anomalous value of CFC-12 (interference during the analysis).

The atmospheric concentrations calculated during the recharge period are based on an average recharge altitude of 1000 m.a.s.l. and a recharge temperature of about 21°C, as highlighted in *Chapter 3*.

The results are particularly well illustrated in **Figure 5. 12** on graphs **b.** (SF_6 vs. CFC-12) and **c.** (SF_6 vs. CFC-11) in. Two main groups can be distinguished:

- Samples from the piedmont area (Umbulan, Banyu Biru and West Umbulan), which spread out between an exponential model and an exponential-piston model.

- The other water samples from the volcano-sedimentary plain, which are aligned according to an exponential model.

Sample AW2 and to a lesser extent Wates Tani 2 are also close to a mixing model.

Based on the flow models previously described, the groundwater points in the "Piedmont area" (Umbulan, Banyu Biru and West Umbulan) show a mean age between 35 and 70 years depending on the flow models considered (Exponential-piston vs. exponential). For example, the Umbulan spring yields a mean age of about 45 years assuming a mix between 60% piston model and 40% exponential model (**Table 5. 3**).
The remaining groundwater points located on the "volcano-sedimentary plain" yield older mean ages ranging from 70 to 250 years assuming an exponential flow model (**Table 5. 3**).

Table 5. 3. Mean age estimation from anthropogenic gases

Groundwater points	Type	Flow models		Model proportion
		Expon.-Piston (year)	Exponential (year)	Piston-Expon. (%)
Piedmont group				
Umbulan	AS	40-50	-	60% PM – 40% EM
Banyu Biru	AS	30-40	40-50	25% PM – 75% EM
West Umbulan	AW	35-50	50-70	30% PM – 70% EM
Volcano-sedimentary plain group				
All groundwater points	AW PW	-	70-250	-

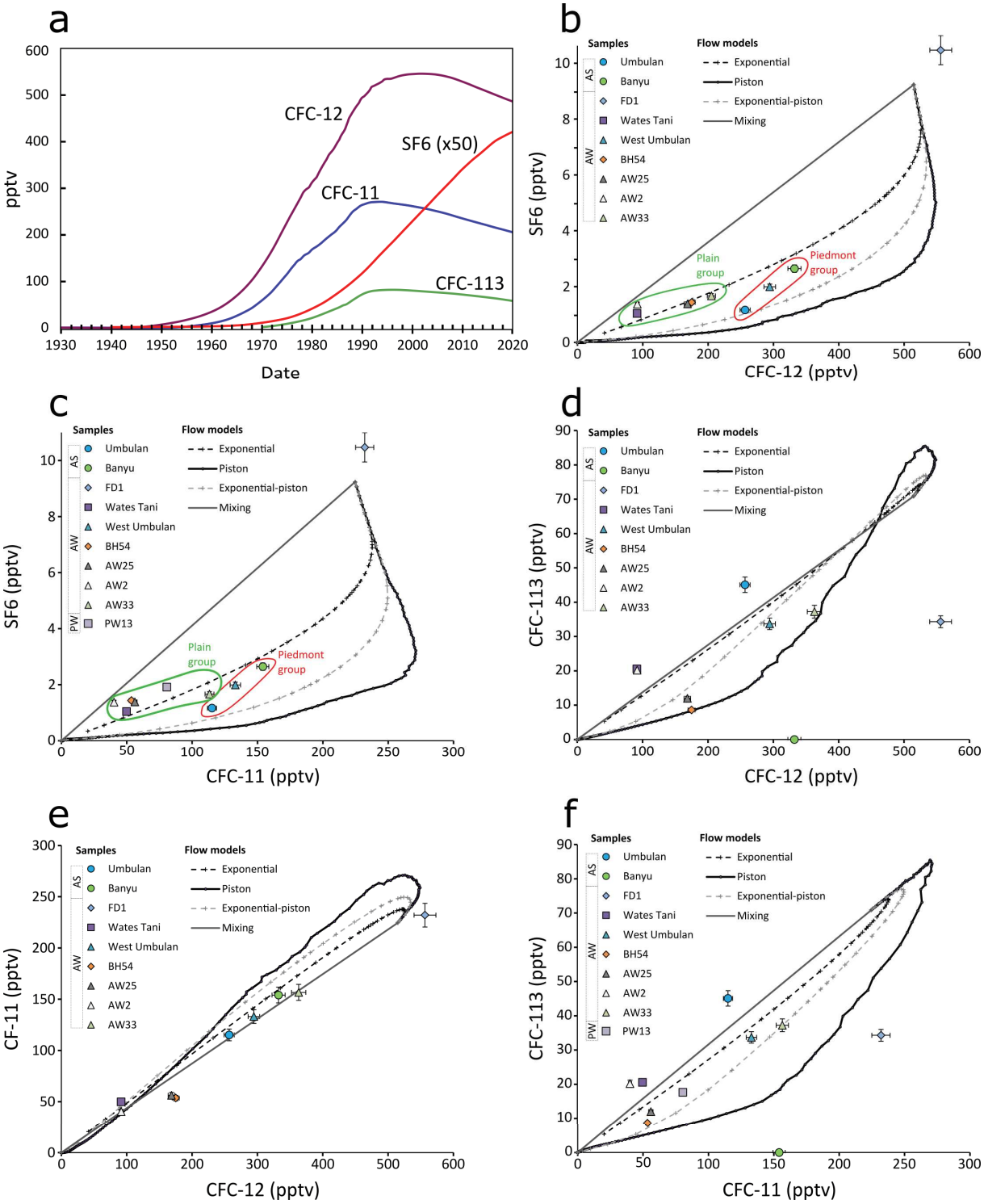

Figure 5. 12. a. Variation in atmospheric concentrations of CFCs and SF_6. **b. c. d.** and **e.** The results of CFCs and SF_6 concentration in groundwater samples according the main flow models.

5.4 Discussion

5.4.1 Groundwater flow modeling

5.4.1.1 Conceptual model

The results of the numerical model are consistent with the conceptual model proposed in *Chapter 3*. Indeed, the steady-state model representative of groundwater flows in 2018 suggests a low-lying basal aquifer within the volcanic edifice (about 400 masl) with a thick unsaturated zone about 1700 m below the caldera floor. Therefore, it is possible to consider a network of perched aquifers at the top of this unsaturated zone. Besides, the extension of artesian conditions across the downstream volcano-sedimentary plain is coherent with field observations since these conditions extend over the whole Pasuruan plain, with piezometric heads located at 1 to 10 m above the ground surface.

5.4.1.2 Calibration

The calibration phase leads to adopt simulation n°53 as the most realistic model. The latter considers a 40% decrease of the initial estimated recharge, which could be explained by a lateral variation in precipitation (rainfall amount unknown in the western and eastern part of the study area). The presence of an impervious layer preventing infiltration, such as the large lahar deposits observed in the eastern part of the volcanic edifice (Madakaripura Valley, section 3.4.1) might also induce a lower recharge in the eastern part of the recharge area. On the contrary, the Nongkojajar caldera in the West could correspond to a preferential recharge area, as suggested in *Chapter 4*. This zone shows a surface drainage network that is much less developed than in the remaining part of the volcanic edifice (see section 1.5.1), suggesting higher infiltration rates in this area. Note that this assumption is consistent with the piezometric map of the plain that shows a groundwater flow direction from SW to NE (section 4.4.3).

The adjustment of the hydraulic head by changing the outflow rate from the unconfined aquifer on the plain was carried out by increasing the upward leakage of the confining unit. Although this leakage of about 11 m^3 s^{-1} is large, it is consistent with the availability of this groundwater resource used for private water supply. There is a very high density of dug wells observed on the Pasuruan plain, particularly in the North. Indeed, almost every house in the city of Pasuruan has its own dug well, mainly used for domestic needs. However, the orders of magnitude of flows must be considered with caution in compare to the simplifications that have been done for this first numerical model (see in section 5.4.1.4).

In terms of calibration parameters, most of the wells where the simulated heads are over or underestimated correspond to wells with high uncertainty with regards to the initial measurement (section 4.4.2). Without these calibration points, the performance of the model would increase, with a RMSE of about 3.3 m, a correlation coefficient of 0.95 and a scaled RMSE of 7.8%, which is close to the 5% recommended by Anderson and Woessner, (1992).

Considering the groundwater fluxes at the scale of the model domain, as well as the head differences (42 m of variation between the upstream and downstream parts of Pasuruan plain), a RMSE that accounts for a variation of more or less 5 m (simulated-observed) is rather satisfactory as a first reference calibration.

5.4.1.3 Present-day flow conditions

The simulations performed in steady state before and after the drilling of artesian wells, based on data from the 1980s and 2018, respectively, do not show any decline of the artesian conditions in the study area.

We note that the change in discharge at Umbulan (≈4.9 in 1980 compared with 3.2 m^3 s^{-1} in 2018) seems to be correlated with the increase of outflow related to the artesian wells, which is of the same order of magnitude as in 2018 (≈2.4 m^3 s^{-1}). Besides, the models suggest that the Umbulan discharge has decreased by about 52% (from 4.2 to 2.2 m^3 s^{-1}), while the monitoring data indicate a decrease of about 35% (5 to 3.2 m^3 s^{-1}). At this stage, the discharge difference observed at Umbulan seems to be correlated with the increase of outflow related to the artesian wells, which is of the same order of magnitude as in 2018 (≈2.4 m^3 s^{-1}). Moreover, the continuous piezometric data recorded by the Aqua piezometer between 2017 and 2019 does not seem to indicate any declining trend (**Appendix 7. C. D.**). The measured piezometric oscillations of about 20 to 30 cm seem to be triggered by seasonal recharge processes with cyclic variations. Longer time-series of piezometric data at such artesian wells could reveal the real trend of artesian conditions in Pasuruan. In the same way, continuous discharge monitoring at a representative free-flowing well could be helpful in estimating an eventual declining trend.

5.4.1.4 Model limitations

The numerical groundwater flow model developed in the present study is a simplified representation of the real aquifer. The following limitations and sources of uncertainty should be taken into consideration when examining the model results:

- The errors associated with the geometry, thickness and structure of the domain (volcanic edifice and multilayered volcano-sedimentary plain) are substantially reflected in the groundwater flow model. Volcanic rocks such as lava flows are usually considered as anisotropic in numerical modelling since their horizontal hydraulic conductivity is generally several times greater than the vertical conductivity (Singhal and Gupta, 2010). The multilayered geometry of the volcano-sedimentary plain is not discretized in this model but simplified into a single confining unit. This could explain the low variation of simulated leakage between the steady-state model in 1980 and the former in 2018.

- In term of calibration, it is debatable to consider the surface water basin elevation as representing the imposed specified head at the Umbulan and Banyu Biru artesian springs. In fact, the head value is probably more than the simple outflow elevation. Therefore, some adjustments of the imposed head value could allow to refine the

expected outflow at Umbulan to reach a value of about 3.2 $m^3 s^{-1}$ in 2018. In the same way, the Ranu Grati lake outflow could be simulated as an imposed specified head instead of a simple flow constraint of the mean discharge.

- Finally, even if there is no indication of submarine outflows, this possibility cannot be completely excluded as it is frequently mentioned in volcanic contexts (Custodio, 2007; Heilweil et al., 2012; Nichols et al., 1996), and other outflows, such as the continuous large releases of water vapour from the Mt. Bromo crater, could also be considered. A complementary inventory of artesian wells in the west could allow to determine the total artesian well outflow of the Bromo-Tengger aquifer.

- The non-uniqueness of the solution arises when different parameter sets lead to an equally good performance of the model in terms of calibration. This aspect was already discussed in *Chapter 3*. The manual trial-and-error calibration carried out here does not overcome this problem. However, to address this issue, it could be interesting to solve the inverse problem, which consists of constraining the model parameters with the available observation data (Aster et al., 2005). The inverse problem could be solved using an mathematical parameter estimation approach such as the Gauss Levemberg Marqart Algorithm (GLMA), which is a non-linear Newton method for parameter estimation, implemented, for example, in PEST (Doherty, 2010). Mathematical parameter estimation should be coupled with regularization methods (Tikhonov regularization and/or singular value decomposition (SVD)) that would guide us towards a "well-posed" problem to improve the inversion of groundwater models (Doherty and Skahill, 2006).

- As a perspective, the natural flow conditions before the exploitation of artesian wells (pre-1980) could be obtained using a transient flow model constrained with the evolution of discharge at the artesian wells since the 1980s. In this way, we could assess the evolution of the discharge at Umbulan from 1980 to 2018, and compare this with the recharge monitored over the last ten years.

5.4.2 Identification of conceptual models for groundwater flow

The results of the age dating analyses reveal two main groundwater groups probably corresponding to different flow systems.

The first group corresponds to groundwater sampled at the foot of the Bromo-Tengger volcano, near the northernmost outcrops of lava flows from the volcanic edifice. These groundwater samples represent the “piedmont group”, and show mean residence times that can be considered as “modern”:

1) Artesian springs: Umbulan and Banyu Biru springs show ^{3}H and ^{14}C concentrations indicating "modern" groundwater and ages estimated from dissolved gases (CFCS and SF_6) ranging from 35 to 50 years, depending on the considered flow model. Considering an Exponential-piston model (EPM) for Umbulan and an Exponential mixing model (EMM) for Banyu Biru, we obtain a similar mean groundwater age of about 45 years. These results are consistent with the physico-chemical monitoring carried out at the springs since 2017, which shows very stable temperature and electrical conductivity, suggesting transit times long enough to explain an inertial system. In addition, the fault identified in *Chapter 2* could explain the influence of an Exponential-piston flow model in the case of the Umbulan spring.

2) Artesian wells: groundwaters sampled in the wells from the piedmont area yield scattered values of residence time. For well FD1, consistent tritium concentration (0.9 TU) and ^{14}C results indicate the presence of "modern" groundwater. Unfortunately, gas contamination at this water point prevents a more precise determination of the mean groundwater age. In contrast, the West Umbulan water point shows inconsistent results from the various age tracers. Indeed, measurable ^{3}H values (0.6 UT) and dissolved gases (CFCS and SF_6) indicate a maximum age of about 70 years according to an exponential mixing model (EMM), thus suggesting modern groundwater, while the ^{14}C data suggest an age of about 600 years.

The second group of groundwater samples corresponds to the “volcano-sedimentary plain group” which show longer groundwater residence times than those obtained for the piedmont group. Two types of groundwater can be distinguished:

1) Artesian wells: with the exception of the BenbyAlix water point, ^{3}H concentrations measured at wells are below the analytical detection limit, which is consistent with the groundwater ages derived from ^{14}C, highlighting a mean residence time ranging from 200 to 2800 years. On the contrary, analysis of the dissolved gases suggests younger groundwater ages, with residence time ranging between 70 and 250 years according to an exponential mixing model (EMM).

2) Pump well: the water point PW13 is a shallow well which is supposed to extract groundwater from the unconfined aquifer. Considering the relatively shallow depth of

this well, it could easily be influenced by "modern" surface water. However, the tritium concentration is below the detection limit, which is in agreement with the mean age of 180 years obtained from ^{14}C dating. This relatively old apparent age might result from mixing between deep and shallow groundwaters due to upward leakage within the confining unit (artesian aquifer?).

At this stage, two hypotheses can explain the apparent discrepancy between age tracers on the Pasuruan plain.

- Hypothesis 1: The recurrent presence of anthropogenic gases in the groundwater samples constrains to consider a mixing of water with a proportion of recent recharge. Thus, groundwaters on the plain would result from the mixing between ≈50% young groundwater similar to the piedmont group (mean residence time of ≈ 50 years according to exponential model) and older groundwater formed about 4000 years BP (**Figure 5. 12. b**). This mixing would lead to an apparent mean residence time of 2000 years as determined by ^{14}C. In this case, the $\delta^{13}C$ increase observed on the plain could result from fractionation processes during plagioclase alteration (Clark and Fritz, 1997).

- Hypothesis 2: The relatively old ^{14}C mean residence time measured on the plain (≈ 2000 years) could be overestimated due to the input of dead carbon from magmatic CO_2 (^{14}C= 0 pmC) as suggested by the observed $\delta^{13}C$ increase on the plain. For example, a first rough estimation shows that the enriched $\delta^{13}C$ value from well BH54 bis could result from the input of 26% of magmatic CO_2. The corrected mean residence time would be about 230 years BP, in better accordance with the gas mean residence time.

In any case, the age distribution with older ages on the plain is consistent with the piezometric map, which suggests an increase in transit times towards the North of the plain. However, there is a difference with the effective velocities previously calculated for the plain, on the basis of the piezometric map (see section 4.4.4). These effective velocities were previously estimated at about 40 m y^{-1} corresponding to relatively good flow conditions (with a porosity of 0.3 and $K_{mean} \approx 10^{-4}$ m s^{-1}). However, based on the same flow line and considering a Piston flow model (PFM) between wells AW33 and AW25 (**Figure 5. 13**), the ^{14}C results would suggest a lower effective velocity of about 6 m y^{-1}. This indicates that either a higher effective porosity should be considered (0.57), which however seems to be overestimated, or that the PFM model is not consistent with groundwater flow circulation on the plain.
Considering the depth difference between wells AW33 and AW25, (200 m and 93 m, respectively), it may be inappropriate to consider the PFM model.

To conclude, it is necessary to perform further analysis of the water dating results through (i) calculation of lumped parameter models including ^{3}H data or (ii) Netpath ^{14}C modelling to specify the most robust hypothesis to be considered for further interpretations. In addition, more information is required about ^{13}C fractionation processes during silicate alteration.

Conceptually, it is already possible to consider two types of groundwater flow in the Bromo-Tengger aquifer system (**Figure 5. 13**):

- An exponential flow system uniformly receiving recharge along the whole northern flank of the volcano, with groundwater flowing within the volcanic edifice and then into the volcano-sedimentary plain. This flow model represents the main artesian wells on the volcano-sedimentary plain. The deepest wells, and those furthest from the volcano, are assumed to show the oldest mean ages (up to 250 years or 4000 years, respectively, depending on the hypothesis considered). A thick unsaturated zone combined with a slow vertical flow could favour a longer residence time.

- Exponential-piston flow involving lateral downslope flow within lava units, feeding water points such as the artesian springs in piedmont areas. Indeed, the layered anisotropic character of the volcanic rocks (Custodio, 2007; Singhal and Gupta, 2010) could favour inter-flow circulation, inducing faster flow and therefore younger mean ages (between 35 and 50 years). The strong trend towards a piston flow model for some points (e.g. Umbulan) could be related to the fault described in *Chapter 2*.

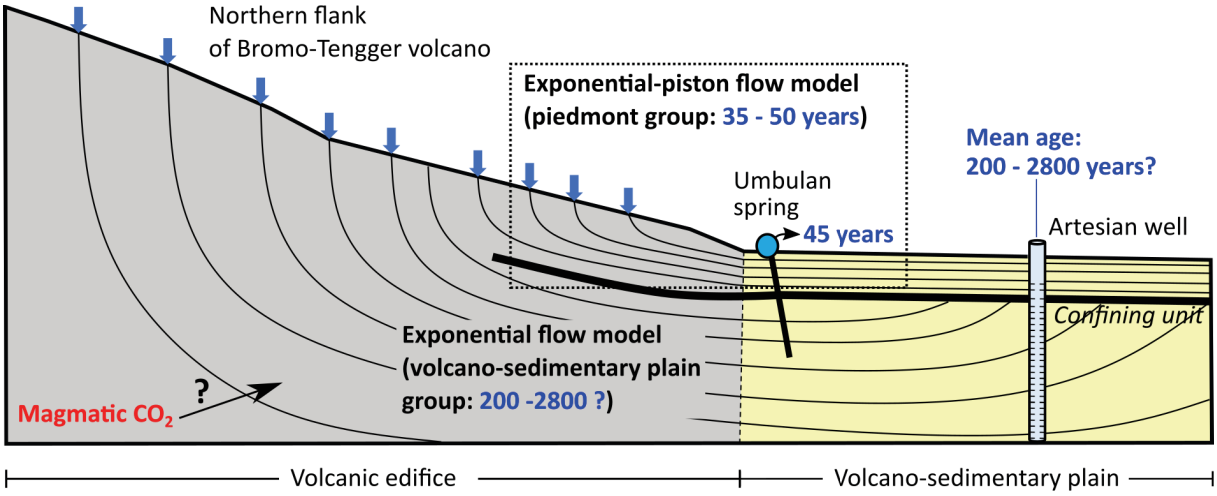

Figure 5. 13. Conceptual models for groundwater flow paths in the Bromo-Tengger aquifer system.

In a similar context, the Caribbean coastal plain at the foot of Volcano Brava, in Costa Rica, is characterized by a mixing of two hydrogeochemically distinct groundwaters with (1) deep bedrock groundwater receiving recharge along the flanks in upland areas, with mean ages of 2400 to 4000 years, influenced by magmatic CO_2 and, (2) local groundwater recharged locally in the lowlands, with the presence of dissolved gases (CFCs and SF6) and a mean age younger than 55 years (Genereux et al., 2009; Solomon et al., 2010). In the above case, bedrock groundwater is much older than local groundwater: the high solute load of bedrock groundwater is related to its subsurface residence time in volcanic rock, and local groundwater has no significant interaction with volcanic rock. Among the different mixing models, an exponential distribution of groundwater travel times (EMM) would lead to mean residence times that range from less than 10 years to more than 1000 years.

This above conceptual model could be in agreement with the model necessary to explain the groundwater ages measured in the Bromo-Tengger aquifer system. Therefore, a more detailed analysis of the ^{14}C and dissolved gases results should be carried out to investigate the potential influence of magmatic CO_2 on groundwater age dating.

5.5 Conclusion

Results from the numerical modeling presented here are consistent with the conceptual model proposed in *Chapter 3*. The latter model implies a decrease of about 40% in the initial estimated recharge (i.e. recharge of about 18.5 m^3 s^{-1}). This model also involves a significant amount of upward leakage through the confining unit, yielding flows which could partially supply the unconfined aquifer of the Pasuruan plain. The steady-state flow model representative of hydrogeological functioning in 2018 shows a low-lying basal aquifer within the volcanic massif and an artesian basin extending across the whole Pasuruan plain. The significant decrease of discharge at Umbulan spring since the 1980s can be explained by increased discharge related to the outflow of artesian wells onto the plain, which is of the same order of magnitude as the decline in outflow observed at Umbulan (≈2 m^3 s^{-1}). However, since long-term piezometric data are not available, it is not possible to assess the evolution of artesian conditions on the Pasuruan volcano-sedimentary plain.

The age dating results from the downstream flanks of the volcano allow to highlight two main flow systems:

- The first flow system corresponds to groundwater sampled at the base of the volcanic edifice. The groundwater circulation probably occurs through lateral downslope flow in lavas units, resulting in relatively long transit times (between 35 and 50 years). The groundwater flows can be explained according to an exponential-piston model which gives a mean age of about 45 years at the Umbulan artesian spring.

- The second flow system correspond to groundwater showing older mean ages, which were sampled on the volcano-sedimentary plain. The groundwater flows can be explained by an exponential model or other mixing models. However, the age results differ according to whether the results are obtained from dissolved gases or ^{14}C, with respective maximum ages of 200 and 2800 years. Two hypotheses are proposed: (i) a binary mixing model with 50% of water coming from recent recharge (≈ 50 years BP) and 50% of older groundwater (≈ 4000 years BP), and (ii) an exponential mixing model with the influence of magmatic CO_2 requiring an age correction of ^{14}C results that may lead to a mean residence time of about 250 years BP in better accord with the gas results.

Transient simulations based on the evolution of discharge at artesian wells since the 1980s should be carried out to assess the trend in discharge at Umbulan over the last ten years. In the same way, future scenarios may lead to anticipate the over-exploitation of groundwater resources in Pasuruan. Complementary monitoring should be carried out at free-flowing artesian wells to record piezometric head and discharge trend, which could be used to assess the trend in artesian conditions on the Pasuruan plain.

Further analyses will be carried out to determine whether or not there is any influence from magmatic CO_2 requiring a ^{14}C age correction. In parallel, an advanced study through lumped parameter models should refine the mean ages derived from the analysis of dissolved gases.

Conclusion

Conclusion and Perspectives

Conclusion

This thesis aims to improve the hydrogeological knowledge of aquifers developed in tropical climates on stratovolcanoes including a summit caldera and a downstream artesian volcano-sedimentary plain.

This type of setting is shown by the Bromo-Tengger volcano (located in East Java, Indonesia), which provides the object of the case study presented in this thesis. Over the past few decades, this volcano has become a tourist attraction known for its sunrises over the Sand Sea caldera. However, besides being a famous touristic site, this volcano also represents a strategic resource of regional importance owing to its high aquifer potential, which is now impacted by increasing anthropogenic pressures.

This thesis aims to improve the knowledge of the Bromo-Tengger volcano aquifer system, which up to now has been only poorly studied. Particular attention is paid to the northern flank and downstream plain of the volcano, where most of outflow occurs through major artesian springs and free-flowing artesian wells.

To attain this objective, a multidisciplinary approach is applied at the scale of the volcano's northern flank. This approach not only combines geological and geophysical data from field investigations, hydro-climatological data from a new monitoring network, hydrogeochemical and isotopic analyses, but also hydraulic tests and piezometric mapping, supplemented by a first groundwater flow model. Each groundwater point inventoried during this thesis project is incorporated into a new database.

The insights derived from each discipline are used to i) characterize the structure and geometry of the volcanic edifice and its coastal volcano-sedimentary plain, ii) quantify the inputs and outputs of the water budget and propose a first hydrogeological conceptual model at the scale of the volcano's northern flank, iii) characterize the groundwater flow circulation and model at the scale of the whole aquifer system. The main results of this thesis can be summarized in the five points presented below.

Structure and geometry

The geological and geomorphological surveys enable to refine the structure and the architecture of deposits on the northern flank of Bromo-Tengger. The previous geological map (Santosa et al., 1992; Zaennudin et al., 1994) is updated and a first conceptual geological model is used to explain the artesian conditions of the Pasuruan Plain. Volcanic formations are heterogeneous and make up complex structures, especially on the volcano-sedimentary plain at the foot of the volcanic massif, where stream networks give rise to intense remobilization and lateral variations of volcanoclastics. The artesian aquifer is mainly hosted within reworked coarse-grained volcanic sands, while cemented layers such as pyroclastic breccias and lahar deposits control a complex multilayered configuration. Lava flows can either act as aquitards related to weathered clayey boulders and non-fractured massive formations, or favour enhanced

groundwater flow through the fresh and fractured massive lavas associated with highly porous autoclastic breccias. In spite of the paleochannels observed in the field, there is no evidence that these act as a preferential groundwater flow paths since artesian conditions are homogeneously developed over the entire Pasuruan plain.

The geometry of the artesian aquifer on the volcano-sedimentary plain is probably bounded by local tectonic features in the north associated with clayey distal deposits near the coast. Low-permeability ignimbrites delimit the eastern part of aquifer, while the western limit is still unknown since artesian wells are identified at the base of the Arjuno volcano. The artesian aquifer reaches an estimated depth of about 300 m in agreement with the literature and the drilling survey on the Pasuruan Plain. The whole Pasuruan Plain hosts an unconfined aquifer associated with an impermeable/semi-permeable pyroclastic cap that is about 30 m thick. This shallow geological unit provides groundwater for the Pasuruan population through numerous dug wells. This area and its relationship with the underlying artesian aquifer are still not clearly defined, but upward leakage may probably occur. Complementary geophysical surveys show that the existence of a conductive fault is the most reliable hypothesis to explain the outflow context of artesian springs in the Bromo-Tengger volcanic piedmonts, which is in agreement with the regional tectonic setting.

Recharge estimation

Based on the new hydro-climatological monitoring, the input parameters of the water budget at the scale of the volcano's northern flank have been defined over a representative hydrological year (2017-2018). Recharge occurs over the entire northern flank of the volcano within the massive fractured lava flows series and the upstream pyroclastic complex. New insights from quantitative modeling combining water budget calculations and isotopic analyses suggest that 80% of the recharge occurs between 150 and 1450 m.a.s.l. The recharge is mainly controlled by the spatial distribution of rainfall, which is strongly impacted by seasonal and elevation effects. A significant rainfall gradient can be observed and reaches 4000 mm $year^{-1}$ at 1200 m.a.s.l., 79 to 91% of which occurring during the wet season. The water budget estimation on a representative watershed indicates high effective rainfall infiltration: of about 90.5% (i.e. 66% of rainfall).

Based on the quantitative modeling, the extrapolated volume of the whole northern flank including half of the caldera (540 km^2) is estimated at approximately 980 million m^3 (i.e. 1800 mm y^{-1}) over the studied hydrological year 2017-2018. This value must be very carefully taken into consideration since it is based on the maximum hypothetical East-West limits of the hydrogeological system and assumes there is no lateral variation of the recharge rate along the northern volcano profile. Even if the caldera summit represents a large endoreic zone, its contribution to recharge is very limited compared to the flank. Complementary data such as groundwater temperature and hydrochemical analyses confirm that recharge occurs at high elevations. However, the lateral extent of the recharge remains to be defined, especially regarding the contribution to this recharge area from the old caldera of Nongkojajar in the South-West, where the lower density of the stream network suggests a high infiltration of rainfall.

Hydrogeological conceptual model

Convergence of evidences from the different approaches enabled to propose a first hydrogeological conceptual model. The Bromo-Tengger complex aquifer comprises two distinct but linked hydrogeological systems:

- The upstream part of the aquifer within the volcano, where the host aquifer rock is composed of andesitic lava flows series topped with a pyroclastic series. These formations, which are geologically complex in detail, appear homogeneous and permeable at the scale of the whole volcano. They host perched aquifers that are either independent or connected to each other, and characterized by low discharge gravity springs (more than 50 inventoried). Groundwater transit time is generally close to the time scale of the hydrological year, being easily impacted by surface contamination. Part of the infiltration over the volcano flank penetrates downwards through a thick unsaturated zone (> 1000 m) and supplies the main low-lying basal aquifer of the volcano. The latter provides groundwater to high-discharge artesian springs (such as Umbulan) and to the volcano-sedimentary aquifer located on the downstream Pasuruan plain.

- The downstream part of the aquifer, corresponding to a multilayer volcano-sedimentary artesian aquifer with high productivity provides groundwater to numerous free-flowing artesian wells (approximately 600 in 2018) on the Pasuruan Plain. The hydrochemical analyses indicate good-quality groundwater with low mineralization and free from any bacterial contamination as expected from the confining conditions. The volcanic edifice associated with the multilayered system seems to be an efficient filter against chemical pollutants. In addition, the confining unit on the plain and its upward leakage component prevent potential surface contamination on the plain from reaching the deep artesian aquifer. Nevertheless, considering that the main recharge occurs at high elevation, the pollution observed in the upstream systems could represent a long-term risk of contamination in the future. In 2018, the total outflow from the Bromo-Tengger complex aquifer towards artesian springs and free flowing wells on the plain is estimated at about 6500 L s^{-1}.

Groundwater flow characterization

Using a new hydraulic test device, the hydrodynamic survey allows to assess the hydrodynamic properties and hydraulic heads at the scale of the Pasuruan artesian plain:

- The volcano-sedimentary confined aquifer is permeable ($K_{mean} \approx 10^{-4}$ m s^{-1}) and shows a local hydraulic conductivity anomaly probably linked to more permeable volcanic materials derived from the collapse of the Nongkojajar caldera.

- Based on the 2018 piezometric mapping, the main groundwater flow direction is from Southwest to Northeast. This result is consistent with the increase in mineralization, temperature and water ages towards the North. It also supports the hypothesis of a preferential groundwater flow path related to the Nongkojajar caldera. A groundwater age gradient of 2 to 25 y km^{-1} can be inferred from the low hydraulic gradient (≈0.001) of the artesian basin,

assuming a piston flow model. This represents a good water flow circulation, clearly influenced by the depression cone developed by the numerous free-flowing artesian wells. In fact, this abstraction from wells remains a major regional issue since no regulations has been enacted to prevent groundwater waste. In addition, the depletion of artesian conditions caused by the increase of free-flowing artesian wells could favour downward vertical transfer from surface pollution to the deep artesian aquifers.

As a first modeling approach, simulations were conducted in 3D and 2D vertical cross sections, in steady-state flow conditions using all the new hydrogeological data acquired during this thesis. The modelling aims to validate the previous conceptual model simulating the groundwater flow in agreement with the proposed piezometric map and the spring discharge measurements in 2018. The calibration phase leads to reconsider the recharge rate of the hydrosystem as well as estimate a higher leakage through the confining unit towards the unconfined aquifer of the Pasuruan plain.

- The initial recharge rate (66% of rainfall), based on the maximum hypothetical hydrogeological limit of the system, is reduced by 40% (18. 5 m^3 s^{-1}) and the initial leakage increased to 11 m^3 s^{-1}. Despite the orders of magnitude of flows must be considered with caution in compare to the model simplifications, this calibration allows to reproduce a realistic distribution of hydraulic heads and representative values for spring discharge, in agreement with the measurements performed in 2018. This first model is consistent with the previous conceptual model. The latter suggests a low-lying basal aquifer (up to 400 m.a.s.l.), with a thick unsaturated zone over the volcanic edifice and artesian conditions developed in the downstream volcano-sedimentary formations of the Pasuruan Plain.

- Considering this first model as a representative "steady state," and imposing a zero flux at the artesian wells, we can simulate the natural conditions in 1980 when the discharge of the Umbulan spring was probably about 5 m^3 s^{-1}.

Groundwater residence time

The age dating analyses performed in the downstream part of the volcano make it possible to highlight two main flow systems:

- The first system is represented by groundwater circulation occurring through lateral downslope flow in lavas units, resulting in relatively fast transit times (between 35 and 50 years). The groundwater flows are mainly consistent with an exponential-piston model (EPM), and correspond to groundwater sampled at the foot of the volcanic edifice (e.g. Umbulan).

- The second system is represented by groundwaters sampled on the volcano-sedimentary plain, which yield older mean ages. The groundwater flows are mainly consistent with an exponential mixing model (EMM). However, different age results are obtained from the dissolved gases and from ^{14}C, with maximum ages of 200 and 2

800 years, respectively. Two hypotheses are proposed: (i) a mixing of recent and older waters, (ii) an overestimated ^{14}C mean age influenced by the input of deep magmatic CO_2. Further analyses should allow to identify the most reliable hypothesis.

Perspectives

Scientific

Several aspects of the hydrogeology of the Bromo-Tengger aquifer system are addressed in this thesis. However, the results obtained raise additional questions that remain unanswered. In the following, we propose a non-exhaustive list of further studies that could significantly improve the global understanding of the aquifer system:

- Maintaining the hydro-climatological monitoring network on the northern flank of the volcano. First, it is a priority to use the current instrumentation to collect long-term records of physico-chemical and discharge parameters at the Umbulan and Banyu Biru springs. This monitoring could help clarify the hydrodynamic behavior of these subsystems, such as the decreasing discharge trend, and allow to anticipate the consequences of lower groundwater availability in the future if confirmed by the data. Continuous physico-chemical monitoring could be used as a preliminary indicator related to pollution observed in the upstream part of the volcano. Based on the acquired records, a hydrodynamic study including rainfall-discharge analysis could improve the understanding of the functioning of such a complex stratovolcano system, which has so far hardly been addressed in the literature.
  In addition, long-term records from weather stations could help characterize the influence of climate change on the groundwater resource as well as the impact of phenomena such as El Niño on the recharge of recurrent atmospheric circulation in Java. It would also be interesting to pursue monitoring of the piezometric level at Aqua for long-term piezometric data. However, the continuous monitoring of discharge and piezometric head at free-flowing artesian wells (about 100 m depth) would be more representative of the current artesian condition.

- A new piezometric campaign based on the same water points as those used in this thesis should be performed to assess the evolution trend of artesian conditions.

- The study of the negative thermal anomaly observed on the artesian volcano-sedimentary plain of Pasuruan would be an interesting scientific topic for further research. Such thermal tracers are still being improved for recharge assessment, and a large amount of field data collected in the Bromo-Tengger system could be used in such an approach, until now scarcely used in a volcanic context.

- Complementary well logging (e.g. gamma-ray, resistivity) and camera investigations could improve the understanding of the multilayered structure of the volcano-sedimentary plain as well as the lithologies accounting for the confining conditions.

- An additional inventory of groundwater points would define more precisely the total outflow of the plain, especially towards the West where deep free-flowing artesian wells (200 m depth) are identified. It would be interesting to define the water divide between the aquifer of Bromo-Tengger and the aquifer of the Arjuno volcano in the West. A supplementary drilling survey would confirm the absence of artesian aquifers east of the Ranu Grati maar.

- A further groundwater age dating study, taking account of diverse conceptual flow models (e.g. piston, exponential, dispersion) with a lumped parameter model using ^{3}H and ^{14}C atmospheric input functions, could help refine groundwater flow circulation and better characterize groundwater residence times. In addition, ^{14}C models should be used to investigate the potential influence of magmatic CO_2 on groundwater age dating.

- Finally, efforts could be focused on groundwater flow modeling in a transient state. The calibration should be based on the discharge evolution of the free-flowing artesian wells and the decreasing discharge trend of Umbulan spring over the years. Then, numerical simulations would offer future scenarios of the artesian conditions in response to increased exploitation of artesian wells. Simulations with unsaturated flow (Richards equation) could allow to estimate the infiltration transfer time through the thick vadose zone, and this transport simulation could be calibrated on the age dating data acquired in this thesis.

Sustainable water management

Recent conservation actions have been carried out to preserve the quality and quantity of the water resource. These actions are supported by the Rejoso Kita project, a collaborative initiative grouping together various socio-environmental organizations. A sustainable tree planting project in the upstream part of the volcano was initiated by ICRAF (the World Agroforestry Centre). Further downstream, on the Pasuruan Plain, efforts are focused on improving the productivity of rice cropping using a rice variety that requires less water. A prototype of the closing valve system for free-flowing artesian wells is currently being designed by Danone Ecosystem Foundation and is expected to be installed on numerous abandoned but still flowing artesian wells. Such conservation actions must be encouraged and further discussion with the government will contribute to increasing awareness of the groundwater issue of the Bromo-Tengger aquifer system.

In this perspective, the transfer of technology to local organizations has already started. The monitoring of weather stations should be continued by the Bromo-Tengger-Semeru National Park (TNBTS) and the Badan meteorologi dan klimatologi (BMKG) in Malang. The spring monitoring should come under the responsibility of the local water supply company (PDAM Pasuruan). The long-term time-series data should be used as a guideline for current and further sustainable water abstraction projects.

Collaborations

The international collaboration between the University of Gadjah Mada (Indonesia), the University of Montpellier (France) and the local industrial partnership (Danone Aqua Indonesia) enabled to organize a field course every year focused on an introduction to volcanic hydrogeology. Through these field courses, professionals and students are able to discover hydrogeological investigation tools as well as raise awareness about social and environmental issues related to groundwater resources in this type of volcanic environment.
Such collaborations should continue, as Indonesian professionals trained through these courses will take the lead and manage sustainable water projects in the future.



Group photo of the second international hydrogeology field course organized in Pasuruan in April 2019

References

References

Abidin, H.Z., Andreas, H., Gamal, M., Hendrasto, M., Suganda, O.K., Purbawinata, M.A., Meilano, I., Kimata, F., 2004. The Deformation of Bromo Volcano (Indonesia) as Detected by GPS Surveys Method. J. Glob. Position. Syst. 3, 16–24. https://doi.org/10.5081/jgps.3.1.16

Abram, N.J., McGregor, H. V., Gagan, M.K., Hantoro, W.S., Suwargadi, B.W., 2009. Oscillations in the southern extent of the Indo-Pacific Warm Pool during the mid-Holocene. Quat. Sci. Rev. 28, 2794–2803. https://doi.org/10.1016/j.quascirev.2009.07.006

Aiuppa, A., Bani, P., Moussallam, Y., Di Napoli, R., Allard, P., Gunawan, H., Hendrasto, M., Tamburello, G., 2015. First determination of magma-derived gas emissions from Bromo volcano, eastern Java (Indonesia). J. Volcanol. Geotherm. Res. 304, 206–213. https://doi.org/10.1016/j.jvolgeores.2015.09.008

Aldrian, E., Dwi Susanto, R., 2003. Identification of three dominant rainfall regions within Indonesia and their relationship to sea surface temperature. Int. J. Climatol. 23, 1435–1452. https://doi.org/10.1002/joc.950

Amaruzaman, S., Khasanah, N., Tanika, L., Dwiyanti, E., Lusiana, B., Leimona, B., Janudianto;, 2018. Landscape characteristics of Rejoso Watershed: land cover dynamics, farming systems and community strategies. Bogor, Indonesia: World Agroforestry.

Anderson, M.., Woessner, W.., 1992. Applied groundwater modeling: simulation of flow and advective transport. Gulf Professional Publishing.

Appelo, C.A.J., Postma, D., 2004. Geochemistry, Groundwater and Pollution, 2n edition. ed. CRC Press, London. https://doi.org/10.1201/9781439833544

Ardhana, W., Lunt, P., Burgon, G.E., 1993. The deep amrine sand facies of the Ngrayong formation in the tuban block, East Jav basin. Indones. Pet. Assoc. 117–175.

Ashley, G.M., Goman, M., Hover, V.C., Owen, R.B., Renaut, R.W., Muasya, A.M., 2002. Artesian blister wetlands, a perennial water resource in the semi-arid rift valley of East Africa. Wetlands 22, 686–695. https://doi.org/10.1672/0277-5212(2002)022[0686:ABWAPW]2.0.CO;2

Aster, R.., Borchers, B.., Thurber, C., 2005. Parameter estimation and inverse problems. Elsevier Academic Press : Burlington.

Audebert, M., 2015. Développement d'une méthode de contrainte des modèles hydrodynamiques par une stratégie d'analyse des données géophysiques ERT : Application aux écoulements de lixiviat dans les massifs de déchets. Université Grenoble Alpes. https://doi.org/tel-01228499

Bachri, S., Stötter, J., Monreal, M., Sartohadi, J., 2015. The calamity of eruptions, or an eruption of benefits? Mt. Bromo human-volcano system a case study of an open-risk perception. Nat. Hazards Earth Syst. Sci. 15, 277–290. https://doi.org/10.5194/nhess-15-277-2015

Baltassat, J.M., Mathieu, F., Ambroise, B., Barbet, C., Béon, O., Dewandel, B., Lachassagne, P., Norie, A., Wyns, R., 2015. Méthodologie et résultats d'application de la tomographie électrique de résistivité par courant continu pour l'exploration hydrogéologique des aquifères discontinus en domaine de socle. Vingtièmes journées Tech. du Com. Français d'Hydrogéologie l'Association Int. des Hydrogéologues 5. https://doi.org/10.13140/RG.2.1.1667.6966

Bani, P., Surono, Hendrasto, M., Gunawan, H., Primulyana, S., 2013. Sulfur dioxide emissions from papandayan and bromo, two indonesian volcanoes. Nat. Hazards Earth Syst. Sci. 13, 2399–2407. https://doi.org/10.5194/nhess-13-2399-2013

Berenbrock, C., 1993. Effects of Well Discharges on Hydraulic Heads in and Spring Discharges from the Geothermal Aquifer System in the Bruneau Area, 0wyhee County, Southwestern

Idaho 1–63.
Bertani, R., 2016. Geothermal power generation in the world 2010-2014 update report. Geothermics 60, 31–43. https://doi.org/10.1016/j.geothermics.2015.11.003
Blavoux, B., Lachassagne, P., Henriot, A., Ladouche, B., Marc, V., Beley, J.J., Nicoud, G., Olive, P., 2013. A fifty-year chronicle of tritium data for characterising the functioning of the Evian and Thonon (France) glacial aquifers. J. Hydrol. 494, 116–133. https://doi.org/10.1016/j.jhydrol.2013.04.029
Blyth, F.G.H., 1940. The nomenclature of pyroclastic deposits. Bull. Volcanol. 6, 145–156. https://doi.org/10.1007/BF02994876
BMKG, 2018. Badan Meteorologi Klimatologi Dan Geofisika (BMKG), rainfall dataset 2018. Malang.
Bourdet, D., Ayoub, J.A., Pirard, Y.M., 1983. Use of Pressure Derivative in Well Test Interpretation. SPE Form. Eval. 4, 293–302. https://doi.org/10.2118/12777-pa
Bourlier, P.Y., Lachassagne, P., Desprats, J.F., Gille, E., 2005. Nouveaux éléments sur la structure et le fonctionnement hydrogéologique du plateau basaltique de l'Aubrac (Massif central, France). Première évaluation des potentialités en eau souterraine. Comptes Rendus - Geosci. 337, 663–673. https://doi.org/10.1016/j.crte.2005.01.014
BPS-Statistics Indonesia, 2017. Statistical Yearbook of Indonesia 2017. BPS-Statistics Indones. xl+708. https://doi.org/10.2307/2541047
Breuer, B.A.., Koch, M.., Bardsley, E.W.., 2000. Modeling the feasibility of tapping artesian flow to augment winter baseflows in a hydropower catchment in New Zealand. Water Stud. 7, 325–334.
Busenberg, E., Plummer, L.N., 2008. Dating groundwater with trifluoromethyl sulfurpentafluoride (SF 5CF3), sulfur hexafluoride (SF6), CF 3Cl (CFC-13), and CF2Cl2 (CFC-12). Water Resour. Res. 44. https://doi.org/10.1029/2007WR006150
Cabusson, B., 2012. Formation de caldera par fluage d'un système hydrothermal volcanique. Université Blaise Pascal - Clermond Ferrand.
Caine, J.S., Evans, J.P., Forster, C.B., 1996. Fault zone architecture and permeability structure. Geology 24, 1025–1028. https://doi.org/10.1130/0091-7613(1996)024<1025:FZAAPS>2.3.CO;2
Camacho, A.G., Fernández, J., González, P.J., Rundle, J.B., Prieto, J.F., Arjona, A., 2009. Structural results for La Palma island using 3-D gravity inversion. J. Geophys. Res. Solid Earth 114, 1–12. https://doi.org/10.1029/2008JB005628
Campbell, J., 1913. Artesian Waters of Oahu.
Cartwright, I., Cendón, D., Currell, M., Meredith, K., 2017. A review of radioactive isotopes and other residence time tracers in understanding groundwater recharge: Possibilities, challenges, and limitations. J. Hydrol. 555, 797–811. https://doi.org/10.1016/j.jhydrol.2017.10.053
Caudron, C., Syahbana, D.K., Lecocq, T., Van Hinsberg, V., McCausland, W., Triantafyllou, A., Camelbeeck, T., Bernard, A., Surono, 2015. Kawah Ijen volcanic activity: a review. Bull. Volcanol. 77. https://doi.org/10.1007/s00445-014-0885-8
Charlier, J., 2008. Fonctionnement et modélisation hydrologique d'un petit bassin versant cultivé en milieu volcanique.
Charlier, J.B., Lachassagne, P., Ladouche, B., Cattan, P., Moussa, R., Voltz, M., 2011. Structure and hydrogeological functioning of an insular tropical humid andesitic volcanic watershed: A multi-disciplinary experimental approach. J. Hydrol. 398, 155–170. https://doi.org/10.1016/j.jhydrol.2010.10.006
Chen, J., Wilson, C.R., Famiglietti, J.S., Scanlon, B.R., 2017. Groundwater Storage Monitoring From Space, Comprehensive Remote Sensing. Elsevier. https://doi.org/10.1016/b978-0-12-409548-9.10361-6
Chotin, P., Giret, A., Rampnoux, J.-P., Rasplus, L., Suminta, Priyomarsono, S., 1984. Etude de

la fracturation dans l'île de Java, Indonesie. Bull. la Société Géologique Fr. S7-XXVI, 1325–1333. https://doi.org/10.2113/gssgfbull.S7-XXVI.6.1325
CKNet, 2015. Lampiran data sumur dan mata air di Pasuruan.
Clark, I., Fritz, P., 1997. Environmental isotopes in hydrogeology. CRC Press.
Clarke, A.J., 2014. El Niño Physics and El Niño Predictability. Ann. Rev. Mar. Sci. 6, 79–99. https://doi.org/10.1146/annurev-marine-010213-135026
Clements, B., Hall, R., Smyth, H.R., Cottam, M.A., 2009. Thrusting of a volcanic arc: A new structural model for Java. Pet. Geosci. 15, 159–174. https://doi.org/10.1144/1354-079309-831
Cochrane, J., 2006. Indonesian national parks. Understanding Leisure Users. Ann. Tour. Res. 33, 979–997. https://doi.org/10.1016/j.annals.2006.03.018
Cochrane, J.E., 2003. Ecotourism, conservation and sustainability: a case study of Bromo Tengger Semeru National Park, Indonesia. PQDT - UK Irel.
Cole, J.W., Milner, D.M., Spinks, K.D., 2005. Calderas and caldera structures: A review. Earth-Science Rev. 69, 1–26. https://doi.org/10.1016/j.earscirev.2004.06.004
Cook, P.G., Hatton, T.J., Pidsley, D., Herczeg, A.L., Held, A., O'Grady, A., Eamus, D., 1998. Water balance of a tropical woodland ecosystem, Northern Australia: A combination of micro-meteorological, soil physical and groundwater chemical approaches. J. Hydrol. 210, 161–177. https://doi.org/10.1016/S0022-1694(98)00181-4
Cooper, H.H.J., Jacob, C.E., 1946. A generalized graphical method of evaluating formation constants and summarizing well-field history. Trans. Am. Geophys. Union 14.
Craig, H., 1961. Isotopic Variations in Meteoric Waters. Science (80-.). 133, 1702–1703. https://doi.org/10.1126/science.133.3465.1702
Cruz-Fuentes, T., Heredia, J., Cabrera, M.C., Custodio, E., 2014. Behaviour of a small sedimentary volcanic aquifer receiving irrigation return flows: La Aldea, Gran Canaria, Canary Islands (Spain)Fonctionnement d'un petit aquifère volcano-sédimentaire bénéficiant de l'excédent d'eaux d'irrigation: La Aldea, Grande Cana. Hydrogeol. J. 22, 865–882. https://doi.org/10.1007/s10040-013-1094-9
Cruz, J.V., 2003. Groundwater and volcanoes: Examples from the Azores archipelago. Environ. Geol. 44, 343–355. https://doi.org/10.1007/s00254-003-0769-2
Custodio, E., 2007. Groundwater in volcanic hard rocks, Groundwater in Fractured Rocks. https://doi.org/10.1201/9780203945650.ch5
Custodio, E., 2004. Hydrogeology of Volcanic Rocks. Groundw. Stud. 395–425.
Custodio, E., 1985. Low permeability volcanics in the Canary Islands (Spain).
Custodio, E., Cabrera, M. del C., Poncela, R., Puga, L.O., Skupien, E., del Villar, A., 2016. Groundwater intensive exploitation and mining in Gran Canaria and Tenerife, Canary Islands, Spain: Hydrogeological, environmental, economic and social aspects. Sci. Total Environ. 557–558, 425–437. https://doi.org/10.1016/j.scitotenv.2016.03.038
CVGHM, (Center for Volcanology and Geological Hazard Mitigation), 2010. Laporan penyelidikan 25 pasca bencana letusan gunung api Bromo. Indonesia.
Dahlin, T., Zhou, B., 2006. Multiple-gradient array measurements for multichannel 2D resistivity imaging. Near Surf. Geophys. 4, 113–123. https://doi.org/10.3997/1873-0604.2005037
Dahlin, T., Zhou, B., 2004. A numerical comparison of 2D resistivity imaging with 10 electrode arrays. Geophys. Prospect. 52, 379–398. https://doi.org/10.1111/j.1365-2478.2004.00423.x
Davis, S.N., 1999. Humboldt, Arago, and the temperature of groundwater. Hydrogeol. J. 7, 501–503. https://doi.org/10.1007/s100400050223
De Deckker, P., 2016. The Indo-Pacific Warm Pool: critical to world oceanography and world climate. Geosci. Lett. 3, 20. https://doi.org/10.1186/s40562-016-0054-3
De Genevraye, P., Samuel, L., 1972. Geology of the Kendeng zone (Central & East Java). Proc.

Indones. Pet. Assoc. Annu. Conv. 1st 17–30.
De Marsily, G., 2004. Cours d'hydrogéologie.
De Marsily, G., 1986. Quantitative hydrogeology. Groundwater hydrology for engineers. Academic press.
de Roever, W.P., 1966. Dacitic ignimbrites with upwards increasing compactness near sibolangit (NE Sumatra, Indonesia) and their peculiar hydrology. Bull. Volcanol. 29, 105–111. https://doi.org/10.1007/BF02597147
del Potro, R., Hürlimann, M., 2008. Geotechnical classification and characterisation of materials for stability analyses of large volcanic slopes. Eng. Geol. 98, 1–17. https://doi.org/10.1016/j.enggeo.2007.11.007
Detay, M., Thomas, P., Olivier, D., 2012. Hydrovolcanologie appliquée à la phase hydrothermale. Lave 17–26.
Dewandel, B., Alazard, M., Lachassagne, P., Bailly-Comte, V., Couëffé, R., Grataloup, S., Ladouche, B., Lanini, S., Maréchal, J.C., Wyns, R., 2017. Respective roles of the weathering profile and the tectonic fractures in the structure and functioning of crystalline thermo-mineral carbo-gaseous aquifers. J. Hydrol. 547, 690–707. https://doi.org/10.1016/j.jhydrol.2017.02.028
Diersch, H.-J.G., 2014. FEFLOW: finite element modeling of flow, mass and heat transport in porous and fractured media. Springer Berlin Heidelberg, Berlin, Heidelberg. https://doi.org/10.1007/978-3-642-38739-5
Doherty, J., 2010. PEST, Model-independent parameter estimation, 5th editio. ed. Watermark numerical computing.
Doherty, J., Skahill, B.E., 2006. An advanced regularization methodology for use in watershed model calibration. J. Hydrol. 327, 564–577. https://doi.org/10.1016/j.jhydrol.2005.11.058
Dominguez, C., 2017. Integrated hydrogeological study of San Cristobal Island (Galapagos). Université Pierre et Marie Curie. https://doi.org/https://tel.archives-ouvertes.fr/tel-01431034
Duffield, G.M., Court, H., 2007. AQTESOLV for Windows Version 4.5 User ' s Guide.
Farr, T.G., Rosen, P.A., Caro, E., Crippen, R., Duren, R., Hensley, S., Kobrick, M., Paller, M., Rodriguez, E., Roth, L., Seal, D., Shaffer, S., Shimada, J., Umland, J., Werner, M., Oskin, M., Burbank, D., Alsdorf, D., 2007. The Shuttle Radar Topography Mission. Rev. Geophys. 45, RG2004. https://doi.org/10.1029/2005RG000183
Fetter, C., 1994. Applied hydrogeology, Macmillan. ed.
Flint, L.E., Selker, J.S., 2003. Use of porosity to estimate hydraulic properties of volcanic tuffs. Adv. Water Resour. 26, 561–571. https://doi.org/10.1016/S0309-1708(02)00182-3
Folio, J.L., 2001. Distribution de la perméabilité dans le massif du Piton de la Fournaise : apport à la connaissance du fonctionnement hydrogéologique d'un volcan-bouclier. Unidersité de La Réunion. https://doi.org/https://www.theses.fr/2001LARE0022
Forkasiewicz, J., 1972a. Interprétation des données de pompages d'essai pour l'évaluation des Paramétres Des Aquiféres.
Forkasiewicz, J., 1972b. Interprétation des données de pompages d'essai pour l'évaluation des paramètres aquifères.
Forster, C., Smith, L., 1988. Groundwater flow systems in mountainous terrain: 2. Controlling factors. Water Resour. Res. 24, 1011–1023. https://doi.org/10.1029/WR024i007p01011
Freeze, R.A., Cherry, J.A., 1979. Groundwater. Prentice-Hall. Inc., Englewood Cliffs.
Gat, J.R., 1996. Oxygen and hydrogen isotopes in the hydrologic cycle. Annu. Rev. Earth Planet. Sci. 24, 225–262. https://doi.org/10.1146/annurev.earth.24.1.225
Genereux, D.P., Webb, M., Kip Solomon, D., 2009. Chemical and isotopic signature of old groundwater and magmatic solutes in a Costa Rican rain forest: Evidence from carbon, helium, and chlorine. Water Resour. Res. 45. https://doi.org/10.1029/2008WR007630
Gertisser, R., Keller, J., 2003. Trace element and Sr, Nd, Pb and O isotope variations in

medium-K and high-K volcanic rocks from Merapi Volcano, Central Java, Indonesia: evidence for the. J. Petrol. 44.

Gingerich, S.B., 1999. Estimating transmissivity and storage properties from aquifer tests in the southern Lihue Basin, Kauai, Hawaii. U.S. Geol. Surv. Water-Resources Investig. Rep. 99-4066.

Gingerich, S.B., Oki, D.S., 2000. Ground water in Hawaii. U.S. Geol. Surv. Fact Sheet 126-00 6 p.

Glover, R.E., 1987. Transient Ground Water Hydraulics, Water Resources Publications. Fort Collins.

Gonfiantini, R., Roche, M.., Olivry, J.., Fontes, J.., Zuppi, G., 2001. The altitude effect on the isotopic composition of tropical rains., in: Chem Geol 181. pp. 147–167.

Gottschämmer, E., Surono, I., 2000. Locating tremor and shock sources recorded at Bromo Volcano. J. Volcanol. Geotherm. Res. 101, 199–209. https://doi.org/10.1016/S0377-0273(00)00171-2

Guillet, S., Corona, C., Stoffel, M., Khodri, M., Lavigne, F., Ortega, P., Eckert, N., Sielenou, P.D., Daux, V., Churakova Sidorova, O. V., Davi, N., Edouard, J.L., Zhang, Y., Luckman, B.H., Myglan, V.S., Guiot, J., Beniston, M., Masson-Delmotte, V., Oppenheimer, C., 2017. Climate response to the Samalas volcanic eruption in 1257 revealed by proxy records. Nat. Geosci. 10, 123–128. https://doi.org/10.1038/ngeo2875

Habermehl, M.A., 2001. Hydrogeology and environmental geology of the Great Artesian Basin, Australia. Geol. Soc. Aust. Spec. Publ. 21, 127–143.

Hadi Nugroho, F., Winarni, T., Hayuddin, Z., Suprayetno, J., Rully, F., Muhajir, Kadarusman, A., 2018. The influence of fault and stress contributed on overpressure mechanism for Neogen Formation (Mundu, Wonocolo, Ngrayong) East Java Basin, Indonesia. MATEC Web Conf. 159, 02034. https://doi.org/10.1051/matecconf/201815902034

Hadisantono, R.D., 1990. The Sakapura and other ignimbrites, in the Sapikerep-Sakapura valley and the relationship to caldera formation of Bromo-Tengger volcanic complex, Probolinggo, est Java, Indonesia. Victoria University of Wellington.

Hakim, L., Miyakawa, H., 2013. Plant trees species for restoration program in Ranupani, Bromo Tengger Semeru National Park Indonesia. Biodivers. J. 4, 387–394.

Hall, R., 2002. Cenozoic geological and plate tectonic evolution of SE Asia and the SW Pacific: Computer-based reconstructions, model and animations. J. Asian Earth Sci. 20, 353–431. https://doi.org/10.1016/S1367-9120(01)00069-4

Hamada, J.I., Yamanaka, M.D., Matsumoto, J., Fukao, S., Winarso, P.A., Sribimawati, T., 2002. Spatial and temporal variations of the rainy season over Indonesia and their link to ENSO. J. Meteorol. Soc. Japan 80, 285–310. https://doi.org/10.2151/jmsj.80.285

Hamilton, W.., 1988. Plate tectonics and island arcs, Geological Society of America Bulletin 100.

Hamm, S.Y., Cheong, J.Y., Jang, S., Jung, C.Y., Kim, B.S., 2005. Relationship between transmissivity and specific capacity in the volcanic aquifers of Jeju Island, Korea. J. Hydrol. 310, 111–121. https://doi.org/10.1016/j.jhydrol.2004.12.006

Hantush, M.S., 1959. Nonsteady flow to flowing wells in leaky aquifers. J. Geophys. Res. 64, 1043–1052. https://doi.org/10.1029/jz064i008p01043

Healy, R.W., Scanlon, B.R., 2010. Estimating groundwater recharge. Cambridge University press.

Heilweil, V.M., Healy, R.W., Harris, R.N., 2012. Noble gases and coupled heat/fluid flow modeling for evaluating hydrogeologic conditions of volcanic island aquifers. J. Hydrol. 464–465, 309–327. https://doi.org/10.1016/j.jhydrol.2012.07.019

Heilweil, V.M., Solomon, D.K., Gingerich, S.B., Verstraeten, I.M., 2009. Oxygen , hydrogen , and helium isotopes for investigating groundwater systems of the Cape Verde Islands , West Africa 1157–1174. https://doi.org/10.1007/s10040-009-0434-2

Hemmings, B., Gooddy, D., Whitaker, F., George Darling, W., Jasim, A., Gottsmann, J., 2015a. Groundwater recharge and flow on Montserrat, West Indies: Insights from groundwater dating. J. Hydrol. Reg. Stud. 4, 611–622. https://doi.org/10.1016/j.ejrh.2015.08.003

Hemmings, B., Whitaker, F., Gottsmann, J., Hughes, A., 2015b. Hydrogeology of Montserrat review and new insights. J. Hydrol. Reg. Stud. 3, 1–30. https://doi.org/10.1016/j.ejrh.2014.08.008

Hendon, H.H., 2003. Indonesian Rainfall Variability: Impacts of ENSO and Local Air-Sea Interaction. J. Clim. 16, 1775–1790.

Herrera, C., Custodio, E., 2014. Groundwater flow in a relatively old oceanic volcanic island: The Betancuria area, Fuerteventura Island, Canary Islands, Spain. Sci. Total Environ. 496, 531–550. https://doi.org/10.1016/j.scitotenv.2014.07.063

Herrera, C., Custodio, E., 2008. Conceptual hydrogeological model of volcanic Easter Island (Chile) after chemical and isotopic surveys. Hydrogeol. J. 16, 1329–1348. https://doi.org/10.1007/s10040-008-0316-z

Hildenbrand, A., Gillot, P.Y., Marlin, C., 2008. Geomorphological study of long-term erosion on a tropical volcanic ocean island: Tahiti-Nui (French Polynesia). Geomorphology 93, 460–481. https://doi.org/10.1016/j.geomorph.2007.03.012

Hildenbrand, A., Marlin, C., Conroy, A., Gillot, P., Filly, A., Massault, M., 2005. Isotopic approach of rainfall and groundwater circulation in the volcanic structure of Tahiti-Nui (French Polynesia) 302, 187–208. https://doi.org/10.1016/j.jhydrol.2004.07.006

Hinds, J., Ge, S., Fridrich, C., 1999. Numerical Modeling of perched water under Yucca Mountain, Nevada. Ground Water 37(4), 59.

Hughes, C., Crawford, J., 2012. A new precipitation weighted method for determining the meteoric water line for hydrological applications demonstrated using Australian and global GNIP data, Journal of Hydrology. https://doi.org/10.1016/j.jhydrol.2012.07.029

Hunt, C.., 1996. Geohydrology of the Island of Oahu, Hawaii, U.S. Geological Survey Professional Paper 1412-B. https://doi.org/http://dx.doi.org/10.18632/oncotarget.22814

Husein, S., 2015. Indonesia Universiti Teknologi Petronas - Malaysia " Petroleum and Regional Geology Northeast Java Basin , Indonesia ." Int. Geol. Course Program. 17. https://doi.org/10.13140/RG.2.1.2408.3280

IAEA, 2008. Isotopes de l'environnement dans le cycle hydrologique. https://doi.org/IAEA-TCS-32F

IAEA, 1961. Global Network of Isotopes in Precipitation (GNIP) [WWW Document]. URL http://www-naweb.iaea.org

Inamdar, P., Kumar, D., 1994. On the origin of bole beds in Deccan traps. J. Geol. Soc. India (3), 31–34.

Ingebritsen, S., Scholl, M., 1993. The hydrogeology of Kilauea volcano, Geothermics. https://doi.org/10.1016/0375-6505(93)90003-6

Izquierdo, T., 2014. Conceptual hydrogeological model and aquifer system classification of a small volcanic island (La Gomera; Canary Islands). Catena 114, 119–128. https://doi.org/10.1016/j.catena.2013.11.006

Izquierdo, T., 2011. Hydrogeology of La Gomera (Canary Islands): contributions to conceptual models of volcanic contributions to conceptual mode 237.

Izuka, S.K., Gingerich, S.B., 2003. A thick lens of fresh groundwater in the southern Lihue Basin, Kauai, Hawaii, USA. Hydrogeol. J. 11, 240–248. https://doi.org/10.1007/s10040-002-0233-5

Izuka, S.K., Oki, D.S., Engott, J.A., 2010. Simple method for estimating groundwater recharge on tropical islands. J. Hydrol. 387, 81–89. https://doi.org/10.1016/j.jhydrol.2010.03.034

Jacob, C.E., 1947. Radial flow in a leaky artesian aquifer. Eos, Trans. Am. Geophys. Union 28, 481–484. https://doi.org/10.1029/TR028i003p00481

Jacob, C.E., 1940. On the flow of water in an elastic artesian aquifer. Eos, Trans. Am. Geophys.

Union 21, 574–586. https://doi.org/10.1029/TR021i002p00574
Jacob, C.E., Lohman, S.W., 1952. Nonsteady Flow to a Well Of Constant Drawdown. Am. Geophys. Union 33, 10.
Join, J., Coudray, J., Longworth, K., 1997. Using principal components analysis and Na/Cl ratios to trace groundwater circulation in a volcanic island: the example of Reunion. J. Hydrol. 190, 1–18.
Join, J.L., 1991. Caractérisation hydrogéologique du milieu volcanique insulaire : Piton des Neiges, Île de la Réunion. Universtié de Montpellier 2.
Join, J.L., Folio, J.L., Bourhane, A., Comte, J.C., 2016. Groundwater Resources on Active Basaltic Volcanoes: Conceptual Models from La Réunion Island and Grande Comore. Act. volcanoes Southwest Indian Ocean Pit. la Fournaise Karthala 1–428. https://doi.org/10.1007/978-3-642-31395-0_5
Join, J.L., Folio, J.L., Robineau, B., 2005. Aquifers and groundwater within active shield volcanoes. Evolution of conceptual models in the Piton de la Fournaise volcano. J. Volcanol. Geotherm. Res. 147, 187–201. https://doi.org/10.1016/j.jvolgeores.2005.03.013
Jones, I.C., Banner, J.L., Humphrey, J.D., 2000. Estimating recharge in a tropical karst aquifer, Water Resources Research. https://doi.org/10.1029/1999WR900358
Jurgens, B.C., Böhlke, J.K., Eberts, S.M., Survey, U.S.G., 2012. Tracer LPM (Version 1): An Excel® workbook for interpreting groundwater age distributions from environmental tracer data. Tech. Methods.
Kasenda, A., Komara, A.M., Sutisna, S., 2011. The Indonesian Gravity Field and the Geoid Model. https://doi.org/10.1007/978-3-642-59745-9_51
Kendall, C., McDonnell, J.., 1998. Isotope tracers in catchment hydrology. Elsevier.
Kereszturi, G., Nmeth, K., 2012. Monogenetic Basaltic Volcanoes: Genetic Classification, Growth, Geomorphology and Degradation, in: Updates in Volcanology - New Advances in Understanding Volcanic Systems. InTech. https://doi.org/10.5772/51387
Kiernan, K., Wood, C., Middleton, G., 2003. Aquifer structure and contamination risk in lava flows: Insights from Iceland and Australia. Environ. Geol. 43, 852–865. https://doi.org/10.1007/s00254-002-0707-8
Knapp, K.M., 1988. The Interpolation of Hydraulic Head Contours. Rose-Hulman Undergrad. Math. J. 1.
Knödel, K., Lange, G., Voigt, H.J., 2007. Environmental Geology: Handbook of field methods and cases studies. Springer.
Koh, D.C., Plummer, L.N., Busenberg, E., Kim, Y., 2007. Evidence for terrigenic SF6 in groundwater from basaltic aquifers, Jeju Island, Korea: Implications for groundwater dating. J. Hydrol. 339, 93–104. https://doi.org/10.1016/j.jhydrol.2007.03.011
Kottek, M., Grieser, J., Beck, C., Rudolf, B., Rubel, F., 2006. World Map of the Köppen-Geiger climate classification updated. Meteorol. Zeitschrift 15, 259–263. https://doi.org/10.1127/0941-2948/2006/0130
Koulali, A., McClusky, S., Susilo, S., Leonard, Y., Cummins, P., Tregoning, P., Meilano, I., Efendi, J., Wijanarto, A.B., 2016. The kinematics of crustal deformation in Java from GPS observations: Implications for fault slip partitioning. Earth Planet. Sci. Lett. 458, 69–79. https://doi.org/10.1016/j.epsl.2016.10.039
Kumalasari, R., Srigutomo, W., Djamal, M., 2017. Location and Pressures Change Prediction of Bromo Volcano Magma Chamber Using Inversion Scheme. J. Phys. Conf. Ser. 846. https://doi.org/10.1088/1742-6596/846/1/012002
Kummerow, C., Barnes, W., Kozu, T., Shiue, J., Simpson, J., 1998. The Tropical Rainfall Measuring Mission (TRMM) sensor package. J. Atmos. Ocean. Technol. 15, 809–817. https://doi.org/10.1175/1520-0426(1998)015<0809:TTRMMT>2.0.CO;2
Lachassagne, P., Aunay, B., Frissant, N., Guilbert, M., Malard, A., 2014. High-resolution conceptual hydrogeological model of complex basaltic volcanic islands: A Mayotte,

Comoros, case study. Terra Nov. 26, 307–321. https://doi.org/10.1111/ter.12102
Lachassagne, P., Marechal, J.C., 2011. Les ressources en eau souterraine en contexte volcanique insulaire. Geosciences 42–49.
Legette, R., Taylor, G., 1934. The transmission of pressure in artesian aquifers, U.S. Geological Survey Professional Paper.
Lin, L., 2007. Hydraulic properties of the Table Mountain Group (TMG) aquifers. Faculty of Natural Sciences, University of the Western Cape.
Lohman, S.W., 1965. Geology and artesian water supply, Grand Junction area, Colorado. Geol. Surv. water-supply Pap. 451.
Machard de Gramont, H., Noel, C., Oliver, J.-L., Pennequin, D., Rama, M., Stephan, R.., 2010. Vers une gestion concertée des systèmes aquifères transfrontaliers : guide méthodologique, A Savoir.
Małoszewski, P., Zuber, A., 1982. Determining the turnover time of groundwater systems with the aid of environmental tracers. 1. Models and their applicability. J. Hydrol. 57, 207–231. https://doi.org/10.1016/0022-1694(82)90147-0
Maréchal, J.C., Lachassagne, P., Ladouche, B., Dewandel, B., Lanini, S., Le Strat, P., Petelet-Giraud, E., 2014. Structure and hydrogeochemical functioning of a sparkling Natural mineral water system determined using a multidisciplinary approach: A case study from southern France. Hydrogeol. J. 22, 47–68. https://doi.org/10.1007/s10040-013-1073-1
Margat, J., Pennequin, D., Roux, J.-C., 2013. Histoire de l'hydrogéologie française, Associatio. ed. Orléans.
Marliyani, G.I., 2016. Neotectonics of Java, Indonesia: Crustal Deformation in the Overriding Plate of an Orthogonal Subduction System. Arizona state University.
Marliyani, G.I., Arrowsmith, J.R., Helmi, H., 2019. Evidence for Multiple Ground-Rupturing Earthquakes in the Past 4,000 Years Along the Pasuruan Fault, East Java, Indonesia: Documentation of Active Normal Faulting in the Javan Backarc. Tectonics 38, 1489–1506. https://doi.org/10.1029/2018TC005255
Marrero-Diaz, R., Alcalá, F.J., Pérez, N.M., López, D.L., Melián, G. V., Padrón, E., Padilla, G.D., 2015. Aquifer recharge estimation through atmospheric chloride mass balance at Las Cañadas Caldera, Tenerife, Canary Islands, Spain. Water (Switzerland) 7, 2451–2471. https://doi.org/10.3390/w7052451
Martens, B., Miralles, D.G., Lievens, H., Schalie, R. Van Der, Jeu, R.A.M. De, 2017. GLEAM v3 : satellite-based land evaporation and root-zone soil moisture 1903–1925. https://doi.org/10.5194/gmd-10-1903-2017
Martorana, R., Capizzi, P., D'Alessandro, A., Luzio, D., 2017. Comparison of different sets of array configurations for multichannel 2D ERT acquisition. J. Appl. Geophys. 137, 34–48. https://doi.org/10.1016/j.jappgeo.2016.12.012
Mathers, S.. an., Zalasiewicz, J., 1994. A guide to the sedimentology of unconsolidated seimentary aquifers, British Geological Survey.
Matter, J.M., Goldberg, D.S., Morin, R.H., Stute, M., 2006. Contact zone permeability at intrusion boundaries: New results from hydraulic testing and geophysical logging in the Newark Rift Basin, New York, USA. Hydrogeol. J. 14, 689–699. https://doi.org/10.1007/s10040-005-0456-3
Mazzini, A., Scholz, F., Svensen, H.H., Hensen, C., Hadi, S., 2017. The geochemistry and origin of the hydrothermal water erupted at Lusi, Indonesia. Mar. Pet. Geol. 15. https://doi.org/10.1016/j.marpetgeo.2017.06.018
Meinzer, O.E., 1928. Compressibility and elasticity of artesian aquifers. Econ. Geol. 23, 263–291. https://doi.org/10.2113/gsecongeo.23.3.263
Meinzer, O.E., Herbert, A.H., 1925. Contributions to the hydrogeology of the unites states. Geol. Surv. water-supply Pap.
Merritt, M.L., 1995. Computation of the time-varying flow rate from an artesian well in central

Dade County, Florida, by analytical and numerical simulation methods, Open-File Report. https://doi.org/10.3133/ofr94457

Miftakhul Fajar, M.H., Nogroho, D., 2018. Geology and hydrogeological study of the Bromo, Progress Report 2018. Yogyakarta.

Montgomery, E., Rosko, M., Castro, S., Keller, B., Bevacqua, P., 2003. Interbasin underflow between closed Altiplano basin in Chile. Ground Water 41, 523–531.

Morales, I., Villanueva-Estrada, R.E., Rodríguez, R., Armienta, M.A., 2015. Geological, hydrogeological, and geothermal factors associated to the origin of arsenic, fluoride, and groundwater temperature in a volcanic environment "El Bajío Guanajuatense", Mexico. Environ. Earth Sci. 74, 5403–5415. https://doi.org/10.1007/s12665-015-4554-9

Morgenstern, U., Stewart, M.K., Stenger, R., 2010. Dating of streamwater using tritium in a post nuclear bomb pulse world: Continuous variation of mean transit time with streamflow. Hydrol. Earth Syst. Sci. 14, 2289–2301. https://doi.org/10.5194/hess-14-2289-2010

Moscariello, A., Do Couto, D., Mondino, F., Booth, J., Lupi, M., Mazzini, A., 2018. Genesis and evolution of the Watukosek fault system in the Lusi area (East Java). Mar. Pet. Geol. 90, 125–137. https://doi.org/10.1016/j.marpetgeo.2017.09.032

Moscariello, A., Do Couto, D., Mondino, F., Booth, J., Lupi, M., Mazzini, A., 2017. Genesis and evolution of the Watukosek fault system in the Lusi area (East Java). Mar. Pet. Geol. https://doi.org/10.1016/j.marpetgeo.2017.09.032

Mudd, G.M., 2000. Mound springs of the Great Artesian Basin in South Australia: A case study from Olympic Dam. Environ. Geol. 39, 463–476. https://doi.org/10.1007/s002540050452

Mulligan, B.M., Ryan, M.C., Cámbara, T.P., 2011. Delineating volcanic aquifer recharge areas using geochemical and isotopic tools. Hydrogeol. J. 19, 1335–1347. https://doi.org/10.1007/s10040-011-0766-6

Mulyadi, E., 1992. Le complexe de Bromo-Tengger (Est Java, Indonesie): Etude structurale et volcanologique. PhD thesis, Université Blaise Pascal - Clermont Ferrand.

Murakami, H., Kato, Y., Akutsu, N., 2000. Construction of the Largest Geothermal Power Plant for Wayang Windu Project, Indonesia. World Geotherm. Congr. 2000 3239–3244.

Naud, G., 1971. Contribution à l'étude géologique et hydrogéologique du massif du Coiron partie orientale) (Ardèche). Université de Provence.

Neumann van Padang, M., 1951. Catalogue of the active volcanoes of Indonesia. International Volcanological Association.

Newhall, C.G., Dzurisin, D., 1988. Historical unrest at large calderas of the world. https://doi.org/10.3133/b1855

Newhall, C.G., Self, S., 1982. The volcanic explosivity index (VEI) an estimate of explosive magnitude for historical volcanism. J. Geophys. Res. 87, 1231–1238. https://doi.org/10.1029/JC087iC02p01231

Nichols, W.D., Shade, P.J., Hunt Jr., C.D., 1996. Summary of the Oahu, Hawaii, regional aquifer-system analysis, U.S. Geological Survey Professional Paper 1412-A.

Oberlander, P.L., Almy, R.B., 1979. Aquifer tests report for stage Gulch Ranch well no 3, Standfield, Oregon.

Pambudi, N.A., 2018. Geothermal power generation in Indonesia, a country within the ring of fire: Current status, future development and policy. Renew. Sustain. Energy Rev. 81, 2893–2901. https://doi.org/10.1016/j.rser.2017.06.096

Pambudi, N.A., 2017. Geothermal power generation in Indonesia, a country within the ring of fire: Current status, future development and policy. Renew. Sustain. Energy Rev. 1–9. https://doi.org/10.1016/j.rser.2017.06.096

Parisi, S., Paternoster, M., Kohfahl, C., Pekdeger, A., Meyer, H., Hubberten, H.W., Spilotro, G., Mongelli, G., 2011. Groundwater recharge areas of a volcanic aquifer system inferred from hydraulic, hydrogeochemical and stable isotope data: Mount Vulture, southern Italy.

Hydrogeol. J. 19, 133–153. https://doi.org/10.1007/s10040-010-0619-8
Parkinson, B., Spilker, J., 1996. Global Positioning System: Theory and Applications.
Paternoster, M., Parisi, S., Caracausi, A., Favara, R., Mongelli, G., 2010. Groundwaters of Mt. Vulture volcano, southern Italy: Chemistry and sulfur isotope composition of dissolved sulfate. Geochem. J. 44, 125–135. https://doi.org/10.2343/geochemj.1.0050
Peel, M.C., Finlayson, B.L., McMahon, T.A., 2007. Updated world map of the Köppen-Geiger climate classification. Hydrol. Earth Syst. Sci. 11, 1633–1644. https://doi.org/10.5194/hess-11-1633-2007
Peter, J., Mehringer, J., 1967. Late quaternary vegetation in the Mohave desert (USA). Rev. Palaeobot. Palynol. 2.
Peterson, D.W., Morre, R.B., 1987. Geologic and History and Evolution of Geologic Concepts, Island of Hawaii, in: U.S. Geological Survey Professional Papers 1350 - Volcanism in Hawaii, Chapter 7. pp. 149–189.
Peterson, F.L., 1972. Water Development on Tropic Volcanic Islands - Type Example: Hawaii. Groundwater. https://doi.org/10.1111/j.1745-6584.1972.tb03586.x
Pierrehumbert, R.T., 2000. Climate change and the tropical Pacific: The sleeping dragon wakes. Proc. Natl. Acad. Sci. U. S. A. 97, 1355–1358. https://doi.org/10.1073/pnas.97.4.1355
Plummer, L.N., Bohlke, J.-K., Busenberg, E., 2000. Approaches for ground-water dating.
Ponce, V.., Shetty, A. V., 1995. A conceptual model of catchment water balance : 1 . Formulation and calibration. Elsevier, J. Hydrol. 173, 27–40.
Poorter, R.P.E., Varekamp, J.C., Poreda, R.J., Van Bergen, M.J., Kreulen, R., 1991. Chemical and isotopic compositions of volcanic gases from the east Sunda and Banda arcs, Indonesia. Geochim. Cosmochim. Acta 55, 3795–3807. https://doi.org/10.1016/0016-7037(91)90075-G
Prada, S., Prada, S., Cruz, J.V., Figueira, C., 2016. Using stable isotopes to characterize groundwater recharge sources in the volcanic island of Madeira , Portugal Using stable isotopes to characterize groundwater recharge sources in the volcanic island of Madeira , Portugal. J. Hydrol. 536, 409–425. https://doi.org/10.1016/j.jhydrol.2016.03.009
Prada, S.N., da Silva, M.O., Cruz, J.V., 2005. Groundwater behaviour in Madeira, volcanic island (Portugal). Hydrogeol. J. 13, 800–812. https://doi.org/10.1007/s10040-005-0448-3
Pryet, A., 2011. Hydrogeology of volcanic islands : a case-study in the Galapagos Archipelago (Ecuador). Université Pierre et Marie Curie.
Pryet, A., D'Ozouville, N., Violette, S., Deffontaines, B., Auken, E., 2012. Hydrogeological settings of a volcanic island (San Cristobal, Galapagos) from joint interpretation of airborne electromagnetics and geomorphological observations. Hydrol. Earth Syst. Sci. 16, 4571–4579. https://doi.org/10.5194/hess-16-4571-2012
Pryet, Alexandre, Domínguez, C., Tomai, P.F., Chaumont, C., D'Ozouville, N., Villacís, M., Violette, S., 2012. Quantification of cloud water interception along the windward slope of Santa Cruz Island, Galapagos (Ecuador). Agric. For. Meteorol. 161, 94–106. https://doi.org/10.1016/j.agrformet.2012.03.018
R, J.M. trian, R, J.F.H., R, C.A.R., A, O.M.C., M, J.A. henao, Williams, C.D., Roberts, C.L., 2012. Natural zeolites filling amygdales and veins in basalts from the British Tertiary Igneous Province on the Isle of Skye, Scotland. Earth Sci. Res. J. 16, 41–53.
Renard, P., 2005. Hydraulics of Well and Well Testing. Encycl. Hydrol. Sci. 18. https://doi.org/10.1002/0470848944
Renard, P., Glenz, D., Mejias, M., 2009. Understanding diagnostic plots for well-test interpretation. Hydrogeol. J. 17, 589–600. https://doi.org/10.1007/s10040-008-0392-0
Ritter, A., Regalado, C.M., Aschan, G., 2008. Fog water collection in a subtropical Elfin Laurel forest of the Garajonay National Park (Canary Islands): A combined approach using artificial fog catchers and a physically based impaction model. J. Hydrometeorol. 9, 920–935. https://doi.org/10.1175/2008JHM992.1

Roberts, C.R., Mitchell, C.W., 2019. Spring mounds in southern Tunisia Environment of the Tunisian spring mounds Downloaded from http://sp.lyellcollection.org/ at Bibliotheque Interuniversitaire de 321–334.

Rodysill, J.R., Russell, J.M., Crausbay, S.D., Bijaksana, S., Vuille, M., Edwards, R.L., Cheng, H., 2013. A severe drought during the last millennium in East Java, Indonesia. Quat. Sci. Rev. 80, 102–111. https://doi.org/10.1016/j.quascirev.2013.09.005

Romario, I.F.B., Mindasari, D., Suprapto, R.E., Yusuf, M.A., 2015. Oligo-Miocene Tectonic of Java and The Implication for Flexural Basin of Southern Mountain in Affecting Depositional System in Kerek Formation. Jt. Conv. Balikpapan 2015.

Rotzoll, K., El-Kadi, A.I., Gingerich, S.B., 2007. Estimating hydraulic properties of volcanic aquifers using constant-rate and variable-rate aquifer tests. J. Am. Water Resour. Assoc. 43, 334–345. https://doi.org/10.1111/j.1752-1688.2007.00026.x

Rouquet, S.I., Boivin, P.I., Lachassagne, P.A., Ledoux, E.M., 2012. A 3-D genetic approach to high-resolution geological modelling of the volcanic infill of a paleovalley system . Application to the Volvic catchment (Chaîne des Puys , France) 395–407.

Rovida, A., Tibaldi, A., 2005. Propagation of strike-slip faults across Holocene volcano-sedimentary deposits, Pasto, Colombia. J. Struct. Geol. 27, 1838–1855. https://doi.org/10.1016/j.jsg.2005.06.009

Rutter, A.J., Kershaw, K.A., Robins, P.C., Morton, A.J., 1972. A predictive model of rainfall interception in forests, Derivation of the model from observation in a plantation of corsican pine. Agric. Meteorol. 9, 367–384.

Samouëlian, A., Cousin, I., Tabbagh, A., Bruand, A., Richard, G., 2005. Electrical resistivity survey in soil science: A review. Soil Tillage Res. 83, 173–193. https://doi.org/10.1016/j.still.2004.10.004

Santosa, S., Suwarti, T., Suharsnono, 1992. Geological map of Bromo-Tengger (Malang, Probolinggo, Turen and Lumajang quadrangle). Bandung.

Satyana, A.H., Erwanto, E., Prasetyadi, C., 2004. Rembang-Madura-Kangean-Sakala (RMKS) Fault Zone, East Java Basin: The Origin and Nature of a Geologic Border. Indones. Assoc. Geol. 33rd Annu. Conv. 1–23.

Scholl, M., Gingerich, S., W Tribble, G., 2002. The influence of microclimates and fog on stable isotope signatures used in interpretation of regional hydrology: East Maui, Hawaii, Journal of Hydrology. https://doi.org/10.1016/S0022-1694(02)00073-2

Scholl, M.A., Ingebritsen, S.E., Janik, C.J., Kauahikaua, J.P., 1996. Use of Precipitation and Groundwater Isotopes to Interpret Regional Hydrology on a Tropical Volcanic Island: Kilauea Volcano Area, Hawaii, in: Volume32, Issue12. pp. 3525–3537.

Selles, A., 2014. Multi-disciplinary study on the hydrogeological behaviour of the eastern flank of the Merapi volcano, Central Java, Indonesia. PhD thesis, Université Pierre et Marie Curie - Paris.

Selles, A., Deffontaines, B., Hendrayana, H., Violette, S., 2015. The eastern flank of the Merapi volcano (Central Java, Indonesia): Architecture and implications of volcaniclastic deposits. J. Asian Earth Sci. 108, 33–47. https://doi.org/10.1016/j.jseaes.2015.04.026

Simandjuntak, T.O., 1993. Neogene tectonics and orogenesis of Indonesia. Bull. Geol. Soc. Malaysia 33, 43–64. https://doi.org/10.7186/bgsm33199305

Singhal, B.B.S., 1997. Hydrogeological characteristics of Deccan trap formations of India. Hard Rock Hydrosystems 241, 78–80.

Singhal, B.B.S., Gupta, R.P., 2010. Applied hydrogeology of fractured rocks: Second edition. Appl. Hydrogeol. Fract. Rocks Second Ed. 1–408. https://doi.org/10.1007/978-90-481-8799-7

Smyth, H., 2005. East Java: Cenozoic basins, volcanoes and ancient basement. Thirtieth Annu. Conv. Exhib. 251–266. https://doi.org/10.29118/ipa.629.05.g.045

Smyth, H.R., Hall, R., Nichols, G.J., 2008. Cenozoic volcanic arc history of East Java,

Indonesia: The stratigraphic record of eruptions on an active continental margin. Spec. Pap. Geol. Soc. Am. 436, 199–222. https://doi.org/10.1130/2008.2436(10)

Soekardi Puspowardoyo, R., 1985. Hydrogeological map of Indonesia (1:250 000). bandung, Indonesia.

Solikhin, A., 2017. Geology , tectonics and post-2001 eruptive activity interpreted from high-spatial resolution satellite imagery : the case study of Merapi and Seremu volcanoes , Indonesia. Université Blaise Pascal, U.F.R Sciences et Technologies. https://doi.org/https://tel.archives-ouvertes.fr/tel-01555688

Solomon, D.K., Genereux, D.P., Plummer, L.N., Busenberg, E., 2010. Testing mixing models of old and young groundwater in a tropical lowland rain forest with environmental tracers. Water Resour. Res. 46, 1–14. https://doi.org/10.1029/2009WR008341

Stearns, H.T., Clark, W.O., Meinzer, O.E., 1930. Geology and water resources of the Kau District, Hawaii. U.S. Geol. Surv. Water Supply Pap. 616 194 p.

Sun, X., Xu, Y., 2014. A hydraulic test device for free-flowing artesian boreholes with a case study in Table Mountain Group (TMG) aquifers, South Africa. Water SA 40, 445–452. https://doi.org/10.4314/wsa.v40i3.7

Sun, X., Xu, Y., Lin, L., 2015. The diagnostic plot analysis of artesian aquifers with case studies in Table Mountain Group of South Africa. Hydrogeol. J. 23, 567–579. https://doi.org/10.1007/s10040-014-1203-4

Surya Nugraha, A.M., Hall, R., 2013. Cenozoic Stratigraphy of the East Java Forearc. Indones. J. Sediment. Geol.

Susilohadi, 1995. Late tertiary and quaternary geology of the East Java Basin, Indonesia.

Swamee, P.K., Mishra, G.C., Chahar, B.R., 2002. Simple Approximation for Flowing Well Problem. J. Irrig. Drain. Eng. 126, 65–67. https://doi.org/10.1061/(asce)0733-9437(2000)126:1(65)

Takahashi, T., Tsujimoto, H., 2000. A mechanical model for Merapi-type pyroclastic flow. J. Volcanol. Geotherm. Res. 98, 91–115. https://doi.org/10.1016/S0377-0273(99)00193-6

Thompson, D., 1929. Origin of artesian pressure. Econ. Geol. 24, 758–771.

Thornthwaite, 1948. Water balance.

Thouret, J.C., 1999. Volcanic geomorphology-an overview. Earth Sci. Rev. 47, 95–131. https://doi.org/10.1016/S0012-8252(99)00014-8

Toulier, A., Baud, B., de Montety, V., Lachassagne, P., Leonardi, V., Pistre, S., Dautria, J.M., Hendrayana, H., Miftakhul Fajar, M.H., Satrya Muhammad, A., Beon, O., Jourde, H., 2019. Multidisciplinary study with quantitative analysis of isotopic data for the assessment of recharge and functioning of volcanic aquifers: Case of Bromo-Tengger volcano, Indonesia. J. Hydrol. Reg. Stud. 26, 100634. https://doi.org/10.1016/j.ejrh.2019.100634

Tropical Rainfall Measuring Mission (TRMM) [WWW Document], 2011. https://doi.org/10.5067/TRMM/TMPA/3H/7

Tsuji, K., Grouting, F., Co, E., 1986. Groundwater Development in the Mountain Skirts of Volcanic Massifs in Eastern Java , Indonesia.

UNESCO, U.N.E. and S.O., 2012. International glossary of hydrology, IHP/OHP-Berichte.

Ungemach, P., Bonnet, M., Suzanne, P., 1968. Interprétation des essais de pompage en régime transitoire. Cas des mesures effectuées dans le puits. L'effet de puits et la postproduction (Terres et Eaux, 1968, 21, 54, p. 3). Sci. Géologiques, Bull. mémoires 21, 325.

Untung, M., Sato, y, 1978. Gravity and Geological Studies in Java, Indonesia: Geological Survey of Indonesia and Geological Survey of Japan Joint Research Program on Regional Tectonics of Southeast Asia, Geological Survey of Indonesia.

USGS, 1996. Shuttle Radar Topography Mission (STRM), 1 arc-second for global coverage (~30 meters) [WWW Document].

Van Bemmelen, R.W., 1949. The geology of Indonesia, Special ed. ed.

Van Gerven, M., Pichler, H., 1995. Some aspects of the volcanology and geochemistry of the

Tengger Caldera, Java, Indonesia: eruption of a K-rich tholeiitic series. J. Southeast Asian Earth Sci. 11, 125–133. https://doi.org/10.1016/0743-9547(95)00003-B

Vasquez, J., 2010. Hydraulique Generale. Laboratoire Systèmes Hydrauliques Urbains - ENGEES.

Versey, H.R., Singh, B.K., 1983. Groundwater in Deccan basalts of Betwa Basin, India. J. Hydrol. 58.

Versluys, J., 1930. The origin of artesian pressure. Econ. Geol. 214–222.

Violette, S., Ledoux, E., Goblet, P., Carbonnel, J.-P., 1997. Hydrologic and thermal modeling of an active volcano: the Piton de la Fournaise, Reunion. J. Hydrol. 191, 37–63.

Vittecoq, B., Lachassagne, P., Lanini, S., Maréchal, J.C., 2010. Assessment of Martinique (FWI) water resources: effective rainfall spatial modelling and validation at catchment scale. Rev. des Sci. l'eau 23, 361. https://doi.org/10.7202/045098ar

Vittecoq, B., Reninger, P.A., Violette, S., Martelet, G., Dewandel, B., Audru, J.C., 2015. Heterogeneity of hydrodynamic properties and groundwater circulation of a coastal andesitic volcanic aquifer controlled by tectonic induced faults and rock fracturing - Martinique island (Lesser Antilles - FWI). J. Hydrol. 529, 1041–1059. https://doi.org/10.1016/j.jhydrol.2015.09.022

Volk, C.M., Elkins, J.W., Fahey, D.W., Dutton, G.S., Gilligan, J.M., Loewenstein, M., Podolske, J.R., Chan, K.R., Gunson, M.R., 1997. Evaluation of source gas lifetimes from stratospheric observations. J. Geophys. Res. Atmos. 102, 25543–25564.

Vuković, M., Soro, A., 1992. Hydraulics of Water Wells: Theory and Application. Water Resources Publications.

Walker, G.P.L., 1971. Compound and simple lava flows and flood basalts. Bull. Volcanol. 35, 579–590. https://doi.org/10.1007/BF02596829

Waltham, D., Hall, R., Smyth, H.R., Ebinger, C.J., 2008. Basin formation by volcanic arc loading. Spec. Pap. Geol. Soc. Am. 436, 11–26. https://doi.org/10.1130/2008.2436(02)

Webster, P.J., Magaña, V.O., Palmer, T.N., Shukla, J., Tomas, R.A., Yanai, M., Yasunari, T., 1998. Monsoons: Processes, predictability, and the prospects for prediction. J. Geophys. Res. Ocean. 103, 14451–14510. https://doi.org/10.1029/97jc02719

Weijden, C.H. Van Der, Pacheco, F.A.L., 2003. Hydrochemistry , weathering and weathering rates on Madeira island. J. Hydrol. 283, 122–145. https://doi.org/10.1016/S0022-1694(03)00245-2

Wentworth, C.K., 1951. Geology and ground-water resources of the Honolulu-Pearl Harbor area Oahu, Hawaii.

Whittier, R.B., Rotzoll, K., Dhal, S., El-Kadi, A.I., Ray, C., Chang, D., 2010. Groundwater source assessment program for the state of Hawaii, USA: methodology and example application. Hydrogeol. J. 18, 711–723. https://doi.org/10.1007/s10040-009-0548-6

Willmann, M., Carrera, J., Sánchez-Vila, X., Vázquez-Suñé, E., 2007. On the meaning of the transmissivity values obtained from recovery tests. Hydrogeol. J. 15, 833–842. https://doi.org/10.1007/s10040-006-0147-8

Winograd, I.J., 1971. Hydrogeology of Ash Flow Tuff: A Preliminary Statement. Water Resour. Res. 7, 994–1006. https://doi.org/10.1029/WR007i004p00994

Wyrick, G., Floyd, O.E., 1961. Microtime Measurements in Aquifer Tests on Open-Hole Artesian Wells - Method of aquifer tests. Geol. Surv. water-supply Pap. 11.

Zaennudin, A., 2010. The characteristic of eruption of Indonesian active volcanoes in the last four decades. J. Lingkung. dan Bencana Geol. 1, 113–129.

Zaennudin, A., 1990. The stratigraphy and nature of the stratocone of Mt. Cemorolawang in the Bromo-Tengger caldera, East Java, Indonesia. Research School of Earth Science, Victoria University of Wellington.

Zaennudin, A., Hadisantono, R.D., Erfan, R.D., Mulyana, A.., 1994. Geological map of Bromo-Tengger volcano, east Java. Bandung: Direktorat Vulkanologi, 1992-2004 (Indonesia).

Appendices

Appendices.

Appendix 1. Interface of the new Bromo-Tengger database

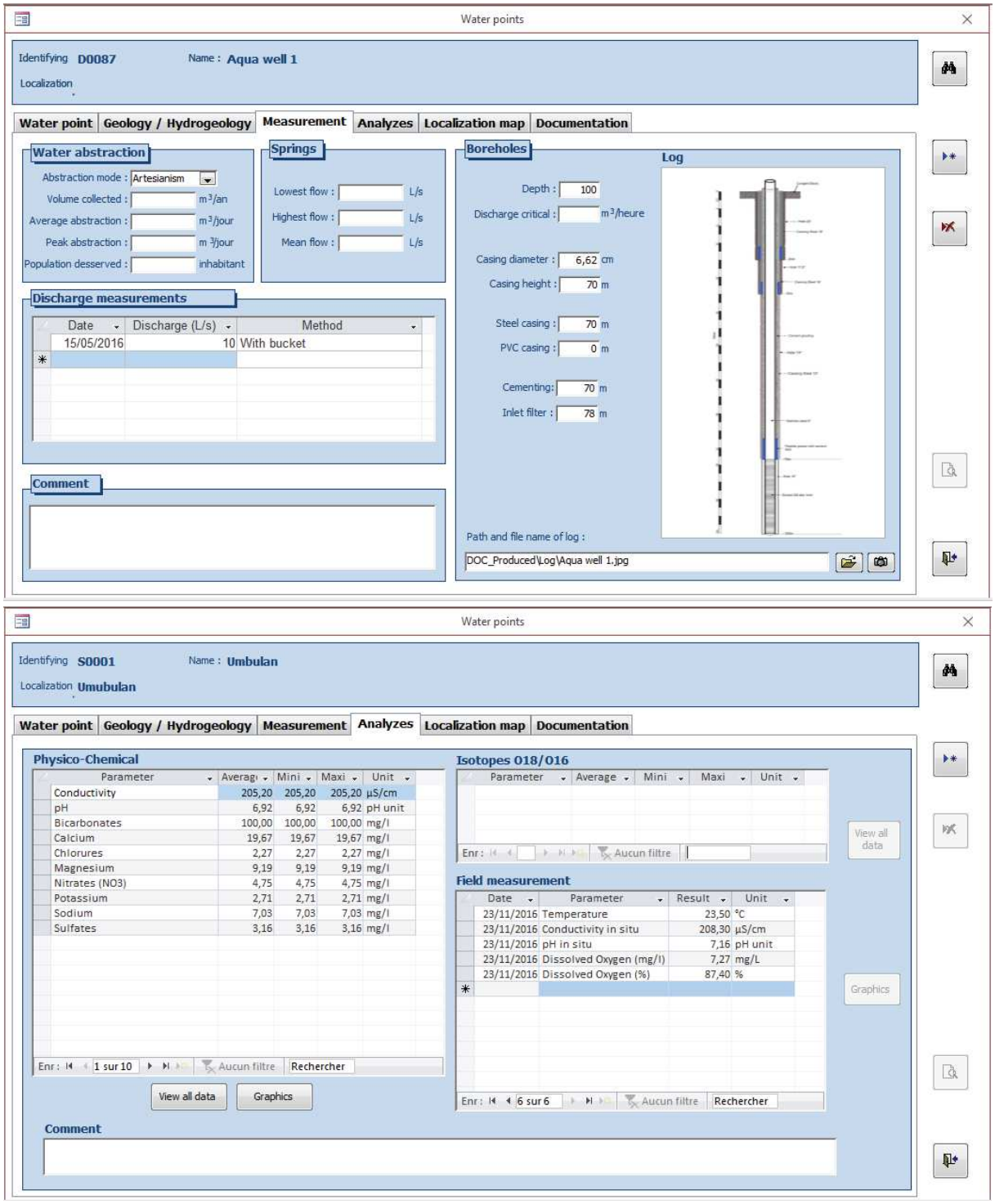

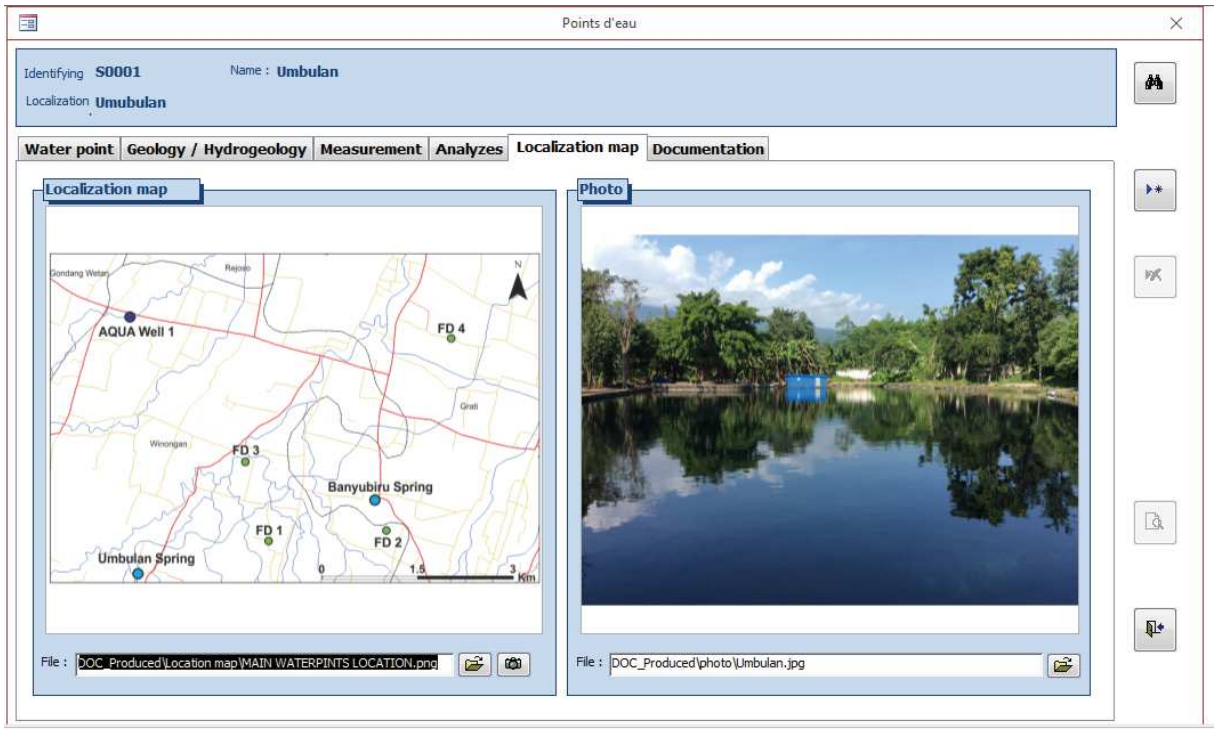
Points d'eau
Identifying S0001
Name : Umbulan
Localization Umubulan
Water point
Geology / Hydrogeology
Measurement
Analyzes
Localization map
Documentation
Localization map
AQUA Well 1
FD 4
FD 3
Banyubiru Spring
FD 1
FD 2
Umbulan Spring
N
0
1.5
3
Km
File : DOC_Produced\Location map\MAIN WATERPINTS LOCATION.png
Photo
File : DOC_Produced\photo\Umbulan.jpg

Appendix 2. Design of the video logging device for investigations in artesian well.

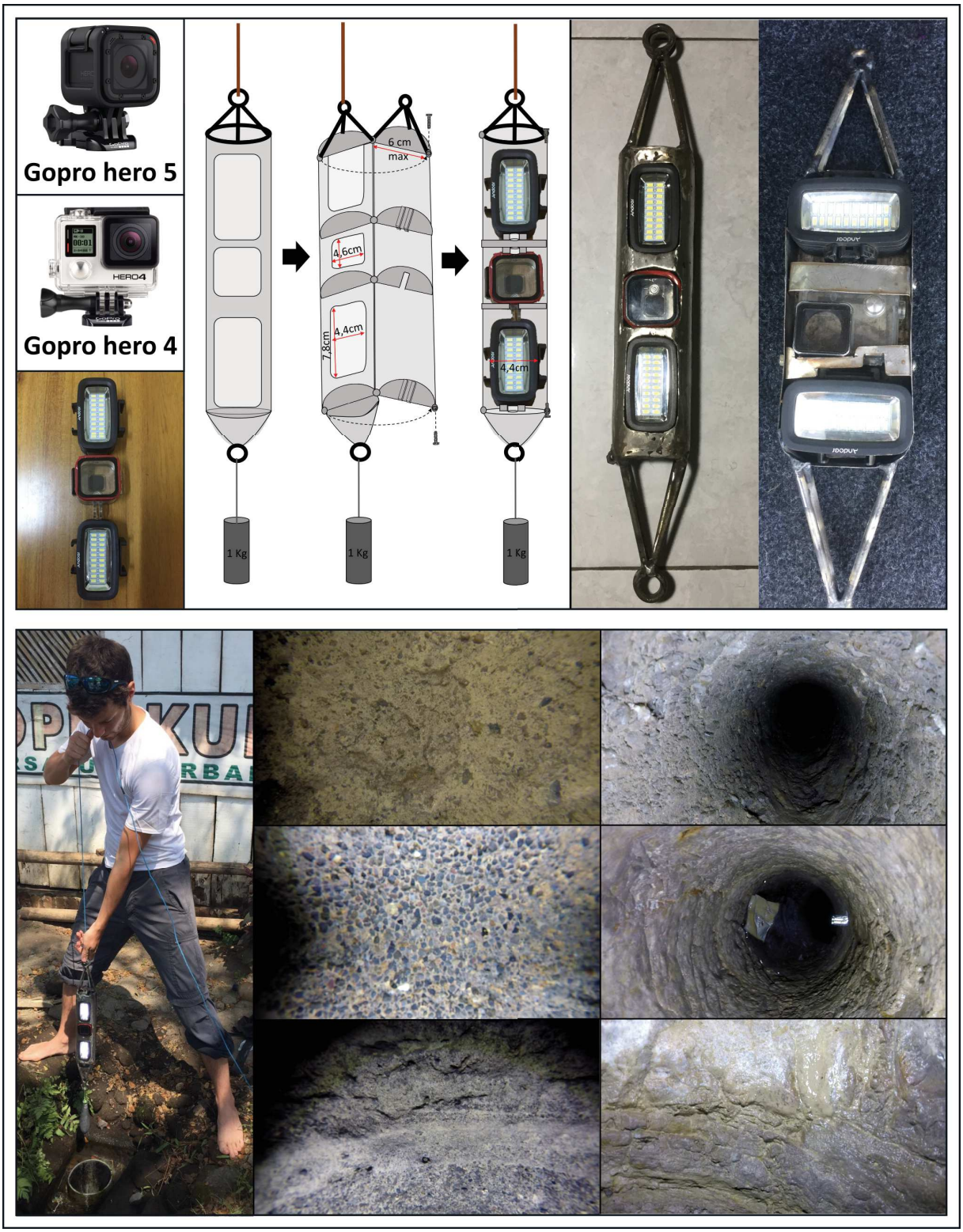

Appendix 3. Description of the main springs of the Bromo-Tengger-Semeru volcanic complex



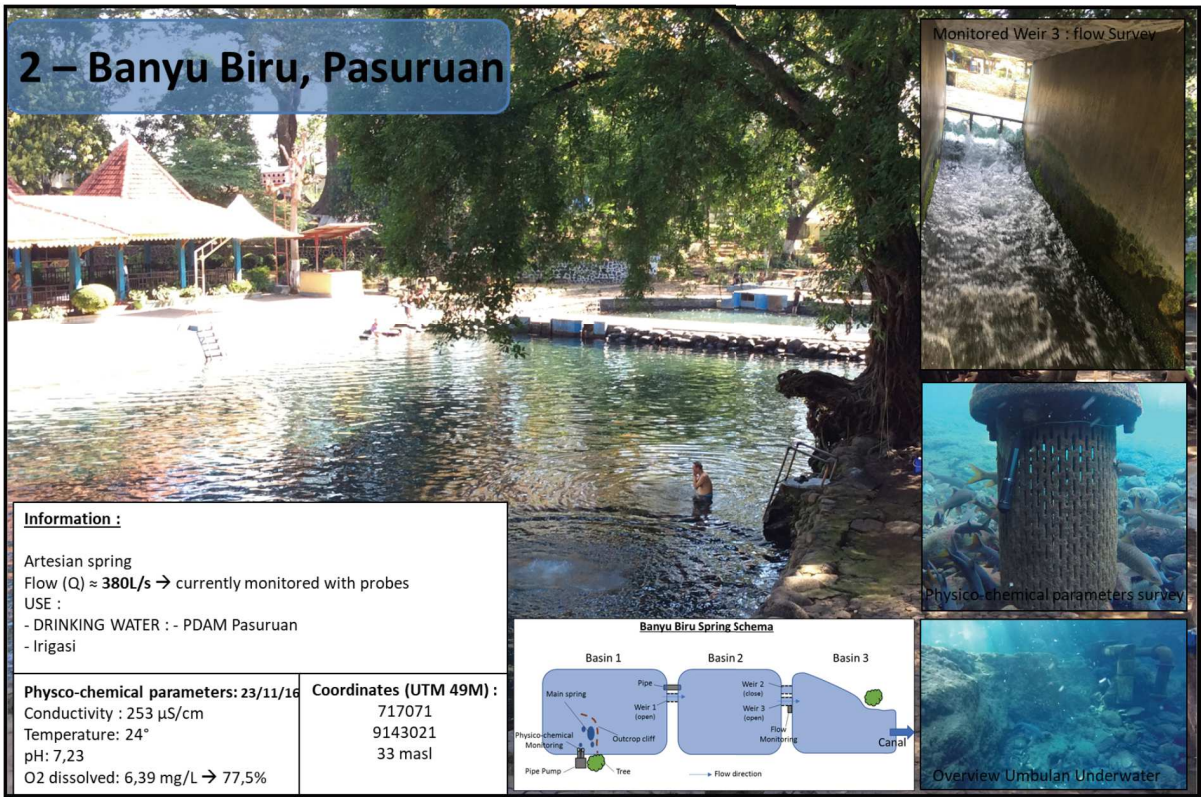


3 – Madakaripura, Probolinggo
One of the main spring from cliff
Madakaripura statue
Information :
Gravity spring
Flow (Q) ≈ 200L/s
USE :
- DRINKING WATER : - PDAM Probolinggo
- Village
Physco-chemical parameters : 19/05/17
Conductivity : 121,9 µS/cm
Temperature: 20,9
pH: 8,19
O2 dissolved: 7,92 mg/L → 96,7%
Coordinates (UTM 49M) :
722063
9131614
810 masl
One of the spring from the cliff
Pyroclastic flow

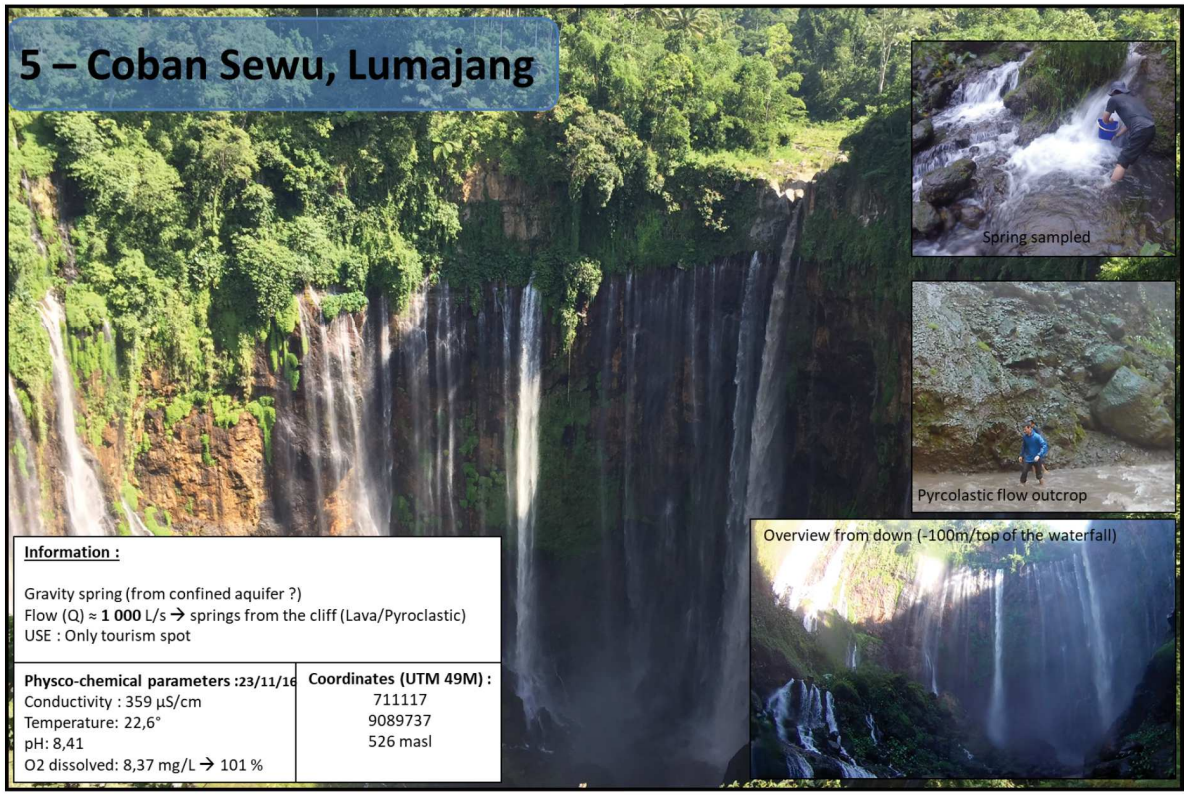
5 – Coban Sewu, Lumajang
Spring sampled
Pyrcolastic flow outcrop
Overview from down (-100m/top of the waterfall)
Information :
Gravity spring (from confined aquifer ?)
Flow (Q) ≈ 1 000 L/s → springs from the cliff (Lava/Pyroclastic)
USE : Only tourism spot
Physco-chemical parameters :23/11/16
Conductivity : 359 µS/cm
Temperature: 22,6°
pH: 8,41
O2 dissolved: 8,37 mg/L → 101 %
Coordinates (UTM 49M) :
711117
9089737
526 masl

6 – Umbulan, Malang


Weir 1 installation


Numerous springs in the bottom of the basin (-3m/surface)


Pyroclastic outcrop

Information :

Artesian spring
Flow (Q) ≈ **100** L/s →
USE : Recreation (and drinking water ?)

Physco-chemical parameters :11/04/17	**Coordinates (UTM 49M) :**
Conductivity : 200 µS/cm Temperature: 20,9° pH: 7,5 O2 dissolved: 7,12 mg/L → 101 %	694643 9095612 465 masl

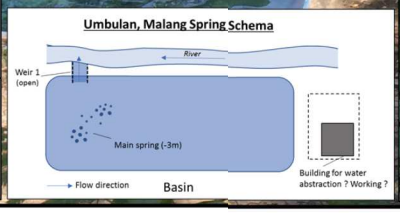

7 – Sumber Pitu, Malang


Under lava spring

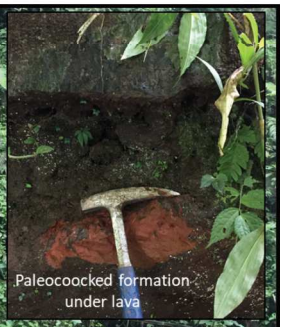
Paleocoocked formation under lava

Information :

Gravity spring ; Under lava spring
Flow (Q) ≈ **500-1000** L/s
USE : - Tourism spot
- Drinking water – PDAM Malang

Physco-chemical parameters : To do	**Coordinates (UTM 49M) :**
Conductivity : 628 µS/cm Temperature: 20,6°C pH: O2 dissolved:	700778 9113788 870 masl

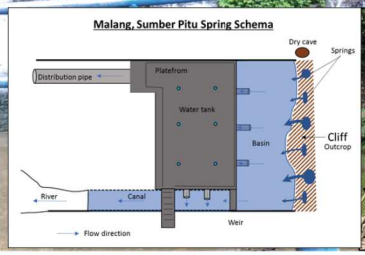



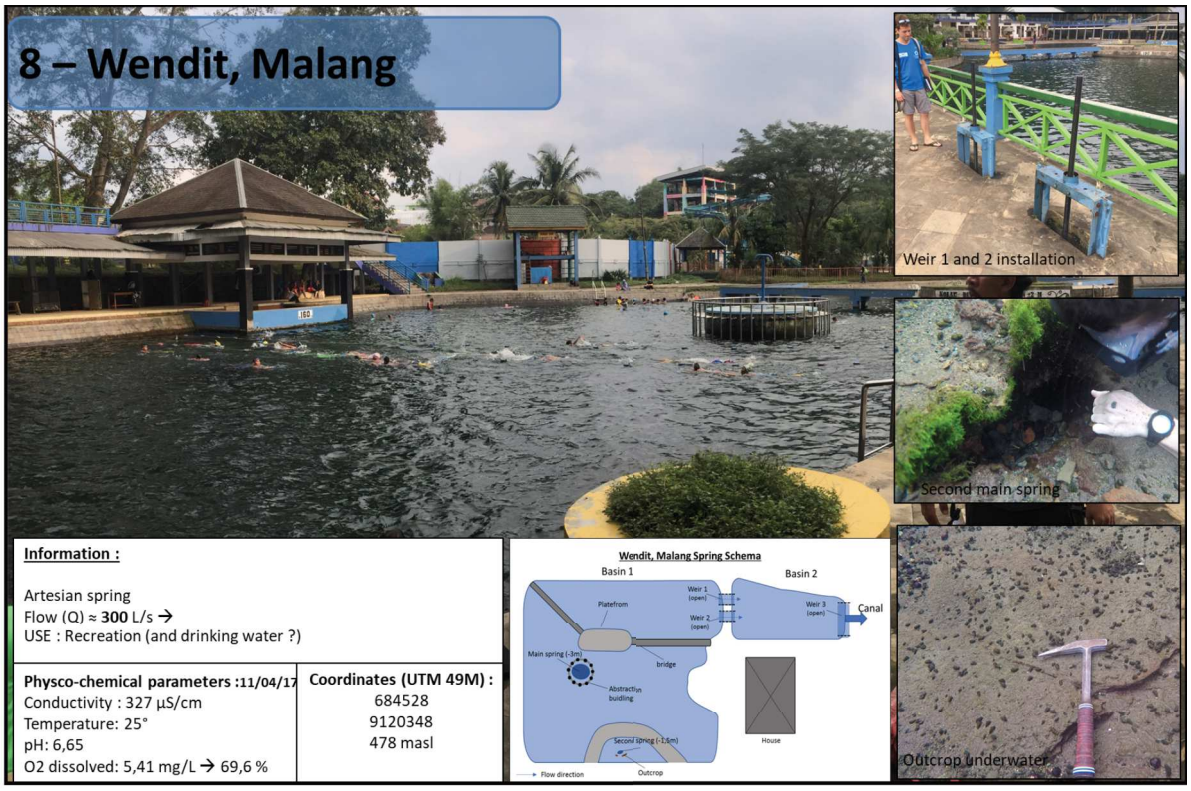
8 – Wendit, Malang
Weir 1 and 2 installation
Second main spring
Outcrop underwater
Information :
Artesian spring
Flow (Q) ≈ 300 L/s →
USE : Recreation (and drinking water ?)
Physco-chemical parameters :11/04/17
Conductivity : 327 µS/cm
Temperature: 25°
pH: 6,65
O2 dissolved: 5,41 mg/L → 69,6 %
Coordinates (UTM 49M) :
684528
9120348
478 masl
Wendit, Malang Spring Schema
Basin 1
Basin 2
Platefrom
Weir 1 (open)
Weir 2 (open)
Weir 3 (open)
Canal
Main spring (-3m)
bridge
Abstraction building
House
Second spring (-1.6m)
Flow direction
Outcrop

Appendix 4. Key outcrops descriptions

Ranu Grati quarry (Key outcrop n°7)



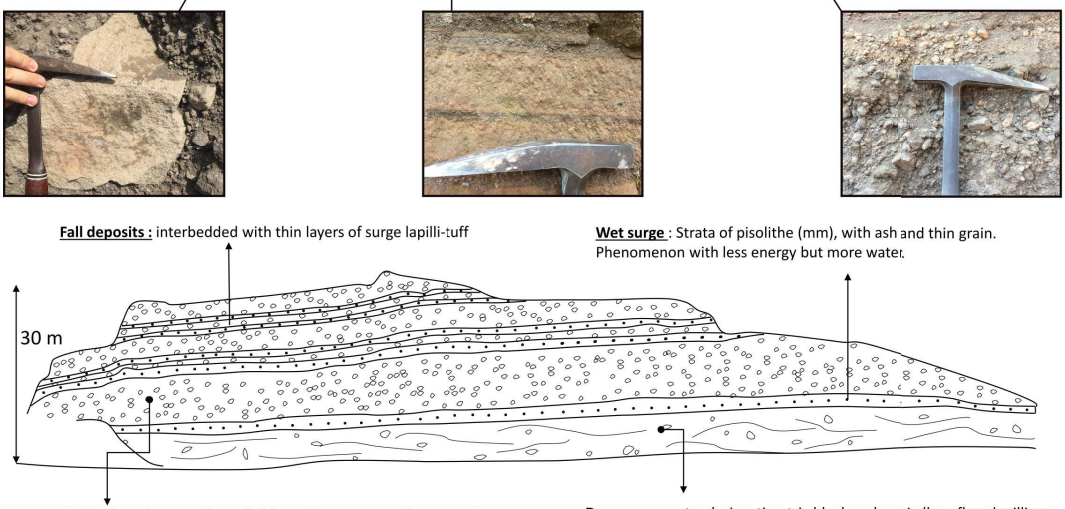

Carbonbates and alluviales quarry (Key outcrop n°1)

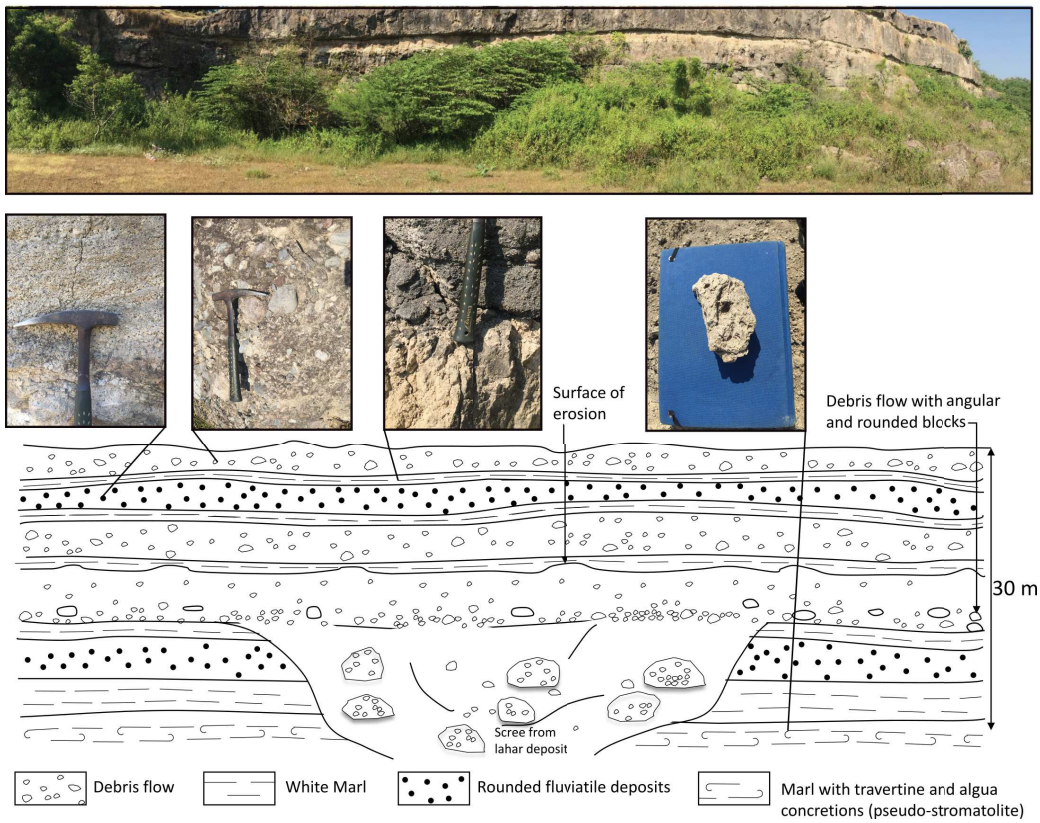

Ignimbrite quarry (Key outcrop n°14)

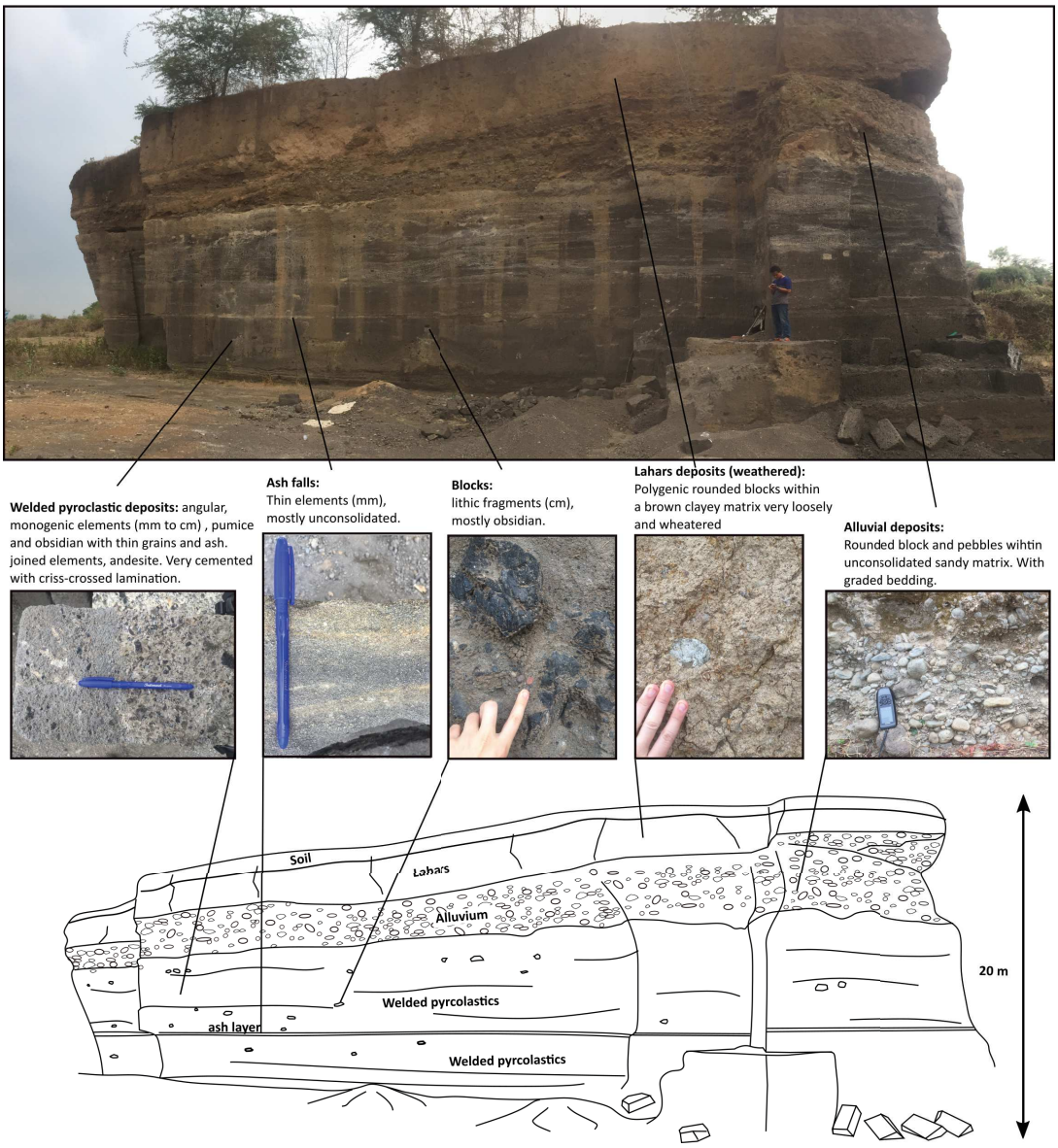

Appendix 5. Geophysical calibration from key outcrop and log drilling

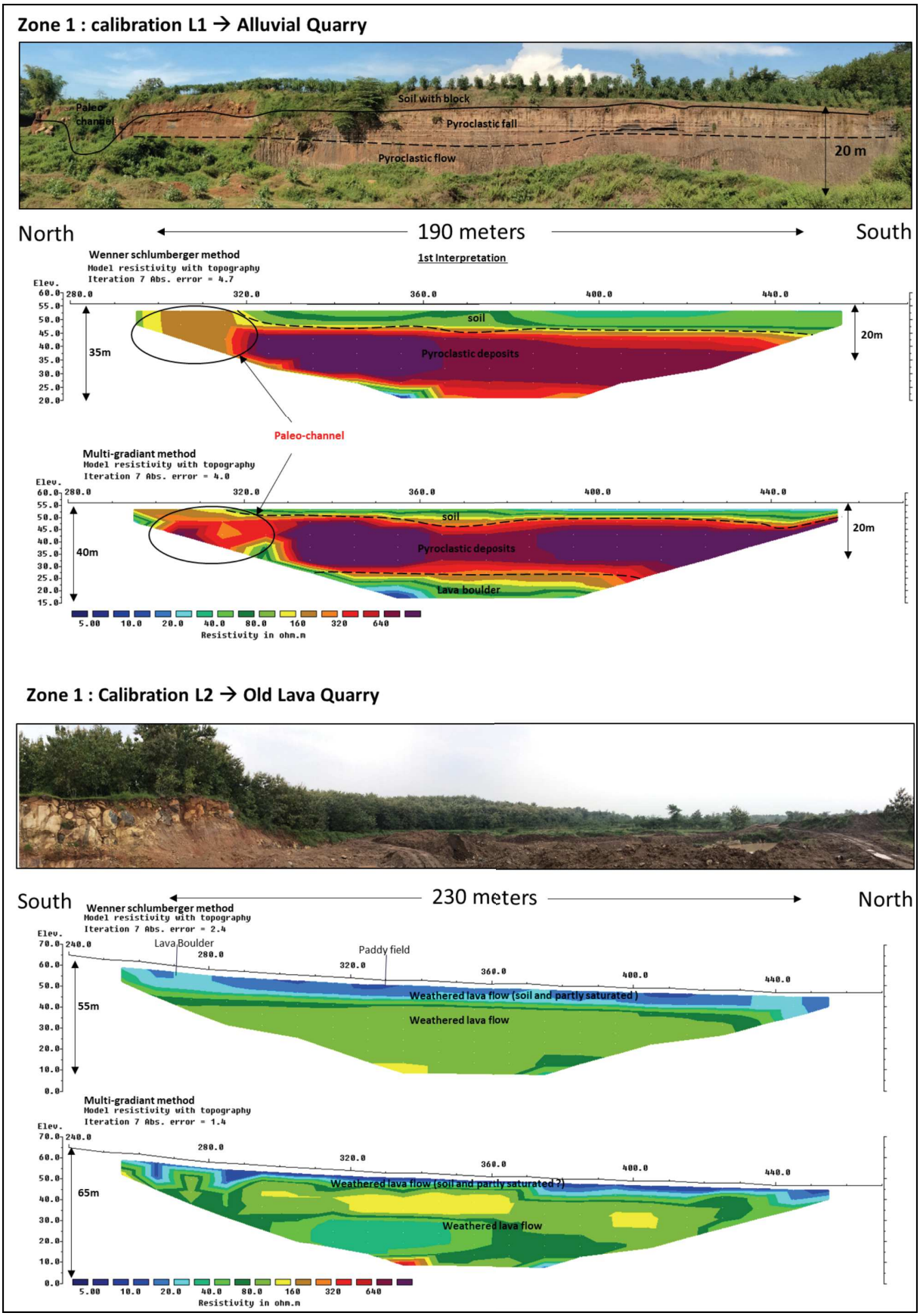

Zone 3 : calibration L10 → Fresh Lava Quarry



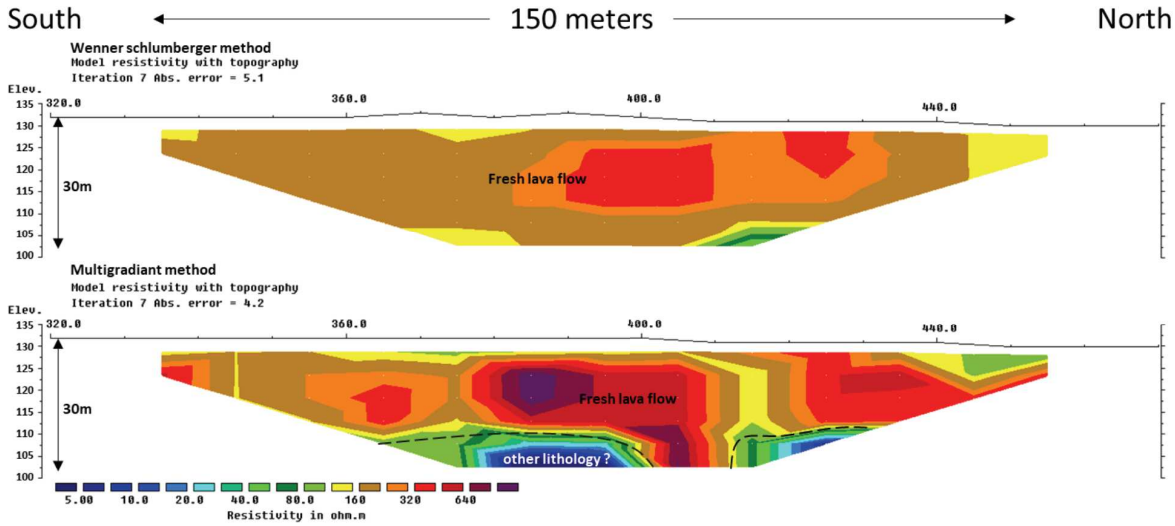

Zone 3 : calibration L11 → Aqua KBC well



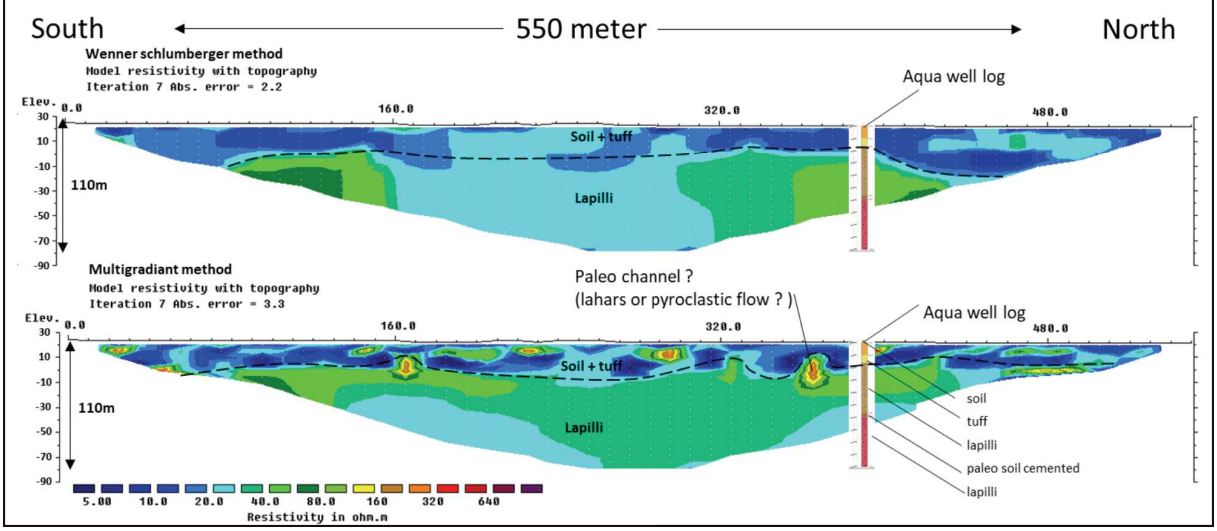

Appendix 6. Geophysical calibration from groundwater points inventory

1 - Electrical conductivity from artesian springs and wells

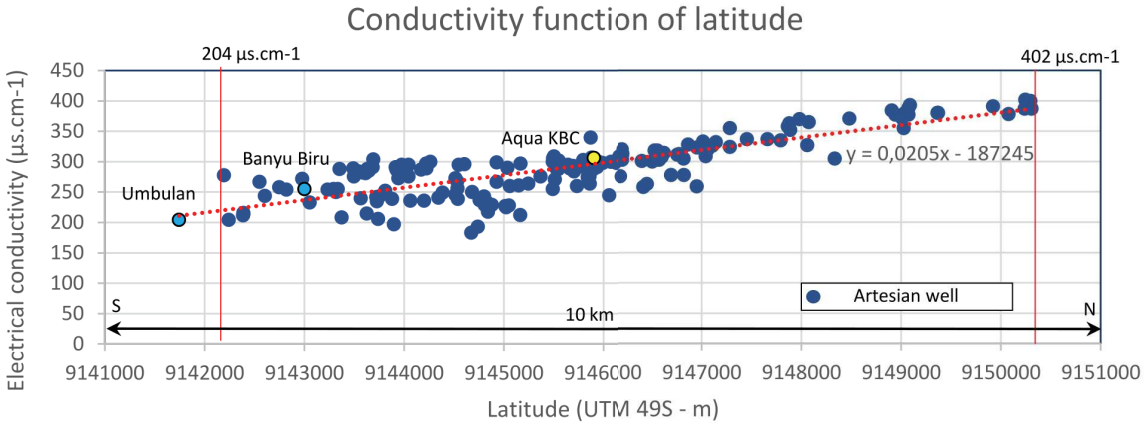

2 - Electrical conductivity from dug wells

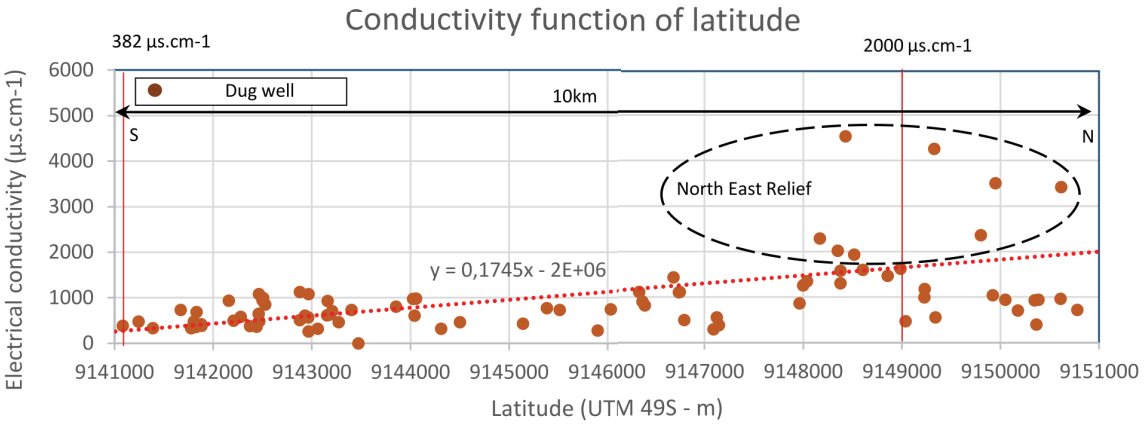

3 - Calibration synthesis

b	Aquifer formation calibration				
Resistivity (Ohm m $^{-1}$)	Unconfined / Confined: 5	10	20	40	80	160	320	640
Confined aquifer (from artesian wells & springs)					
Electrical conductivity (µS cm^{-1})	400	350	300	250	200
Resistivity (Ohm m $^{-1}$)	25	29	33	40	50
Range color resistivity					
Unconfined aquifer (from dug wells)					
Electrical conductivity (µS cm^{-1})	2000	1500	1000	700	400
Resistivity (Ohm m $^{-1}$)	5	6	10	20	25
Range color resistivity					

Appendix 7. Results of the phD instrumentation

A. Hourly electrical conductivity and temperature data monitoring of the Umbulan and Banyu Biru artesian springs. The probes show a drift of about 9.97E-06 and 1,01E-05 °C h^{-1}, respectively for Umbulan and Banyu Biru which are corrected below (in green).

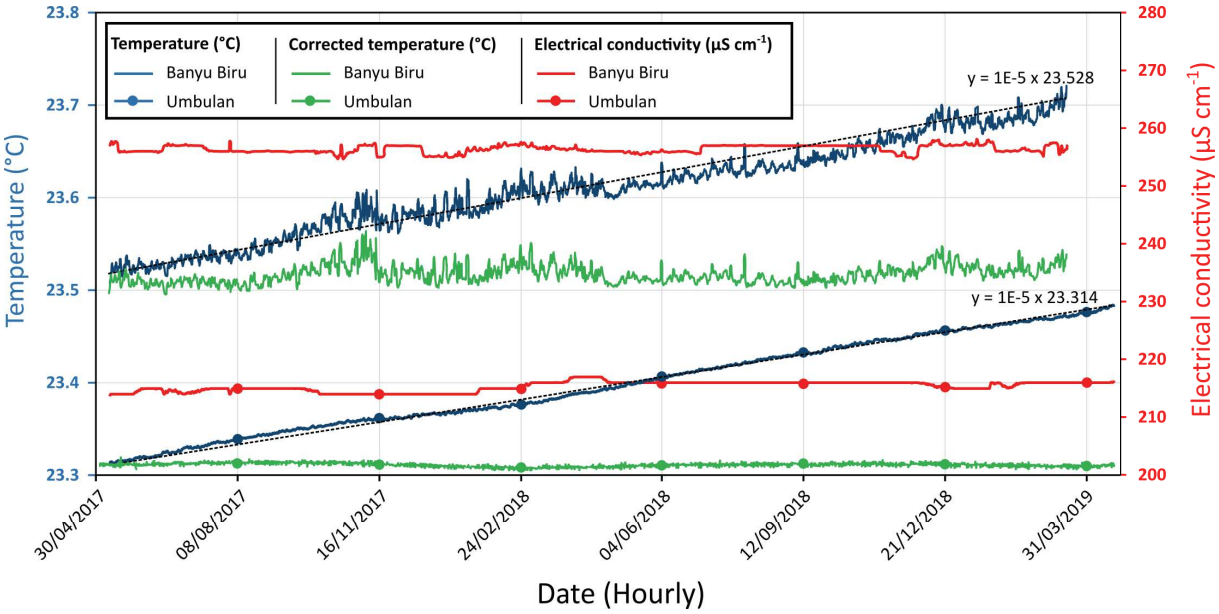

B. Compilation of the discharge data of Umbulan and Banyu Biru springs. The discharge of Umbulan spring includes the previous manual discharge measurements performed by CKnet organization from 2007 to 2015. The phD instrumentation covers the period from May 2017 to April 2019.

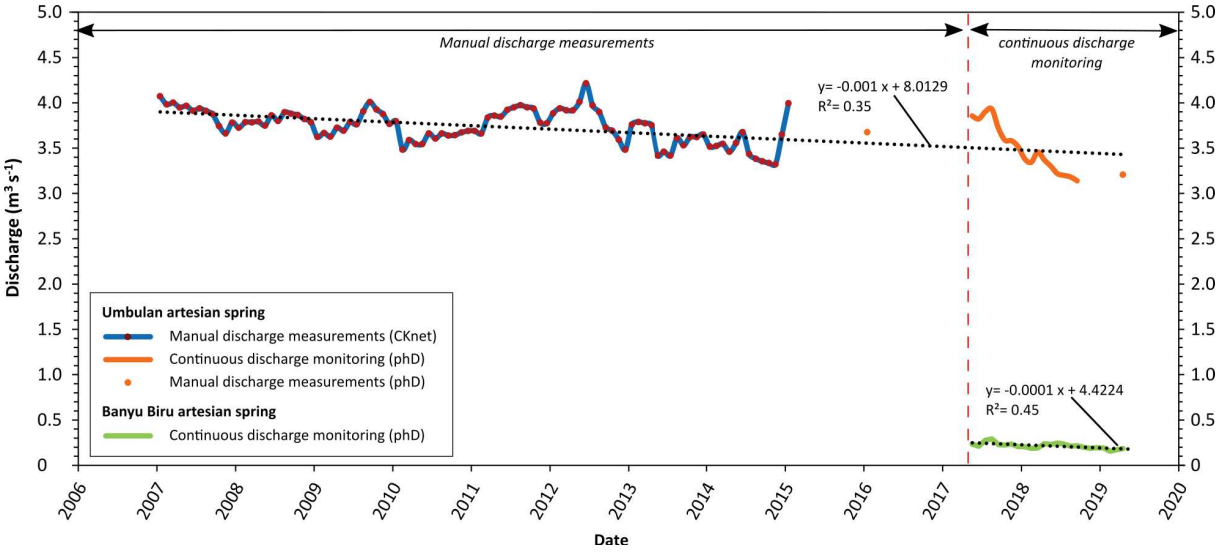

C. Monitoring results of Banyu Biru and Umbulan artesian springs, completed by the piezometric level recorded in Aqua piezometer.

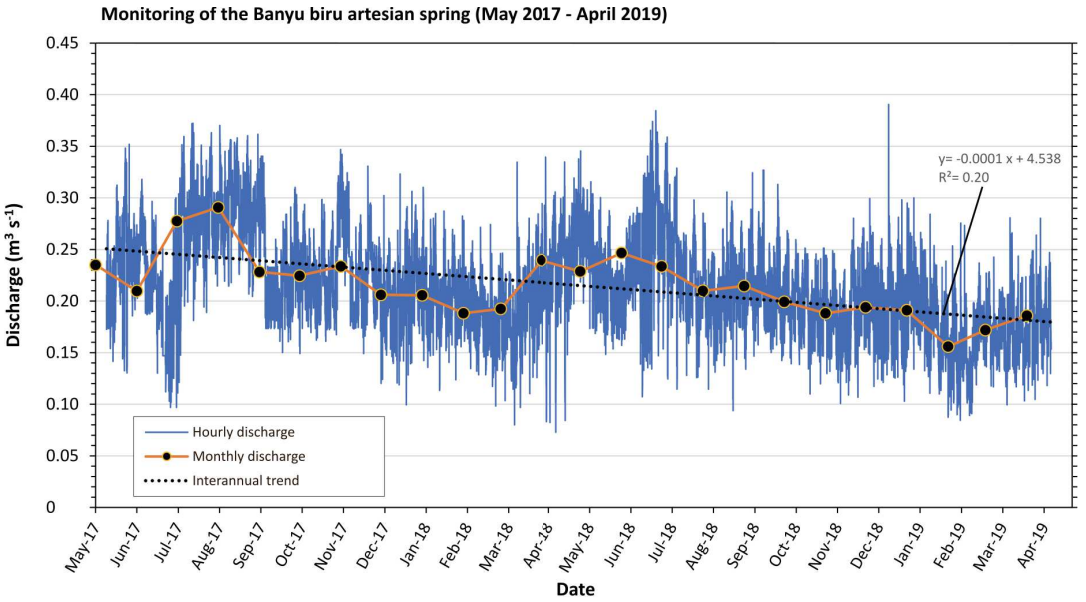

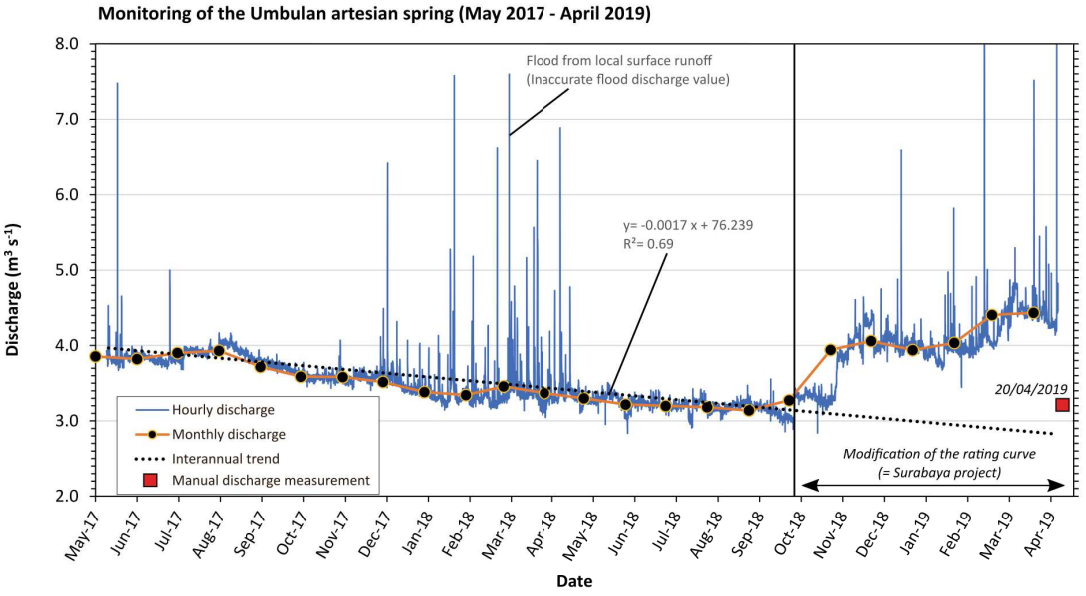

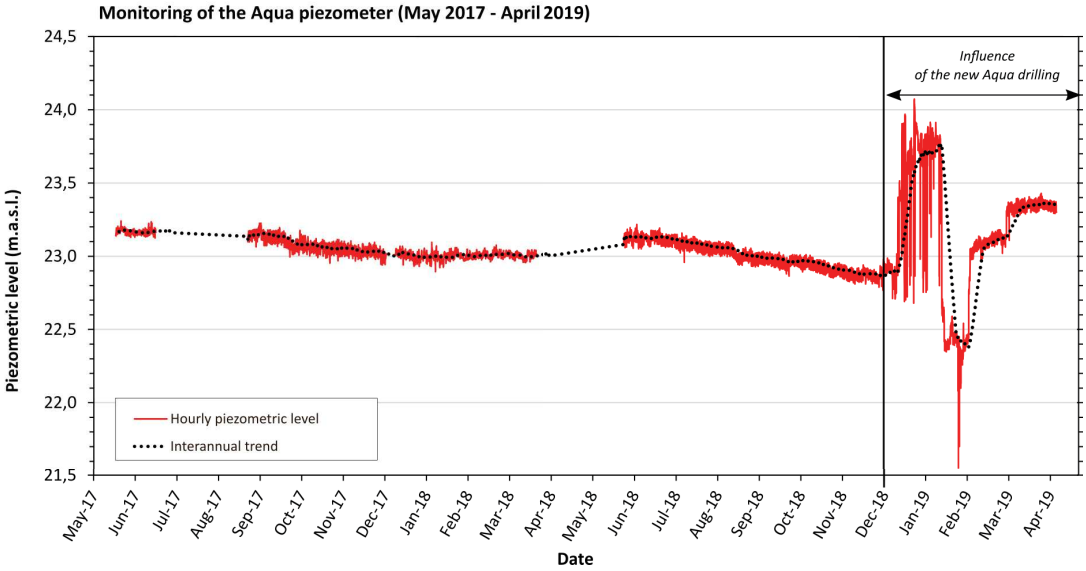

D. Compilation of the results from Umublan, Banyu Biru and Aqua piezometer.

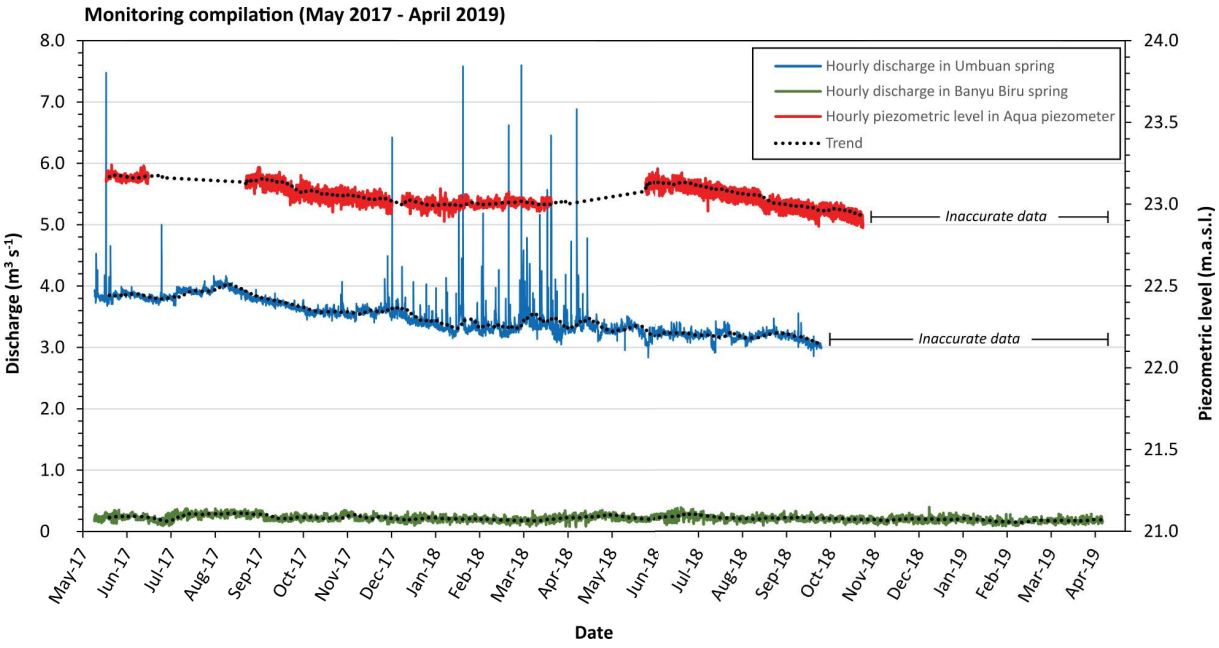

Appendix 8. Example of extrapolation or interpolation of the hydraulic head values to reach a residual drawdown of 1m.

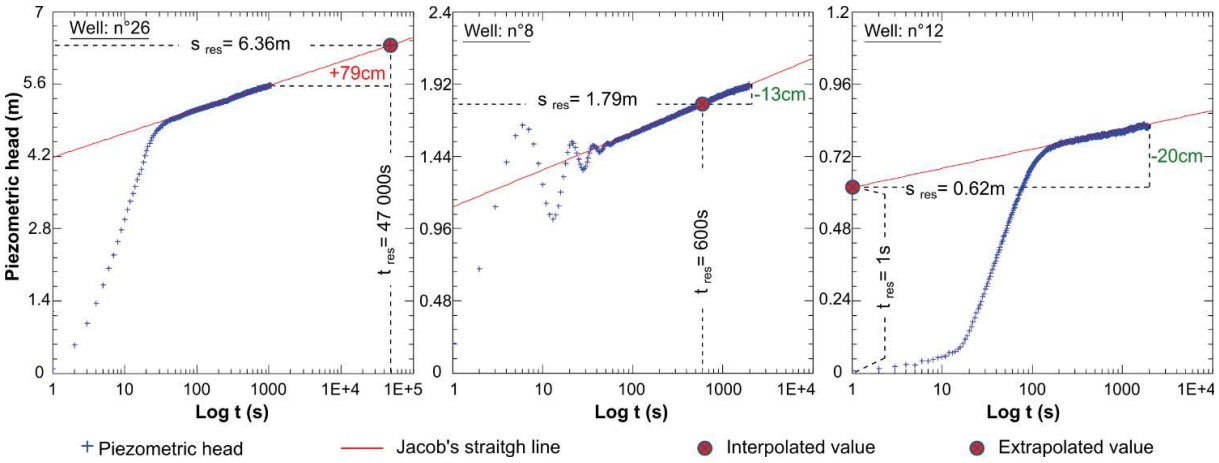

Appendix 9. Calculation results to reach a residual drawdown of 1m for each artesian well tested with the device.

n°	Depth	Flow	Recovery time	T	Piezometric level t4	Drawdown steady Dupuit	Drawdown transient Jacob	t residual drawdown = 1m	Correction by interpolation or extrapolation	Corrected piezometric level
	(m)	(m^3 s^{-1})	(s)	(m^2 s^{-1})	(s)	(m)	(m)	(s)	(m)	(m.a.s.l.)
3	32	0,0002	2999	3.15E-03	38.35	0.12	(-0.87)	1.00E-79	-0.02	38.33
5	60	0,0009	2093	8.83E-03	40.57	0.20	(-0.80)	1.00E-47	-0.06	40.51
6	103	0,0019	1903	1.06E-03	41.93	3.48	2.48	15000	0.02	41.95
8	63	0,0048	1973	3.45E-03	19.64	2.70	1.70	600	-0.13	19.51
12	120	0,0001	1924	4.01E-04	17.87	0.48	(-0.50)	1.00E-14	-0.20	17.67
13	70	0,0127	25397	1.11E-02	23.09	2.22	1.22	27	-0.37	22.71
15	93	0,006	2097	2.64E-03	30.63	4.42	3.41	26600	0.39	31.02
18	38	0,006	1420	2.91E-02	26.04	0.4	(-0.57)	1.00E-20	-0.10	25.94
19	60	0,0043	1878	2.36E-03	38.4	3.54	2.54	7600	0.09	38.28
20	52	0,0067	679	1.00E-02	40.58	1.3	0.29	1.00E-02	-0.20	39.88
21	88	0,0021	610	4.05E-02	46.03	0.1	(-0.90)	1.00E-100	-0.02	46.01
22	133	0,0182	2129	4.32E-02	49.37	0.82	(-0.16)	1.00E-07	-0.04	46.03
25	79	0,0031	1935	2.04E-03	39.29	2.95	1.95	2200	0.18	39.47
26	83	0,0052	1069	2.14E-03	37.73	4.72	3.72	47000	0.79	38.52
27	60	0,008	225	2.62E-02	24.28	0.59	(-0.40)	1.00E-12	-0.10	24.18
28	81	0,0112	2097	5.24E-03	42.46	4.15	3.15	9500	0.21	42.57

(.) negative value caused by artefact from the non-validity of the Cooper-Jacob's solution (1/u> 100).

Appendix 10. Groundwater flow model (Slice 1 = top layer) in steady state 2018.

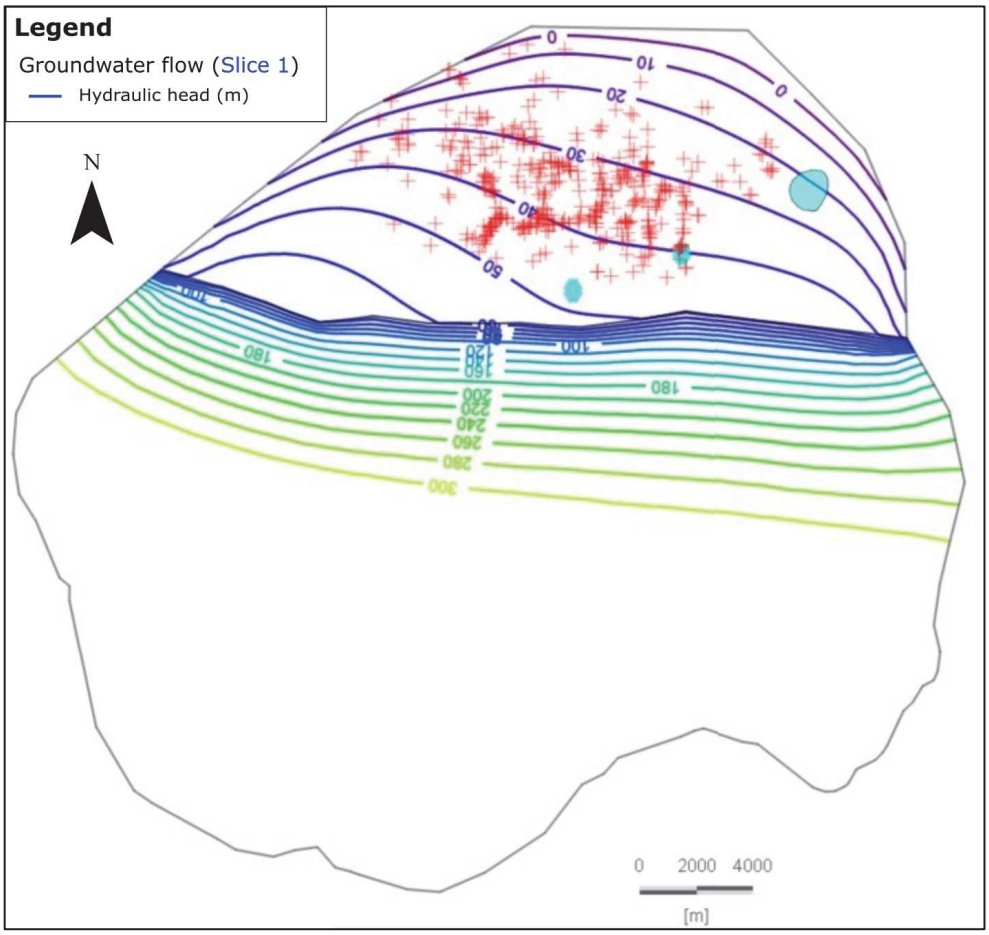

Appendix 11. Saturation Index of the dated groundwater samples

Datation No.	BDD No.	Water point name	Elevation	Type	Saturation Index by phase										
			(m.a.s.l.)		Anhydrite (CaSO4)	Aragonite (CaCO3)	Calcite (CaCO3)	CO2(g) (CO2)	Dolomite (CaMg(CO3)2)	Fluorite (CaF2)	Gypsum (CaSO4:2H2O)	H2(g) (H2)	H2O(g) (H2O)	Halite (NaCl)	O2(g) (O2)
1	3	Banyu Biru e	33	artesian spring	-3,83	-0,85	-0,71	-2,07	-1,34	-3,29	-3,61	-22,4	-1,53	-9,37	-38,62
2	43	Pump Well 13 b	28	pump well	-2,76	-0,47	-0,32	-1,74	-0,49	-2,46	-2,54	-22,22	-1,49	-8,64	-38,45
3	39	Artesian well 19 b	4	artesian well	-3,99	-0,66	-0,52	-2,67	-0,33	-3,6	-3,79	-24,04	-1,39	-7,11	-33,49
4	52	Wates Tani 2	34	artesian well	-3,79	-0,29	-0,15	-2,57	-0,08	-2,88	-3,57	-23,5	-1,53	-9,35	-36,36
5	53	BH54 bis	13	artesian well	-3,22	-0,45	-0,31	-2,17	-0,4	-2,63	-3	-22,88	-1,5	-8,52	-37,23
6	54	AWQ	43	artesian well	-3,55	-1,09	-0,95	-1,72	-1,8	-2,82	-3,33	-21,76	-1,48	-9,05	-39,27
7	22	FD1 b	20	artesian well	-3,86	-0,75	-0,61	-2,37	-1,19	-3,23	-3,64	-22,84	-1,52	-9,46	-37,57
8	55	BenbyAlix	18	artesian well	-3,84	-0,93	-0,78	-2,15	-1,38	-2,79	-3,61	-22,52	-1,54	-9,17	-38,48
9	4	Umbulan e	33	artesian spring	-3,76	-1,27	-1,12	-1,93	-2,23	-2,96	-3,53	-21,92	-1,55	-9,33	-39,75
10	56	AW2	27	artesian well	-3,48	-0,6	-0,45	-1,94	-0,74	-2,49	-3,27	-22,46	-1,47	-8,2	-37,73
11	57	West Umbulan	46	artesian well	-3,28	-0,95	-0,81	-1,93	-1,43	-2,87	-3,07	-22,18	-1,48	-8,62	-38,33
12	35	Artesian well 33 b	39	artesian well	-3,15	-0,81	-0,66	-1,99	-1,13	-2,97	-2,94	-22,36	-1,5	-8,51	-38,23
13	34	Artesian well 25 b	31	artesian well	-3,5	-0,02	0,13	-2,47	0,49	-2,54	-3,29	-23,62	-1,44	-8,25	-34,95
		Min			-3,99	-1,27	-1,12	-2,67	-2,23	-3,6	-3,79	-24,04	-1,55	-9,46	-39,75
		Max			-2,76	-0,02	0,13	-1,72	0,49	-2,46	-2,54	-21,76	-1,39	-7,11	-33,49

Appendix 12. Hydrochemical and isotopic results of the dated groundwater samples

No.	Water point name	Elevation	Type	Date	pH	EC	T	O2	HCO3-	Ca2+	Mg2+	K+	Na+	Cl-	SO42-	NO3-	Ionic Balance	δ18O	δD
		(m.a.s.l.)				(µS cm-1)	(°C)	(mg L-1)				(mg L-1)					(%)	(‰)	(‰)
3	Banyu Biru e	33	AS	05/06/2018	7.2	253	24.1	6.2	136.6	22.9	12.7	2.3	7	2.2	2.1	3.5	3%	-7.11	-42.42
43	Pump Well 13 b	28	PW	05/06/2018	7.11	483	25.7	1.62	236.7	43.6	27.3	6	14.7	5.8	17.3	26.7	4%	-7.3	-44.15
39	Artesian well 19 b	4	AW	05/06/2018	8.02	476	29.7	0.28	214.7	3.2	6.4	11.7	94.2	30.5	10.6	-	5%	-7.37	-44.75
52	Wates Tani 2	34	AW	05/06/2018	7.75	304	24.3	6.29	152.7	21.5	16.2	3	7.8	2	2.6	1.1	3%	-7.24	-43.14
53	BH54 bis	13	AW	05/06/2018	7.44	335	25.4	3.79	185.9	25	18.2	6.6	15.5	7.1	8.8	3.5	1%	-7.04	-43.08
54	AWQ	43	AW	04/06/2018	6.88	262	26	5.22	143	25.2	13.6	2.6	9	3.6	3.8	7.9	3%	-6.84	-41.65
22	FD1 b	20	AW	04/06/2018	7.42	200	24.6	7.4	111.8	20.3	9.9	2	6.1	2	2.1	3.1	4%	-7.25	-42.28
55	BenbyAlix	18	AW	05/06/2018	7.26	216	23.8	6.31	131.3	17.5	12.5	4.2	9.7	2.4	2.6	2.8	2%	-7.29	-42.63
4	Umbulan e	33	AW	04/06/2018	6.96	198	23.6	6.97	108.3	18.9	9.2	2.5	6.6	2.4	2.8	5.1	2%	-7.29	-43.26
56	AW2	27	AW	06/06/2018	7.23	371	26.4	0.88	192.8	27.1	17.3	8.2	20.4	11.4	4.4	1.8	4%	-6.92	-41.24
57	West Umbulan	46	AW	06/06/2018	7.09	300	26.3	6.05	142	21.4	14.5	5	11.7	7.5	8.2	7.7	1%	-6.78	-40.33
35	Artesian well 33 b	39	AW	06/06/2018	7.18	335	25.5	5.92	153.7	23.7	16.4	5.8	13.2	8.5	10.4	9.6	2%	-6.95	-41.12
34	Artesian well 25 b	31	AW	06/06/2018	7.81	398	27.8	1.23	214.7	23.9	16.9	6.9	26.4	7.9	4.8	-	1%	-6.52	-39.78